

Distribution Agreement

In presenting this thesis or dissertation as a partial fulfillment of the requirements for an advanced degree from Emory University, I hereby grant Emory University and its agents the non-exclusive license to archive, make accessible, and display my thesis or dissertation in whole or in part in all forms of media, now or hereafter known, including display on the world wide web. I understand that I may select some access restrictions as part of the online submission of this thesis or dissertation. I retain all ownership rights to the copyright of the thesis or dissertation. I also retain the right to use in future works (such as articles or books) all or part of this thesis or dissertation.

Signature:

Hans Peter Verkerke

Date

Viral and Immune Factors in Acute Respiratory Virus Infections: Evaluating the Role of SARS-CoV-2 Nucleocapsid Antigenemia in the Diagnosis and Pathogenesis of SARS-CoV-2 Infection

By

Hans Peter Verkerke
Doctor of Philosophy
Graduate Division of Biological and Biomedical Sciences
Microbiology and Molecular Pathogenesis

Sean Robinson Stowell, MD, PhD
Advisor

Anice Lowen, PhD
Committee Member

Jacob Kohlmeier, PhD
Committee Member

Haydn Kissick, PhD
Committee Member

Kenneth Moberg, PhD
Committee Member

David Steinhauer, PhD
Committee Member

Accepted:

Kimberly Jacob Arriola, PhD, MPH
Dean of the James T. Laney School of Graduate Studies

Date

Viral and Immune Factors in Acute Respiratory Virus Infections:
Evaluating the Role of SARS-CoV-2 Nucleocapsid Antigenemia in the Diagnosis and
Pathogenesis of SARS-CoV-2 Infection

By

Hans Peter Verkerke
B.S. (*Biology, Highest Distinction*), University of Virginia, 2013

Advisor: Sean R. Stowell, MD, PhD

An abstract of
A dissertation submitted to the Faculty of the
James T. Laney School of Graduate Studies of Emory University
in partial fulfillment of the requirements for the degree of
Doctor in Philosophy
in Microbiology and Molecular Pathogenesis
2022

Abstract

Viral and Immune Factors in Acute Respiratory Virus Infections:

Evaluating the Role of SARS-CoV-2 Nucleocapsid Antigenemia in the Diagnosis and Pathogenesis of SARS-CoV-2 Infection

By Hans Peter Verkerke

In the first months of the SARS-CoV-2 pandemic, we undertook several translational studies as part of the COVID-19 response at Emory to evaluate early biomarkers of disease severity and investigate the use of serological tests as adjunctive diagnostic tools. As part of these efforts, we aided in the development, validation, and implementation of the FDA authorized SARS-CoV-2 IgG test, still the primary serological test used in the Emory system for COVID-19. We then employed versions of this test in studies evaluating the antibody components of therapeutic COVID-19 convalescent plasma units, finding significant heterogeneity in levels of SARS-CoV-2 IgG, IgA, and IgM. Finally, we have spearheaded the development of novel, high-throughput testing platforms for SARS-CoV-2 neutralizing antibody activity, a primary correlate of vaccine efficacy and protection after natural infection.

While developing these tools, we conducted several clinical studies to uncover biomarkers of COVID-19 severity. In these studies, we found that viral nucleocapsid antigenemia could reliably be measured in blood samples taken during the acute phase of infection. This observation led us to test whether nucleocapsid antigenemia may be a specific diagnostic biomarker of acute SARS-CoV-2 infection. To this end, we conducted a large retrospective serological survey of COVID-19 patients, quantifying antigenemia in 1860 specimens from 1607 patients. In this cohort, antigenemia exhibited 85.8% sensitivity and 98.6% specificity in diagnosing acute COVID-19 cases, suggesting its possible utility as a screening tool for SARS-CoV-2 infection in blood samples.

Infection with SARS-CoV-2 results in a broad spectrum of clinical manifestations from asymptomatic carriage to severe respiratory failure and death. Notably, many patients with severe COVID-19 suffer from systemic disease involving microvascular inflammation, thromboembolism, and multi-system organ failure. However, the viral and immune factors driving these complications remain incompletely understood. Our work on viral antigenemia as a diagnostic tool led us to also evaluate its utility as a prognostic biomarker and potential driver of systemic pathology. We found that early nucleocapsid antigenemia levels predict disease severity and mortality and are associated with specific patterns of antiviral cytokine response. Furthermore, SARS-CoV-2 nucleocapsid itself can stimulate endothelial cells to elicit antiviral cytokine secretion and upregulation of leukocyte adhesion molecules. Together these studies provide a novel framework for understanding nucleocapsid antigenemia as both a diagnostic marker of acute infection and a clinical biomarker of severe COVID-19 that may itself contribute to endothelial dysfunction and systemic disease.

Viral and Immune Factors in Acute Respiratory Virus Infections:
Evaluating the Role of SARS-CoV-2 Nucleocapsid Antigenemia in the Diagnosis and
Pathogenesis of SARS-CoV-2 Infection

BS

Hans Peter Verkerke
B.S. (*Biology, Highest Distinction*), University of Virginia, 2013

Advisor: Sean R. Stowell, MD, PhD

A dissertation submitted to the Faculty of the
James T. Laney School of Graduate Studies of Emory University
in partial fulfillment of the requirements for the degree of
Doctor in Philosophy
in Microbiology and Molecular Pathogenesis
2022

Acknowledgements

First, I would like to thank my PI Sean Stowell, a truly excellent mentor for his unwavering support from the time I joined his lab through developing projects in response to a global pandemic. His enthusiasm for science and medicine is truly infectious and he has created an extraordinary environment for his students to succeed while exploring their own curiosities. I truly feel I have found a lifelong friend and intellectual advisor during my time in his lab.

I am also grateful to Andy Neish, John Roback and the members of the asymptomatic screening program and translational lab, without whose support my work on COVID-19 would not have been possible. Being part of this response has been the greatest learning experience in science and life that I have experienced so far. I would also like to thank the many collaborators that I have collected along the way, particularly Greg Damhorst, whose guidance and mentorship have enriched my PhD immensely.

I would like to thank my committee members for their insights and guidance on all of my projects. In particular, I am very grateful to Jake Kohlmeier for opening his lab to me so that I could continue work on my flu project during challenging times. I would also like to profusely thank Kirsten Kost and others in his group. Their guidance, technical and intellectual support have been invaluable in my training.

I am also grateful to former mentors who shaped my love for science and passion for medicine. Bill Petri, who took me on as a high school student to purify proteins and stuck with me throughout my undergraduate career and Fulbright research year in Bangladesh. His mentorship set me on the road to becoming a physician scientist and I am forever grateful for the start he gave me.

No part of this work would have been possible without my loving family and supportive friends. I am eternally grateful to my husband, Clinton, who has been and continues to be a steadfast and loving companion on this long and challenging road. To my parents who lovingly encouraged my curiosity for all things including science throughout my life. To my sister and brother, who have been amazing examples as older siblings following their interests and cheering me on to follow my passions.

Table of Contents

Chapter 1	<i>SARS-CoV-2 diagnosis and pathogenesis</i>	10
Abstract		11
SARS-CoV-2 Diagnostics		11
Detection of SARS-CoV-2 Infection		12
SARS-CoV-2 Infection and infectiousness		14
Viral Life Cycle		16
Spike Protein		18
Nucleocapsid Protein		19
Membrane		20
Envelope		21
Accessory Proteins		21
Pathogenesis		22
Innate Response		22
Adaptive Response		23
Humoral Response		25
Autoantibody formation		26
Cytokine storm		26
COVID-19 Coagulopathy		28
Conclusions and outlook		30
Thesis Objectives		31
Figures for Chapter 1		33
Chapter 2	<i>Nucleocapsid Antigenemia in the diagnosis of SARS-CoV-2 Infection</i>	36
Abstract		36
Introduction		37
Results		39
Discussion		42
Experimental Procedures		45
Author Contributions		48
Tables Chapter 2		48
Figures Chapter 2		51
Chapter 3		56
Abstract		57
Introduction		58
Results		60
Discussion		66
Experimental Methods		68
Chapter 3 Tables		75
Figures for Chapter 3		76

Chapter 4	<i>SARS-CoV-2 antibody class-specific serology: applications in diagnostics and characterization of COVID-19 convalescent plasma</i>	83
	Abstract	84
	Introduction	86
	Results	89
	Discussion	99
	Experimental Methods	103
	Chapter 4 Tables	108
	Chapter 4 Figures	109
Chapter 5	<i>Rapid, automated detection of SARS-CoV-2 neutralizing antibodies against native-like vaccine and delta variant spike trimers</i>	121
	Abstract	122
	Introduction	122
	Results	124
	Discussion	129
	Experimental Methods	130
	Figures for Chapter 5	134
Chapter 6	<i>Conclusions and Outlook</i>	142
	SARS-CoV-2 Serological Tests: Then and Now	143
	Viral antigenemia: Implications for diagnosis	145
	Viral Antigenemia: implications for COVID-19 pathology	146
Appendix 1	<i>Supplementary materials to Chapter 2</i>	150
	Supplementary Experimental Methods	151
	Supplementary Figures and Tables	152
Appendix 2	<i>Galectins, An Ancient Family of Carbohydrate Binding Proteins with Modern Functions</i>	3
	Abstract	4
	Introduction	5
	The Evolution of Carbohydrate Recognition	7
	Galectin Evolution and Biochemistry	9
	Galectin Evolution	10
	The Galectin CRD	12
	Synthesis of Galectin Carbohydrate Ligands	14
	Mammalian Galectin Expression and Localization	17
	Nuclear and Cytoplasmic Galectins	20
	Galectin Secretion	20
	Modern Galectin Functions	21
	Regulation of Pre-mRNA Splicing and mRNA Stability	21
	Intracellular Signaling: Proliferation and Apoptosis	24
	The Galectin Lattice	25

Homeostasis.....	27
Cancer	29
Roles in the Mammalian Immune System	31
Engagement and Crosslinking of Surface Receptors.....	32
Regulation of Immune Cell Turnover	35
Modulation of Inflammatory Intracellular Signaling Pathways.....	37
Intracellular Pattern Recognition and Damage Sensing.....	38
Galectin-Pathogen Interactions	40
Summary and Conclusions.....	43
<i>Appendix 3 Evaluating the Role of Galectin-1 during Influenza A Virus Infection</i>	<i>53</i>
Abstract	54
Introduction	55
Results	57
Conclusion	59
Experimental Procedures	60
Figures for Appendix 3	64
<i>References.....</i>	<i>7</i>

*Author contributions are included in chapters that include co-first authored materials

Chapter 1 SARS-CoV-2 Diagnosis and Pathogenesis

Abstract

Severe acute respiratory syndrome coronavirus 2 (SARS-CoV-2) is the causative agent of (COVID-19), cumulatively accounting for close to 500 million cases and 6.1 million deaths worldwide to date(1). Health care providers recognized early in the pandemic that infection with SARS-CoV-2 can result in a broad range of clinical presentations from asymptomatic to decompensated respiratory failure. Since this time, a massive scientific effort has dissected the biology of the evolving virus as well as the host immune response during infection. These basic studies in human populations and newly employed animal models have come far in defining essential parameters that mediate viral transmission, infectivity, immune protection, and evasion while at the same time identifying important viral, immune, and host factors associated with disease severity. Orthogonally to these lines of investigation, translational work has produced an immense armamentarium of diagnostic tools, therapeutic strategies, vaccines, and now antiviral therapies to be employed at the bedside. In this introductory chapter to our work on COVID-19 diagnostics and disease severity, we present an overview of SARS-CoV-2 diagnostics, virology, and pathogenesis, emphasizing the clinical implications that have arisen from basic lines of inquiry.

SARS-CoV-2 Diagnostics

SARS-CoV-2 infection results in a broad array of clinical manifestations, from asymptomatic carriage to respiratory failure and multi-system end-organ damage involving the heart, kidney, brain, and immune system(2, 3). And while clinical suspicion is warranted in any patient presenting with signs or symptoms of respiratory infection, the lack of their specificity for COVID-19 and the urgency of case identification and management, have necessitated the development of a diverse array of robust diagnostic tools. The first set of these tools, targeting viral nucleic acid with conventional real time reverse transcriptase polymerase chain reaction (RT-PCR), were assembled within days

of identification and sequencing of SARS-CoV-2(4). As the pandemic set in, additional methods for detection relied on less conventional modes of nucleic acid amplification or modified platforms offering faster turnaround times with varying performance characteristics(5). At the same time, synthesis of viral antigens allowed for isolation of monoclonal antibodies which could be employed in new antigen detection assays, which are simpler to adapt for rapid testing and can be less demanding for the clinical laboratory or surveillance operation to employ. These antigens were also used in the development of clinical serology tests for SARS-CoV-2 antibodies, which provide evidence of exposure and potential correlates of immunity(6). While many challenges arose and remain in the deployment of effective diagnostic tools during the pandemic, the speed and breadth of innovation in translation of basic science to the clinical laboratory has been unprecedented.

Detection of SARS-CoV-2 Infection

The clinical performance of any diagnostic test for a viral pathogen is multifactorial. Test subject characteristics affect pre-test probability and mostly involve factors that influence viral load. These include timing post infection or symptom onset and exposure to infected individuals, which itself is dependent on the density or prevalence of disease in a population. Operational factors involve sampling and are usually specific to a class or modality of testing—including the type of specimen to be tested, transport conditions, sampling technique, and laboratory protocols for sample handling. Together, these pre-analytical variables are independent of the test itself, but are essential factors in determining test performance. In fact, the majority of variability and error in test performance is attributable to pre-analytical factors(7).

Tests for SARS-CoV-2 fall into three categories (1) nucleic acid amplification tests (NATs) (2) antigen tests (3) and antibody tests. Each testing modality has its advantages

and disadvantages depending on the needs of those employing them. For instance, the high sensitivity of NATs can be advantageous in the hospital setting, where contact precautions prevent transmission among closely housed patients. However, one dilemma posed by the sensitivity of SARS-CoV-2 NAT testing arises from the long tail of RNA positivity, which can persist well beyond the period of transmissibility(8–10). Triggering contact precautions for patients or community members who test persistently positive by PCR can impact care and have enormous repercussions in the societal impact of the pandemic response.

Antigen tests are lower cost, have a rapid turnaround time, and fewer requirements for specialized personnel or facilities. They are, however, less sensitive and exhibit varying specificity compared to NATs. Thus, antigen tests may require confirmatory results particularly in symptomatic individuals testing negative or asymptomatic individuals testing positive, where varying pre-test probability increases the risk of false classification. One proposed strategy to overcome these limitations is for individuals to employ lower sensitivity antigen tests more frequently(11, 12). This approach targets identification of infected individuals with higher viral loads than are typically detected by the low analytical thresholds of NAT tests, which mitigates the mis-classification of recovered, PCR positive individuals, while increasing the likelihood of detecting the most transmissible cases.

SARS-CoV-2 antibody tests have limited use in diagnosing acute infection in the community setting due to the timing of the humoral immune response and, more recently, the rollout of vaccination(13). However, early in the pandemic when resources for NATs were limited, numerous studies explored the diagnostic performance of serology testing in SARS-CoV-2 infection(14–18). Performance of these tests depended on the timing of presentation and the class of antibody evaluated. Issues with cross-reactivity perhaps

due to pre-existing coronavirus immunity also contributed to a lack of specificity for these platforms(19). Nonetheless, with the advent of vaccines and larger scale studies of natural immunity, the utility of COVID-19 serology has shifted from diagnosis to the characterization of neutralizing antibodies, which are a primary correlate of immune protection. Because SARS-CoV-2 is a BSL3 pathogen, adaptation of gold-standard virus neutralizing assays has been required to develop tests that are suitable for clinical use. Many of these new tests use a blockade of binding approach, which measure the inhibitory activity of a sample for the high affinity interaction between SARS-CoV-2 spike glycoprotein and human angiotensin converting enzyme (ACE2)(20, 21). In principle, these tests can be adapted to measure neutralizing activity against any virus with a defined host receptor, and their development clinical use may represent a promising new tool in pandemic preparedness. In **Figure 1.1** we outline the role of diagnostic testing at various stages and population levels in the SARS-CoV-2 pandemic.

SARS-CoV-2 Infection and infectiousness

Like SARS-CoV-1, SARS-CoV-2 enters cells through binding of the receptor binding domain (RBD) of spike glycoprotein with ACE2(22–24). A second host protein, the transmembrane serine protease 2 (TMPRSS2) is also important for priming of S protein during viral entry(25). Though genetically similar, SARS-CoV-2 has a longer incubation period and consequently a higher replication number (R_0), meaning that each infected individual, on average, will transmit the virus to more contacts than will those infected with SARS-CoV-1(26). This may also, in part, be due to structural differences in SARS-CoV-2 spike that increase affinity for ACE2 binding and may increase infectivity at the upper respiratory mucosa(27).

In studies detailing the dynamics of viral replication in human subjects, the peak of SARS-CoV-2 viral load and infectiousness typically precedes or coincides with the onset

of symptoms, adding to the challenges of case detection and contact tracing in a pre-symptomatic population(28). In a metanalysis of studies using viral culture as well as highly sensitive quantitative reverse transcriptase polymerase chain reaction (qRT-PCR) for detection, SARS-CoV-2 viral RNA persisted by PCR in the upper respiratory tract for an average of 15 days after symptom onset (range of 9.3 to 20 days with a maximum of 83 days)(29). However, the duration of infectiousness appears to be more limited based on two lines of evidence. The first comes from epidemiological studies of transmission, which show that very few linked transmission events occur after the first two weeks of symptoms. The second is that viral culture rarely detects infectious virus in the upper respiratory tract after 10 days of symptomatic disease(28, 30). Thus, PCR status may, in some cases, extend past the period in which active viral replication and risk of transmission occur. While these findings do not rule out persistence of replication competent virus in other compartments, they are consistent with the resolution of infectiousness from the respiratory compartment no more than two weeks after the onset of symptoms in the majority of immunocompetent hosts.

During this period of infectiousness, transmission of SARS-CoV-2 occurs primarily through inhalation or transfer of respiratory droplets to mucosal surfaces of the respiratory tract in the upper airway, where ACE2 can be found on host target cells(31). Because ACE2 expression is not isolated to respiratory tissue(32), other ACE2 bearing cells, including those of the gastrointestinal (GI) tract, can become infected with virus and drive symptomatology. Clinical studies show that 15-20% of COVID-19 patients experience GI specific symptoms(33), though the proportion of these patients with active GI infection remains unclear. Virologic studies using explants and isolated cells in culture also indicate that SARS-CoV-2 has tropism for this compartment, which is permissive to the life cycle of the virus(34–38). In addition to potentially causing GI symptoms through direct infection

of the intestinal epithelium, the role that SARS-CoV-2 may play in altering the microbiome of infected hosts or driving dysbiosis remains poorly understood(39). Intriguingly, viral shedding in stool persists for an equivalent period after symptom onset compared to the respiratory compartment(40), suggesting that involvement of the GI tract likely occurs throughout the course of infection. Regarding the potential for fecal-oral transmission, speculation comes from the proven ability of the virus to replicate in the GI compartment as well as several isolated outbreak investigations wherein the details were consistent with this route of transmission. However, further investigation is needed to determine whether this constitutes a significant route for both SARS-CoV-1 and SARS-CoV-2(41).

Viral Life Cycle

SARS-CoV-2 is in the family *Coronaviridae* within the suborder *Coronavirineae* of the order *Nidovirales*, composed of enveloped, positive-strand RNA viruses with a broad host range among vertebrates and invertebrates. Within the family *Coronaviridae* lies four genera of the subfamily *Orthocoronavirinae*: *alphacoronaviruses* and *betacoronaviruses*, which only infect mammals and are known to primarily cause respiratory and GI symptoms; as well as *gammacoronavirus* and *deltacoronavirus*, which are known to also infect avian species(42). SARS-CoV-1 and SARS-CoV-2 along with other SARS-like bat coronaviruses are in the *Sarbecovirus* lineage of *betacoronaviruses*, whereas Middle East respiratory syndrome-related coronavirus (MERS-CoV) is in the *Merbecovirus* lineage(43–45). Human cold coronaviruses come from both *alpha* and *beta* genera (*alpha*: 229E and NL63; and *beta*: OC43 and HKU1). These latter viruses affect populations in seasonal cycles and cause mild symptoms of upper respiratory tract infection(46). Pandemic coronaviruses cause more severe disease through infection of a broader range of host cells including pneumocytes, upper respiratory epithelial cells, bronchial epithelial cells, and intestinal epithelial cells. This expanded tropism and permissiveness of additional cell types to pandemic coronavirus infection likely

contributes to the devastating pathogenic potential of these viruses. This section will focus on what is known about the life cycle of SARS-CoV-2 set within the broader context of coronavirus biology(47).

Priming by serine protease TMPRSS2 and binding to ACE2 initiates cell entry of SARS-CoV-2 through the endosomal compartment(48–50). While TMPRSS2 is required for receptor-mediated entry, endosomal cathepsin B and cathepsin L serve as accessory proteases for S protein priming, increasing efficiency of infection(51, 52). Next, fusion of the endosomal and viral membranes allows for uncoating and release of genomic RNA into the cytoplasm, resulting in early translation of two large, overlapping open reading frames (ORF1a and ORF1b) into polyproteins pp1a and pp1ab(53). A lower efficiency -1 ribosomal entry site to ORF1b dictates an approximated 2:1 stoichiometry for the translation of pp1a relative to pp1ab, which privileges the production of nsps required to hijack translation machinery (nsp1)(54–56) and remodel the cell in preparation for genome replication and virion formation (nsps2-11), mediated by pp1ab nsps and structural proteins(57). These polyproteins are co-translationally processed by host and viral (nsp3, nsp5) protease activity into nsps, which are involved in the biogenesis of perinuclear viral replication factories (VRFs) consisting of multiple membranous structures (e.g. double membrane vesicles and convoluted membranous networks)(58, 59). These structures shield the activity of core replicative nsps (nsps12-16), which drive synthesis of double stranded RNA intermediates (RdRP or nsp12, with accessory nsps 7 and 8) that are potent substrates for cytoplasmic pattern recognition receptors (PRRs)(60).

RNA synthesis itself begins with full length negative strand template synthesis. These templates in turn allow for synthesis of full-length positive strand genomes that can be packaged into virions. They can also mediate translation of additional viral proteins

needed to maintain replication machinery and synthesize virion components. In addition to full length genome synthesis, coronavirus negative strand transcription involves a discontinuous process resulting in the production of functionally monocistronic subgenomic RNAs (sgRNAs), which template synthesis of positive sense sg mRNAs encoding structural proteins—S protein, envelope (E), membrane (M) and nucleocapsid (N)—as well as an unknown number of accessory proteins, designated ORFs(61, 62). For most well-characterized coronaviruses, virion assembly occurs in the transitional endoplasmic reticulum to golgi compartment with egress through the exocytic pathway. SARS-CoV-2 may exhibit a somewhat different route of egress as recent studies have suggested exit is also possible through the lysosomal compartment, where the virus was able to disrupt enzymes required for antigen processing and presentation(63–65). In **Figure 1.2** we outline some of the major functional components of the SARS-CoV-2 genome and the formation of viral replication factories.

Spike Protein

SARS-CoV-2 S protein is an extensively glycosylated type I homotrimeric viral membrane protein, responsible for host cell receptor binding and fusion(22, 66–68). Extending from the surface of the virus like the points of a crown, ~25-30 S proteins stud the surface of individual virions in various conformations. Cryo-electron microscopy studies of intact, native virions have demonstrated considerable heterogeneity in the conformation of S protein on the surface(69). In addition to adoption of both pre-fusion and post-fusion states on native virions, evidence of breathing was observed of the N-terminal hinge-like receptor binding domain (RBD) between “up” and “down” conformations, dynamically exposing or masking the binding surface or receptor binding motif (RBM), which recognizes the N terminal helix of ACE2. The most N terminal structure of S protein is the N terminal domain (S NTD), which adopts a galectin-like fold

and has been shown in multiple studies to exhibit carbohydrate binding activity(70). This activity, along with the shown lectin activity of RBD itself for structures including blood group antigens(71) and interactions with integrins may play a role in initial stages of attachment or could, in theory, mediate receptor independent entry in some cases(72).

Cleavage of full-length S protein by furin and other golgi proteases forms S1 and S2. The N terminal S1 domain encompasses the aforementioned RBD and NTD while S2 contains four functional regions: the fusion peptide, two heptad repeat domains (HR1 and HR2), and a transmembrane domain. Thus, S1 contains the domains necessary for host receptor recognition and binding while S2 contains the machinery for membrane fusion. Upon receptor binding, RBD is frozen in the up conformation and proteolytic cleavage by TMPRSS2 and cathepsins results in shedding of S1 and formation of a six helical bundle from HR1 and HR2. This structure brings the viral and host membrane into close apposition and allows insertion of the hydrophobic fusion peptide thus accomplishing membrane fusion(73, 74).

S protein is a primary target for naturally occurring and therapeutic neutralizing antibodies, whose activities directly block viral entry by preventing ACE-2 binding or in some way preventing the conformational changes needed for membrane fusion to occur(75, 76).

Nucleocapsid Protein

SARS-CoV-2 N protein is a 5-domain nucleic acid binding protein with three intrinsically disordered regions (N terminal arm, SR-rich linker domain, and C terminal tail) flanking and linking ordered N and C terminal domains with RNA binding and dimerization activity respectively. The NTD is composed of a four stranded antiparallel β -sheet in the shape of a right-handed fist with extended charged loops facilitating RNA

binding. The crescentic CTDs associate through complementary double β -hairpins at the dimer interface that extend into each cavity and form a stable four β -strand structure(77). ~12 nucleocapsid proteins dimerize and then polymerize like beads on a string along a stretch of approximately ~800 nucleotides to package the genome of the virus. In the native virion, nucleocapsid is the only internal structural protein, but appears to associated closely with the membrane of the virus perhaps through interaction with the internally facing features of other structural proteins including M and E(78–80). In **Figure 1.3** we outline the structure of nucleocapsid protein and its domains.

Several studies have identified activities of N protein in modulating the host immune response including as a suppressor of anti-viral RNA silencing through sequestration of RNAi targeting guides. Exogenous expression of N protein is also sufficient to interfere directly with IFN-I production and signaling in target cells.

Membrane

SARS-CoV-2 membrane glycoprotein (M) is an integral membrane protein that interacts with S, N, and E to regulate virion assembly, size, and morphology. Through its interactions with S protein, M is thought to localize and organize the topology of viral membrane assembly(81). It may also play a role in viral entry as M proteins of other coronaviruses have been shown to interact with ubiquitous and non-specific ligands like heparin sulfate. M is also an inhibitor of innate immune signaling pathways by inducing degradation of TBK1(82) and by blocking assembly of RIG-I, MAVS, TRAF signaling complexes and preventing activation of IRF3(83). M protein has also been shown to engage and promote mitochondrial apoptosis pathways through interactions with B-cell lymphoma 2 (BCL-2) ovarian killer (BOK), which may be sufficient to cause pulmonary edema in mouse models(84).

Envelope

In addition to S protein, E protein is a structural protein likely involved in viral membrane fusion and genome release from the endolysosomal compartment as well as virion assembly (85). E is a small five helix bundle transmembrane protein which can form an ion channel in the viral membrane. While the exact mechanism by which E protein aids in fusion and genome release is unknown, the well studied M2 protein of influenza A virus illustrates how ion channels can impact this process for other viruses. IAV M2 is an ion transporter that controls endolysosomal acidification (86). While this specific mechanism may not directly apply to SARS-CoV-2 biology and the mechanism of action for E protein, it is clear that ion transport can be a key regulatory feature in the life cycle of a virus. In addition to its potential conserved role in the life cycle of the virus, E protein may have off target effects for the virus by causing NLRP3 inflammasome activation through triggering Ca²⁺ release as it accumulates during virion synthesis in transitional ERGIC structures(85, 87).

Accessory Proteins

Accessory proteins of SARS-CoV-2 are primarily encoded by alternative ORFs, for which they are named, in sg mRNAs for structural proteins. While a comprehensive understanding of their functions remains to be determined, some activities and structural features have been elucidated. ORF3a, for instance, has been shown to induce apoptosis and may also serve as a scaffold for NF- κ B activation through a conserved TRAF binding domain(88, 89). ORF9b is translated from the sgRNA encoding N protein and is known to modulate the activity of mitochondrial antiviral signaling protein (MAVS) through interaction with TOM70(90). Other accessory proteins like ORF7a and ORF8 have membrane associated structural features and may regulate protein trafficking and virion formation in membranous viral replication factories where they localize(91). Other

putative accessory proteins with less well-defined function include ORF3b, 6, 7b, 9c and 10(92).

Pathogenesis

Innate Response

After entry into target cells of the respiratory epithelium through interactions with ACE2 as well as non-receptor mediated entry, SARS-CoV-2 undergoes a period of active replication and viral release from host cells (described above). Intracellular and extracellular pattern recognition receptors are activated by viral RNA (vRNA), resulting in type I interferon production and the induction of a coordinated antiviral state through autocrine and paracrine signaling to upregulate a broad array of interferon stimulated genes (ISGs), whose corresponding proteins have evolved to disrupt various aspects of the viral life cycle (93). Any virus adapted to replicate within the mammalian immune system must evolve strategies sufficient to circumvent these innate immune programs. Though more work remains to be done to validate these specific findings, Shi et al. used a systematic approach to screen all SARS-CoV-2 structural and non-structural proteins (nsps) for activity against the conserved RIG-I/Type I interferon signaling pathways resulting from viral pattern recognition upon infection. They found that SARS-CoV-2 nsps and translated open reading frames (ORFs) hit multiple levels of these sentinel pathways including phosphorylation of TBK1 and IRF3 downstream of RIG-1, which would reduce transcription of interferons. Additional inhibition was identified at the level of STAT1/2 phosphorylation and nuclear translocation downstream of the receptors for IFN- α and β (94). Together these finding lay the groundwork for our evolving understanding of mechanisms by which, like other successful human viruses, SARS-CoV-2 subverts innate immune pathways to permit its replication and release. The pathology associated with this stage of infection include hallmark symptoms of viral infection like fever, headache,

muscle aches, and cough(95). Intriguingly, these early stages of SARS-Cov-2 infection may also be accompanied by loss of taste and smell, which animal studies suggest may be a direct result of viral infection of olfactory epithelial cells (96, 97), raising concern for the potential of neurotropism or the evolution of that phenotype in new variants.

Several studies have observed a reduce systemic IFN-I response in COVID-19, particularly in patients with severe disease(98–100). And treatment with IFN-I therapy may improve outcomes(101). These observations may in part be due to the innate immune evasion described above. Others have suggested that the multilineage lymphopenia accompanying SARS-CoV-2 infection includes depletion of plasmacytoid dendritic cells (pDCs)(102, 103)p, which are major IFN- α secreting cells during viral infection(104). Consistent with the latter hypothesis, despite suppressed early systemic IFN-I responses, exuberant IFN-I and ISG signatures have been observed in bronchial alveolar lavage samples from severe COVID-19 patients later in their disease course(105). Cumulatively, the evidence suggests that a delayed or poorly timed IFN-I response may contribute, at least in part, to immune dysregulation associated with severe COVID-19.

Adaptive Response

In the majority of COVID-19 patients, despite viral evasion, the innate response described above initiates cellular and humoral responses, first non-specific to the virus and then resolving in production of virus specific immunoglobulin and the recruitment of antigen specific cytotoxic and helper T cells to the site of infection(106). Several studies have suggested that pre-existing memory B and T cells specific for circulating human cold coronaviruses may play a role in shaping this antigen specific response to SARS-CoV-2 infection(107–110), though the exact etiology of the cross reactivity observed in these studies remains unresolved. It is during this adaptive phase of the immune response that

dysregulation can drive severe pathological outcomes. Autopsies of patients who die from COVID-19 show inflammatory changes consistent with immunopathological damage (hyaline membranes, endothelial disruption and damage to the alveoli with infiltrating lymphocytes)(111). In addition to findings of respiratory pathology, many patients exhibit more systemic disease including severe end organ damage of the cardiovascular system, acute kidney injury, and hepatobiliary dysfunction (3). Despite the absence of replicating virus in circulation, COVID-19 coagulopathy and endothelial dysfunction have also emerged has hallmarks of more severe disease, in some cases clearly driving multisystem organ failure(112).

A common laboratory finding in COVID-19 patients is a reduction in circulating lymphocytes below normal (lymphopenia) and a concomitant increase in circulating neutrophils (neutrophilia). This skewed neutrophil to lymphocyte ratio is a major prognostic indicator of disease severity and progression(113, 114). Detailed immunologic characterization of the circulating lymphocyte compartment by multiple groups has revealed that all major lymphocyte populations are depleted with the T cell compartment carrying markers of functional exhaustion in many studies (115, 116). The mechanism remains unclear but could in part be driven by elevation in certain immunomodulatory cytokines or potential destruction of secondary lymphoid tissues during more severe infection (117, 118) While some evidence supports unique features of neutrophilia in COVID-19—including metabolic changes, altered NETosis, and changes in maturation—other studies describing these changes use healthy controls as a comparison and cannot exclude the possibility that these observations represent a normal, if pathological, response to the severity of infection(119).

Humoral Response

The humoral immune response to SARS-CoV-2 is initiated by antigen presentation with T cell help to germinal center B cells, which proliferate and undergo affinity maturation into antibody secreting plasma cells(120). Plasma cells facilitate synthesis of multiple classes and subtypes of immunoglobulin, which serve multiple functions from direct neutralization to facilitating antibody dependent cytotoxic and phagocytic (ADCC and ADCP) responses from natural killer cells and macrophages respectively(121, 122). In SARS-CoV-2 infection, virus-neutralizing antibody responses correlate with disease severity and are a primary correlate of protection after natural infection and vaccination. Despite a relatively low mutation rate for coronaviruses, escape from these neutralizing antibodies through amino acid substitutions in S protein are thought to be a primary mechanism for breakthrough infections and waning immunity(123). While many studies have claimed to characterize specific and generalizable patterns of antibody class specific immunity in COVID-19, the emergent pattern is clearly that the timing, magnitude, and specificity of responses are heterogeneous with most patients mounting anti-S IgM, IgG and IgA responses within the first two weeks of symptom onset that variably wane within months of infection(124, 125). Virus specific IgG and IgM antibodies persist for longer periods than IgA, lending some specificity of high IgA levels in serum for proximity to acute infection(126). Another theme that has emerged in studying both T cell and B cell responses is evidence for pre-existing or cross-reactive immunity to cold coronaviruses influencing the immune response during SARS-CoV-2 infection. This pre-existing memory compartment with cross-reacting specificity has been shown in some studies to protect against SARS-CoV-2 infection(108, 127).

Autoantibody formation

While we have yet to achieve a complete understanding of COVID-19 immunopathology, several mechanistic themes have emerged over the course of the pandemic. These findings have come from comprehensive immune profiling with the goal of identifying correlates of disease severity. Among these emerging correlates of severity is formation of autoantibodies, particularly against immunomodulatory proteins (chemokines, cytokines, complement pathway components and receptors). In a systematic study of this question, Wang et al., used high throughput autoantibody profiling in COVID-19 patients with severe, mild, and asymptomatic disease compared to uninfected controls and found that immune system reactive antibodies were more commonly found in patients with more severe COVID-19. They went on to infuse murine versions of several candidate immunopathological autoantibodies in a mouse model of SARS-CoV-2 infection finding that they induced dysregulated immune responses and worsened outcomes in the model(128). Other groups identified autoantibodies against type I interferons as mendelian deficiencies in interferon signaling as risk factors for severe COVID-19(129, 130). While these studies provide compelling information about associated risk factors, many lack the study design to specifically understand whether the tendency toward autoantibody production occurs in response to COVID-19 or represents a pre-existing phenotype. Longitudinal assessment of individual immune responses during COVID-19 are need to determine the direction of this association with clinical outcomes.

Cytokine storm

A well-controlled cytokine response—one that may result in symptoms but not extensive immunopathology—arises from effective crosstalk between virally infected cells and cellular components of the immune system. Dysregulation of this response,

particularly over production of pro-inflammatory cytokines, can result in a clinical syndrome known as cytokine storm (CS)—first described in patients with graft-versus-host disease(131, 132). Hyperstimulation of immune cell populations amplifies a positive feedback loop and can lead to aberrant tissue infiltration by immune cells in high mortality syndromes such as hemophagocytic lymphohistiocytosis (HLH)(133). In addition, because non-immune cells also express receptors for cytokines, uncontrolled systemic CS results in a host of physiologic dysregulation including thrombotic changes like disseminated intravascular coagulopathy (DIC), capillary leak syndromes, and severe end-organ damage(134–136).

Specific cytokines involved in COVID-19 CS include numerous members of the interleukin family (1,2,6,7,8,10,12,17,18), type I-III interferons, tumor necrosis factor α (TNF- α), monocyte chemoattractant protein 1 (MCP-1), as well as granulocyte-macrophage colony-stimulating factor (GM-CSF)(99, 136–140). While the early events that drive CS during SARS-CoV-2 infection are not well understood, the process may emerge from innate immune evasion involving disruption of IFN-I signaling cascades by M protein, N protein, and open reading frame 3a (ORF3a) protein (among others). This immune modulation coupled with positive feedback amplification of the systemic immune response, may be sufficient to drive over production of cytokines and hyper activation of immune cells involved in high mortality processes like macrophage activation syndrome (MAS) and HLH(133, 135).

Observations of CS in COVID-19 as well as studies showing that high levels of IL-6 and later other cytokines were predictive of outcomes in SARS-CoV-2 infection(141) have led to translational efforts aimed at identifying biomarkers of disease severity as well as therapeutic interventions that target cytokine signaling pathways. These efforts include marshaling existing clinical laboratory tests to develop diagnostic criteria for a complex,

multisystem immune syndrome like COVID-19 CS. A proposal by Caricchio et al.(142), suggested multi-test guidelines for identifying CS in a COVID patient. These criteria cluster into three categories in the context of systemic inflammation (e.g. elevated CRP, ferritin, or specific cytokines). (1) markers of immune dysregulation (low albumin, lymphopenia, neutrophilia); (2) markers of end organ damage (elevated ALT and AST, elevated d-dimer, elevated LDH, elevated troponin); (3) markers of electrolyte imbalance and kidney dysfunction (hyperkalemia, anion gap, elevated blood urea nitrogen (BUN) to creatinine ratio). While these guidelines are non-specific to SARS-CoV-2 pathogenesis they may serve to guide application of specific immunomodulatory therapies such as the IL-6 receptor antagonist tocilizumab, which has been shown to have variable impact on mortality in COVID-19 generally(143, 144), but may provide particular benefit in a more specific, hyper-inflamed population. Despite this progress, there remains a pressing need to characterize biomarkers of COVID-19 severity and better understand the role specific cytokines may play in disease progression.

COVID-19 Coagulopathy

Patients with SARS-CoV-2 infection frequently experience coagulation abnormalities and thromboembolic event. This process can be conceptualized using Virchow's triad, a framework for understanding the factors that contribute to life-threatening thrombosis which is defined by endothelial injury, stasis, and hypercoagulability.

Many studies have identified microvascular endothelial injury and endothelial dysfunction as hallmarks of SARS-CoV-2 systemic disease(145). The rate of venous thromboembolism among COVID-19 intensive care unit patients is up to 30% with incidence rising to between 70 and 100% among patients who died from COVID-19(146). And while the mechanisms by which this dysfunction remain unclear, endothelial injury is

likely to play a key role in predisposing patients to coagulopathy by contributing to a hypercoagulable state. In the lung, the tropism of SARS-CoV-2 for type II pneumocytes(147, 148) brings the virus in apposition to the microvasculature associated with alveoli. Thus, local pulmonary inflammation and damage can drive endotheliitis in the lung. In addition, direct infection of both pericytes and perivascular cells has been reported and findings consistent with endothelial cell infection have been seen on autopsy in multiple compartments including capillary loops of the glomerulae and intestinal capillary beds(149). Endothelial damage and dysfunction are also direct consequences of hyperinflammation seen in COVID-19 CS, macrophage activation syndrome, and HLH. The hemophagocytes associated with HLH cause consumptive coagulopathy, which can result in disseminated intravascular coagulation (DIC)(150). However, while DIC may be a consequence of hyperinflammation in some cases, isolated COVID-19 coagulopathy is distinct from DIC in that the primary pathology is thrombosis rather than bleeding(151). Complement mediate endothelial injury has also been described. Levels of C5b-9 are elevated in patients with severe COVID-19 relative those with non-COVID-19 respiratory failure or severe influenza, suggesting some degree of specificity for SARS-CoV-2 infection(152–154).

All patients receiving intensive care are at higher risk of thromboembolic events due to inactivity and venous stasis(155). However, COVID-19 patients have also been shown to have increased plasma viscosity, which itself can decrease flow and contribute to the stasis arm of Virchow's triad(156). Specific mechanisms of COVID-19 hyperviscosity have not been described but may involve extrusion of neutrophil extracellular traps (NETs), elevated fibrinogen, or elevated immunoglobulin levels.

Evidence of hypercoagulopathy in COVID-19 patients comes from abnormal coagulation tests. Patients often have elevated prothrombin time (PT), thrombocytosis,

fibrinogen elevation, and high D-dimer levels—which have been independently associated with disease severity in several studies. VWF and Factor VII are less commonly measured, but are also elevated in COVID-19 coagulopathy.

Conclusions and outlook

Since the emergence of SARS-CoV-2 in 2019, the scientific community has responded en masse to characterize the virus and its pathogenesis. Arising from these basic virological and immunological studies have been numerous insights on which our clinical tools for managing the pandemic have been built. Identification of the causative agent of COVID-19 by electron microscopy and sequencing of the viral genome, coupled with informatics and decades studying basic coronavirus biology allowed researchers to quickly identify viral proteins and infer their likely functions. This early molecular characterization rapidly led to selection of targets for vaccination and nucleic acid-based diagnostics. PCR tests allowed widespread case identification, opening the door to clinical study of the disease and its sequelae. Synthesis of recombinant spike, nucleocapsid, and other viral proteins formed the basis for serological tests and enabled B cell sorts for new monoclonal antibodies. These antibodies could then be tested in passive immunization studies as therapeutics while simultaneously being deployed as critical reagents in new antigen testing platforms. This coordinated scientific response has saved millions of lives and expanded our understanding of SARS-CoV-2 biology.

Efforts have progressed in parallel to better understand the pathophysiology and unique features of COVID-19, particularly its most severe consequences. A diversity of clinical outcomes and manifestations have emerged as hallmarks of COVID-19 in adults and pediatric populations. These include endothelial dysfunction, cytokine storm, hyper-immune activation, and autoimmune mediated sequelae such as multisystem inflammatory syndrome (MIS) in pediatric and adult populations. The viral and immune

processes underlying these phenomena remain active lines of investigation. Early studies identified comorbidities like older age, diabetes, obesity, male sex as significant correlates of disease severity. In addition, growing evidence suggests that the dynamics and magnitude of viral load, in addition to influencing diagnostic test performance, are key correlates of severity in COVID-19. And while a link between viral load and immunopathology in the lung is clear, the mechanisms underlying the devastating systemic features of COVID-19 remain to be fully characterized.

Thesis Objectives

The main goal of this thesis work was to better understand the phenomenon of nucleocapsid antigenemia in SARS-CoV-2 infection, a project which emerged from our early involvement in the pandemic response at Emory. This work has since evolved into a multifaceted set of studies spanning from the population level surveillance to cellular mechanisms of endothelial damage in severe COVID-19. In **Chapter 2** of this dissertation, we present data from a large serological survey describing the diagnostic value of viral antigenemia in the detection of acute COVID-19. Our finding that antigen levels in blood can help distinguish active infection from persistently PCR positive recovered individuals highlights the potential value of blood antigen testing in multiple clinical and community contexts. In **Chapter 3**, we expand upon this observation to evaluate the longitudinal dynamics of antigenemia in humans and rhesus macaques as well as its association with disease severity. Our results demonstrate an association of early antigenemia with COVID-19 severity and mortality as well as specific patterns of antiviral cytokine response. These correlations prompted us to evaluate the potential direct effects of viral antigenemia on endotheliitis, a hallmark of COVID-19 severity. We found that nucleocapsid interacts with human endothelial cells, eliciting antiviral cytokine production from human endothelial cells and upregulation of leukocyte adhesion molecules. Furthermore, nucleocapsid-mediated endothelial activation can be modulated

by pre-incubation with antibodies against the RNA binding N terminal domain. These studies identify viral antigenemia as a correlate of disease severity and introduce possible contributor to endothelial damage during SARS-CoV-2 infection.

In **Chapter 4**, we present work from two studies on the development and validation of serological tests for SARS-CoV-2, which were adapted in Emory's EUA clinical serology test and with which we characterized components of COVID-19 convalescent plasma to better understand potential correlates of its efficacy. And in **Chapter 5**, we describe a novel high-throughput blockade of binding assay for SARS-CoV-2 neutralizing antibodies, which we developed as an alternative to cell-based neutralization assays.

Figures for Chapter 1

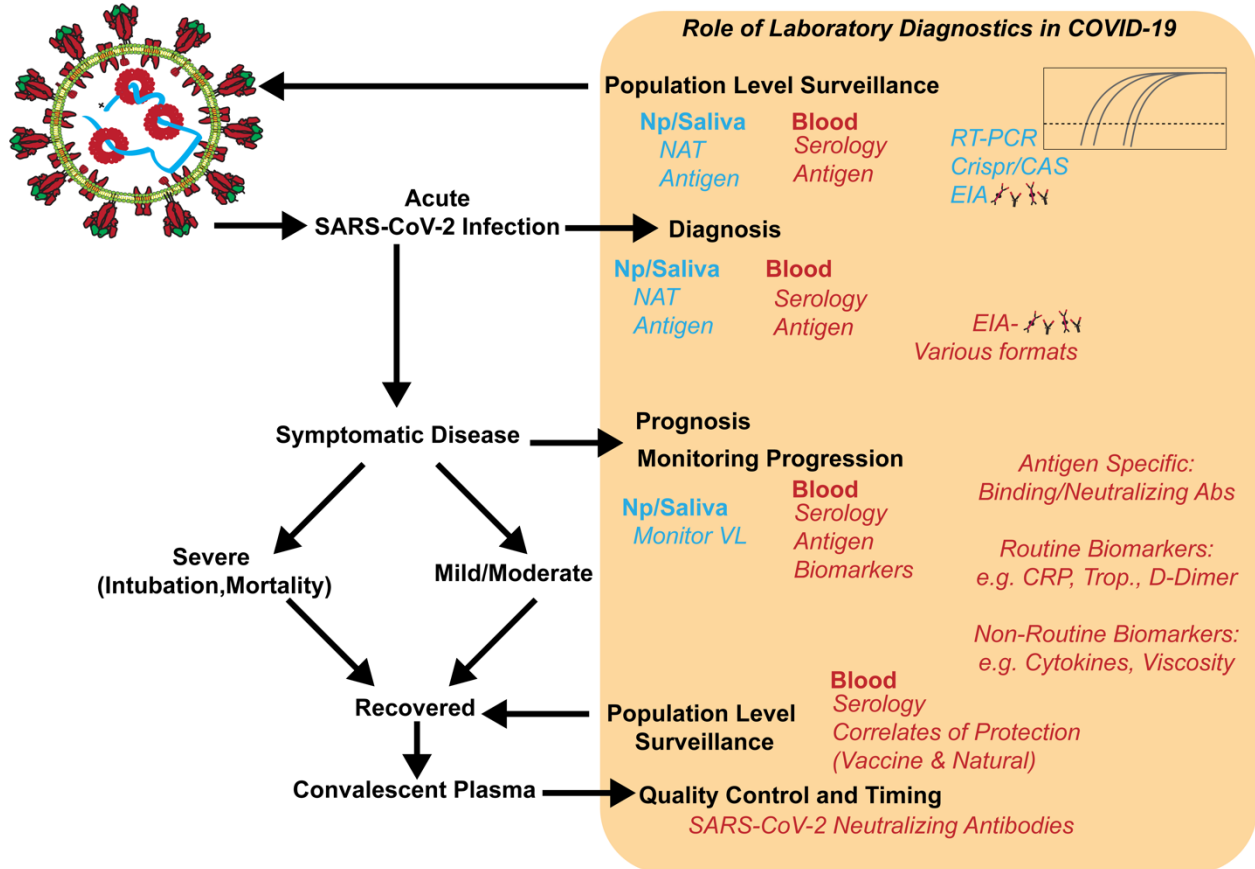


Figure 1.1 Role of laboratory diagnostics in COVID-19. From acute infection to symptomatic disease and recovery, diagnostic tools are essential for the detection and management of COVID-19. Most diagnostics use respiratory sampling to detect components of the virus. However, blood testing has also proven useful in serological evaluation and more recently in the detection of circulating antigen. In addition, blood sampling allows the simultaneous detection of biomarkers that may offer prognostic value for severe disease.

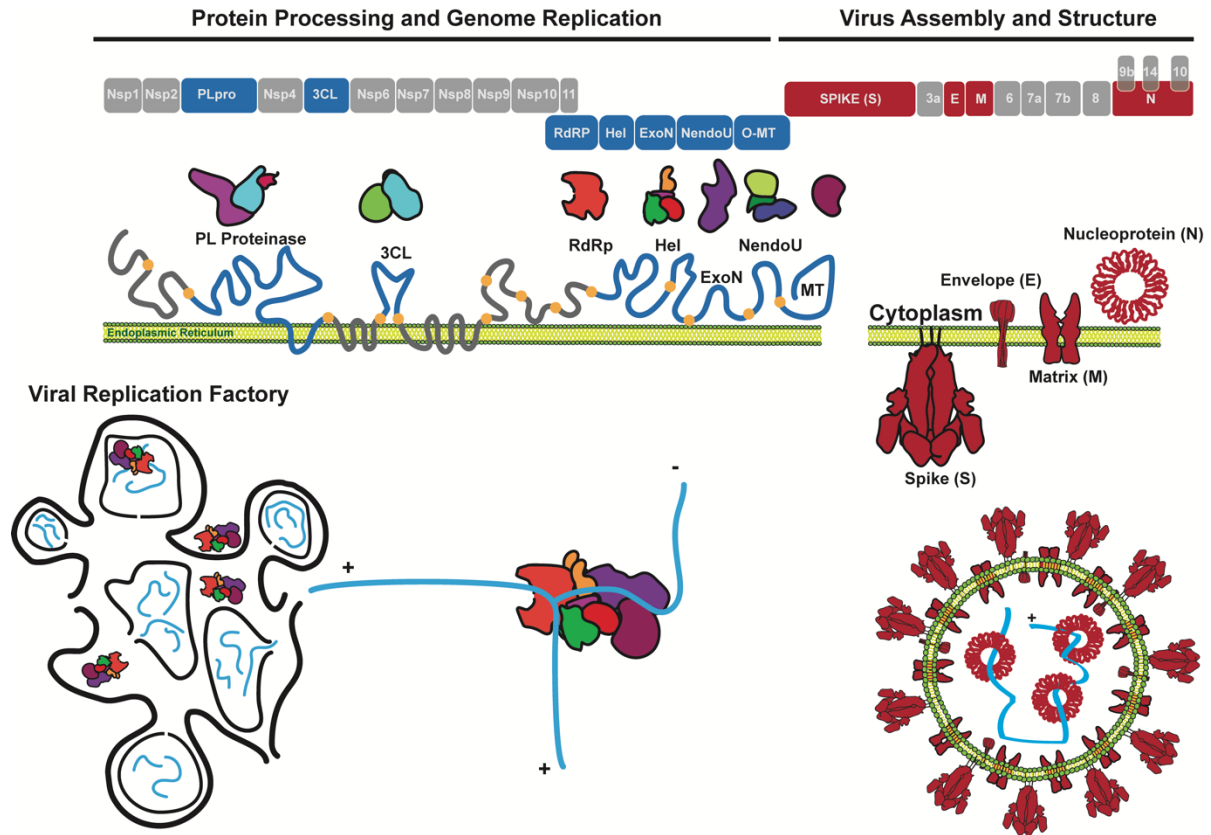


Figure 1.2 SARS-CoV-1 genome structure and major functional proteins. A schematic of the SARS-CoV-2 genome highlights proteins involved in viral protein processing, genome replication and virion assembly. Replication factories are shown with associated RdRp complexes as sites of genome replication.

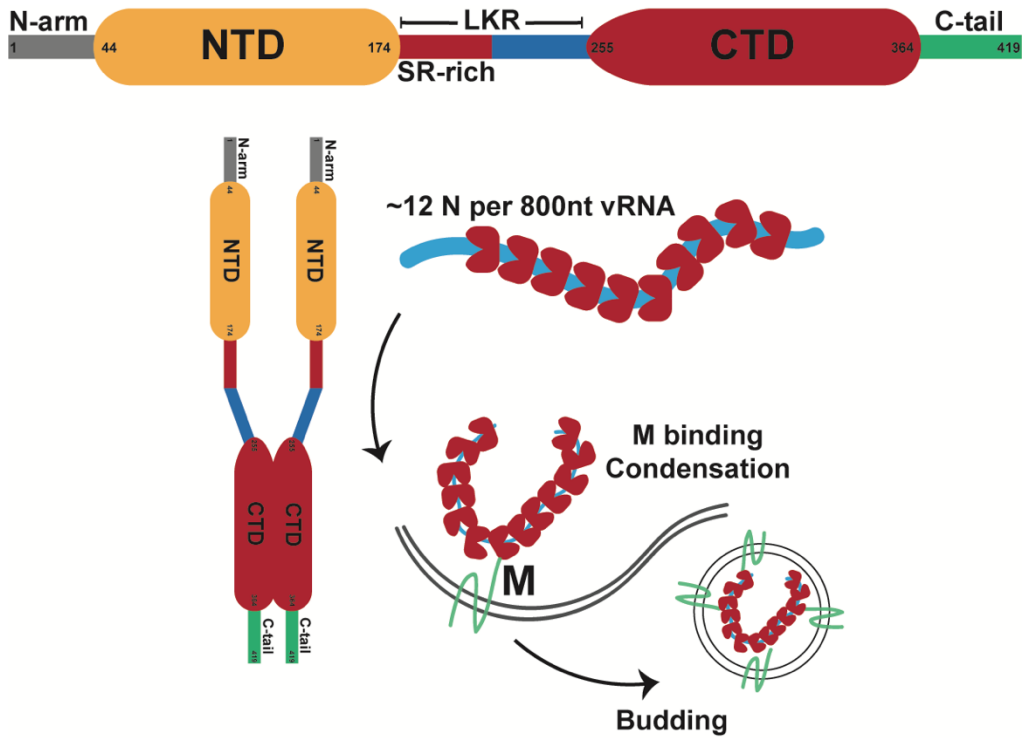


Figure 1.3 SARS-CoV-2 Nucleocapsid protein. Domain structure and basic structural features of SARS-CoV-2 nucleocapsid protein are shown. Three intrinsically disordered regions link an N terminal RNA binding domain (NTD) with a dimerization domain at the C terminus (CTD). Approximately 12 nucleocapsid units assemble and polymerize with viral RNA to condense the ribonucleoprotein during virion formation.

Chapter 2 Nucleocapsid Antigenemia in the diagnosis of SARS-CoV-2 Infection

Abstract

Reliable detection of SARS-CoV-2 infection is essential for diagnosis and treatment of COVID-19 as well as infection control and prevention during the ongoing pandemic. Existing nucleic acid tests do not reliably distinguish acute from resolved infection, as residual RNA is frequently detected in the absence of replication-competent

virus. Based on our observations in longitudinal samples from hospitalized COVID-19 patients, we hypothesized that viral nucleocapsid in serum or plasma (nucleocapsid antigenemia) may be a specific diagnostic biomarker of acute infection that could enhance isolation and treatment strategies at an individualized level. To test this, we conducted a retrospective serological survey targeting a convenience sample from adult inpatient and outpatient encounters from January through March of 2021. Using available SARS-CoV-2 testing data and symptomatology extracted from the medical record, each sample was categorized by COVID-19 status and the along a timeline of infection (e.g. acute, late presenting, convalescent). In this serosurvey cohort, we quantified nucleocapsid levels in 1860 specimens from 1607 patients, finding the highest frequency and level of antigenemia in samples obtained during acute SARS-CoV-2 infection (sensitivity: 85.8%; specificity 98.6%). In this cohort, levels of antigenemia were highest in samples from seronegative individuals and in those with more severe disease.

Introduction

Although the standard of care for SARS-CoV-2, reverse transcription polymerase chain reaction (RT-PCR) remains an imperfect diagnostic marker for coronavirus disease 2019 (COVID-19) because SARS-CoV-2 RNA commonly persists beyond the period of acute infection(29, 157, 158). Accordingly, Centers for Disease Control and Prevention (CDC) guidelines do not recommend re-testing most individuals by RT-PCR within 90 days following diagnosis. Instead, isolation guidelines are based on time from symptom onset (159, 160). This creates a dilemma when screening tests detect SARS-CoV-2 RNA in a patient without well-defined onset or resolution of COVID-like illness. Alternative molecular markers for acute infection are not widely available(161) and low sensitivity respiratory antigen testing may be effectively applied at a population level(11, 162), but

there remains a need for more sensitive and specific diagnostics to provide individualized guidance.

The presence of viral nucleocapsid protein in peripheral blood (antigenemia) has been demonstrated in SARS-CoV-1 and SARS-CoV-2 infection(163–175). A blood-based antigen biomarker may have inherent advantages over upper respiratory tract antigen testing, or biomarkers such as RT-PCR cycle threshold (Ct) value and sub-genomic RNA (sgRNA), because specimen quality and quantity can be standardized. Reports of antigenemia test performance as a diagnostic biomarker are inconsistent, likely due to varying assay composition and inconsistent reference standards as many studies compare against respiratory RT-PCR as a gold standard and fail to account for the persistence of RNA beyond acute infection.

In the study presented here, we evaluate evidence from a large serosurvey of adults in inpatient and outpatient settings to explore the hypothesis that nucleocapsid antigenemia is a sensitive and specific marker of acute infection as defined by a clinical timeline. Specifically, each blood sample was categorized through rigorous review of clinical history and respiratory SARS-CoV-2 testing in a schema that assumes a typical course of COVID-19 for all subjects. Our study is novel among others evaluating nucleocapsid antigenemia in that we were able to capture blood samples from each stage of infection in order to evaluate the performance of antigenemia testing for staging acuity, which we define based on onset of symptoms and timing of respiratory SARS-CoV-2 positivity. We find a strong association between acute infection and nucleocapsid antigenemia, which also correlates with serostatus and disease severity. Together our findings suggest antigenemia may clarify disease timing and provide needed insight in many clinical settings.

Results

Specimens & COVID-19 status assignment

2,498 serum and plasma samples were targeted for evaluation during the study period (**Figure 2.2**). Eleven samples were not evaluated for antigenemia due to pre-analytical factors such as insufficient sample volume. 2,487 samples were available for quantification of antigenemia, of which 255 (10.2%) exhibited detectable nucleocapsid. 115 of 2,487 were excluded due to lack of patient identifiers and five additional samples were excluded as they had been collected on the same day as another blood sample from a single patient. Clinical data were examined for the remaining 2,367 samples from 2,101 unique patients (**Table 2.1**). 507 of 2,367 samples were excluded because of no record of SARS-CoV-2 testing, and 11 of these 507 (2.1%) had detectable antigenemia.

The remaining 1,860 samples from 1,607 patients had SARS-CoV-2 testing records to guide categorization and were classified as described in (**Figure 2.1b** and **Table 2.2**).

Diagnostic performance of antigenemia for acute COVID-19

Nucleocapsid antigenemia was present at higher frequency and with a higher median concentration in acute COVID samples compared to samples categorized as late-presenting, convalescent, pre-COVID, or same-day negative ($p < 0.001$ for all comparisons; (**Figure 2.3a**). ROC analysis demonstrated area under the curve (AUC) of 0.902 in distinguishing samples from patients experiencing acute infection from all non-acute categories, and sensitivity and specificity were 85.2% and 89.9%, respectively (**Figure 2.3b**). Test characteristics with censoring of the potentially ambiguous late-presenting group showed AUC 0.914, sensitivity 85.8%, and specificity 93.7% while the most stringent comparison (censoring of the convalescent and late-presenting groups) demonstrated AUC 0.972, sensitivity 85.8%, and specificity 98.6%. Sensitivity improved

to 93.9% when the comparison was only made among seronegative individuals (**Supplemental Figure 2.1**).

Test characteristics were also examined when adjusting the reference standard by varying parameters of the acuity window. Sensitivity decreased as the window start period increased beyond -11 days (**Figure 2.3c**). Meanwhile, specificity consistently increased as the period of the acuity window was lengthened. Maximum AUC was observed with a window period opening at -12 days (AUC = 0.912 with window close at +3 days) with minimal effect of varying the post-sampling period from 0 to +3 days (**Figure 2.3d**).

Ct values from positive nasopharyngeal RT-PCR were available from the same day as a blood sample for 49 specimens. Only 6 of 17 samples with corresponding Ct values greater than 33 had antigenemia and four of six of these were from the GeneXpert assay (**Figure 2.3e**). All except for two samples with corresponding Ct values less than 30 exhibited antigenemia.

Temporal trends in antigenemia

We analyzed the dynamics of antigen level over time in samples from the acute, late-presenting and convalescent groups. The frequency of detectable nucleocapsid and antigen concentration decreased over time following diagnosis and reported symptom onset (**Figure 2.4a-b**). 18 samples were identified from patients who were asymptomatic at the time of COVID-19 diagnosis, 5 (27.7%) of which had detectable nucleocapsid antigenemia. Nucleocapsid antigen was detected more frequently (50.0%) in the subset of samples available from asymptomatic patients within 3 days of their diagnosis (**Figure 2.4c**). Among 55 samples from individuals with positive respiratory RT-PCR testing on the same day, seven convalescent samples did not exhibit antigenemia (**Figure 2.4d, supplementary table 2.1**) and acute infections primarily exhibited high antigenemia.

Among this subset of patients, no antigenemia was observed more than fourteen days after the earliest known positive test (**Figure 2.4d**).

Examination of outliers

We reviewed medical records for individuals with unexpected presence or absence of antigenemia. Twenty-one samples in the convalescent group had antigenemia (**supplementary table 2.2, supplementary figure 2.2**). Among these, two individuals had clinical history consistent with re-infection by SARS-CoV-2, two were highly immunocompromised, and eleven samples (median time from diagnosis 20 days, IQR 16.5-28.5 days) had severe COVID-19 marked by need for high-flow oxygen, intubation or death. End-stage renal disease or dialysis was more common among samples in the convalescent group with antigenemia compared to those without antigenemia (fraction [95% confidence interval] = 0.41 [0.20-0.61] vs 0.13 [0.07-0.18]) whereas other co-morbidities were not significantly different (**supplementary figure 2.3**). Three individuals had negative respiratory SARS-CoV-2 testing and antigenemia on the same day, none of which had evidence of COVID-related symptoms (**supplementary table 2.3**). Eighteen samples had antigenemia after more than fourteen days of symptoms, of which fourteen were seropositive for both N IgG and RBG IgG, two seropositive for RBD IgG only, and two were seronegative for both. Thirteen had nucleocapsid level less than 46 pg/mL while the other five exceeded 700 pg/mL including both N and RBD seronegative patients and N-/RBD+ sample (**supplementary table 2.4, supplementary figures 2.4 & 2.5**). Twenty individuals with samples categorized in the acute COVID group did not have antigenemia – ten of these were collected ten or more days after symptom onset (**supplementary table 2.5, supplementary figure 2.6**).

Antigenemia trends by antibody serostatus

Distribution of nucleocapsid levels in the acute COVID group were significantly different with higher median values in seronegative samples compared to seropositive

samples for nucleocapsid IgG, RBD IgG, RBD IgA, and RBD IgM ($p < 0.001$ for each comparison, **Figure 2.5**). Seropositive samples were also more likely to have undetectable antigenemia. Similar trends were seen in the late-presenting group except for the comparison based on IgM which was not significant (**Supplementary Figure 2.7**).

Association of antigenemia with COVID-19 severity

In the acute COVID group, distribution of nucleocapsid antigen was significantly different and median value was higher in samples from patients who died or required intubation within 30 days of sampling compared to those who survived or did not require intubation (**Figure 2.6a-c**). This observation held true for comparison based on the composite of intubation or mortality. Levels of nucleocapsid antigenemia were not significantly associated with elevated D-dimer (cutoff 500 ng/mL) but were associated with elevated CRP ($p = 0.002$ in comparison based on 40 mg/L cutoff; **Figure 2.6d-e**).

Discussion

This analysis of blood samples from routine clinical specimens collected during the ongoing COVID-19 pandemic demonstrates the following: First, antigenemia is a sensitive and specific marker for acute SARS-CoV-2 infection. Second, nucleocapsid is elevated in samples without evidence of anti-nucleocapsid (IgG) and anti-spike (IgG, IgM, and IgA) seroconversion. Third, antigenemia is associated with disease severity.

Evolving CDC isolation guidance during the COVID-19 pandemic reflects the difficulty of objectively defining resolution of SARS-CoV-2 infection. Underlying this is the persistence of RNA targets beyond a period during which the immunocompetent individual is reasonably believed to harbor replication-competent virus(29, 157, 158). Meanwhile, persistence of replication-competent virus for months has been demonstrated by viral culture in immunocompromised hosts(8, 176–178). This creates a diagnostic dilemma when RT-PCR is persistently positive for weeks after diagnosis, when re-

infection with SARS-CoV-2 is a consideration, or when encountering positive SARS-CoV-2 RT-PCR test results in an asymptomatic individual without history of prior objective diagnosis or prior COVID-like illness. Our data suggest assessment of nucleocapsid antigenemia may assist providers in making judgments in these scenarios.

Further, our data compels interest in whether antigenemia may provide direct evidence of active viral replication, which aid in evaluation of infectiousness or guide therapeutics at an individualized level. For example, antiviral agents are not likely to benefit a patient without active SARS-CoV-2 replication. Clinical trial data therefore may be confounded by failure to stratify patients according to such a marker, as late presenters after cessation of viral replication would likely fail to show benefit or may even suffer harm from investigatory antiviral agents. In fact, recent evidence emphasizes benefit of antivirals early in infection(179). In showing its association with acute SARS-CoV-2 infection and characterizing outliers, our data suggest that nucleocapsid should be further investigated as a marker of viral activity, infectiousness, and a predictor of therapeutic response.

Strengths of our study include a diverse cohort that is among the largest in which nucleocapsid antigenemia has been quantified to date and rigorous assignment of COVID-19 status through medical record review. Prior studies restricting the definition of a positive case to no more than two weeks after symptom onset report sensitivities between 90.9% and 97.5% and specificities between 94.2% and 100%(167–172)(see **supplementary Table 2.6**, and our data are consistent with these findings. Of further interest, our data revealed detectable antigen in 11 (2.1%) of the blood samples obtained in the primary serosurvey even though these patients were never screened with nasopharyngeal RT-PCR testing in our healthcare system. These represent likely infectious patients who may have had a missed SARS-CoV-2 diagnosis and suggest a

potential role for antigenemia screening in a population for whom blood is already being sampled to complement existing infection control measures.

We also detected antigenemia in a small number of patients with subclinical SARS-CoV-2 infection. Individuals who test positive for SARS-CoV-2 without antecedent or subsequent COVID-like symptoms either represent shedding of replication-competent virus *during* subclinical disease or persistent RNA shedding *following* subclinical disease. While we corroborate previous findings that levels of antigenemia are associated with disease severity, the presence of antigenemia in five asymptomatic individuals with SARS-CoV-2 demonstrates that antigenemia can also be present in subclinical infection. Despite the difficulty associated with identifying these cases, further investigation of the prevalence of antigenemia in acute asymptomatic infection is needed to clarify its role in screening broad populations.

This study is limited by use of a convenience sampling approach and retrospective data collection. Symptom onset as recorded in the medical record can be subjective and influenced by recall bias. Because of the ubiquity of community-based testing, SARS-CoV-2 diagnosis was documented prior to evaluation in our healthcare system for a subset of these patients and was only known to us when documented in the clinical narrative in addition to being subject to biases and imprecision. In addition, nucleocapsid-specific immunoglobulin may interfere with quantitation of antigenemia in individuals who have seroconverted although it is currently unknown whether total (Ig-bound and unbound) antigen or free (unbound only) antigen is a more meaningful clinical indicator. The primary analysis relies on the assumption that each subject is immunocompetent, that immunocompetent hosts have similar duration of acute COVID-19, and that there are no other confounding factors which may result in prolonged antigenemia. Recognizing these limitations, we performed a post-hoc investigation of outlier cases, which facilitated hypothesis generation regarding reasons for prolonged antigenemia such as reduced

renal function, prolonged critical illness, and immune compromise (**supplementary Table 2.1-2.5 & 2.7**). Several studies have demonstrated high specificity of antigenemia by evaluation of pre-pandemic samples(167, 169, 172), suggesting many false positives in our study are likely to have active infection beyond the parameters for acute infection defined in our reference standard schema. This will be further clarified as more robust comparisons to viral culture, sgRNA, RT-PCR Ct value, and respiratory antigen testing can be achieved.

Together our data demonstrate that nucleocapsid antigenemia is a sensitive and specific biomarker of acute COVID-19 wherein COVID-19 status is defined by time since earliest positive testing and symptom onset. We conclude that nucleocapsid antigenemia is a promising candidate biomarker for active viral replication – the definition of which is the presence of replication-competent virus in a host – recognizing that the available evidence points to this being an individualized process that cannot be broadly defined based on a timeline. Further prospective studies with rigorous documentation of clinical course and correlation with viral culture and other potential biomarkers of viral replication are needed.

Experimental Procedures

Clinical specimens

We collected a convenience sample of residual plasma, serum, and whole blood specimens from the clinical chemistry laboratory of Emory Medical Laboratories one day per week between January 11, 2021 and March 12, 2021. These specimens were originally collected for routine clinical testing from inpatient (medical/surgical wards, intensive care, obstetrics) and outpatient settings (clinics, emergency department, infusion centers, ambulatory surgery). Samples were transferred to a –80C repository

after clinical testing was completed, but prior to being discarded. More than one blood sample from the same patient was permitted with a minimum time of five days between samples. This study was approved and granted complete HIPAA and consent waiver by the Emory University Institutional Review Board (STUDY00000510).

Nucleocapsid detection

Nucleocapsid antigenemia was quantified on the Quanterix HD-X platform. Residual serum and plasma samples were thawed once after storage at -80°C and diluted 1 to 3 in assay sample diluent. Diluted samples were then run using the ultrasensitive SIMOA SARS-CoV-2 N Protein Antigen assay on the automated Quanterix HD-X platform (Quanterix, Billerica, MA, USA) which has a validated limit of detection of 0.099 pg/mL in respiratory and saliva samples. Samples with antigen levels too high for the linear range of the assay were further diluted 1 to 20 and re-tested. Final antigen concentrations were determined by interpolation after sigmoidal fitting of duplicate calibration curves run on each test plate.

Serological testing

In-house developed single-dilution serological screening assays for SARS-CoV-2 receptor binding domain (RBD) and nucleocapsid antibodies were used to establish serological status at the time of antigenemia testing. Antibody class-specific RBD serologies were performed as previously described(14). Nucleocapsid antibody testing was performed using an in-house developed ELISA (supplementary information).

Medical record review

Patient medical record number was recorded at the time of specimen collection. The Emory Healthcare Clinical Data Warehouse (CDW) was queried for SARS-CoV-2 nucleic acid amplification tests (NAAT), clinical notes, ICD-10 codes, laboratory values,

mechanical ventilation, and date of death. All Ct values were obtained directly from reports produced by the manufacturer's software (**supplementary information**).

A COVID-19 status label (positive or negative) and a category (convalescent, late-presenting, acute, pre-COVID, and same-day negative) were assigned to each blood sample based on that patient's (1) SARS-CoV-2 respiratory testing (including NAAT or antigen), (2) date of earliest positive test, and (3) date of symptom onset (**Figure 2.2**).

Chart review began with automated review of NAAT results available in the medical record. Blood samples from a patient with a positive NAAT more than fourteen days prior to sample collection were labeled *convalescent* and no further review of the medical record for categorization purposes was performed. History and physical clinical notes dated within fourteen days before or after the date of the blood sample were then reviewed, if available, for all patients not labeled *convalescent*. Date of COVID-like symptom onset (including fever, fatigue, malaise, myalgia, headache, dyspnea, cough, wheezing, anosmia, ageusia, congestion, rhinorrhea, or diarrhea) and earliest positive SARS-CoV-2 testing (NAAT or antigen) was recorded if these had been described in the history narrative or clinician's assessment and plan.

The original medical records were then reviewed for all patients (other than those labeled *convalescent*) with a positive SARS-CoV-2 test who did not yet have date of symptom onset recorded in our data set. The entire medical record was available during this stage, but the reviewer was blinded to antigenemia status which was not considered in labeling of COVID-19 status or category assignment.

Our approach assumed that no re-infection events were captured in our sample set, which spanned 3 months. Patients without any record of SARS-CoV-2 testing were excluded from analysis. Further detail is provided in Supplementary Information.

Data analysis

Data obtained during specimen collection were stored in Microsoft Excel. CDW reports were provided in .csv format. All data were then imported into MATLAB (The MathWorks, Inc.) for analysis. Wilcoxon rank-sum test was used for comparisons.

Author Contributions

This chapter is adapted from the manuscript below, currently under review at JID. HV tested the samples, conceived of the study and analytical approach, and performed chart review to gather the clinical data. GD planned the chart review and performed the data analysis in MATLAB. Both authors contributed to the drafting of the manuscript and assembly of figures.

Nucleocapsid antigenemia is a marker of acute SARS-CoV-2 infection

Hans P. Verkerke*, Gregory L. Damhorst*, Daniel S. Graciaa, Kaleb McLendon, William O'Sick, Chad Robichaux, Narayanaiah Cheedarla, Sindhu Potlapalli, Shang-Chuen Wu, Kristin R.V. Harrington, Andrew Webster, Colleen Kraft, Christina A. Rostad, Jesse J. Waggoner, Neel R. Gandhi, Jeannette Guarner, Sara C. Auld, Andrew Neish, John D. Roback, Wilbur A. Lam, N. Sarita Shah[†], Sean R. Stowell[†]

*,[†] Equal contribution

Under review, JID

Tables Chapter 2

Table 2.1

	SARS-CoV-2 Infection Status		
	Positive	Negative	Undefined
N	130	385	1622
Age mean (IQR)	60.6 (52.2–73.0)	54.2 (39.2–69.6)	55.0 (39.8–70.2)
Female %	47.7	57.1	55.5
Vaccinated %	1.5	4.7	9.9
Race %			
African American or Black	78.5	72	60.7
American Indian or Alaskan Native	0	0	0.2
Asian	0.8	1	1.6
Caucasian or White	13.1	20	29
Native Hawaiian or Other Pacific Islander	0	0.3	0.2
Multiple	0	0.5	0.4
Unknown, Unavailable or Unreported	7.7	6.2	7.9
Ethnicity			
Non-Hispanic or Latino	83.9	86	84.4
Unreported, Unknown, Unavailable	13.9	7.8	11.9
Hispanic or Latino	0.8	5.5	3
Not Recorded	1.5	0.8	0.7
Antigenemia* %	85.8	10.1	3.9
Setting*			
Inpatient	70.9	42.9	39.3
ER or CDU	29.1	27.2	14.1
Outpatient	0	26.7	45.3
Peripartum	0	3.3	1.1

Table 2.1. Summary of patient characteristics by COVID status.

*Reflects all included samples (including multiple samples for a unique patient). CDU = clinical decision unit

Table 2.2

	Samples	Unique patients
Never SARS-CoV-2 positive	1416	1249
Same-day negative test	194	194
Ever SARS-CoV-2 positive*	444	360
Convalescent	182	153
Late-presenting	30	30
Acute	141	130
Sampled three or more days prior to diagnosis	42	34
Negative interim testing	21	16

Table 1.2. Categories determined by chart review for samples and patients included in the analysis.

*Includes in-hospital NAAT as well as community NAAT or antigen testing if reported in the clinical narrative

Figures Chapter 2

Figure 2.1.

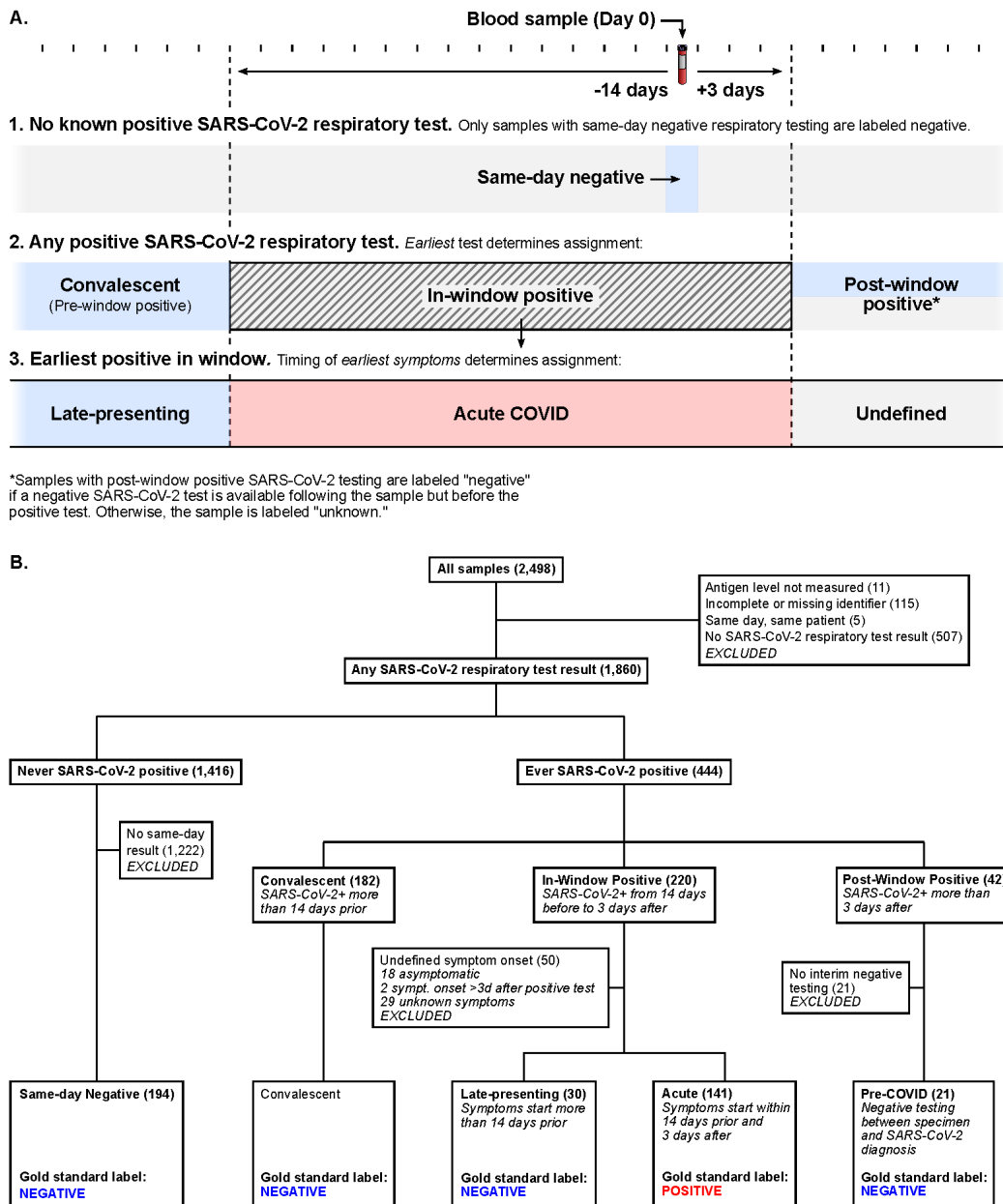


Figure 2.1 Study outline and sample categorization schema (A) Schematic of process for COVID status assignment. Samples from patients with no record of positive SARS-CoV-2 respiratory testing were only considered negative if corresponding negative respiratory testing occurred on the same day. Due to the lack of a gold standard for active SARS-CoV-2 infection, samples from individuals with history of positive SARS-CoV-2 testing are labeled based on earliest known positive SARS-CoV-2 respiratory test and time since symptom onset. (B) Flow chart of categorization and labeling process indicating number of samples assigned to each group.

Figure 2.2.

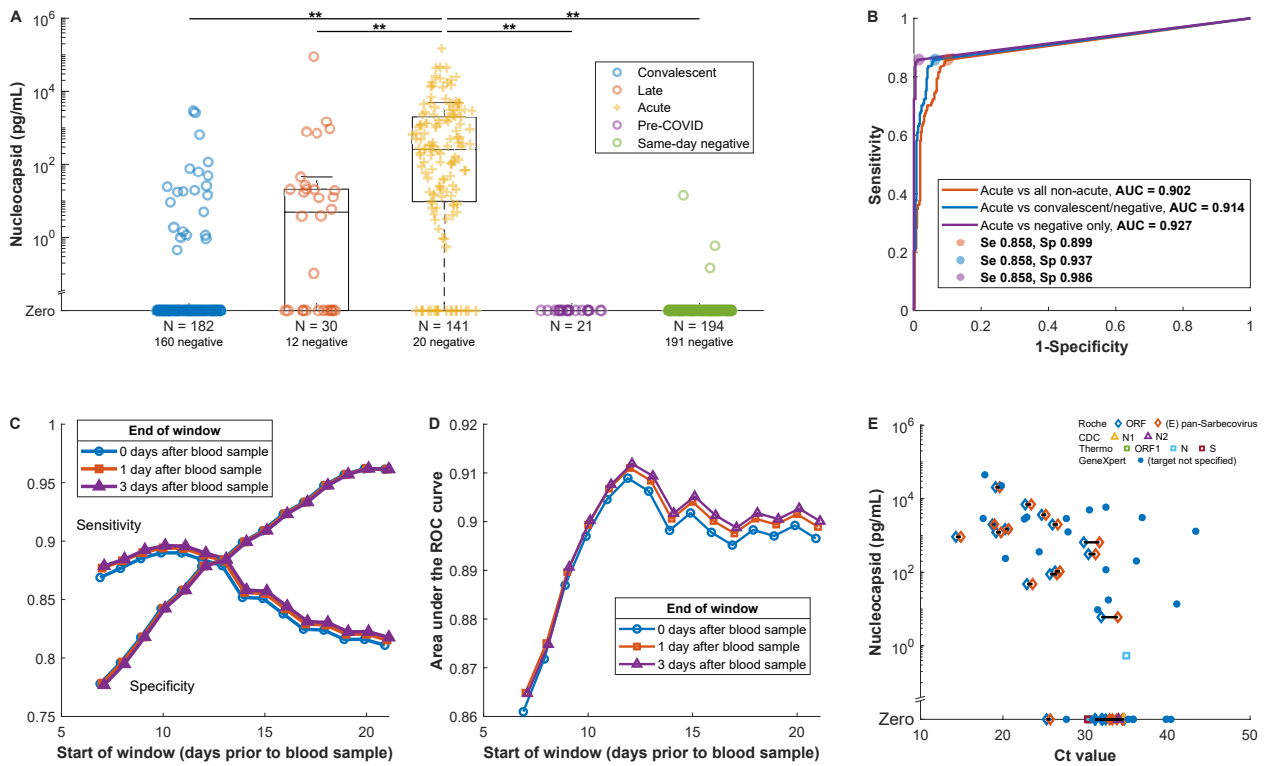


Figure 2.2 Diagnostic performance of SARS-CoV-2 nucleocapsid antigenemia. (A) Prevalence of antigenemia and serum or plasma nucleocapsid levels for blood samples by category. Unexpected results (presence of nucleocapsid in the convalescent and same-day negative groups, absence of nucleocapsid in the acute group) are examined in Supplementary Information Tables 2-5. (B) ROC curve for diagnostic performance of detectable antigenemia with reference to a -14/+3 day window for acute infection. The additional curves progressively exclude ambiguous categories. (C) Impact on sensitivity and specificity of varying the window period, which defines the reference standard for acute COVID. (D) AUC for the same varied window periods. (E) Antigenemia compared to RT-PCR Ct value for those specimens with a Ct value available from the clinical laboratory on the same day. Symbols correspond to assay and gene target with horizontal line linking Ct values for different targets detected in the same sample. This includes data from four assays on three thermocycler platforms described in further detail in Supplementary Information.

Figure 2.3

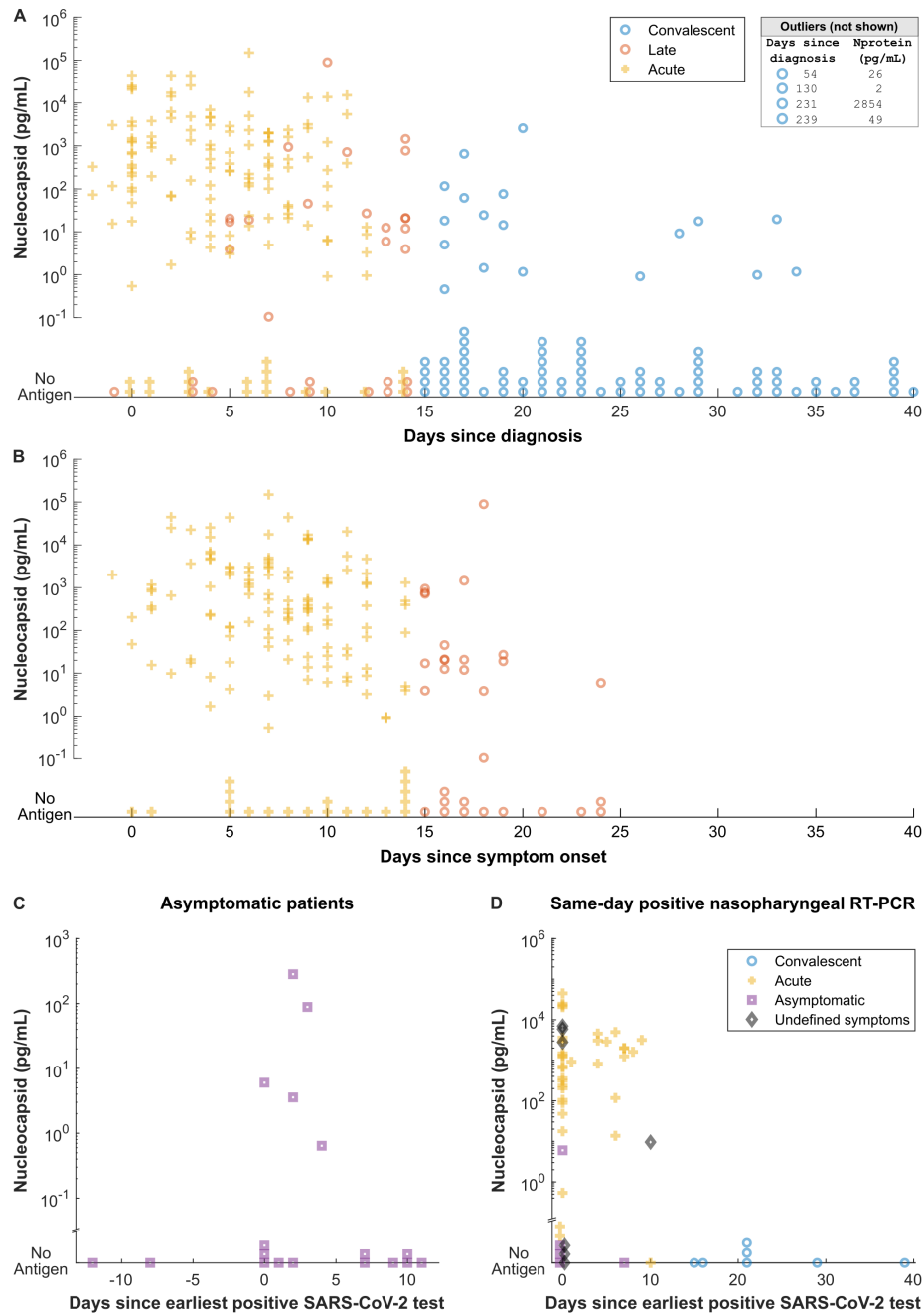


Figure 2.3 Temporal trends in antigenemia. (A) Serum or plasma nucleocapsid plotted against time since diagnosis (top) and symptom onset (bottom, shown with an inverted y axis). Samples without antigen detected are shown stacked on the common horizontal axis. Four samples with antigenemia beyond 41 days are listed in the box and 93 samples without antigenemia between 41 and 351 days after earliest diagnosis are not shown. (B) Serum or plasma nucleocapsid in patients whose COVID-19 course was described as asymptomatic in clinical records. The x axis reflects time in between first known positive respiratory test and the day the blood sample used in our analysis was collected. (C) Serum or plasma nucleocapsid for individuals with positive nasopharyngeal RT-PCR on the same day as blood sample collection.

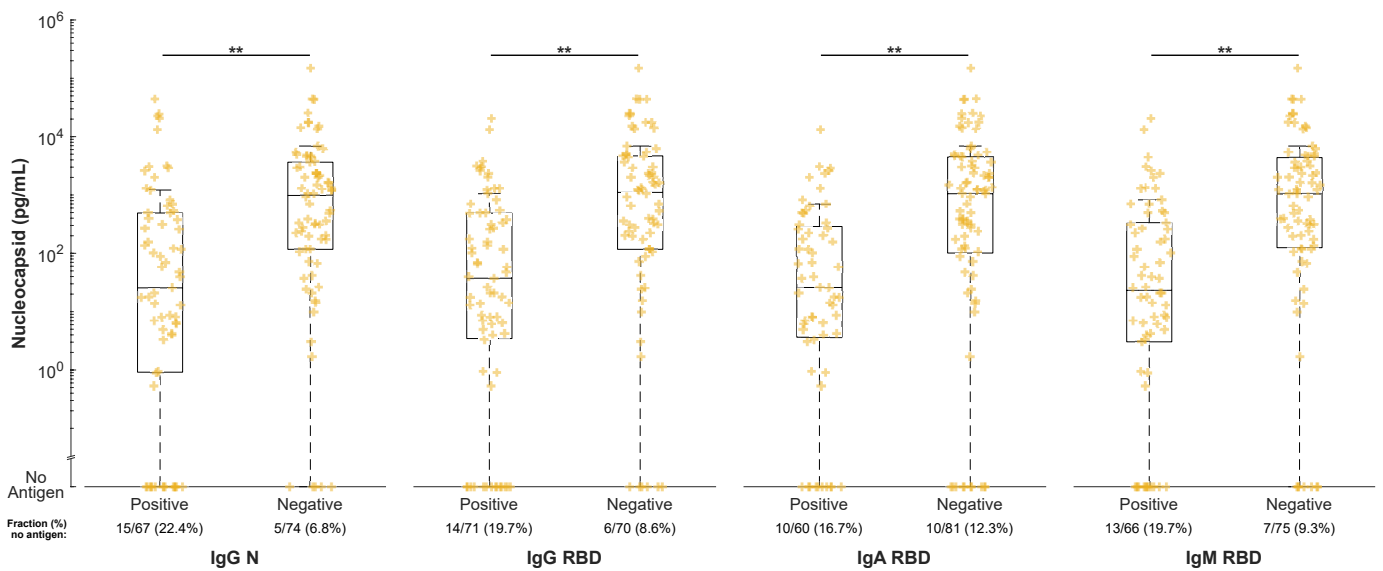


Figure 2.4. Association with serostatus. Comparison of serum or plasma nucleocapsid levels in individuals with and without SARS-CoV-2-specific antibodies. Samples were tested by in-house developed serological tests for nucleocapsid and receptor binding domain specific IgG as well as receptor binding domain specific IgA and IgM. Levels of nucleocapsid are plotted and compared in samples stratified by seropositivity for each antibody type.

Figure 2.5

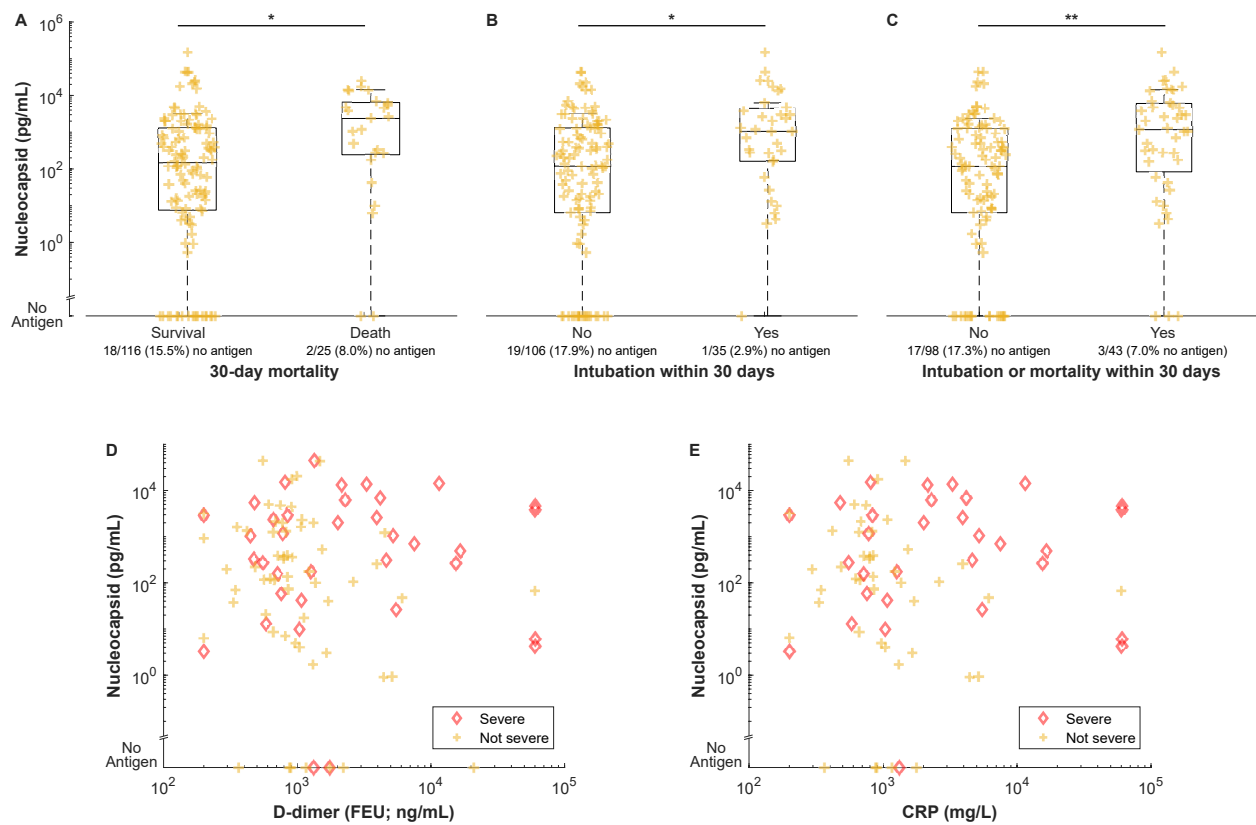


Figure 2.5. Comparison of serum or plasma nucleocapsid levels by (A-C) severity and (D-E) inflammatory biomarkers. Intubation in figures B and C includes intubation within 30 days before or after the blood sample was collected. Individuals with severe COVID as defined by the composite of 30-day intubation or mortality are highlighted in D and E.

**Chapter 3 SARS-CoV-2 nucleocapsid antigenemia is associated with
COVID-19 disease severity and directly drives endothelial activation**

Abstract

Though many patients have been infected with SARS-CoV-2, only a fraction develop severe disease. Those who do often suffer from endotheliitis, which can lead to microvascular complications, thromboembolism, and multi-system organ dysfunction. While numerous viral and immune factors have been associated with COVID-19 severity, the mechanisms that contribute to systemic pathophysiology remain incompletely understood. To examine this, we developed an analytical approach to evaluate a wide variety of clinical and immune biomarkers in blood samples taken early during hospitalization and at the peak of severe disease. Along with previously characterized markers of inflammation and organ dysfunction, our studies identified early levels of viral nucleocapsid antigenemia as a significant correlate of severe disease and mortality. Furthermore, we found that higher levels of antigenemia were associated with the magnitude of systemic antiviral cytokine responses in patients with severe disease, which led us to hypothesize that circulating nucleocapsid may itself contribute to systemic inflammation and endothelial dysfunction. We found that incubation of human endothelial cells with nucleocapsid elicits secretion of antiviral cytokines and upregulation of leukocyte adhesion molecules, which can be modulated by monoclonal antibodies against the RNA binding domain of the protein. We further show that nucleocapsid binds stably to endothelial cells under flow in an endothelialized microfluidic model and in static culture. Finally, we demonstrate for the first time that nucleocapsid antigenemia is also a feature of SARS-CoV-2 infection in rhesus macaques and that levels of peak antigenemia correlate most strongly with viral load in the lower respiratory tract, suggesting a possible source of antigen leak. Together our studies provide a novel framework for understanding nucleocapsid antigenemia as both a clinical biomarker of severe COVID-19 and as a potential driver of systemic endothelial pathology at the cellular level.

Introduction

SARS-CoV-2 is a respiratory viral pathogen that primarily infects epithelial cells of the upper and lower respiratory tracts. However, since its emergence and uncontrolled global spread, a broad array of systemic clinical manifestations and syndromes have been observed in COVID-19 patients. These include cytokine storm, capillary leak syndrome, COVID-19 coagulopathy, and severe end-organ damage as well as autoimmune mediated sequelae exemplified by multisystem inflammatory syndromes in adults and children (MIS-A and MIS-C). Studies investigating the pathophysiology of COVID-19 have suggested that among other factors, endotheliitis and endothelial dysfunction underly or exacerbate many of these life-threatening processes(152, 180–183). Supporting these findings, pathology on autopsy often includes evidence of severe endothelial injury in multiple organ systems, loss of basal membranous structures in blood vessels, and disrupted endothelial junctions(184). Despite this, the specific viral and immune mechanisms resulting in damage to endothelial cells during SARS-CoV-2 infection remain incompletely characterized.

Many studies have focused on elements of cellular and humoral antiviral immunity, including the aberrant formation of autoantibodies, which may skew the balance between efficacious and immunopathogenic responses(128–130). A second line of investigation has probed for specific viral factors directly involved in immune evasion and pathogenesis. These latter studies have uncovered numerous putative intracellular mechanisms by which SARS-CoV-2 may activate as well as thwart innate immune pathways, including direct inhibition of type I interferon signaling and viral pattern recognition by structural and non-structural proteins(94). While these studies of immune evasion provide rationale for the ability of SARS-CoV-2 to replicate in human airways and other epithelial compartments, they are not sufficient to explain the systemic pathology seen in severe COVID-19.

One line of investigation exploring this further concerns the discovery and characterization of blood biomarkers of disease severity with diagnostic and prognostic value(139, 185–187). While antigenemia and viremia are both hallmark features of several systemic viral infections(188, 189), respiratory viruses and their proteins are not typically detected at high levels in the blood of immunocompetent hosts. Early in our investigations of host and viral factors that may serve as blood biomarkers of severity we made the observation that high levels of viral nucleocapsid protein could be detected in blood samples from SARS-CoV-2 infected individuals soon after the onset of symptoms. Since this discovery, several groups including our own have described the diagnostic and prognostic value of measuring nucleocapsid antigenemia in both adult and pediatric cohorts. Nucleocapsid levels in blood mark the acute phase of infection and have consistently been associated with poor outcomes(169, 172, 190, 191). These studies have highlighted SARS-CoV-2 viral antigenemia as a biomarker of COVID-19 severity with diagnostic value in the acute setting.

To further explore COVID-19 severity including the potential role of nucleocapsid antigenemia, we developed an analytical approach in a longitudinal cohort of COVID-19 patients using receiver operator characteristic (ROC) analysis in combination with fold change estimates to identify biomarkers associated with disease severity present in samples early and at the peak of disease. We found that early and peak nucleocapsid antigenemia levels along with other markers of inflammation and organ damage are associated with disease severity and mortality. Furthermore, independent of outcome, higher levels of antigenemia were associated with specific patterns of antiviral cytokine response, suggesting a possible direct role for nucleocapsid antigenemia in systemic inflammation.

This led us to test the hypothesis that SARS-CoV-2 nucleocapsid in blood might contribute to endothelial dysfunction directly. To this end, we stimulated human endothelial cells with recombinant nucleocapsid protein and evaluated signs of endotheliitis. Nucleocapsid-stimulated endothelial cells produced high levels of antiviral cytokines and upregulated leukocyte adhesion molecules VCAM-1 and ICAM-1. Furthermore, we show that nucleocapsid-induced endotheliitis can be modulated using monoclonal antibodies against the N terminal RNA binding domain of the protein—suggesting a rationale for therapeutic intervention as well as a possible interaction of viral antigenemia-induced endotheliopathy with the endogenous nucleocapsid antibody response. Finally, we demonstrate that nucleocapsid antigenemia is a feature in the well-characterized rhesus macaque model of SARS-CoV-2 infection, wherein antigen levels are dependent on the dose of inoculate and most closely correlated with viral load in samples taken from the lower respiratory tract. Together our findings are consistent with a model in which nucleocapsid leaks from the lower respiratory tract at the peak of viral load into the blood, where it may directly interact with and stimulate endothelial cells in the microvasculature of multiple organ systems, contributing to the systemic pathophysiology of COVID-19.

Results

Cohort characteristics and disease severity

We enrolled 138 PCR confirmed patients hospitalized with COVID-19 from March to August of 2020. Patients were included in the cohort only if an accurate date of symptom onset could be abstracted during clinical chart review. Cases varied in their hospital courses, which were categorized by severity using the world health organization (WHO) ordinal scale (**Table 3.1**). In our study, we define severe COVID-19 as a score of 6 or greater on this scale, which included patients who required intubation and mechanical ventilation, use of vasopressors and organ replacement therapy or who died during the

encounter. 50 patients fell into this severe category while 88 were classified as moderate (WHO score of 5 or less).

Systematic Evaluation of Blood Biomarkers of COVID-19 Severity

To systematically evaluate candidate biomarkers of COVID-19 severity, we collected 1221 samples from 138 COVID-19 patients throughout their hospital courses and longitudinally tested for a variety of biomarkers including nucleocapsid antigenemia, multiplex antiviral cytokine levels, neutralizing antibody activity, and antibody class specific spike receptor binding domain (RBD) and nucleocapsid binding antibody titers (**Figure 3.1A**). We supplemented these measured variables with an inclusive extraction of longitudinal laboratory test results from a clinical data warehouse, from which we were able to abstract earliest and peak values for each variable during the relevant encounter. In order to identify useful biomarkers of COVID-19 severity, we calculated the fold change relative to moderate for two severity outcomes—mortality (WHO ordinal scale of 8), and severe (WHO ordinal scale 6 or greater; a composite outcome of requirement for mechanical ventilation or mortality). We observed a significant fold change increase over moderate cases (WHO ordinal scale <6) for several candidate biomarkers taken early and at the peak of disease including nucleocapsid antigenemia, IL-6, CXCL10, IFN- λ 1, IL8, IFN- β , IL-10, and creatinine kinase (CK). Several candidate biomarkers were most associated with severity at their peak levels including IL10, hyperkalemia, creatinine, liver function tests (ALT and AST), Ferritin, and markers of cardiac damage--troponins and BNP (**Figure 3.1B**).

To further evaluate the predictive and associative value of our candidate biomarkers. We used a second approach—multi-marker ROC analysis, which also takes into account the specificity or overlap between outcome and baseline groups for each variable. Here, we saw that early levels of fibrin and fibrinogen, IL-6, and the composite neutrophil to lymphocyte ratio exhibited the best performance in predicting mortality

(**Figure 3.1C and 3.1E**). While fewer biomarkers performed well early on, many markers at their peak were able to distinguish severe from moderate COVID-19 (**Figure 3.1D and 3.1F**). Importantly, nucleocapsid antigenemia exhibited the best performance (ROC AUC 0.71) as a biomarker using the earliest measurement available for each patient in predicting mortality.

Early nucleocapsid and antiviral cytokine levels predict mortality and are associated with disease severity.

In order to further dissect the associative value of candidate biomarkers, we developed an approach that combines ROC analysis with a fold change estimate to visualize markers that most accurately separated patients who experienced our severity outcomes (**Figure 3.2A**). We found that early and peak levels of IL-6 were the best performing biomarkers in both severity outcomes. In addition, Nucleocapsid antigenemia was a strong predictor of mortality along with early CXCL10 levels (**Figure 3.2B and 3.2C**). Maximum levels of several organ injury markers (troponin, BNP, AST, ALT, creatinine) and coagulation markers (Ddimer) were also associated with these outcomes (**Figure 3.2D and 3.2E**).

Nucleocapsid antigenemia is associated with inflammatory cytokine responses.

In order to better characterized the inflammatory signature associated with nucleocapsid antigenemia and severe outcomes, we evaluated a possible association of varying levels of early nucleocapsid antigenemia with early and maximum levels of various antiviral cytokines. Using ROC analysis (**Figure 3.3A**), we identified three pg/mL cutoffs (750, 2000, and 5000) and compared levels of early and maximum antiviral cytokines in groups defined by each cutoff (comparison for cutoff of 750 pg/mL shown in **Figure 3.2B**). Significantly increased levels of several cytokines including early CXCL10 and maximum levels of IL6, CXCL10, and IL8 were associated with the higher level of

antigen. Importantly, sequentially increasing the antigenemia cutoff value increased the magnitude of difference in the level of each of these cytokines (**Figure 3.3C**). In addition to the cytokines analyzed above, several other cytokines including maximum levels of IFN- λ 1, IFN- β , and IFN- γ correlated to some degree with antigen levels in the cohort at large.

Recombinant full-length nucleocapsid elicits secretion of antiviral cytokines by human endothelial cells

Sharing significant homology with nucleocapsid proteins from other coronaviruses, SARS-CoV-2 N protein is a five domain RNA-binding protein with important functions in several aspects of the viral life cycle, including virion assembly, genome packaging, and innate immune evasion. Three intrinsically disordered domains connect RNA binding and dimerization domains at the N and C terminus respectively (CTD and NTD). While the N terminal RNA binding region is most associated with genome packaging, all five regions have been implicated in the protein-RNA and protein-protein interactions required to effectively condense and organize viral nucleic acid(192, 193).

To test the hypothesis that viral antigenemia directly causes endothelial activation, we purified native, non-glycosylated nucleocapsid protein and an isolated C terminal dimerization domain (CTD). Stimulation of human umbilical vein endothelial cells with full-length nucleocapsid (**Figure 3.3E**) resulted in secretion over a 48hr time course of antiviral cytokines including CXCL10, IFN- β , TNF- α , IL-6, IL-1 β , GMCSF, and IL8 (**Figure 3.3F**)—many of which were seen to be directly associated with nucleocapsid antigenemia levels in our cohort. Importantly, the isolated CTD of nucleocapsid (Schematic in **Figure 3.4A**) did not elicit significant cytokine secretion under the same conditions. Together, these results suggest that full-length nucleocapsid is sufficient to induce cytokine secretion in human endothelial cells.

Nucleocapsid stimulation induces upregulation of leukocyte adhesion molecules

Stimulation with full-length nucleocapsid, but not CTD, also induced expression of VCAM-1, a terminal marker of endothelial activation and a functional leukocyte adhesion molecule (**Figure 3.4B**). By flow cytometry, surface ICAM-1 was elevated in full-length nucleocapsid stimulated HUVECs, particularly in cells with high levels of detectable nucleocapsid associated at 48 hours post stimulation (**Figure 3.4C**). Induction of VCAM-1 by nucleocapsid stimulation was dose dependent and associated with higher levels of stably associated (either surface or internalized) nucleocapsid at 48 hours as evaluated in whole cell lysates by western blot (**Figure 3.4D**).

Opposing effects of N terminal domain (NTD) antibodies on endothelial activation by full length nucleocapsid

To further dissect the domains of nucleocapsid involved in endothelial activation, we pre-incubated full length nucleocapsid with monoclonal antibodies against different epitopes within the N terminal RNA binding domain (NTD) of the protein prior to stimulation (**Figure 3.5A**). Pre-incubation with M08, but not R04 resulted in some blockade of nucleocapsid induced VCAM-1 expression (**Figure 3.5C**). In fact, R04 appears to some degree to enhance nucleocapsid induced endothelial activation. Furthermore, reducing the concentration of stimulating nucleocapsid, we were able to achieve complete blockade of VCAM-1 induction after pre-incubation with M08 (**Figure 3.5D**).

Next, to investigate the fate of nucleocapsid in HUVEC culture, we evaluated levels of stably associated nucleocapsid in WCL at various time points with and without these monoclonal antibodies. Interestingly, with nucleocapsid alone, we found a significant reduction in HUVEC associated nucleocapsid levels at 48hrs relative to 24hrs post stimulation, suggesting that the protein is either processed or dissociated over time. Furthermore, pre-incubation with M08 and R04 resulted in opposing effects on N protein

processing between 24 and 48hrs. while M08 appears to have moderately stabilized the protein, pre-incubation with R04 resulted in complete processing or dissociation of nucleocapsid (**Figure 3.6A**). Together, these findings suggest that antigenemia-induced endothelial activation is likely to depend on the structure and stability of the RNA binding domain and that it can be modulated by specific antibodies. Future work will seek to evaluate the specific mechanisms underlying the opposing effects of M08 and R04.

SARS-CoV-2 nucleocapsid protein binds to human endothelial cells

We next evaluated the interaction of FL nucleocapsid with endothelial cells by flow cytometry, microfluidics and immunofluorescence (IF) microscopy. By flow cytometry, we observed increasing levels of FL nucleocapsid on the surface of HUVECs over a four-hour time course. In permeabilized HUVECs at 48hrs, significant levels of nucleocapsid were also seen (histogram inset) (**Figure 3.6B**). The interaction of nucleocapsid with endothelial cells was observed in an endothelialized microfluidic model, where FL nucleocapsid bound to HUVECs seeded in microscopic synthetic capillaries under flow (**Figure 3.6C**). In live-stained IF microscopy, nucleocapsid could be seen on the surface of endothelial monolayers, mostly localized in cellular junctions (**Figure 3.6D**). Together, these studies show that nucleocapsid binds to endothelial cells in multiple contexts and that this association is stable under microvascular flow rates. Further studies will evaluate the functional consequences of viral nucleocapsid adhesion to the endothelium.

SARS-CoV-2 infected rhesus macaques develop nucleocapsid antigenemia, which is dependent on challenge dose and strongly correlated with peak lung viral loads

In our longitudinal cohort, the highest antigenemia levels are found within the first 2 weeks after self-reported onset of symptoms. These high levels decay rapidly with the evolution of the humoral immune response, which can be seen in **Figure 3.7A**. These early levels correlate weakly with RT PCR Ct values, typically generated from sampling of the upper respiratory tract (nasopharynx or anterior nares). It remains an open question

which compartment(s) are the source of antigen leak, but presumably an epithelial compartment where active replication occurs is involved. To evaluate this question more rigorously, we tested for antigenemia in two cohort of SARS-CoV-2 infected, untreated rhesus macaques challenged at $2.3E5$ and $1E6$ pfu per animal. Importantly, the development of antigenemia was dose dependent—found sporadically in the lower dose challenge cohort, but consistently in all but one of nine animals challenged at the higher dose (**Figure 3.7C and 3.7D**). In the latter cohort, antigenemia peaked at day 2 post infection at the same timepoint as viral load in the lung. The correlation between antigenemia and compartment specific viral load increased as sampling progressed lower into the respiratory tract, with the strongest correlation found in BAL sampling. This is consistent with an LRT source of antigenemia coincident with the peak of viral load in that compartment, perhaps reflecting a combination of viral and host factors leading to capillary leak of antigen into the blood (**Figure 3.7E and 3.7F**). The use of subgenomic RNA viral load as a surrogate for active viral replication has been proposed, but evidence remains conflicting as to its correlation with infectiousness. Nonetheless, we observed a similar trend in correlation with sgRNA VL, descending the respiratory tract at the peak of antigenemia and viral load (**Figure 3.7G and 3.7H**). Together, these findings identify the dose of inoculum as an important factor in the development of antigenemia in a well-characterized animal model and are consistent with a model in which antigen leak occurs in the LRT during the peak of viral replication.

Discussion

In this study, we describe the dynamics of SARS-CoV-2 nucleocapsid antigenemia in a cohort of patients hospitalized with COVID-19. Not only does N antigenemia mark acute infection, but higher levels of nucleocapsid in blood were associated with disease severity and mortality. While the maximum level of several cytokines, including IL-6, as well as other blood markers of inflammation were also associated with disease severity,

antigenemia was unique as an early correlate of severity with added value as a diagnostic adjunct or alternative to PCR testing. IFN-I and III as well as levels of CXCL10 were associated with levels of antigenemia. The association we observe with IFN-III is particularly interesting as this class of cytokine displays selectivity for epithelial compartments including the lung through more restricted receptor expression than is seen in the IFN-I axis(35, 194, 195). Early antigenemia levels also correlated with maximum IL6 levels, perhaps reflecting a contribution or association with the pro-inflammatory pathways driving immunopathology in COVID-19.

A consistent association of nucleocapsid antigenemia with disease severity and correlation with antiviral cytokine responses led us to investigate the possibility that extracellular nucleocapsid may exert direct effects on endothelial cells, contributing to endothelial injury and coagulopathy in COVID-19. This line of investigation was further motivated by the recent work of Qian et al., who first demonstrated that glycosylated nucleocapsid produced in mammalian cells could activate endothelial cells derived from multiple organ systems(196). We confirm and expand upon this finding to show native non-glycosylated nucleocapsid could also activate the endothelium and produce the same antiviral cytokines seen systemically in severe COVID-19. We further show that full-length N protein is required for endothelial activation *in vitro* and demonstrate that nucleocapsid binds to endothelial cells in multiple contexts including a flow based endothelialized microfluidics model. Finally, we found that blockade of nucleocapsid-mediated endothelial activation was possible using a monoclonal antibody that binds to the N terminal RNA binding region of the protein. This finding raises the possibility that endogenous or therapeutic nucleocapsid antibodies could be employed to modulate endothelial activation that might be a result of nucleocapsid antigenemia during severe

infection. Furthermore, the inclusion of nucleocapsid as a component of future vaccines could modulate the pathophysiology of breakthrough infections.

Our findings in non-human primates infected with SARS-CoV-2 also add two key pieces of information to our understanding of viral antigenemia, difficult to obtain retrospectively in human subjects. (1) The development of antigenemia depends on the dose of inoculate and (2) the correlation of viral load with antigenemia increases dramatically in the middle and lower respiratory compartments compared to the upper airway. Indeed, the latter observation may reflect the source of antigen in the blood as infection of pneumocytes and pulmonary epithelial tissue brings the virus in close apposition to pulmonary capillary beds.

Limitations of these studies include the use of convenience sampling, which resulted in variability in the timing of enrollment during each patient's hospital stay. Abstraction of symptom onset data also relied on chart review and the interpretation of self-reported data, which could be subject to bias. While efforts were made to standardize this process, self-reported information filtered through multiple clinicians can be inaccurate or difficult to interpret. While further work to confirm the relevance of these findings *in vivo*, our human, animal, and cellular studies expand our understanding of SARS-CoV-2 nucleocapsid antigenemia and its potential direct role in endothelial activation during COVID-19.

Experimental Methods

Sample collection and processing

Hospitalized patients diagnosed or under investigation for COVID-19 who were seen in the emergency department and/or admitted at Emory University Hospital and Emory University Hospital Midtown March to August of 2020 were identified by SARS-CoV-2 PCR testing records. PCR results were obtained from the medical records of each

admitting institution. Nasopharyngeal swabs were collected by the admitting medical team according to standard hospital procedure for each hospital. Residual serum and heparinized plasma samples from fully resulted clinical laboratory tests were identified and set aside as “discarded tissue” sample in accordance with clinical laboratory director approval. Residual samples were aliquoted by research staff and stored at -80 C prior to research use. Retrospective chart review of patients in the study cohort was performed by Emory medical students and clinical staff who were in at least year 3 of Medical Doctorate training or currently hold a Medical Doctorate or equivalent degree. Reviewers were blind to results of any testing at the time of chart review. Patient information and clinical course details were entered into a RedCAP database. Additional lab testing data were obtained by extraction for each relevant patient encounter by the Emory clinical data warehouse (CDW).

Nucleocapsid detection

Nucleocapsid antigenemia was quantified on the Quanterix HD-X platform. Residual serum and plasma samples were thawed once after storage at –80°C and diluted 1 to 3 in assay sample diluent. Diluted samples were then run using the ultrasensitive SIMOA SARS-CoV-2 N Protein Antigen assay on the automated Quanterix HD-X platform (Quanterix, Billerica, MA, USA) which has a validated limit of detection of 0.099 pg/mL in respiratory and saliva samples. Samples with antigen levels too high for the linear range of the assay were further diluted 1 to 20 and re-tested. Final antigen concentrations were determined by interpolation after sigmoidal fitting of duplicate calibration curves run on each test plate.

Pseudovirus neutralization assay

SARS-CoV-2 neutralizing antibody activity in was measured using an HIV-based pseudoviral particle bearing SARS-CoV-2 spike, produced from a plasmid encoding a 21

amino acid intracellular domain truncation mutant of the SARS-CoV-2 spike protein (delta 21 spike) based on the strain Wuhan-Hu-1 (GenBank NC_045512). Pseudovirus infection and inhibition of infection (neutralization) in ACE-2 bearing 293T cells were quantified using the Promega Bright-Glo Luciferase Assay System and the luminometer fiber on a synergy BIOTEK plate reader. The 50% inhibitory concentration/dilution (ID50) for each plasma sample tested was determined in duplicate by normalizing the luminescence signal in each sample dilution to the maximum signal in pseudovirus alone controls. ID50s were calculated by imputation after sigmoidal fitting of each neutralization curve using GraphPad Prism.

Coronavirus spike and RBD enzyme linked immunosorbent assays (ELISAs).

In-house purified recombinant his-tagged receptor-binding domain (RBD) from the SARS-CoV-2, Wuhan-Hu-1 (GenPept: QHD43416) was coated on high-bind ELISA plates at 1ug/mL in PBS overnight at 4°C. Plates were then washed 3x with 0.05% PBST and blocked for 30 minutes at RT in ELISA buffer (1% BSA, 0.02% tween 20 in PBS). Plates were then tapped out after blocking and pre-diluted serum or plasma samples added the test plate in 8-well dilution series. Samples were incubated at room temperature for 1hr, washed 3x in 0.05% PBST. HRP-conjugated anti-human IgG (Jackson Labs), IgA (Southern biotek) and IgM (Invitrogen) were used for detection. SigmaFAST OPD was used for development per the manufacturer instructions and reactions were stopped using 1N HCl before reading on a synergy BIOTEK plate reader at a wavelength of 492.

Cytokine measurements

Cytokines were measured in a subset of longitudinal plasma samples from the cohort using BioLegend® LEGENDPlex™ antiviral response kits. Briefly, plasma

samples or duplicate standard curve samples were diluted in assay buffer prior to incubation for 2hrs with multiplex beads. After two washes in assay wash buffer, beads were resuspended with shaking for 1hr in a biotinylated detection antibody cocktail. PE-conjugated streptavidin was added prior to a final wash and reading of the assay using an LSRII flow cytometer. The same kit and procedure were used in quantifying cytokines for endothelial cell stimulation experiments described below using undiluted supernatants.

Production of Recombinant Nucleocapsid Protein

SARS-CoV-2 nucleocapsid (N) protein was cloned into pET-22b vector including amino acids 1-419. A plasmid of the same type encoding the C-terminal domain (CTD) (amino acids 247-365) of N protein was obtained from BEI (NR52434). N protein plasmids were transformed ClearColi-BL21(DE3) Electrocompetent Cells (DUOs, Astral Scientific) according to manufacturer's instruction. Briefly, N protein transformant positive ClearColi were cultured in LB broth containing 100 ug/ml ampicillin with agitation (250 rpm) at 37 °C. When bacteria were grown to the mid-log phase, protein expression was induced by addition of isopropyl 1-thio- β -D-galactopyranoside (final IPTG, 1 mM). After 20hrs of induction in 37°C, bacteria pellets were harvested by centrifugation. Pellets were lysed and N protein was purified by Ni Sepharose Excel resin (Cytiva) using His Buffer Kit (Cytiva) according to manufacturer's instruction. Dialyze eluate with phosphate buffer to remove the imidazole using the Amicon centrifugal filter (10 kDa) at 4°C. The purity of the recovered proteins was confirmed by SDS-PAGE analysis. The protein was aliquoted and stored at -80 °C for further use.

Culture and stimulation of Human Umbilical Vein Endothelial Cells (HUVECs)

Primary umbilical vein endothelial cells were obtained from ATCC (PCS-100-100) and cultured using growth factor supplemented endothelial growth medium (EGM-2 Lonza). All stimulation experiments were performed in minimally passaged cells (Passage 1-5). HUVECs were seeded overnight at 0.5×10^6 cells/mL in 12 well plates. The next day, FL or CTD N proteins were diluted in EGM-2 to the desired concentration, applied directly to confluent monolayers, and allowed to incubate at 37°C for 25 or 48h. A synthetic tiracylated lipopeptide (PAM3CSK4 InvivoGen) was used at 100ng/mL as a positive control for endothelial activation. Negative control conditions were treated with a fresh media change containing equivalent volumes of sterile PBS to the stimulation conditions

Flow cytometry analysis

After stimulation or binding, cells were washed 3 times with cold PBS, and live cells were detached using 2mM EDTA in PBS, pelleted by centrifugation and stained for analysis by flow cytometry. ICAM-1 surface expression was assessed using anti-human CD54 (BioLegend, clone HA58) in BV421. Surface binding of N protein was measured by his-tag using AF647 conjugated anti-His tag mAb (MBL, clone OGHis). Surface levels of ICAM-1 and nucleocapsid were measured by flow cytometry on an LSR II (BD instruments).

Western blotting

After stimulation, cells were harvested into ice cold RIPA buffer, supplemented with protease inhibitors (Roche technologies). Clarified lysates were then boiled for 10 minutes with BME supplemented SDS-PAGE sample buffer before separation by 4-15% SDS PAGE. Proteins were then transferred to nitrocellulose (125V for 90 minutes) and blocked for 30 minutes in 5% milk. Blots were incubated with a VCAM-1 primary antibody (cell signaling technologies) overnight at 4°C with rocking. After washing three times in PBST,

VCAM-1 was detected using an HRP conjugated anti-rabbit IgG (cell signaling technologies) and pierce ECL western blotting substrate (thermofisher). Chemiluminescence was detected on a ChemiDoc imaging system (Bio-Rad). Blots were stripped using Restore stripping buffer (thermofisher) and re-blotted using an N protein monoclonal antibody followed by a beta actin as a loading control.

Immunofluorescence microscopy

After incubation with N protein at 5ug/mL for 24hrs, HUVEC monolayers were washed three times and fixed in 4% PFA followed by permeabilization and staining with an AF657 conjugated anti-His tag mAb (MBL, clone OGHis), phalloidin, and DAPI nuclear stain. Images were acquired using a Keyence digital microscope.

Endothelialized microfluidics experiments

Endothelialized microfluidic devices were generated as described previously by Lam et al.(197). For N protein binding experiments, microfluidic devices were seeded with HUVECs two days prior to the experiment. 5 or 10ug/mL N protein supplemented EGM-2 media was flowed for 2hrs through the devices. EGM-2 alone was used as a negative control. Following fixation, N protein was detected using an anti-His tag mAb (MBL, clone OGHis) with visualization of nuclei by Hoechst staining. Images were acquired using a Keyence digital microscopes

Rhesus Macaque Plasma Samples

Samples from two cohorts of SARS-CoV-2 infected, untreated control rhesus macaques were obtained with the kind help of Mirko Piardini and Sudhir Kasturi. Animals in the low dose challenge cohort were derived from the infected, unvaccinated animals of a study by Pino et al.(198) The remaining samples, from animals challenged at the higher dose

were derived from a yet unpublished study that followed the same protocols described by Hoang et al., in their trial of baricitinib(199)

Chapter 3 Tables

Table 3.1. Cohort characteristics

Variables		All		Moderate		Severe	
Sex		N	%	N	%	N	%
	Male	67	49	40	46	27	54
	Female	71	51	48	55	23	46
Race		N	%	N	%	N	%
	African American	113	83	75	87	38	76
	White	16	12	7	8	9	18
	Asian/Pacific Isander	2	1	0	0	2	4
	Other	5	4	4	5	1	2
WHO Ordinal Scale		N	%	N	%	N	%
	3	24	17	24	27	0	0
	4	56	41	56	64	0	0
	5	8	6	8	9	0	0
	6	5	4	0	0	5	10
	7	23	17	0	0	23	46
	8	22	16	0	0	22	44
Hospital course		N	%	N	%	N	%
	Mortality	22	16	0	0	22	44
	Intubation	45	33	0	0	45	90
	Intubation or Mortality	49	36	0	0	49	98
	Any ICU	56	41	8	9	48	96
	Admitted directly to ICU	25	18	6	7	19	38
	Transferred to ICU	31	22	2	2	29	58
Age/BMI		Mean	Stdev	Mean	Stdev	Mean	Stdev
	Age	64	17	63	17	66	17
	BMI	31	9	31	8	31	10
Admission Vitals		Mean	Stdev	Mean	Stdev	Mean	Stdev
	Temperature (C)	37	1	37	1	37	1
	Systolic BP (mmhg)	137	26	138	27	137	24
	Diastolic BP (mmhg)	76	14	77	14	75	14
	HR (bpm)	93	19	94	19	91	19
	RR (bpm)	21	5	20	4	22	6
	spO2	93	15	92	18	93	8

Table 3.1. Cohort characteristics. Basic demographic information and details regarding the course of hospitalization are described in the whole cohort and each severity category (defined by mortality and requirement for mechanical ventilation). The world health organization (WHO) ordinal COVID-19 severity scoring system is also included. (3=hospitalized, no oxygen therapy; 4=oxygen by mask or nasal prongs; 5=non-invasive ventilation or high flow oxygen; 6 intubation and mechanical ventilation; 7=ventilation & additional organ support—pressors, RRT, or ECMO; 8=death).

Figures for Chapter 3

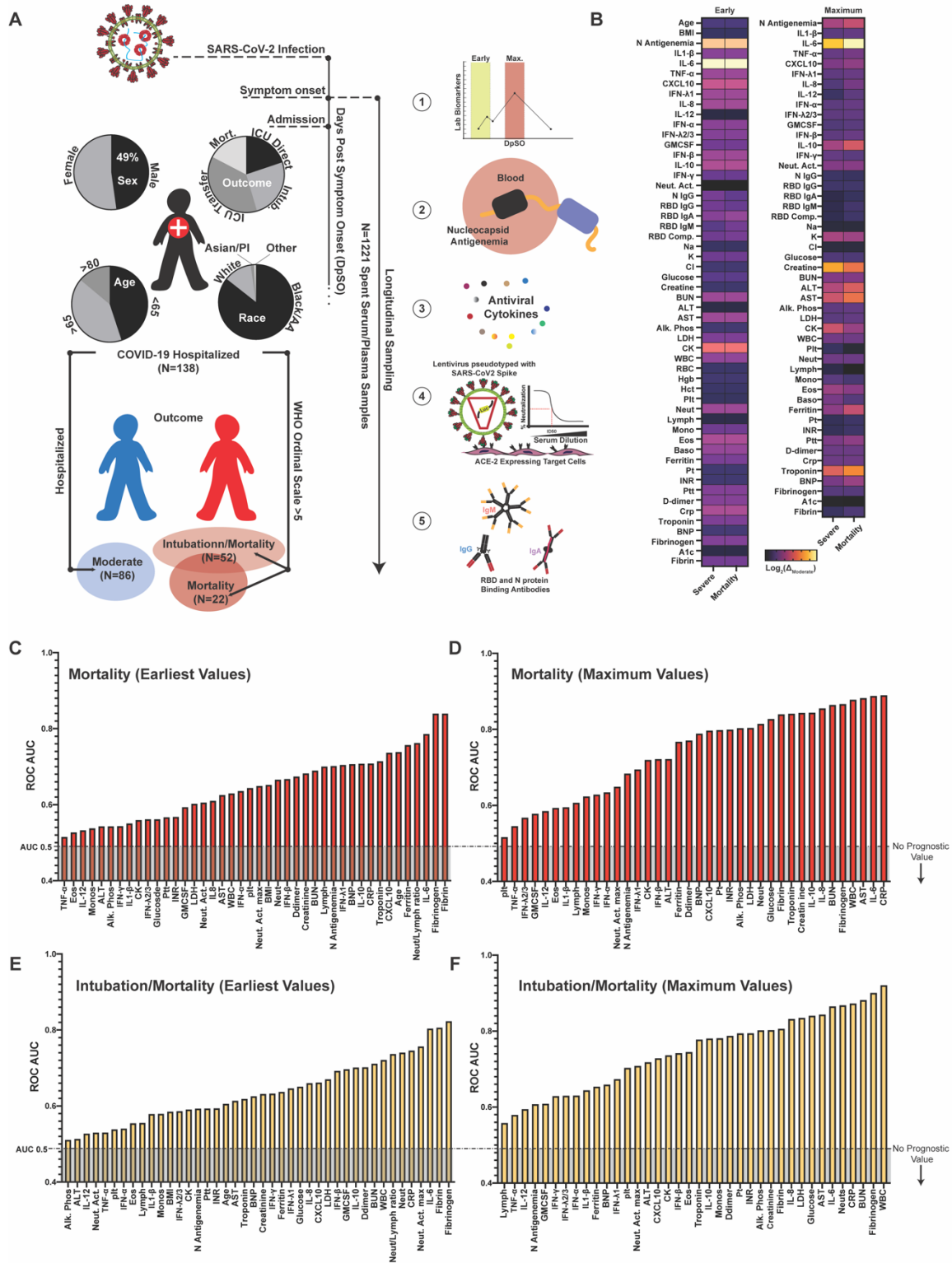


Figure 3.1. Blood biomarkers associated with COVID-19 Disease Severity (A) Overview of study design, cohort characteristics, and blood sampling (B) Heat map showing fold change of early and maximum blood biomarker levels relative to moderate in severe COVID-19. $\text{Log}_2(\text{Severe}/\text{Moderate})$ is used for each biomarker. (C-D) Receiver operator characteristic (ROC) area under curves (AUCs) for early (C and E) and maximum (D, and F) biomarkers ranked and plotted for their prognostic value in predicting mortality (C and D) and COVID-19 severity (E and F).

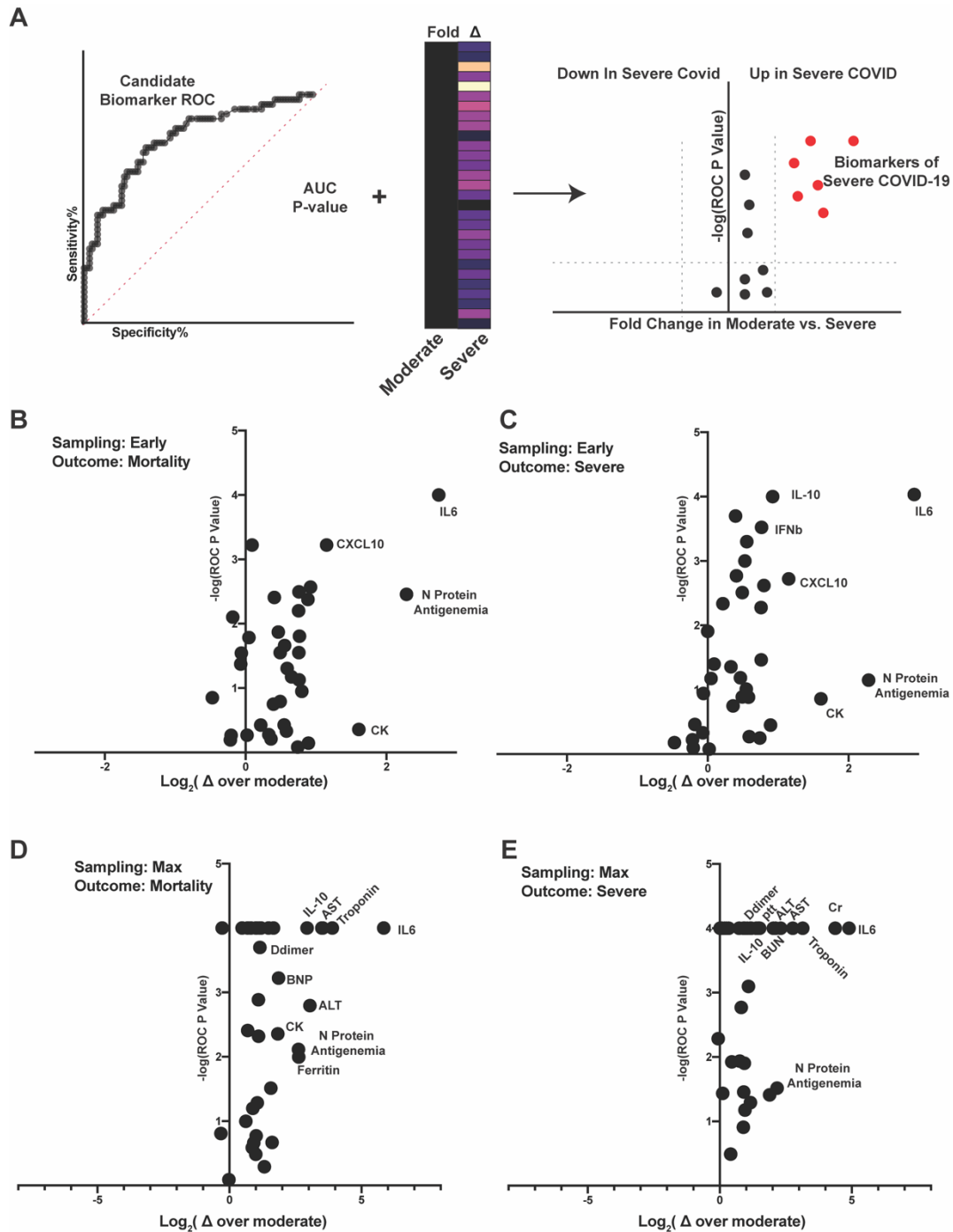


Figure 3.2. Identification of COVID-19 severity biomarkers. (A) Combinatorial screening approach for identification of severity biomarkers. (B-E) Volcano plots of fold change between outcome categories for each candidate biomarker plotted against reciprocal log p values from

receiver operator characteristic (ROC) analyses. Analyses are shown for early (B,C) and maximum (D,E) values of each candidate biomarker.

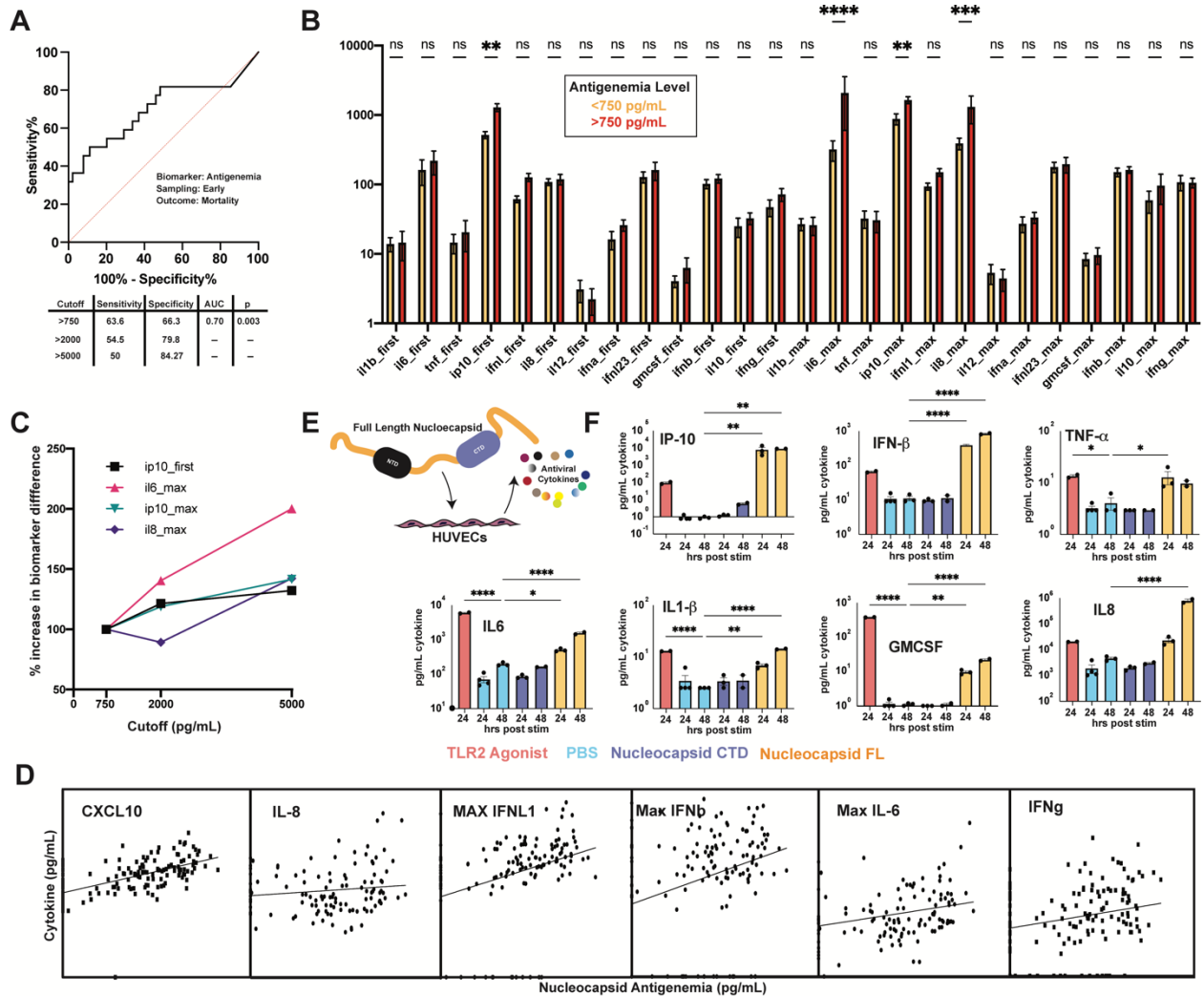


Figure 3.3. Nucleocapsid antigenemia is associated with inflammatory cytokine responses, which can be elicited in endothelial culture by stimulation with full length N protein. (A) ROC analysis of nucleocapsid antigenemia as a predictor of mortality. Sensitivity and specificity at three sequentially higher cutoffs are shown in the table below. (B) Comparison of plasma antiviral cytokine levels in patients grouped by antigenemia level. Statistical significance ($P < 0.05$) was determined by 2-way analysis of variance (ANOVA). (C) Dose dependence of association between cytokine levels and antigenemia plotted as a % increase in difference from the baseline antigenemia cutoff of 750 pg/mL. (D) Linear regression analysis of maximum cytokine levels significantly associated with antigenemia. (E) Experimental schema for *in vitro* endothelial cell stimulation experiments.

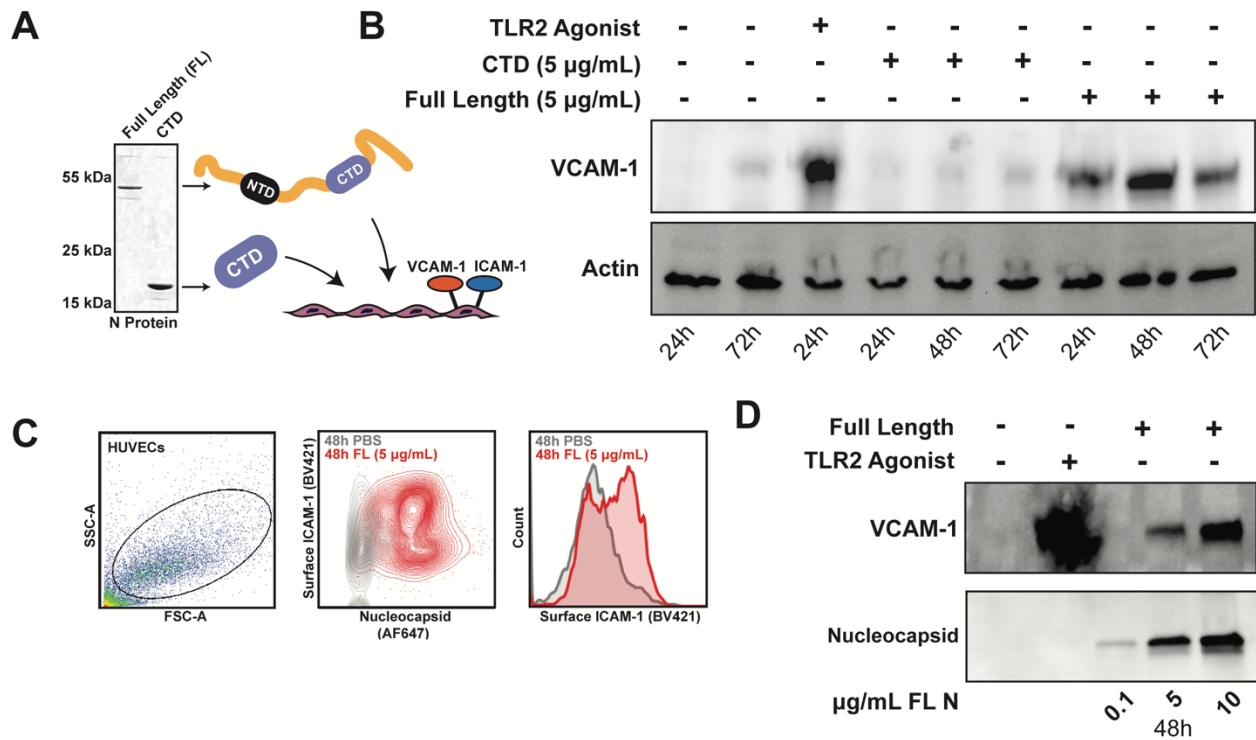


Figure 3.4 Full length nucleocapsid activates human endothelial cells. (A) Experimental schema for HUVEC stimulation experiments. (B) Western blot analysis of VCAM-1 expression following nucleocapsid stimulation over a 72hr time course. A synthesized TLR2 agonist served as a positive control for HUVEC activation (C) Flow cytometry analysis of surface ICAM-1 and total nucleocapsid in HUVECs after stimulation with 5 $\mu\text{g}/\text{mL}$ of full length nucleocapsid over 48hrs. (D) Western blot analysis of VCAM-1 expression and nucleocapsid in whole cell lysates from HUVECs stimulated with 0.1, 5, and 10 $\mu\text{g}/\text{mL}$ FL nucleocapsid over 48 hrs.

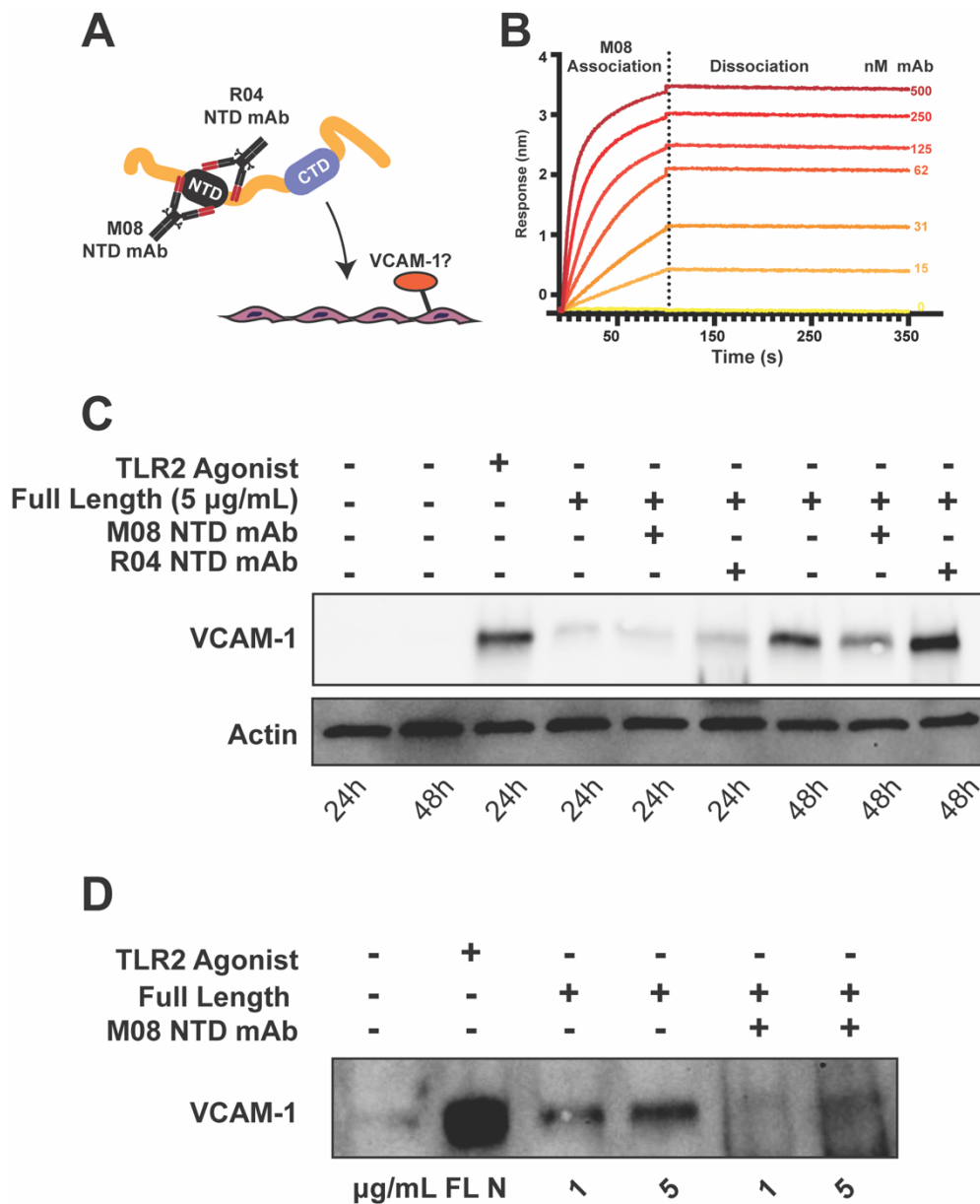


Figure 3.5. Opposing effects of N terminal domain (NTD) antibodies on endothelial activation by FL nucleocapsid. (A) Experimental setup for nucleocapsid endothelial stimulation experiments with two different NTD-specific monoclonal antibodies. (B) Bi-layer interferometry (BLI) binding curves for M08 binding to FL nucleocapsid. (C) Western blot analysis of nucleocapsid stimulated VCAM-1 expression in HUVECs over a 48hr time course with and without pre-incubation with 10ug/mL of M08 or R04. (D) Western blot analysis of VCAM-1 expression after stimulation with 1 or 5ug/mL FL nucleocapsid after pre-incubation with 10ug/mL of the blocking antibody M08.

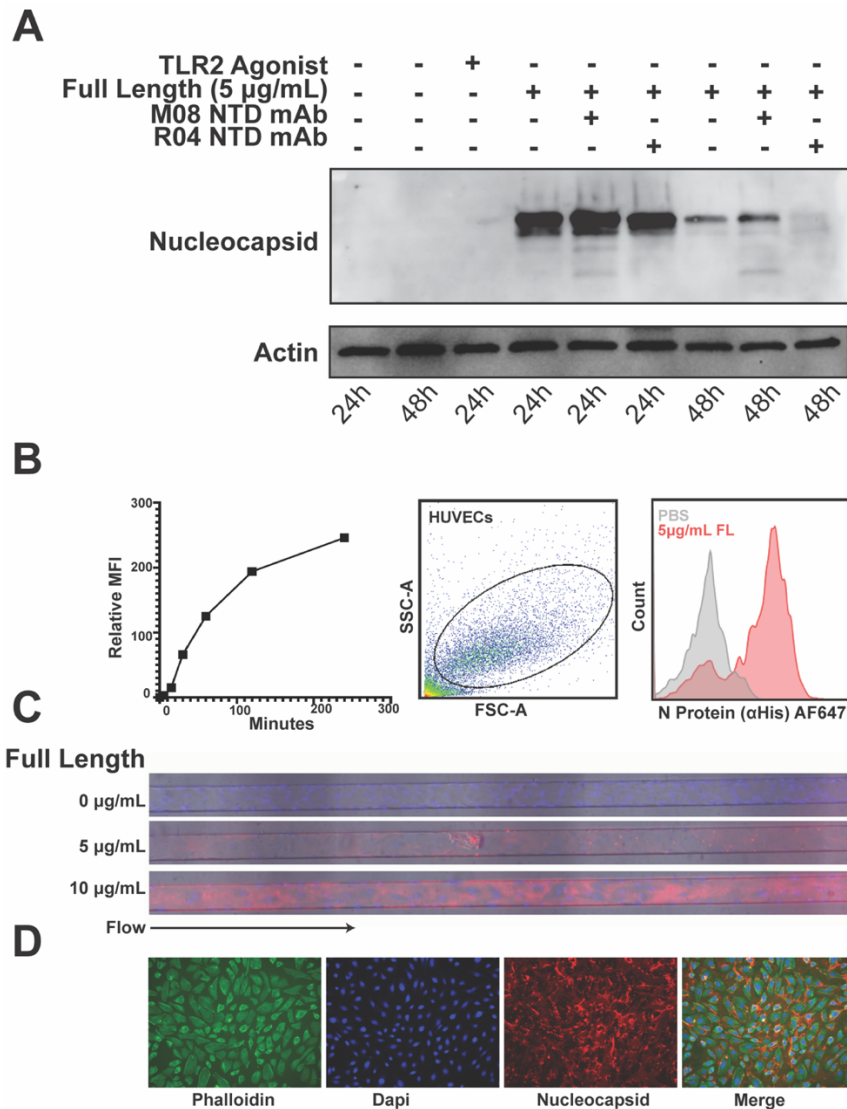


Figure 3.6. Binding and processing of nucleocapsid in HUVECs. (A) Western blot analysis of stably associated nucleocapsid in HUVECs and 24 and 48hrs post stimulation with and without pre-incubation of two NTD specific mAbs at 10µg/mL. (B) Flow cytometry analysis of FL nucleocapsid binding to HUVECs over a 4 hr time course. Histogram of FL nucleocapsid associated with permeabilized HUVECs at 48hrs. (C) FL nucleocapsid binding to HUVECs under flow in endothelialized microfluidic devices. (D) Immunofluorescence microscopy of surface associated nucleocapsid on HUVEC monolayers.

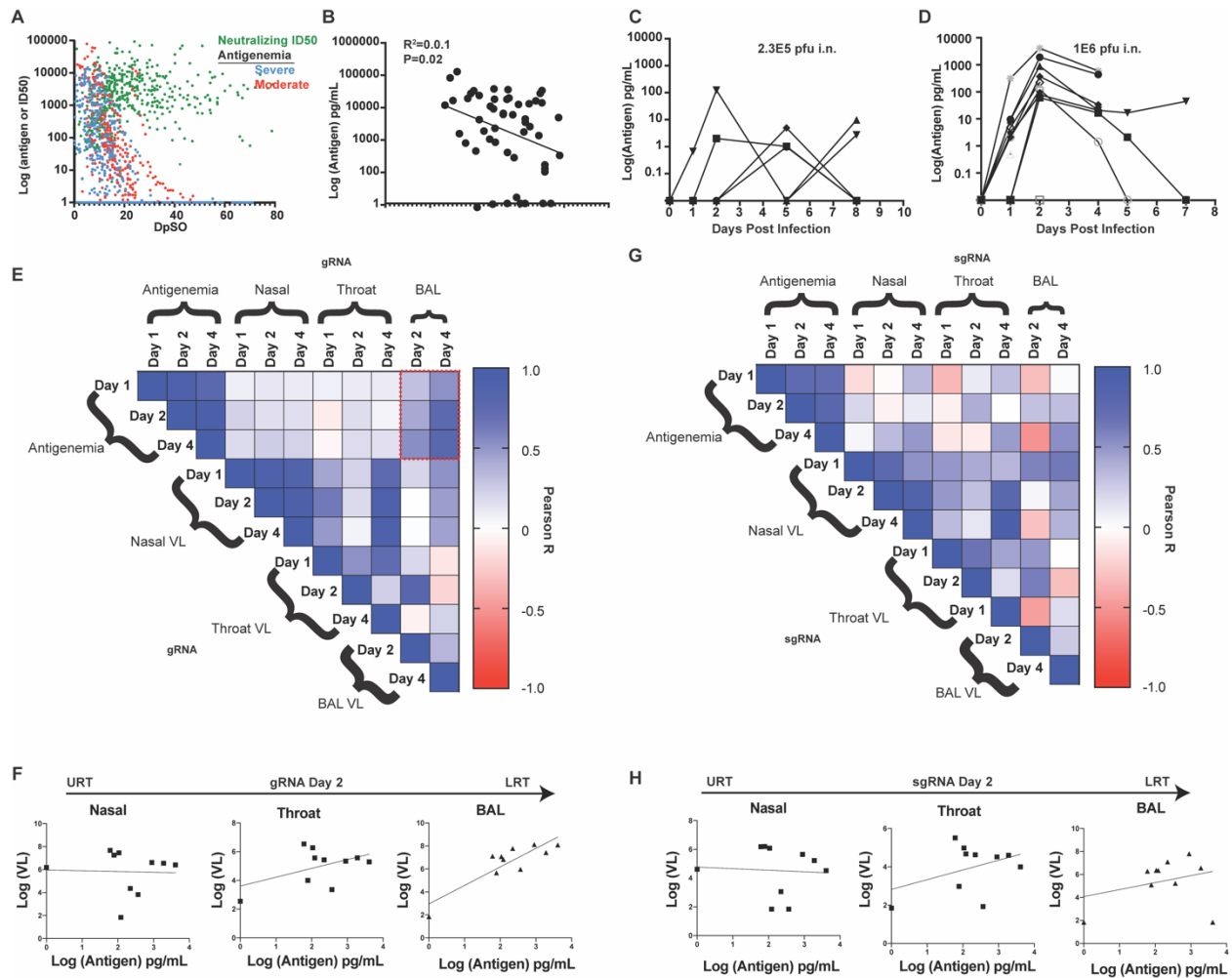


Figure 3.7. Dynamics and compartmental viral load correlates of nucleocapsid antigenemia in the rhesus macaque model of SARS-CoV-2 infection. (A) Human cohort-wide Longitudinal antigenemia decay separated by disease severity and plotted with neutralizing antibody levels against days post symptom onset. (B) Linear association between maximum antigenemia levels and first RT-PCR cycle threshold (Ct) values in the longitudinal cohort. (C) Dynamics of antigenemia in a cohort of rhesus macaques (N=5) after infection with 2.3E6 pfu SARS-CoV-2. (D) Dynamics of antigenemia in a cohort of rhesus macaques (N=9) after infection with a higher dose inoculate (1E6 pfu/animal). (E) Correlation matrix regressing antigenemia at days 1, 2, and 4 post infection with compartment specific genomic viral loads (qRT-PCR). (F) Linear regressions of antigenemia vs genomic viral load at day 2 post infection (peak antigenemia) starting in the upper respiratory tract (URT) and progressing to lung (BAL). (G) Correlation matrix regressing antigenemia as above with compartment specific E gene subgenomic RNA viral loads. (H) Linear regressions of antigenemia vs subgenomic viral load as in (F)

Chapter 4 SARS-CoV-2 antibody class-specific serology: applications in diagnostics and characterization of COVID-19 convalescent plasma

Abstract

Antibody Class-Specific SARS-CoV-2 Serology

In the first months of the SARS-CoV-2 pandemic, limitations in availability and challenges with implementation of gold standard nucleic acid testing prompted evaluation of alternative means of detection. As part of these efforts, we optimized and implemented a lab developed test, which gained FDA emergency use authorization (EUA) for SARS-CoV-2 IgG in the Emory health care system and evaluated the performance of serological testing in general for the diagnosis of COVID-19. Regardless of the modality, accurate diagnosis is critical for appropriate management and establishment of precautions when encountering patients with suspected COVID-19. We examined the possible complementary role of lab developed class-specific serology tests in assessing evidence of SARS-CoV-2 infection in hospitalized patients using nucleic acid amplification testing as the gold standard. In-house serological tests for IgG, IgA, and IgM antibodies against the receptor binding domain (RBD) of SARS-CoV-2 were developed and evaluated using samples from PCR-confirmed inpatients with COVID-19. We analyzed the influence of timing and clinical severity on the diagnostic value of class-specific COVID-19 serology testing. Cross-sectional analysis revealed a higher sensitivity and specificity at lower optical density cutoffs for IgA in hospitalized patients when compared to IgG and IgM serology (IgG AUC: 0.91; 95%CI 0.89 to 0.93 vs. IgA AUC: 0.97; 95% CI 0.96 to 0.98 vs. IgM AUC: 0.95; 95% CI 0.92 to 0.97). Superior performance of IgA serology was seen in the first two weeks after symptom onset and the first week after PCR testing. In samples from patients requiring intubation, all three tests exhibit enhanced sensitivity, while each test showed improved sensitivity over time. Among PCR-negative patients under investigation for SARS-CoV-2 infection 2 out of 61 showed clear evidence of seroconversion. Suspected false-positive results in the latter population were most frequently observed in IgG and IgM serology tests. Our findings suggest the potential

utility of IgA serology in the acute setting and explore the benefits and limitations of class-specific serology as a complementary diagnostic tool to PCR for COVID-19 in the acute setting.

Characterizing COVID-19 Convalescent Plasma

In a second study presented here, we used semi-quantitative versions of the assays described above to evaluate the SARS-CoV-2 antibody components of convalescent plasma, which, prior to the development of vaccines, antiviral therapies, and monoclonal antibodies, was one of the only viable virus specific therapeutic option in cases of severe COVID-19. Fundamental questions remain regarding the efficacy of convalescent plasma, including the components of CP that may contribute to its therapeutic effect. Most serological evaluation of CP have relied on examination of total immunoglobulin or IgG specific anti-SARS-CoV-2 antibody levels. However, IgA antibodies, which also circulate and are secreted along the respiratory mucosa, represent a relatively uncharacterized component of CP. Residual samples from patients and CP donors were assessed for IgM, IgG and IgA antibody titers against the receptor binding domain of SARS-CoV-2. In the clinical case study that motivated this evaluation, increased IgA SARS-CoV-2 antibody levels correlated with clinical improvement and viral clearance in an infant with COVID-19, prompting a broader examination of IgA levels among CP donors and hospitalized patients. Significant heterogeneity in IgA levels was observed among CP donors, which correlated weakly with IgG levels or the results of a commonly employed serological test. Unlike IgG and IgM, IgA levels were also more likely to be variable in hospitalized patients and this variability persisted in some patients >14 days following symptom onset. IgA levels were also less likely to be sustained than IgG levels following subsequent CP donation. IgA levels are heterogeneous among CP donors and hospitalized patients and do not necessarily correlate with commonly

employed testing platforms. Examining isotype levels in CP and COVID-19 patients may allow for a tailored approach when seeking to fill specific gaps in humoral immunity.

Introduction

Severe acute respiratory syndrome-coronavirus 2 (SARS-CoV-2), the cause of COVID-19, first emerged in late 2019 in a cluster of atypical pneumonia linked to a seafood and poultry market in Wuhan, China(200). SARS-CoV-2 is a betacoronavirus, related to a lineage of bat-coronaviruses as well as the zoonotic SARS-CoV and MERS-CoV. The virus targets cells through interaction between the receptor binding domain (RBD) of its spike (S) protein and human angiotensin converting enzyme 2 (ACE2) (23, 200) in the respiratory tract and other target organs, where infection and immune-mediated damage lead to local and systemic disease (201). Sequencing of the viral RNA genome(202) in the early days of the pandemic enabled the rapid development of PCR-based nucleic acid tests (NATs)(4), which have been widely implemented for diagnosis of acute SARS-CoV-2 infection. However, SARS-CoV-2 PCR tests have exhibited limitations in sensitivity for a variety of reasons including variability in nasopharyngeal swab acquisition and processing, and kinetics of the viral infection itself (203–205). Thus, focus has shifted toward the need to develop and validate serological assays, which detect antibody responses elicited by both current and past exposure to the virus and may therefore serve as complementary approaches in diagnosing COVID-19, even following acute presentation of the disease. As the pandemic evolves, antibody testing is also playing a critical complementary role to molecular approaches for a number of additional applications including i) sero-epidemiological surveys ii) screening of donors for convalescent plasma therapy and iii) assessment of vaccine immunogenicity. In addition, since development of RBD-specific antibodies correlates strongly with in-vitro neutralizing activity in both hospital patients and recently developed animal models, RBD-specific serology may provide some insight into the virus neutralization capacity in

ongoing studies examining long-term protection following recovery from SARS-CoV-2 infection(206, 207).

Most clinical serological platforms for detection of pathogen exposure or infection examine the reactivity of patient IgM, IgG, or both against antigenic determinants of the pathogen; some also include direct detection of pathogen antigens. Serological tests for SARS-CoV-2 have largely been no different, with platforms described that test for virus-specific IgG, IgM or pan-Ig. However, given the respiratory nature of the pathogen and the specific immune response predicted to form with respiratory mucosal tissues, examination of IgA SARS-CoV-2 antibodies may hold promise in the serological assessment of this disease. It is now well established that the kinetics of IgG, IgM and IgA responses differ among COVID-19 patients, with some reporting unusual, early onset of an IgG response and persistence of IgM(208). However, less attention has been paid to circulating and mucosal IgA, despite the primary site of infection being respiratory mucosa. Therefore, the potential utility of IgA in the serological evaluation of a patient with suspected COVID-19 remains incompletely understood. Several studies suggest IgA responses may be useful in evaluation of COVID-19 (209–212). However, additional data using longitudinal sampling are needed to accurately assess the class specific responses and their clinical correlates. Such studies will refine the ability of serology in general, in addition to the performance of individual antibody classes, to aid in the diagnosis and potential prognosis of COVID-19. To balance the throughput needs of a clinical diagnostics lab with the value of a semi-quantitative platform, we developed single-dilution ELISA-based screening assays to detect IgG, IgA, or IgM specific for the RBD of SARS-CoV-2 spike (S). We then validated and compared these tests using samples collected from PCR-confirmed COVID-19 patients and pre-pandemic samples from healthy blood donors and patients being screened for other viral infections or HLA

antibodies. Using receiver operator characteristic (ROC) analysis, we found that the IgA serology assay exhibited superior performance overall, especially within the first two weeks after symptom onset or first week after PCR testing.

Using more rigorous, semi-quantitative methods we went on in a second study to use the assays described above to evaluate the antibody components of therapeutic convalescent plasma units. Regarding the efficacy of convalescent plasma therapy, a multi-center study including 35,322 patients from 2,807 acute care facilities by the US expanded access program (EAP) COVID-19 Plasma Consortium found reductions in 7- and 30-day mortality when convalescent plasma (CP) with high levels of SARS-CoV-2 specific IgG antibodies was delivered early during infection¹. High-quality follow-up trials have confirmed the overall findings of efficacy in this analysis(213). In addition to timing, concentration and specificity, antibody isotypes also dictate potency, function, and localization of the humoral immune response to viral pathogens².

Due to the selective secretion of dimeric IgA across mucosal barriers³, these antibodies could provide an important benefit or immunomodulatory capacity when targeting respiratory pathogens^{4,5}. Circulating dimeric and monomeric IgA may also mediate isotype specific function independent of localization⁶. Monomeric, serum IgA lacks the secretory chain of dimeric IgA allowing binding to the Fcα-receptor 1 (FcαR1), engagement of which can contribute to inflammatory programs in myeloid cells(214). There is also experimental evidence for an anti-inflammatory role for serum IgA interactions with FcαR1 and for therapeutic administration of IgA in autoimmune models(215). Furthermore, though beyond the scope of the present study, these effects are likely to be dependent on subclass (IgA1 vs. IgA2) and antibody glycosylation as well as concentration and antigen specificity. Together these studies suggest multiple roles

for this component of serum and strongly support further characterization in CP and other therapeutic blood products.

If the goal of CP therapy is to deliver virus-specific antibodies to the site of infection⁷, assessment of IgA anti-SARS CoV-2 antibody levels in CP may be an important step in defining correlates of CP efficacy in larger studies. Despite the potential contribution of IgA anti-SARS-CoV-2 antibodies in CP efficacy, the relative distribution of these antibodies among CP donors and hospitalized patients remains incompletely understood. Prior to the development of serological tests, early efforts to procure CP understandably relied on donors who recovered from PCR-confirmed infection in the absence of pre-transfusion serological assessment⁸⁻¹⁰. The early inability to characterize antibody levels also made it difficult to determine antibody levels in patients prior to transfusion and therefore define potential gaps in humoral immunity that may benefit from this therapy. Even following the development of tests capable of assessing total or IgG specific anti-SARS-CoV-2 antibody levels or neutralizing titers, the majority of these platforms do not specifically evaluate IgA. Characterization of units and responses to CP have been performed in recent months, but few have focused on class specific components(216). As IgA anti-SARS-CoV-2 antibody levels may reflect an under characterized yet important variable when seeking to establish CP therapeutic efficacy, we sought to define these levels in CP donors and hospitalized patients.

Results

Characteristics of SARS-CoV-2 PCR positive negative cohorts.

Between March and May of 2020, we evaluated longitudinal samples from patients under investigation for COVID-19 at two Emory Healthcare-Affiliated hospitals—Emory University Hospital and Emory University Hospital Midtown. Sampling from 78 patients who tested positive and 61 who tested negative were included in this study. Compiled

data for each group from a retrospective chart review are summarized in **Table 4.1**. On average PCR-confirmed cases were older (64.3 vs 59.8 years) and more likely to be African American (79.5% vs. 63.9%). Clinically, PCR-confirmed COVID-19 cases in this cohort were more likely to present with moderate (57.7% vs. 41.0%) or severe signs and symptoms (11.5% vs 0%). Cases were also more likely to require intubation (46.2% vs. 18.0%) and exhibited higher mortality (19.2% vs. 3.3%).

Cross-sectional comparison of IgG, IgA, and IgM serology assays in hospitalized COVID-19 patients.

We evaluated three enzyme-linked immunosorbent screening assays, developed and characterized in-house, for the detection of SARS-CoV-2 receptor binding domain (RBD)-specific IgG, IgA, and IgM in 508 samples from 78 PCR confirmed COVID-19 cases. 131 pre-pandemic controls including blood donors and patients being screened for HLA antibodies and antibodies against other viruses were used as true negative cases in this analysis. Assay performance was determined in the overall COVID-19 PCR positive cohort using receiver operating characteristic (ROC) analysis. In a ROC analysis, the area under the curve (AUC) for each assay inversely correlates with rates of false positivity and negativity at increasing optical density (OD) value cutoffs. In the overall sample set, the IgA assay exhibited significantly improved characteristics compared to the IgM and IgG assays (**Figure 4.1A & 4.1C**) (AUC 0.97 vs. 0.91 for IgG and 0.95 for IgM; $P < 0.0001$ for IgA vs. IgG and $P = 0.01$ for IgA vs. IgM). This finding was in part due to higher levels of false positivity in the IgG and IgM assays compared to the IgA assay over a range of cutoff values.

For a continuous variable like OD value, the output of a ROC analysis aids in selection of optimal cutoffs, from which clinical labs can determine and report an alpha response (positive or negative) with corresponding sensitivity and specificity at the

chosen cutoff. Inset tables in **Figure 4.1A to 4.1C** illustrate the tradeoffs involved in selecting such a cutoff. For this analysis we selected OD cutoffs with the goal of maintaining sensitivity above 80% at an optimal specificity for each assay (0.2 for IgG, 0.15 for IgA, and 0.35 for IgM). At the cutoff of 0.2 our IgG serology assay achieved a sensitivity of 85.10% (95% CI: 81.75 to 87.93) and a specificity of 80.15% (95% CI: 72.51% to 86.08%). At an OD cutoff of >0.15, the IgA assay achieved a sensitivity of 87.25% (95% CI: 84.08% to 89.87%) and specificity of 99.24% (95% CI: 95.80% to 99.96%). At an OD cutoff of >0.35, the IgM assay reached a sensitivity of 84.31 (95% CI: 80.90 to 87.21) and a specificity of 93.89 (95% CI: 88.41% to 96.87). Because class-specific antibody responses depend on the onset, magnitude, and duration of the antiviral immune response, we hypothesized that the diagnostic performance of our IgG, IgA, and IgM serology assays would change with time post symptom onset. Similar to recent reports(206, 217, 218), improved performance was observed when serology was more than 7 days after PCR testing(206). To address the question of timing in our cohort, we conducted a systematic chart review and estimated the date of symptom onset and time to serology for a subset of samples for which this information was available (N=362 samples from 54 patients). Binning these samples into four-day increments post symptom onset (**Figure 4.1D to 4.1F**) or PCR-testing (**Figure 4.1G to 4.1I**), it was clear that the average OD value in each assay increased over time for each class.

To test for potential cross-reactivity in the IgG and IgA assays, we measured reactivity with purified S1 domain from two human betacoronaviruses that cause human cold (OC43 and HKU1) in a subset of samples from our overall analysis. The latter analysis revealed little correlation (**Figure 4.7K**) in reactivity by OD value between the SARS-CoV-2 RBD ELISAs for IgG and IgA with the cold-coronavirus protein (**Figure 4.7C to 4.7E**), consistent with the polymorphic nature of SARS-CoV2 RBD (**Figure 4.7A and**

4.B). We repeated the latter analyses using recombinant RBD from two endemic alphacoronaviruses, finding a similar lack of strong correlation (**Figure 7G-K**).

Serology performance improves with time after symptom onset and PCR testing.

Based on the observation in the overall cohort that OD increased with time post symptom onset and PCR testing, we repeated ROC analyses binning samples by week post symptom onset (**Figure 4.2A to 4.2C**) or by time post PCR testing (**Figure 4.2D to 4.2F**). For all three assays, performance improved significantly over time, achieving AUCs of >0.99 at three or more weeks post onset or 2 or more weeks post PCR-testing. However, IgA exhibited superior performance in the first and second week post symptom onset compared to IgG serology (WK1: AUC of 0.90 vs 0.74; P=0.01 and WK2: AUC 0.99 vs 0.92; P=0.0005). Together these data corroborate observations for this and other viral infections that time post symptom onset correlates strongly with serology assay performance. This furthermore demonstrates that the overall performance advantage of IgA testing observed in **Figure 4.1** is likely due to superior detection of true positive samples early in the clinical course.

Longitudinal analysis of combinatorial and individual class-specific serology results.

To evaluate combinations of serology in this context, we generated heat maps of OD values and alpha responses for samples collected 1, 2, 3 or 4+ weeks after symptom onset from patients who tested positive for SARS-CoV-2 by PCR and had reliable, adjudicated symptom onset data after chart review (N=54) (**Figure 4.3A to 4.4D**). In **Figure 4.3E** is shown the corresponding % of samples in each week after symptom onset which tested positive by individual or different combinations of assays (i.e. G+A, G+M or M+A; any >2 or all 3). Consistent with our findings in **Figure 4.2**, sensitivity was high and

comparable using any combination of testing more than two weeks after symptom onset (**Figure 4.3E and 4.4F**). Some advantage in sensitivity was observed for combinations of G+A testing or the use of any positive result in the first two weeks after symptom onset. However, the improved sensitivity must be weighed against the combined loss in specificity resulting from combining IgA serology with less specific IgG or IgM (See inset of **Figure 4.1A-C** for specificity comparison at the chosen cutoff).

Analysis of IgG, IgA, and IgM OD values in individuals with longitudinal sampling.

While titering with known standards is the preferred method for quantifying serological responses in ELISA-based assays, ELISA OD values do correlate with the level of the antibody being detected within the linear range of the test. We therefore plotted individual OD responses over time post symptom onset for 6 PCR-positive patients for whom near daily sampling was available in our data set (**Figure 4.4**). Overall, the OD values increased with time within individuals, suggesting that the trends observed in **Figure 4.1** are likely due to the evolution of individual immune responses over time after infection. In addition, patterns of IgG, IgA, and IgM were not always correlated in individuals. In patient #1 for instance, a low level of increasing IgG is observed alongside stable high IgA and a parabolic IgM response. Patient 2 exhibits a late IgM response with a simultaneous sigmoidal increase in IgG signal—again with a stable and high IgA signal. Patients 3 and 4 both exhibit a lower level IgA signal with robust and early IgM occurring prior to a sigmoidal rise in IgG signal. Patients 5 and 6 did not have samples available earlier than day 10 post-symptom onset, but both showed declining IgM and IgA with a stable rise in IgG signal between 20 and 30 days after onset. Although limited to a low number of patients, these data suggest that unique, class specific patterns likely contribute significantly to the overall performance of serology tests over time.

Improved performance of serology in samples from patients requiring intubation.

Given the variable serological responses observed among patients, we next compared OD values in samples collected from patients requiring intubation during their hospital course and investigated serology test performance in these samples relative to samples from patients who never required intubation. Because patients with more severe disease were more likely to have longer hospital stays and therefore more sampling from later in the clinical course (correlating with higher antibody level), we censored the data in both groups to include only samples from the first two weeks after symptom onset. In patients requiring intubation, OD values for IgG, IgA and IgM were higher in the second week compared to the first ($P < 0.0001$) whereas no significant increase was observed in samples from week 2 compared to week 1 in samples from patients who did not require intubation. Interestingly, IgA and IgM, but not IgG OD values were higher in week 1 in samples from individuals requiring intubation compared to samples from those who did not ($P = 0.05$ and $P = 0.005$ respectively) (**Figure 4.5A-C**). For all three assays in samples collected during the first two weeks following symptom onset, ROC analysis revealed higher overall performance in samples collected from those who required intubation compared to those who did not (statistical comparison summarized in **Figure 4.5G**).

Analysis of seroconversion among PCR negative patients under high suspicion of SARS-CoV2 infection.

Due to concerns about the sensitivity of PCR testing for SARS-CoV2 infection, particularly with respect to pre-analytical variables that may significantly influence the likelihood of SARS-CoV-2 nucleic acid detection, we evaluated a cohort of 61 patients admitted to the hospital under high suspicion for COVID-19 for whom some degree of longitudinal sampling was available. Two PCR-negative individuals with longitudinal sampling showed clear evidence of seroconversion (sustained, high levels of SARS-CoV-2 RBD specific IgG, IgA and IgM). Rates of suspected false positive results (low OD value

positive results) were least frequent in the IgA (n=5/61) serology assay compared to the IgG (n=9/61) and IgM (n=12/61) assays (**Figure 4.6A-C**). In suspected false-positive serology results, OD values were low, and did not show a clear pattern of seroconversion seen in specimens collected from PCR-positive individuals.

CP Therapy in an infant with Trisomy 21 and COVID-19.

In our second study presented here, we use the assays described above to examine IgA levels in therapeutic convalescent plasma. We first explored IgA antibody levels in samples acquired before and after transfusion of a recently reported infant where significant clinical improvement and evidence of viral clearance were observed shortly after CP therapy¹². This infant was a 3.1 kg term 9-week-old female with a history significant for Trisomy 21 and an unrepaired balanced complete atrioventricular (AV) canal defect who presented to the hospital with respiratory failure initially thought to be due to decompensated heart failure. However, subsequent testing demonstrated that respiratory compromise in this patient was complicated by infection with SARS-CoV-2. Given the patient's underlying congenital heart disease and respiratory compromise in the face of COVID-19, efforts were taken to eradicate the virus. Initial management of the viral infection was essential given that significant post-operative complications are associated with AV canal defect repair in patients with pre-existing respiratory infection¹³⁻¹⁵.

In an effort to clear the virus, a 14-day trial of remdesivir was initiated. However, despite this intervention, the patient remained PCR positive following repeat SARS-CoV-2 testing (Figure 1A). While very little was known regarding the effectiveness of CP in COVID-19 patients, especially infants with congenital heart disease, the empirical use of CP was considered to treat the ongoing viral infection and prepare the patient for AV repair. At the time of CP therapy, CP units or patients were not routinely evaluated for

anti-SARS-CoV-2 antibodies prior to transfusion. However, we were able to retrospectively perform limiting dilution analysis using SARS-CoV-2 ELISAs for antiviral IgG, IgM, and IgA on residual samples obtained pre- and post-transfusion from the infant as well as samples from the CP donor units themselves.

Characterization of SARS-CoV-2 Antibody Changes after CP.

IgM, IgG and IgA antibody levels against the receptor binding domain (RBD) of SARS-CoV-2 (antibodies that correlate strongly with neutralizing activity¹¹) were found to be high in the first CP unit transfused, while the second unit of CP exhibited low antibody levels overall (**Figure 4.8B**). As samples were available prior to and following the first CP unit, anti-SARS-CoV-2 antibody levels were next evaluated in the patient. Despite having high IgG antibody levels, the first CP unit failed to significantly increase IgG or IgM antibody levels in this patient, perhaps due to the higher titer IgG and IgM antibodies already present (**Figure 4.8B,C**). In contrast, IgA antibody levels increased significantly following CP transfusion (**Figure 4.8B,C**). Shortly after the first CP transfusion, the first SARS-CoV-2 PCR negative results were reported and within 6 days following treatment the patient was extubated and transferred to the floor from the ICU (**Figure 4.8A**)¹². The patient eventually underwent successful repair of the AV defect. While these data do not demonstrate that IgA alone supported viral clearance, the isolated increase in IgA anti-SARS-CoV-2 antibodies following CP transfusion coupled with the proximity of viral clearance and clinical improvement to CP therapy suggests that increases in IgA anti-SARS-CoV-2 antibodies could be associated with infection resolution.

Isotype Specific SARS-CoV-2 Serology in CP Units.

Given the variability in antibody levels between the two CP units used to treat this patient and the possible association of CP-induced increases in IgA anti-SARS-CoV-2

levels and clinical improvement in this patient, we next determined IgM, IgG and IgA levels over a larger pool of CP donor units (n=220). Significant variability was observed in IgM, IgG and IgA levels among CP donors. When stratified based on increasing IgA levels (**Figure 4.9A**), many units also exhibited high levels of IgG and IgM anti-RBD antibodies, suggesting that examination of IgG alone may suffice when seeking to characterize the overall repertoire of anti-SARS-CoV-2 isotypes (**Figure 4.9B**). However, differences between IgA and IgG levels were noted and when units were instead stratified based on IgA negative results, many units were strongly positive for IgG antibodies despite the absence of IgA (**Figure 4.9A**). Similarly, while general correlations across all donor IgM, IgG and IgA levels were observed (**Figure 4.9B**), significant variation existed, suggesting that in addition to total antibody levels, the composition of antibody isotypes can vary between CP units.

Population level longitudinal analysis of SAR-CoV-2 RBD antibodies in hospitalized patients over time.

As differences between IgG and IgA were also observed for our patient, we next examined whether similar differences in isotypes exist among other COVID-19 hospitalized patients (n=201 samples, **Figure 4.10A**). Although lower levels of all three antibody isotypes were observed within the first 10 days following symptom onset, patients nearly uniformly possessed high IgM and IgG anti-RBD antibody levels by 14 days post symptom onset (**Figure 4.10A**). In contrast, some patients continued to exhibit low levels of IgA despite evidence of IgM and IgG seroconversion. To more fully define the overall abundance of IgA, IgG and IgM anti-SARS-CoV-2 antibody levels, we compared their relative levels among CP donors and COVID-19 hospitalized patients. Despite donating 28 days post symptom resolution, IgM antibody levels were sustained in many CP donors, often exceeding corresponding IgA antibody titers (**Figure 4.9B**). IgA

and IgM levels were uniformly lower than corresponding IgG levels in both CP donors and hospitalized patients (**Figure 4.10B,C**). These results suggest that even following prolonged hospitalization, some patients may not generate robust IgA anti-SARS-CoV-2 antibody responses, at least as detected in plasma. Furthermore, as a large percentage of CP units also possess low IgA levels, transfusion of such IgA poor CP units may not possess the ability to increase IgA levels in patients.

Decay rates of SARS-CoV-2 RBD antibodies in repeat convalescent donors.

Differences in IgG, IgM and IgA levels detected between individual CP donors and hospitalized patients motivated us to next define whether differences may also exist in isotype production over time among repeat CP donors. Examination of IgG, IgM and IgA levels in CP units from the same individuals (N=20) at two separate donations demonstrated that while IgG levels were largely sustained, IgM and IgA levels declined more rapidly (**Figure 4.11A-D**). These results suggest that in addition to distinct immune responses that appear to differentially impact the relative abundance of isotypes in a given CP donor, anti-SARS-CoV-2 antibodies have distinct half-lives following symptom resolution.

Correlation of Ortho VITROS COVID-19 antibody test with class-specific RBD endpoint titers in CP units.

While the serological assay we employed is designed to detect isotype specific antibody levels, some blood providers utilize the Ortho VITROS test for total anti-SARS-CoV-2 antibody assessment. This assay is designed to examine the presence of SARS-CoV-2 specific antibodies irrespective of isotype. However, whether this test is influenced by a given isotype or may accurately correlate with IgA levels remains incompletely understood. To determine whether this approach provides sufficient information regarding

IgA antibody levels in particular, we compared titers with signal to cutoff (S/Co) values reported by the instrument. IgG anti-SARS-CoV-2 antibody titers exhibited the highest correlation, with an R^2 value of 0.52 (**Figure 4.9E**). In contrast, neither IgA nor IgM antibody levels exhibited a strong S/Co correlation, suggesting that this approach, while capable of assessing the presence or absence of anti-SARS-CoV-2 antibodies, does not possess the ability to accurately assess IgA anti-SARS-CoV-2 antibody levels.

Discussion

We report a comparative analysis of antibody-class specific SARS-CoV-2 serology testing for diagnosis of COVID-19 in the in-patient setting. Overall, the performance of serology testing improved with time after symptom onset and PCR testing in this population. Our results also suggest that IgA serology may exhibit increased specificity for diagnosis of COVID-19 in hospitalized patients compared to IgG or IgM serology. Most COVID-19 patients show evidence of virus neutralizing antibodies 7-11 days post exposure or within the first two weeks of symptom onset(206). While the timing of seroconversion may seem to preclude the use of serology testing in the acute setting, severe COVID-19 typically presents in the second week after symptom onset(2), coinciding closely with the window in which diagnostic serology testing would be clinically useful—particularly in patients with high pretest probability (PTP). It is reasonable, therefore, to consider and compare the utility of antibody testing for diagnosis of SARS-CoV2 infection in the hospital setting. Serology testing in patients being admitted to the hospital for suspected SARS-CoV-2 infection may therefore complement PCR testing and improve the diagnostic capacity and confidence of healthcare systems and treating physicians.

The majority of tests that have been designed to examine seroreactivity with SARS-CoV-2 to date rely on IgM, IgG or total Ig antibody levels (219). As IgA is the

primary class of antibody produced during active mucosal infections (220), the production of IgA specifically following exposure to SARS-CoV-2 may in part be responsible for the assay characteristics observed in the present study. In addition, with the advent of effective vaccines, which typically produce a robust IgG response, the use of class-specific serology may have additional utility in distinguishing vaccine recipients from those experiencing or recovering from natural infection. While circulating IgA can come from multiple sources, including tissue resident plasma-blasts, bone marrow plasma blasts, and damaged mucosal tissues, its presence in circulation may be a particularly useful biomarker of disease. Two recent studies of the humoral immune response during acute SARS-CoV-2 infection highlight the importance of the IgA response. Sterlin et al. show that the IgA responses occur shortly after symptom onset, peaking in the third week of infection and driven by the clonal expansion of IgA plasmablasts primed for homing to mucosal compartments(212). Wang et al. further demonstrate the potential importance of IgA for protection in a study of convalescent patients, showing that dimeric virus specific IgA more potently neutralizes SARS-CoV-2 than equivalent amounts of IgG (211). These findings suggest that the magnitude and nature of the IgA response is likely to contribute significantly to long term protection and potential efficacy of convalescent plasma therapy.

There are several important strengths and limitations in the present study. The majority of commercial and lab developed tests with EUA report sensitivities and specificities exceeding 95% (219) in samples collected from patients >14 or sometimes >30 days after onset of symptoms(221–223). Specificity analyses also frequently do not focus on pre-pandemic samples from patients under investigation for other infections as well as healthy blood donors(224). We focus our study on a clinically relevant population in our specificity analysis and report the overall sensitivities of our assays regardless of symptom onset in order to provide an accurate picture of the utility of class specific

serology in the acute setting as well as in patients further along in the disease or recovered. Several limitations are also important to note. Sampling was less frequent over the clinical course for the PCR negative population. This was in part due to the nature of our sample collection, which relied on collecting and aliquoting residual sample material from clinical laboratory tests. This lack of available samples, particularly later after symptom onset, may have resulted in an underreporting of serological positivity at later time points for PCR negative individuals in the cohort. Any ELISA based test relies on the performance of detection reagents employed, in this case HRP-conjugated anti human Ig antibodies. In choosing these reagents for a rapidly implemented lab developed clinical test, many practical and analytical variables must be considered, including supply chain, cost, storage requirements, and cold chain. We implemented our assay in the early days of the pandemic using detection reagents that were readily available, stable, and inexpensive. Variability in these reagents is an intrinsic limitation of all ELISA based platforms and should be evaluated as a potential confounding variable. To address these potential issues, we used purified human Ig from each subclass to assess background reactivity of each detection reagent employed. We also tested multiple sample dilutions for negative and positive populations in an effort to maximize sensitivity and address specificity concerns in each assay. Finally, when compared across detection reagents from multiple commercial vendors, relative background signals were consistent in individual samples across conjugate for IgG, IgA, and IgM (**Fig. S5**). The latter finding is most consistent with pre-analytical or sample-intrinsic factors rather than the detection reagent contributing to lack of specificity in the IgG assay. Because of these test-intrinsic factors, strict interpretation of our findings should be limited to the conditions tested for each assay. However, reports of specificity issues on other serology platforms that detect SARS-CoV-2 IgG and our own experience using multiple detection reagents and conditions on pre-pandemic samples add confidence to our observations.

In the second study presented here, we evaluated the distribution of class-specific SARS-CoV-2 antibody levels in convalescent plasma units in order to better understand the heterogeneity that might contribute to reports of varying efficacy of CP. As the implementation of serological assessment tools lagged behind PCR-based diagnostic strategies in the early phases of the pandemic, initial attempts to utilize CP as a therapeutic intervention for COVID-19 understandably relied on PCR confirmed test results in the absence of SARS-CoV-2 antibody assessment prior to transfusion⁸⁻¹⁰. This is exemplified by the clinical case we present here, where the antibody levels were not only unknown, but also found to be highly variable in each unit once tested. This variability, particularly with respect to IgA SARS CoV-2 antibody levels, prompted us to examine a wider number of CP donors, which likewise demonstrated significant differences in both total SARS CoV-2 antibody levels and individual SARS CoV-2 isotypes. Importantly, IgG levels did not correlate sufficiently with IgA levels to infer IgA SARS-CoV-2 content in a given unit. Thus, while serological tests are now routinely employed in blood donor centers and certainly enhance the practice of CP therapy, most of these platforms do not possess the ability to examine individual SARS-CoV-2 isotypes. As IgA is secreted along the respiratory mucosa and little viremia is often detected in patients with COVID-19^{3-5,16,17}, IgA SARS-CoV-2 antibodies represent one variable that may be important when considering optimal approaches to utilizing CP therapy.

In addition to measuring total and isotype specific SARS-CoV-2 antibody levels in CP units, a similar examination of patients prior to CP therapy may be equally beneficial. The results of the present study suggest that most patients develop high titer IgM, IgG and IgA levels >14 days after symptom onset, suggesting that a lack of SARS-CoV-2 antibodies may be less likely to contribute to ongoing symptoms in patients experiencing a protracted course of COVID-19. Consistent with this, several studies suggest that

patients with prolonged COVID-19 often possess low or no detectable virus, while exhibiting responsiveness to anti-inflammatories, such as dexamethasone¹⁸. These results suggest that the later stages of the disease may more likely reflect a misdirected inflammatory response initiated by SARS-CoV-2 than a direct consequence of ongoing uncontrolled SARS-CoV-2 infection. CP therapy may therefore be most promising early in the course of the disease, consistent with recent reports outlining the possible benefit of CP in treating COVID-19¹.

It is important to note that these studies were not designed to examine the exact role of IgA in the overall efficacy of CP therapy; the optimal SARS-CoV-2 titers and overall efficacy of CP therapy in general remains controversial and certainly lies beyond the scope of the present study. Furthermore, whether the lack of IgA SARS CoV-2 antibody levels in plasma reflect a similar deficiency along the respiratory mucosa in an individual patient remains unknown.

Experimental Methods

Sample collection and processing.

Hospital patients diagnosed or under investigation for COVID-19 who were seen in the emergency department and/or admitted at Emory University Hospital and Emory University Hospital Midtown from 3/9/2020 to 5/15/2020 were identified by SARS-COV-2 PCR testing records. In house-validated qRT-PCR results were obtained from the medical records of each admitting institution. Nasopharyngeal swabs were collected by the admitting medical team according to standard hospital procedure for each hospital. Residual serum and heparinized plasma samples from fully resulted clinical laboratory tests were identified and set aside as “discarded tissue” sample in accordance with clinical laboratory director approval. Residual samples were aliquoted by research staff and stored at -80 C prior to research use. The sample cohort utilized in this study had

partial overlap with the smaller cohort utilized in the separate, previously reported clinical IgG ELISA performed in the Emory clinical laboratory (206).

Chart review.

Retrospective chart review of patients in the study cohort was performed by Emory medical students and clinical staff who were in at least year 3 of Medical Doctorate training or currently hold a Medical Doctorate or equivalent degree. Reviewers were blind to the ELISA results at the time of chart review. Patient information and clinical course details were entered into a RedCAP database.

For analysis of disease severity at presentation, four categories were utilized based on COVID-19 specific severity categories developed by the National Health Commission of China and reported in multiple prior studies [citations needed]. These categories were:

- (1) Mild: mild clinical symptoms and no pulmonary changes on imaging;
- (2) Moderate: fever and signs of respiratory infection/ pneumonia changes on imaging;
- (3) Severe: At least one of the following: respiratory rate ≥ 30 /min; oxygen saturation ≤ 93 % in resting condition; arterial partial pressure of oxygen (PaO₂) /oxygen concentration (FiO₂) ≤ 300 mmHg (1 mmHg = 0.133 kPa); respiratory rate ≥ 30 /min; oxygen saturation ≤ 93 % in resting condition; arterial partial pressure of oxygen (PaO₂) /oxygen concentration (FiO₂) ≤ 300 mmHg (1 mmHg = 0.133 kPa)
- (4) Critical: Critical (respiratory failure requiring mechanical ventilation; shock; multiple organ dysfunction/failure; requiring ICU admission).

Retrospective chart review of symptom onset dates was performed using defined criteria. At least one of the following symptoms must have been reported as a new symptom or significant change from the patient's baseline to be considered for symptom onset: cough, shortness of breath or difficulty breathing, fever (including subjective fever), chills, muscle pain, headache, sore throat, loss of taste or smell, rash, or diarrhea. Symptom onset dates were considered valid for this study if a patient-reported exact date or a date approximate within +/- 2 days could be determined with reasonable clinical confidence. For consistency, all symptom onset data entered in the RedCap database were rechecked by one of two reviewers holding medical doctorates (authors MH and HN), with determination of some equivocal dates resolved by consensus.

Chart reviewers were blind to the ELISA results at the time of review. Patient information was entered into a REDCap® database. Symptom onset dates were determined using defined criteria, where at least one of the following needed to be reported as a new symptom on the estimated date of onset (cough, shortness of breath or difficulty breathing, fever (including subjective fever), chills, muscle pain, headache, sore throat, loss of taste or smell, rash, or diarrhea). To enhance symptom onset date reliability, all dates were independently checked by at least one additional chart reviewer.

Coronavirus spike and RBD enzyme linked immunosorbent assays (ELISAs).

Purified recombinant 6x receptor-binding domain (RBD) from the SARS-CoV-2, Wuhan-Hu-1 (GenPept: QHD43416) was kindly provided to the Emory Medical Lab (EML) by Jens Wrammert in the Emory Department of Pediatrics and Vaccine Center (purified as described(206)). A research protocol from the Wrammert group was used as a starting point in the development of the EML assays. HKU1 and OC43 recombinant S1 domains were obtained from the Centers for Disease Control and Prevention. RBDs from alphacoronavirus 229E and NL63 were obtained from SinoBiological. Briefly, coronavirus

RBD or S1 proteins was coated on high-bind ELISA plates at 1ug/mL in PBS overnight at 4°C or at 37°C for 1hr. Plates were then washed 3x with 0.5% PBST and blocked for 30 minutes at RT in ELISA buffer (1% BSA, 0.2% T20 in PBS). Plates were then tapped out after blocking and serum or plasma samples were pre-diluted at 1:20 in ELISA buffer before addition to the test plate at a final dilution of 1:200 for the IgG assays and 1:100 for the IgA and IgM assays. Samples were incubated at room temperature for 30 minutes, washed 3x in 0.5% PBST. HRP-conjugated anti human IgG (Invitrogen, Catalog # 62-8420), IgA (Southern biotek, Catalog # 2050-05) and IgM (Invitrogen, Catalog # 31415) were used for detection. Specificity of each conjugate was tested using IgG, IgM and IgA purified from human serum (Sigma I2511, I8260, I4036) immobilized on high bind plates (**Fig. S1A-C**). Conjugate and sample dilutions were selected to minimize signal loss while avoiding high overall background signal in pre-pandemic negative samples. SigmaFAST OPD was used for development per the manufacturer instructions and reactions were stopped using 1N HCl before reading on a synergy BIOTEK plate reader at a wavelength of 492.

Statistics.

Receiver-operating characteristic (ROC) analysis was performed using Prism 8 (GraphPad). Areas under the curve (AUCs) were compared by generating z scores using the following formula:

$$z = \frac{AUC_1 - AUC_2}{\sqrt{SE_{AUC1}^2 + SE_{AUC2}^2}}$$

To calculate a two-tailed P value, we used the above z scores for each comparison in the normal distribution function (NORMSDIST(z)) of Microsoft Excel. Statistical comparisons of the mean for multiple groups were done using One-way analysis of variance with correction by the Tukey test of p-values for multiple comparisons.

Study approval and ethical statement.

Serum and plasma samples from patients diagnosed with SARS-CoV-2 infection by PCR or under suspicion for COVID-19 (PCR tested with a negative result) were collected in Atlanta, Georgia at Emory University Hospital and Emory University Hospital Midtown. Collection, processing, and storage of these samples was approved under a waiver for the use of discarded samples by the University Institutional Review board (IRB #00022371)

Anti-SARS CoV-2 antibody evaluation.

SARS-CoV-2 PCR confirmed patients were initially identified based on hospital wide SARS-CoV-2 PCR testing results. Residual plasma samples from clinical laboratory tests were collected as “discarded samples”, aliquoted and stored at -80°C prior to analysis for antibody levels. Plasma obtained at the time of CP unit collection was similarly aliquoted and stored at -80°C prior to antibody evaluation. *Purified recombinant receptor-binding domain (RBD) from the SARS-CoV-2 was generated as recently outlined and used as the target¹¹. Briefly, 1ug/mL of purified recombinant RBD in phosphate buffer saline (PBS) was incubated overnight at 4°C or at 37°C for 1hr. Plates were then washed 3x with 0.5% T20 in PBS (PBST) and blocked for 30 minutes at RT in ELISA buffer (1% BSA, 0.2% T20 in PBS). Starting at 1:50, 1:3 serial dilutions were then analyzed for isotype specific anti-RBD antibody levels using anti-human IgA (Southern biotek, Birmingham, AL), IgG or IgM (Invitrogen, Carlsbad, CA) antibodies, followed by O-phenylenediamine dihydrochloride (OPD) for development and a BIOTEK plate reader at 492 nm.*

Study approval and ethical statement.

Sample collection and chart review was accomplished under the approval of the Institutional Review board (IRB #00022371).

Chapter 4 Tables

Table 1. Patient Characteristics		
	SARS-CoV-2 PCR + (n=78)	SARS-CoV-2 PCR- (n=61)
Demographics		
Age, mean years (range)	64.3 (22-100)	59.8 (20-97)
Female, n (%)	29 (47.5%)	33 (42.3%)
Male, n (%)	32 (52.5%)	45 (57.7%)
Race		
African American or Black, n (%)	61 (78.2%)	40 (65.6%)
Asian, n (%)	0 (0.0%)	1 (1.6%)
Caucasian or White, n (%)	15 (19.2%)	20 (32.8%)
Unknown, Unavailable or Unreported, n (%)	2 (2.6%)	0 (0.0%)
Ethnicity		
Hispanic or Latino, n (%)	0 (0.0%)	2 (3.3%)
Non-Hispanic or Latino, n (%)	73 (93.6%)	56 (91.8%)
Unknown or Unavailable, n (%)	5 (6.4%)	3 (4.9%)
*Severity at Presentation		
1 (Mild), n (%)	15 (19.2%)	19 (31.1%)
2 (Moderate), n (%)	45 (57.7%)	25 (41.0%)
3 (Severe), n (%)	9 (11.5%)	0 (0.0%)
4 (Critical), n (%)	9 (11.5%)	17 (27.9%)
Clinical Course		
Intensive Care Unit admission, n (%)	43 (55.1%)	31 (50.8%)
Intubation, n (%)	36 (46.2%)	11 (18.0%)
**Length of hospital stay, mean days (range)	10.2 (0-39)	17.4 (1-48)
Discharge status		
Discharge to home, n (%)	46 (59.0%)	48 (78.7%)
Transfer to another facility, n (%)	14 (17.9%)	6 (9.8%)
Transfer to hospice, n (%)	1 (1.3%)	2 (3.3%)
Deceased, n (%)	15 (19.2%)	2 (3.3%)
Other or still in hospital, n (%)	2 (2.6%)	3 (4.9%)
Sample set characteristics		
Symptom start date available in chart, n (%)	54 (69.2%)	39 (63.9%)
Study samples per patient, mean (range)	6.5 (1-33)	5.1 (1-16)
[†] Symptoms to 1 st study sample, mean days (range)	9.4 (1-25)	5.3 (-2 - 18)
[‡] PCR test to 1 st study sample, mean days (range)	3.6 (-1 - 19)	1.9 (-3 - 14)

Table 4.1. Characteristics for diagnostic serology cohort (evaluated in Figures 4.1-4.7)

Chapter 4 Figures

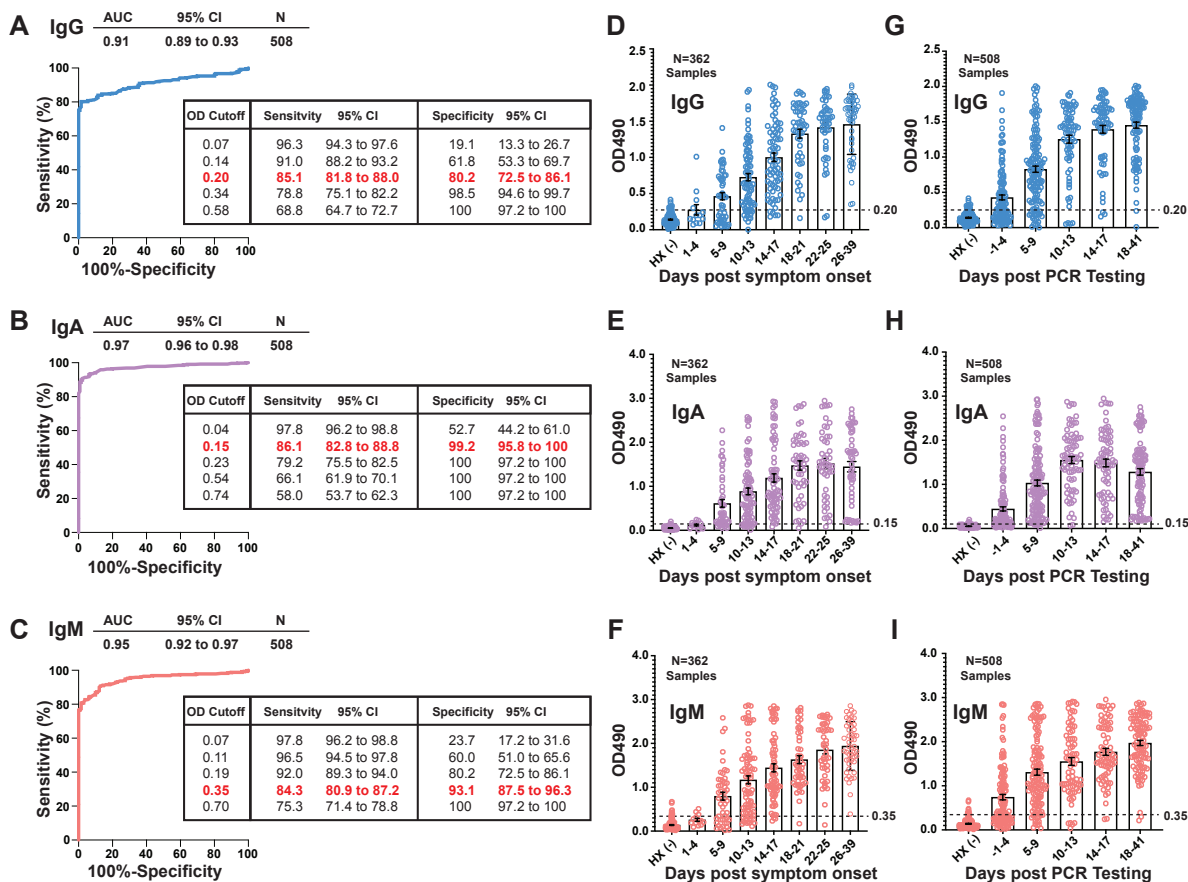


Figure 4.1 Evaluation of class-specific SARS-CoV-2 serology assay performance.

(A-C) Receiver operating characteristic (ROC) analyses of RBD-specific IgG, IgA, and IgM serology in serum and plasma samples from a cohort of hospitalized patients with PCR-confirmed SARS-CoV-2 infection (N=508 samples from 78 individuals). Areas under the curve (AUC), correlative with overall assay performance, are shown with 95% confidence intervals (95% CI). Inset tables indicate sensitivity and specificity at various OD cutoffs with the selected cutoff for each assay highlighted in red. (D-E) IgG, IgA, and IgM OD values are binned and plotted by timing after symptom onset (N=362 samples from 54 individuals). OD values from 131 pre-pandemic serum and plasma samples, which served as negative historical controls (HX -) in these analyses, are plotted to the left of each time series. (G-I) OD values are plotted as in (D-E), instead binning samples using time after PCR testing (N=508 samples from 78 individuals). OD cutoffs are indicated by a dashed line for each assay.

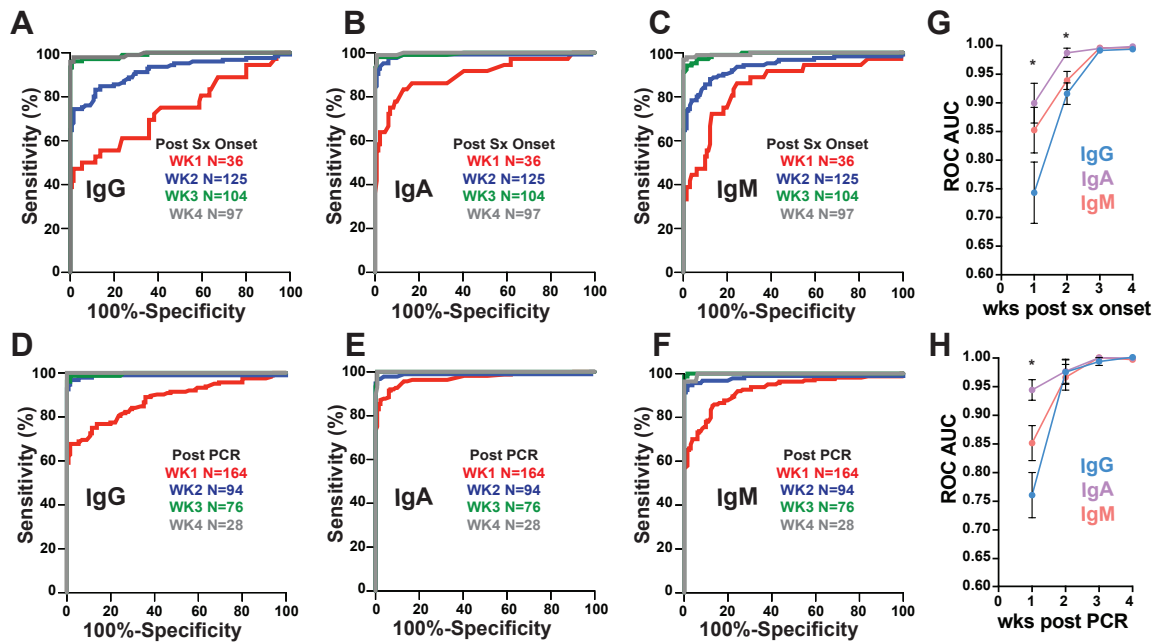
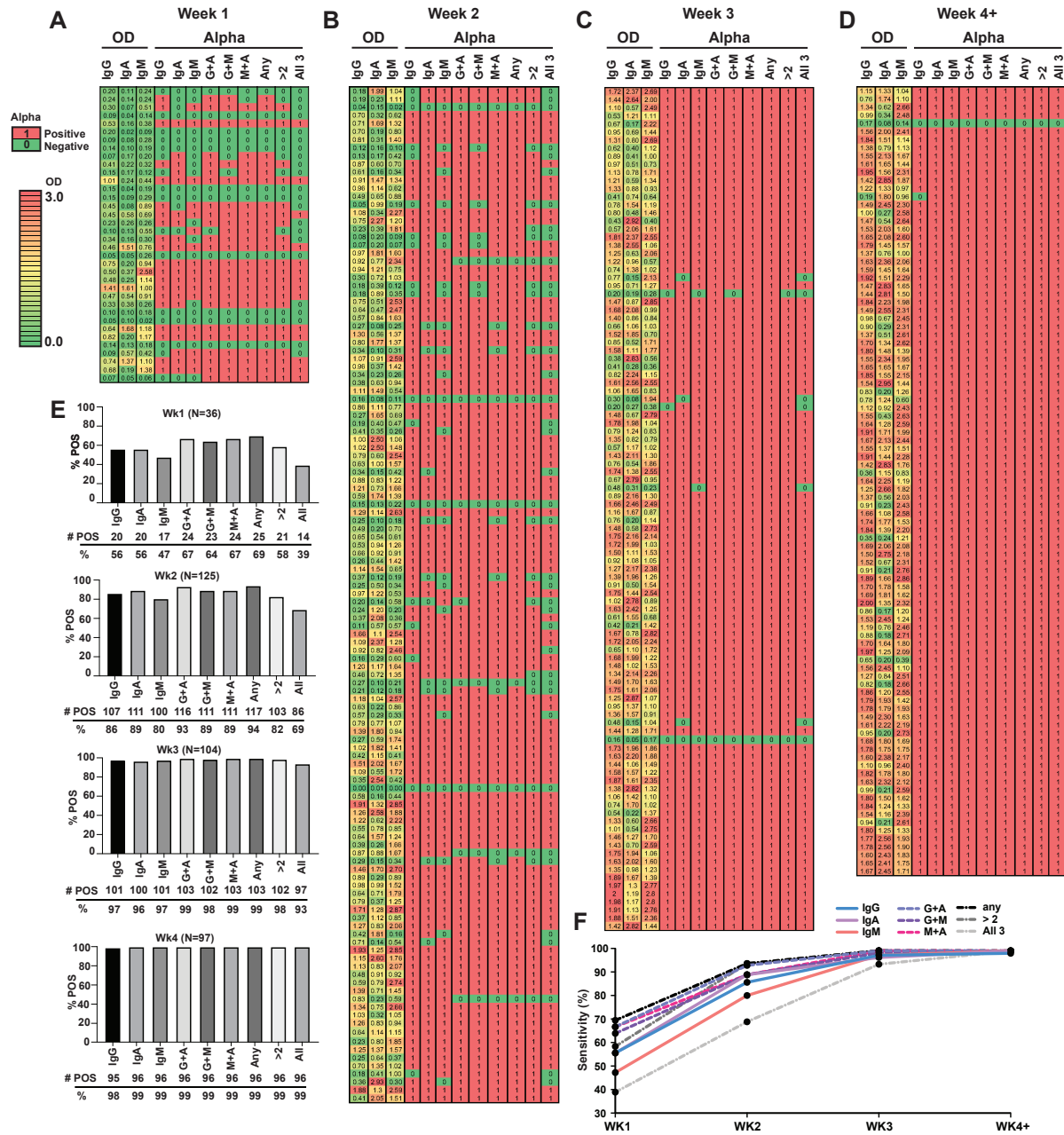


Figure 4.2 Performance of class-specific SARS-CoV-2 serology testing increases over time.

ROC analysis of antibody class specific serology with samples binned into weeks after symptom onset (A-C) or time post PCR (D-F). Areas under the curve (AUC) with standard error (SE) are plotted for these analyses for weeks post symptom onset (G) and weeks post PCR testing (H). Statistical significance was determined by using students' t-tests on Z-scores of AUC and SE values for each ROC curve (* indicates $p < 0.05$). The IgA serology test performed significantly better than IgG serology in samples collected within 1 week of symptom onset (AUC of 0.90 vs 0.74; $P = 0.01$). In addition, IgA (AUC 0.99) performed significantly better than IgG (AUC 0.92) in the second week following symptom onset ($P = 0.0005$). All of the tests exhibited superior performance ($AUC > 0.99$) in samples collected 3 or greater than 4 weeks after symptom onset or > 2 weeks after PCR testing.



Specificity for each assay was determined by testing of 131 historical negatives and is listed for each cutoff in **Fig. 4.1 A-C**.

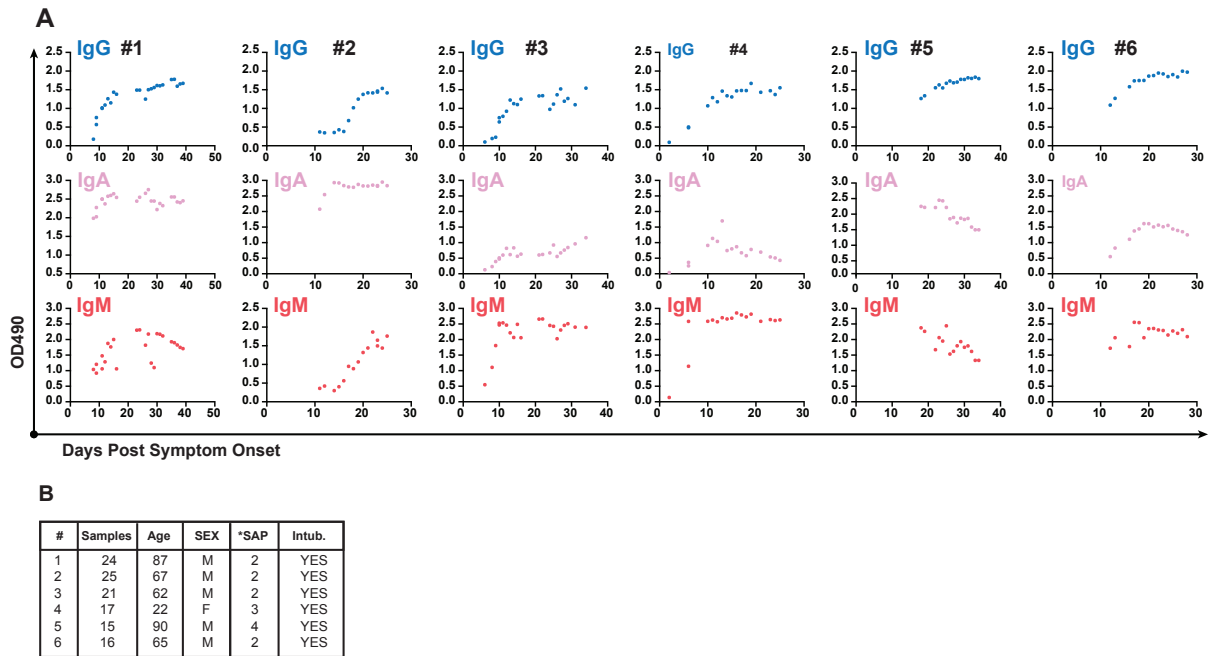


Figure 4.4 Individual antibody responses by OD value over time after symptom onset.

(A) Individual OD values for SARS-CoV-2 RBD-specific IgG, IgA, and IgM are plotted over time post symptom onset for 6 individuals for whom more than 10 simultaneously-tested longitudinal samples were available. (B) Basic characteristics of each individual displayed in A. SAP=symptom severity at presentation.

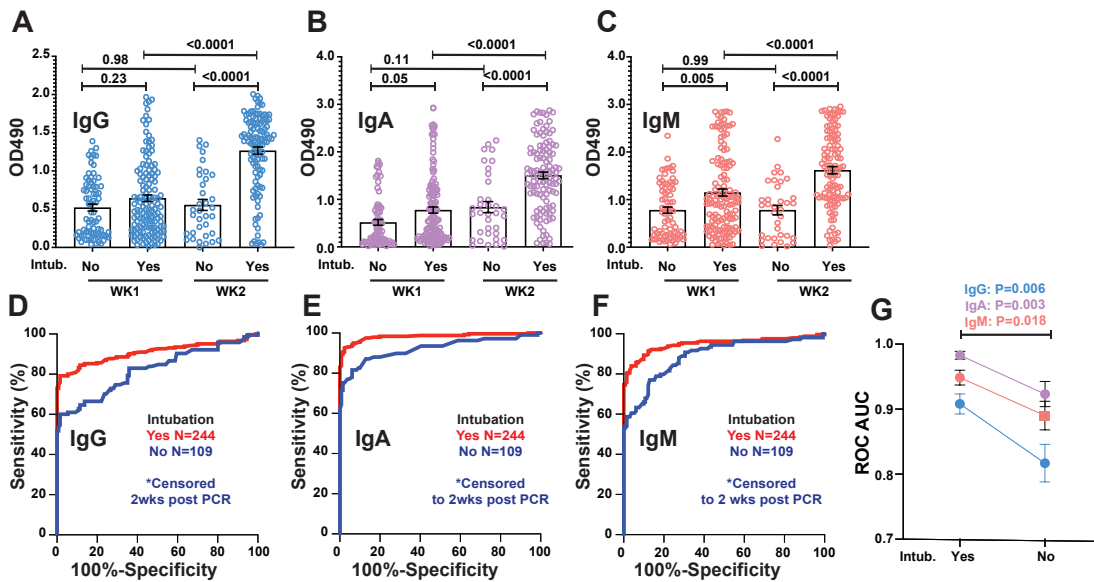


Figure 5 Analysis of assay performance and OD values in samples from COVID-19 patients requiring intubation.

(A-C) OD values are plotted binned by week after PCR testing from 244 samples from COVID-19 patients requiring intubation and 109 samples from patients who did not. To avoid sampling bias due to patients with more severe disease having longer hospital stays, only samples from within the first 2 weeks after PCR testing were included in this analysis. P values with correction for multiple comparison from one-way analysis of variance (ANOVA) are displayed. (D-F) ROC analysis in the above described samples binned by intubation status. (G) Statistical comparison of ROC areas under the curve (AUC) by student's t-test using Z-scores derived from AUC values and standard error (SE).

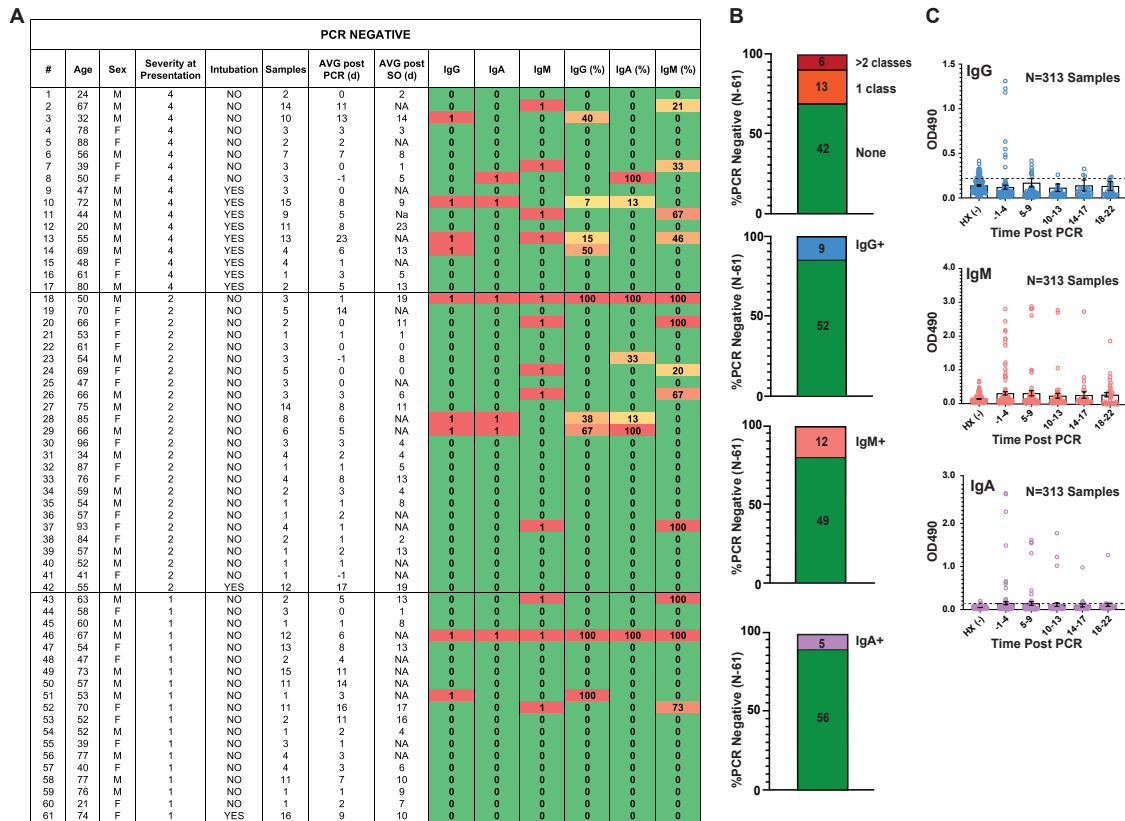
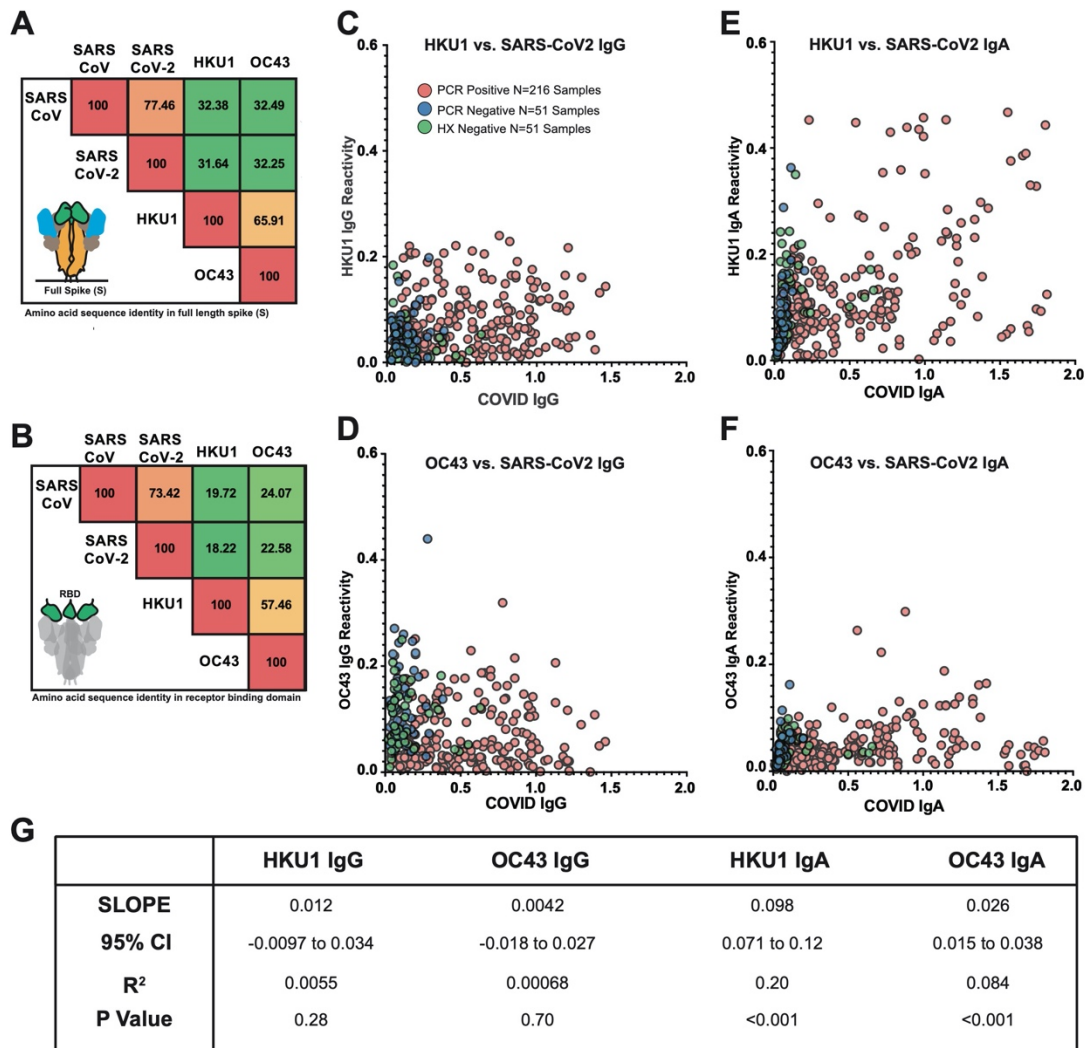


Figure 4.6 Analysis of seroconversion among PCR-negative patients under high suspicion of SARS-CoV-2 infection.

313 samples from 61 patients under high suspicion for COVID-19 were tested for SARS-CoV-2 by PCR during the same time period as the PCR-positive cohort were tested by all three in-house RBD serology assays. (A) The PCR negative cohort and description of sampling is shown organized by severity score at presentation. Alpha responses (1=positive; red, 0=negative; green) for IgG, IgA, and IgM serology are shown along with the percent of samples from a given individual that tested positive by a given assay (also heat mapped to red=high, orange/yellow=intermediate/low, green=no positive results). (B) proportion of individuals who showed evidence of serological positivity by each assay. (C) OD values are plotted over time, binned by time post PCR since very few of these patients provided reliable symptom onset data.



*Linear Regression analysis of cold coronavirus S1 reactivity and SARS CoV-2 IgG and IgA serology among PCR+ COVID-19 Patients

Figure 4.7 Correlation with cold coronavirus reactivity.

(A-B) Amino acid sequence comparison of full-length spike protein (A) and the receptor binding domain (RBD) (B) of human pathogenic coronaviruses SARS-CoV and SARS-CoV-2 with human cold-causing betacoronaviruses OC43 and HKU1. (C-E) OD values from the RBD-ELISA are plotted against reactivity in an ELISA using immobilized S1 domain from OC43 or HKU1 for a subset of samples from PCR positive, PCR negative, and historical pre-pandemic samples. (G) Linear regression analysis between cold coronavirus S1 reactivity and OD in the IgG and IgA SARS-CoV-2 RBD ELISAs.

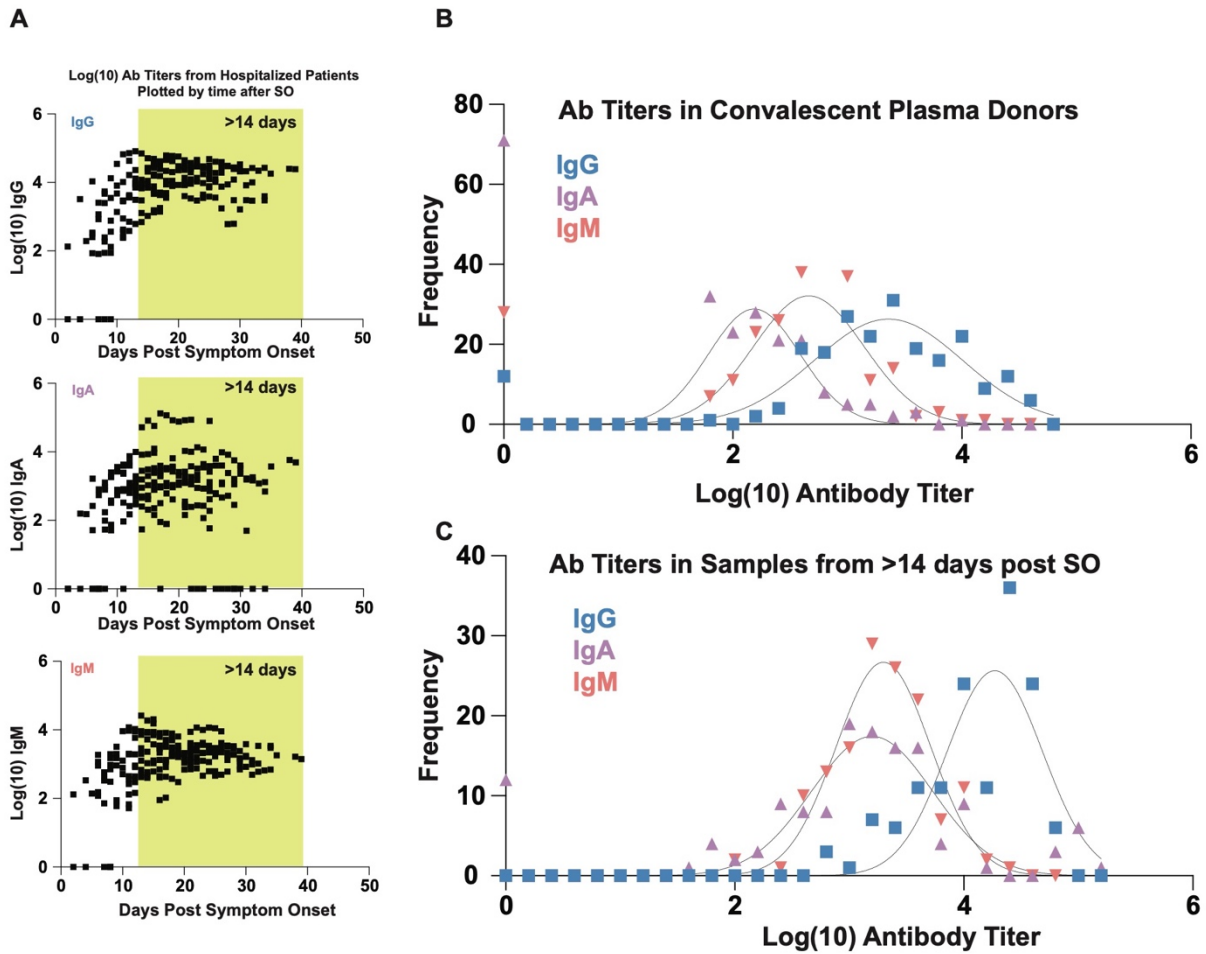


Figure 4.9 Population level longitudinal analysis of SARS-CoV-2 RBD antibodies in hospitalized patients over time.

(A) Logarithmic endpoint titers from 201 samples collected from hospitalized PCR-confirmed COVID-19 patients are plotted over time after symptom onset. (B-C) Frequency distribution (histogram) analysis of class specific SARS-CoV-2 endpoint titers in 220 CP units (B) and 172 longitudinal samples collected >14 days after symptom onset (shaded yellow in 2A)

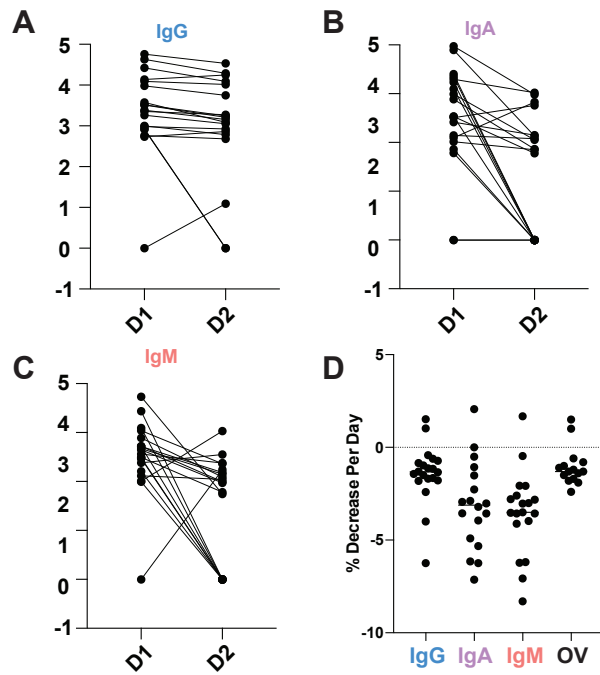


Figure 4.10 SARS-CoV-2 RBD antibodies in repeat convalescent donors.

(A-C) Analysis of antibody levels by log endpoint titer over time in repeat convalescent donors (N=20); repeat donors who did not have detectable antibodies at the outset for a given class were excluded from the % decrease analysis (D).

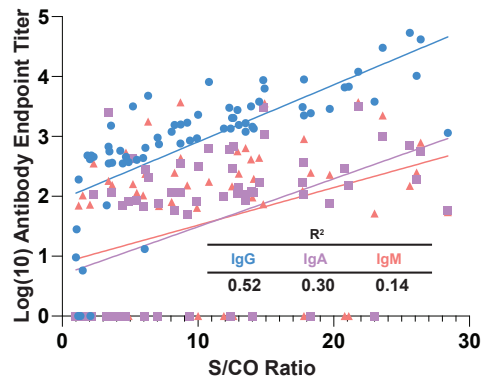


Figure 4.11 Correlation of Ortho VITROS COVID-19 antibody test with class-specific RBD endpoint titers in CP units.

Linear regression analysis of class-specific SARS-CoV-2 antibody levels compared to the signal to cutoff (S/CO ratio) used to characterize units prior to donation. OV = Ortho VITROS; S/CO = Ortho VITROS signal to cutoff ratio value

Chapter 5 Rapid, automated detection of SARS-CoV-2 neutralizing antibodies against native-like vaccine and delta variant spike trimers

Abstract

Traditional cell-based and live-virus methods for detection of SARS-CoV-2 neutralizing antibodies (nAbs) are labor- and time-intensive, and thus not suited for routine use in the clinical lab to predict vaccine efficacy and natural immune protection. Here, we report the development and validation of a rapid, high throughput method for measuring SARS-CoV-2 nAbs against native-like trimeric spike proteins. This assay uses a blockade of ACE-2 binding (BoAb) approach in an automated digital immunoassay on the Quanterix HD-X platform. BoAb assays using vaccine (Wuhan-1) and delta variant viral strains showed strong correlation with cell-based pseudovirus and live-virus neutralization activity. Importantly, we were able to detect similar patterns of delta variant resistance to neutralization in samples with paired vaccine and delta variant BoAb measurements. Finally, we screened clinical samples from patients with or without clinical evidence of SARS-CoV-2 exposure by a single-dilution screening version of our assays, finding significant nAb activity primarily in exposed individuals. In principle, these assays offer a rapid, robust, and scalable alternative to time-, skill-, and cost-intensive standard methods for measuring SARS-CoV-2 nAb levels.

Introduction

Levels of neutralizing antibodies (nAbs) against SARS-CoV-2 and other viruses predict vaccine efficacy and immune protection after natural infection(225–229). In addition, the degree of protection—from sterilizing immunity to prevention of severe disease—correlates strongly with nAb levels at any given time post vaccination or infection(230). Thus, the ability to reliably detect and quantify SARS-CoV-2 nAbs at scale is critical in the ongoing public health effort to reach population level protection in the face of waning immunity and a need for boosters(231). In addition, the emergence of viral variants that escape neutralization by vaccine-induced antibodies underscores the

importance of building efficient and reliable pipelines for nAb assay development as new variants are sequenced and rise to the level of interest or concern (VOI or VOC).

SARS-CoV-2 spike (S) protein is a large homotrimeric glycoprotein, which adopts a metastable prefusion conformation before its high affinity interaction with host-membrane associated angiotensin converting enzyme 2 (ACE-2) (232–234). Native S protein forms two proteolytically cleaved extracellular subunits (S1 and S2), with S1 containing a specific 222 amino acid (AA) receptor binding domain (RBD) that binds to ACE-2(235–237). Thus, S1 promotes receptor recognition and high affinity binding. The S2 subunit, in turn, drives membrane fusion through a fusion peptide (FP), two heptad repeat regions (HR1/2), and a transmembrane domain linked to the cytoplasmic tail(238). To date, studies of neutralizing antibodies elicited by vaccination and natural infection as well as monoclonal antibody therapies have largely focused on antibodies that bind and inhibit interactions through SARS-CoV-2 RBD(239). However, studies have also identified targets of neutralizing activity in SARS-CoV-2 S protein outside of the RBD, including regions in S2 proximal to the FP and HR2¹⁶. These findings were recently bolstered in a study by Garrett et al. using phage deep mutation scanning (Phage-DMS) to comprehensively interrogate immunodominant epitopes of antibodies in SARS-CoV-2 convalescent plasma as well as routes of antibody escape by the virus. This study independently identified non-RBD epitopes for neutralizing antibodies in FP and HR2(76). Together these findings highlight the importance of closely approximating the native structure and domain organization of spike in any robust assay for SARS-CoV-2 neutralizing antibodies.

Current gold-standard assays for measuring nAbs against SARS-CoV-2 require live, replication-competent wild virus isolates or infectious molecular clones(206, 240). While these assays are important tools for research, they require a biosafety level 3

(BSL3) environment, are difficult to standardize, and are poorly suited for any scaled clinical application due to facilities, personnel, and safety requirements. A second tier of widely accepted nAb assays employ replication incompetent reporter viruses—commonly using backbones derived from either HIV or VSV—pseudotyped with SARS-CoV-2 Spike (S)(241–243). These pseudovirus neutralization assays (PNAs) require only BSL2 working conditions and can be scaled for higher throughput. However, both live and pseudoviral assays require use and maintenance of living target cells, which introduces technical variability as well as regulatory complications to clinical testing operations that may seek to employ them. Furthermore, they are manual, labor-intensive assays with turn-around-times of several days. Finally, for lentivirus based PNAs, serum and plasma from patients receiving antiretroviral therapy or pre-exposure prophylaxis for HIV may contain inhibitors of pseudovirus activity non-specific to SARS-CoV-2.

To address these limitations, we developed and validated a rapid, automated, high throughput blockade of ACE2 binding (BoAB) assay for SARS-CoV-2 nAb activity against both vaccine (Wuhan-1) and delta (B.1.167.2) variant native-like trimeric spike proteins. This assay is performed on the ultrasensitive Quanterix-HDX platform, and is amenable to routine clinical use. We validated our BoAB by comparison to gold standard live virus and pseudovirus neutralization assays as well as clinically in samples from a cohort of SARS-CoV-2 exposed and vaccinated individuals collected during a serosurvey in the spring of 2021. In principle, our approach offers a rapid, scalable solution for detection of nAbs against any SARS-CoV-2 variant, against other viral human pathogens, or against emerging viruses of pathogenic potential.

Results

Detection of SARS-CoV-2 neutralizing antibodies by novel automated assay for blockade of ACE-2 binding (BoAB)

The majority of SARS-CoV-2 neutralizing antibodies prevent viral entry by inhibiting the biochemical interaction between S protein and ACE-2. We therefore designed our assay to detect inhibition of this interaction by nAbs in patient samples or select inhibitors using SARS-CoV-2 spike conjugated beads as targets for binding by a biotinylated ACE-2 detector (**Figure 5.1A**). These reagents were then used in a custom three-step assay on the Quanterix HD-X platform (**Figure 5.1B**). To compare and quantify levels of neutralization from our BoAB assays, we engineered two primary readouts of the assay: an eight-point titration to identify the 50% inhibitory dilution or concentration (ID50 or IC50), and a single dilution readout calculated as a % of the maximum ACE-2 binding signal for a given spike target bead set. The latter approach was conceived as a potential screening tool for potent neutralizing antibodies while the former titering approach is appropriate for more rigorous comparison among subjects or between candidate inhibitors (**Figure 5.1C**).

In-house generated vaccine strain and delta variant spike proteins adopt native trimeric structures and bind with high affinity to ACE-2.

In order to present authentic, native-like spike targets for neutralizing antibody detection, we utilized a soluble, stabilized prefusion spike ectodomain construct originally designed in work by Hsieh et al²². This construct contains 6 stabilizing proline mutations in S2, which prevent the spontaneous and irreversible formation of a post-fusion state (**Figure 5.2A**). Spike targets for vaccine strain (Wuhan-Hu-1 GenBank: MN908947) and delta variant (B.1.617.2) were produced in human 293F cells and purified by affinity and size exclusion chromatography (SEC). A soluble, human IgG Fc chimera of ACE-2 was produced in a similar system before affinity and SEC. Purity of all in-house generated protein reagents was determined to be >95% using reducing SDS-PAGE. We next confirmed that our spike targets adopt homotrimeric structures in the prefusion

conformation using negative stain electron microscopy NS-EM (**Figure 5.2D,E**) with 2 dimensional class averaging and 3 dimensional reconstruction. Both purified spike targets adopt structures with 3-fold symmetry at the apex and an expected tapering in the S1 to S2 transition (**Figure 5.2B,C**). Finally, we confirmed that our ACE-2 detector bound stably and with high affinity to both prefusion constructs using biolayer interferometry (**Figure 5.2F,G**). Both the vaccine strain and delta variant spike reagents bound the ACE2 detector at a similar steady state level and showed stable, slow dissociation rates. Together these data confirm the authentic structure of our spike reagents and their binding activity toward the ACE2 detector used in our BoAb assays.

Vaccine strain (Wuh-1) BoAb neutralizing activity correlates strongly with corresponding live virus and pseudovirus neutralization results.

To determine the performance of our new test for SARS-CoV-2 neutralizing antibodies, we evaluated the correlation between titering results with the vaccine strain BoAb assay versus live virus and pseudovirus neutralization assays using plasma samples from patients vaccinated against COVID-19. Results from our vaccine strain assay showed strong correlation with results from a gold-standard live virus focus reduction neutralization test (FRNT) (**Figure 5.3A**) as well as strong performance in a ROC analysis using the lowest reported log ID50 (1.17) as a cutoff for activity (AUC 0.94; $P < 0.0001$) (**Figure 5.3B and 3C**). Similarly, our assay correlated strongly with vaccine strain pseudovirus neutralization activity, particularly in samples above the log ID50 limit of quantification (2.0) for our pseudovirus assay (R squared of 0.72; $P < 0.001$) (**Figure 5.3A**). Using this pseudovirus LOQ as a cutoff for positivity, we performed a second ROC analysis and comparing vaccine strain BoAb activity in samples below and above the PNA LOQ. Our assay showed robust performance (ROC AUC 0.94; $P < 0.0001$) with PNA results as a reference (**Figure 5.3B and 5.3C**). Our new assay also showed strong

correlation with levels of receptor binding domain (RBD) IgG and samples with higher levels of neutralizing antibodies as measured by BoAb contained significantly higher levels of RBD binding IgG (**Figure 5.3G and 5.3H**).

Levels of delta variant (B.1.167.2) BoAb neutralization correlate with live and pseudovirus virus neutralization results, accurately reflecting patterns of escape from neutralizing antibodies.

We next evaluated the performance of our assay for delta variant (B.1.167.2) neutralizing activity. We found a strong correlation and robust performance by ROC analysis for our new delta variant BoAb assay (R squared of 0.80; $P < 0.001$) and live delta variant neutralizing activity by gold standard FRNT (**Figure 5.4A-C**). ID50 results from our delta variant assay also correlated strongly with activity in our vaccine strain PNA and the corresponding live virus neutralizing antibody assay though, as expected, with a lower degree of correlation than that seen within strain (R squared of 0.66) (**Figure 5.4D**). ROC analysis revealed a similar performance of the delta variant BoAb assay to the vaccine strain assay using a vaccine strain PNA log ID50 cutoff of 2 for positivity (**Figure 5.4E and 5.4F**). Delta variant BoAb activity also correlated with vaccine strain RBD binding titers though to a lesser extent (**Figure 5.4G**). Finally, we evaluated the decrement between vaccine strain neutralizing antibody activity and delta variant activity, observed consistently in vaccinated individuals and postulated to be, at least in part, responsible for an increased frequency of delta variant breakthrough infections among vaccinated individuals (ref). Importantly, we found a similar pattern of decrement in vaccine strain and delta variant BoAb activity compared to live virus vaccine strain and delta variant FRNT results (**Figure 5.4H and 5.4I**). Together these data suggest that our delta variant assay correlates strongly with gold standard assays for neutralizing activity and may

similarly detect deficits in delta variant specific activity observed among vaccinated individuals and those who experienced infection prior to the emergence of SARS-CoV-2 spike variants with the ability to escape nAbs.

Screening for neutralizing antibody activity by single dilution BoAB among SARS-CoV-2 exposed patient.

An ideal clinical screening test for SARS-CoV-2 neutralizing activity, in addition to being automated and well correlated with accepted standard assays, should not require limiting-dilution analysis which carries significant costs associated with skilled labor and resources. We therefore generated a single dilution screening test at a sample dilution that was well correlated with live-virus neutralizing activity (1:50) (**Figure 5.5A**). Next, we evaluated the correlation between single-dilution blockade of binding at 1:50 with quantitative spike IgG serology, also performed on the quanterix platform in samples from vaccinated individuals at various times after vaccination. We found a strong linear correlation between blockade of binding and levels of spike IgG in samples with spike specific IgG levels between 5 and 100ug/mL. At higher concentrations, blockade of binding was saturated at 100% inhibition. Significant blockade was not detected in samples with less than 5ug/mL of spike specific IgG (**Figure 5.5B**). Finally, the percentage neutralization at a 1:50 dilution was evaluated in a subset of samples from a serosurvey cohort collected in the Emory University hospital system between January and March of 2021 among inpatients and outpatients who received a blood draw during the relevant encounter. Using available SARS-CoV-2 PCR testing data and serological results, we categorized patients into individuals more likely to have neutralizing activity at the time of sampling (exposed responders) and those unlikely to have nAb activity (unexposed, non-responders). Among 278 patients tested, we identified 115 who were serologically positive with evidence of SARS-CoV-2 exposure. 85 patients were

serologically negative without evidence of SARS-CoV-2 exposure at the time of the blood. All individuals who screened positive for significant neutralizing activity (>50% inhibition at a 1:50 dilution) in vaccine strain and delta variant single dilutions assays fell into the exposed responder category or had an unknown exposure status at the time of blood draw. Significantly more neutralizing activity was detected against the delta variant in this cohort, perhaps due to the fact that the circulating strain at the time (B.1.167-Alpha)²³⁻²⁴ carries many of the same spike mutations as the delta variant (**Figure 5.5C**). Together these data provide proof of concept for use and further validation of our multi-variant BoAb tests as screening tools in patients with evidence of SARS-CoV-2 exposure or vaccination.

Discussion

We report the development and validation of blockade of binding assays for the detection of nAbs against multiple SARS-CoV-2 variants. Results from our assays correlate with established methods for nAb detection including live virus FRNT. Unlike these standard methods, our approach does not require cell culture, BSL3 facilities, or extensive liquid handling(240). In addition, we employ spike antigens with native trimeric structure in our assays to capture the breadth of epitopes bound by vaccine and infection induced antibody responses. This latter point is particularly important with the roll out of boosters, which purportedly broaden the antibody response(229). An enhancement in neutralizing activity mediated by breadth of epitope specificity would be difficult to detect using subdomain and non-native spike targets. Our study is limited by availability of gold-standard live-virus neutralizing antibody data and a need to directly correlate activity measured in our assay with known correlates of nAb activity in gold standard cell-based assays. While our data suggest that biochemical neutralization as measured by BoAb correlates well with results from these more established tests, additional work is needed to evaluate the implications of this association for vaccine efficacy and protection after

natural infection. Our study is limited by availability of gold-standard live-virus neutralizing antibody data and a need to directly correlate activity measured in our assay with known correlates of nAb activity in gold standard cell-based assays. While our data suggest that biochemical neutralization as measured by BoAb correlates well with results from these more established tests, additional work is needed to evaluate the implications of this association for vaccine efficacy and protection after natural infection.

Experimental Methods

Serum and Plasma Samples

Samples were from various studies involved at Emory University Hospitals after obtaining the approval and consent from Institutional Review Board.

Protein expression and purification.

Trimeric SARS-CoV-2 Spike (Wuh-1 and Delta B.1.617.2) as well as Angiotensin Converting Enzyme-2 (ACE-2)-IgFC chimera proteins were produced by transfection in FreeStyle 293-F cells using plasmids. Briefly, FreeStyle 293F cells were seeded at a density of 2E6 cells/ml in Expi293 expression media and incubated with shaking on at 37°C and 127 rpm with 8% CO₂ overnight. The following day, 2.5E6 cells/ml were transfected using ExpiFectamine™ 293 transfection reagent (ThermoFisher, cat. no. A14524) according to the manufacturer protocol. Transfected cells were then incubated with orbital shaking for 4-5 days at 37°C, 127 rpm, 8% CO₂. Supernatants containing secreted trimeric ectodomains were collected by centrifugation at 4,000xg for 20 minutes at 4°C. Clarified supernatants were then filtered using a 0.22 µm stericup filter (ThermoFisher, cat.no. 290-4520) and loaded onto pre-equilibrated affinity columns for protein purification. The SARS-CoV-2 Spike trimer and ACE-2 proteins were purified using His-Pur Ni-NTA resin (ThermoFisher, cat.no. 88221) and Protein-G Agarose (ThermoFisher, cat.no. 20399) respectively. Briefly, His-Pur Ni-NTA resin was washed

twice with PBS by centrifugation at 2000xg for 10 min. The resin was resuspended with the spike-trimer supernatant and incubated for 2 hours on a shaker at RT. Gravity flow columns were then loaded with supernatant-resin mixture and washed (25mM Imidazole, 6.7mM NaH₂PO₄.H₂O and 300mM NaCl in PBS) four times, after which the protein was eluted in elution buffer (235mM Imidazole, 6.7mM NaH₂PO₄.H₂O and 300mM NaCl in PBS). Eluted protein was dialysed against PBS using Slide-A-lyzer Dialysis Cassette (ThermoScientific, Cat# 66030) and concentrated using 100 kDa Amicon Centrifugal Filter Unit, at 2000g at 4°C. The concentrated protein eluate was then run and fractionated on a Sepharose 600 (GE Healthcare) column on an Akta™Pure (GE Healthcare). Fractions corresponding to the molecular weight of each protein were pooled and concentrated as described above. Proteins were quantified by BCA Protein Assay Kit (Pierce) and quality was confirmed by SDS-PAGE and Western blotting.

ACE-2 protein expression and purification

The soluble ACE-2 IgFC chimera was expressed as described above. Clarified supernatants were diluted 1:1 with binding buffer before loading on a protein g gravity flow column, pre-equilibrated with 10 ml of binding buffer (Pierce cat.no.21011). Columns were washed with 20 ml of binding buffer, and the protein was eluted in 40 ml of elution buffer. Following elution, samples were first neutralized to pH 7.5 using 1 M Tris, pH 9.0. Eluted protein was dialysed against 50mM Tris (pH7.5), 150mM NaCl using a Slide-A-lyzer Dialysis Cassette (ThermoScientific, Cat# 66030) and concentrated using 50 kDa Amicon Centrifugal Filter Unit, at 2000g at 4°C. Size exclusion chromatography and quality control was performed on the concentrated protein as described above.

Assessment of Spike-ACE-2 binding by biolayer interferometry

6x His-tagged spike was diluted to 50ug/mL in PBS before immobilization on nickel NTA biosensors (fortebio). Association of ACE-2 was monitored using an OctetRED96e instrument (fortebio) in 2-fold dilutions series starting at 100ug/mL for 600s followed by dissociation in PBS for 500s. Tips were regenerated using 10mM glycine and regenerated in 10 mM NiCl₂ before re-loading with equivalent concentrations of spike.

Generation of detector and conjugated beads.

ACE-2 detector biotinylation and spike bead conjugation were performed per the Quanterix Homebrew Detection Antibody Biotinylation and Bead Conjugation Protocols.

1) ACE-2 Biotinylation

Briefly, ACE-2 was buffer exchanged using Amicon filtration into Quanterix biotinylation reaction buffer prior to mixing at 1mg/mL with a 40x challenge ratio of NHS-PEG4-biotin for 30 minutes at room temperature. Cleanup of the biotinylated detection reagent was achieved by a further round of amicon filtration following recovery in biotinylation reaction buffer and determination of protein concentration. A final detector concentration of 0.5ug/mL was used in the assay.

2) Spike conjugation with magnetic beads

Paramagnetic beads were activated after washing with bead conjugation buffer using 9ug EDC (10mg/mL) in a final bead volume of 300ul containing 4.2E8 beads for 30 minutes at 4C with rocking. Following activation, beads were washed with Bead Conjugation Buffer and 300ul cold spike at 0.2mg/mL to the beads followed by incubation at 4C with rocking for 2 hours. Beads were then washed and blocked for 45 minutes at room temperature, followed by a final wash and resuspension in 300ul bead diluent. Spike capture beads were stored at 4C until use in the assay.

Negative Stain sample preparation, data collection and data analysis.

Spike protein was diluted to 0.05mg/ml in PBS prior to grid preparation. A 3 μ L drop of diluted protein applied to previously glow-discharged, carbon coated grids for ~60 sec, blotted and washed twice with water, stained with 0.75% uranyl formate, blotted and air dried. Between 25-35 images were collected on Talos L120C microscope (Thermo Fisher) at 73,000 magnification and 1.97 Å pixel size. Relion-3.1 was used for particle picking, 2D classification and 3D reconstruction.

Figures for Chapter 5

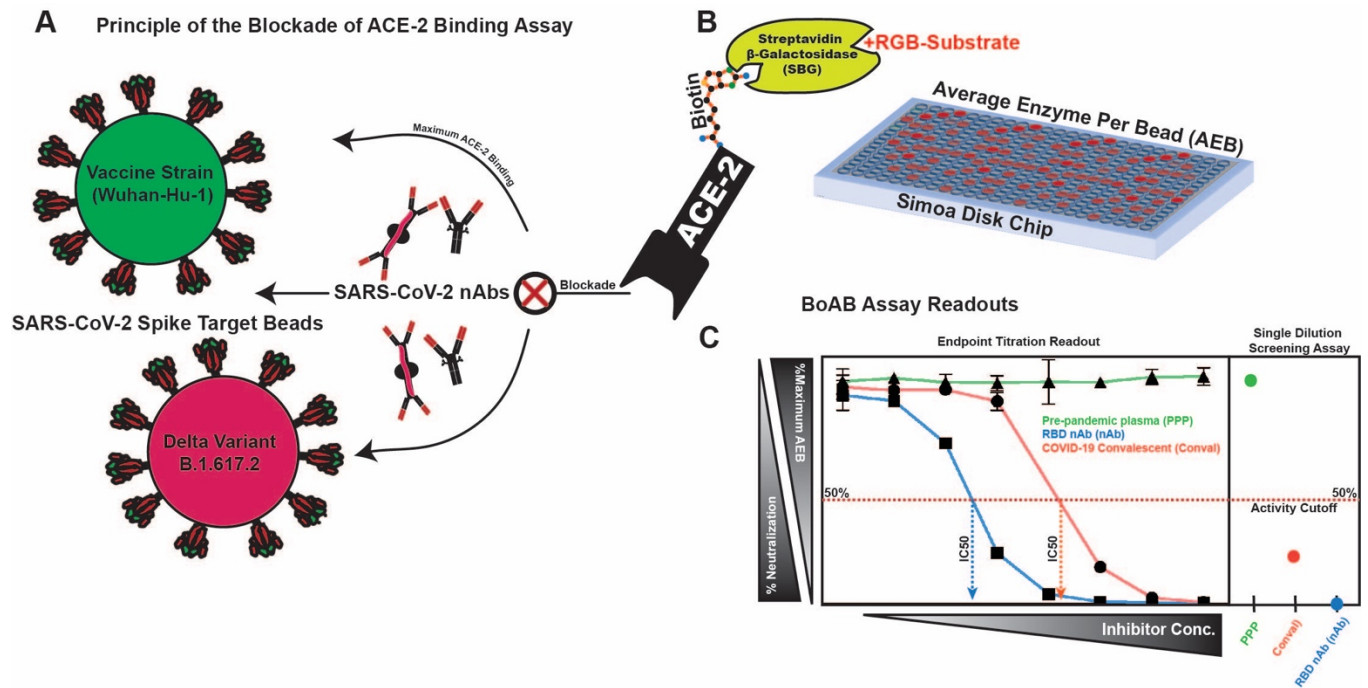


Figure 5.1. Blockade of ACE-2 Binding (BoAB) assay design.

(A) schematic of our blockade of binding assay for SARS-CoV-2 neutralizing antibodies and its primary readouts: 50% inhibitory concentration (IC₅₀) by titration or single dilution screening at a sample dilution of 1:50. **(A)** Detection of inhibitors of the ACE-2/SARS-CoV-2 spike interaction is achieved using an in-house purified and biotinylated human ACE-2 detector reagent. The ACE-2 binding signal is amplified by streptavidin-beta-galactosidase and a fluorescent RGB-Substrate. **(B)** The entire assay is automated and performed using single molecule array (SIMOA) technology on the Quanterix HD-X platform with a readout of average enzymes per bead (AEB). **(C)** Processed data from two assay readouts: titrating for an IC₅₀ (curves to the left) and screening for inhibition at a single sample dilution (right box).

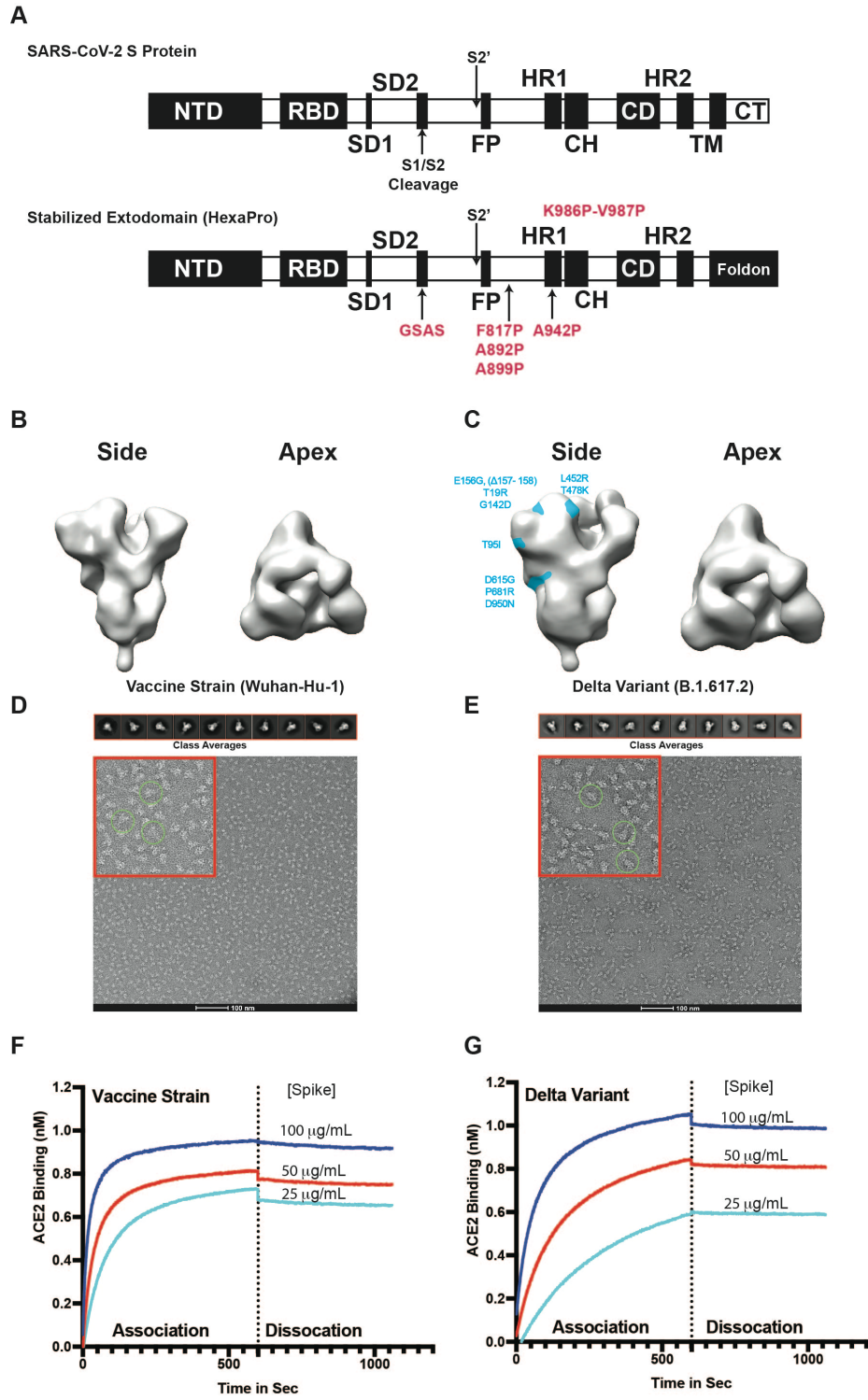


Figure 5.2 Development and validation of SARS-CoV-2 vaccine strain and delta variant prefusion ectodomain spike targets for use in blockade of ACE-2 binding assay (BoAB).

(A) Domain organization diagrams of SARS-CoV-2 S protein and the HexaPro soluble trimeric ectodomain construct used in our assay. (B) 3D reconstruction from negative stain electron microscopy class averages of our purified vaccine strain trimeric ectodomain. (C) 3D reconstruction from negative stain electron microscopy class averages of our purified delta variant (B.1.617.2) trimeric ectodomain with significant amino acid substitutions mapped to the side view in light blue. (D,E) Raw negative stain electron micrographs for purified vaccine strain (left) and delta variant (right) trimers. Examples of native-like structures are encircled in the zoomed view, highlighted in a red cutout for each micrograph. 2D class averages of various trimer orientations derived from the raw micrographs are shown in the upper panel and used for the 3D reconstruction shown in Panels C and D. (F,G) Biolayer interferometry analysis of each spike variant binding to an immobilized recombinant ACE-2 IgG Fc-chimera, the biotinylated form of which serves as the detector in our BoAB assay.

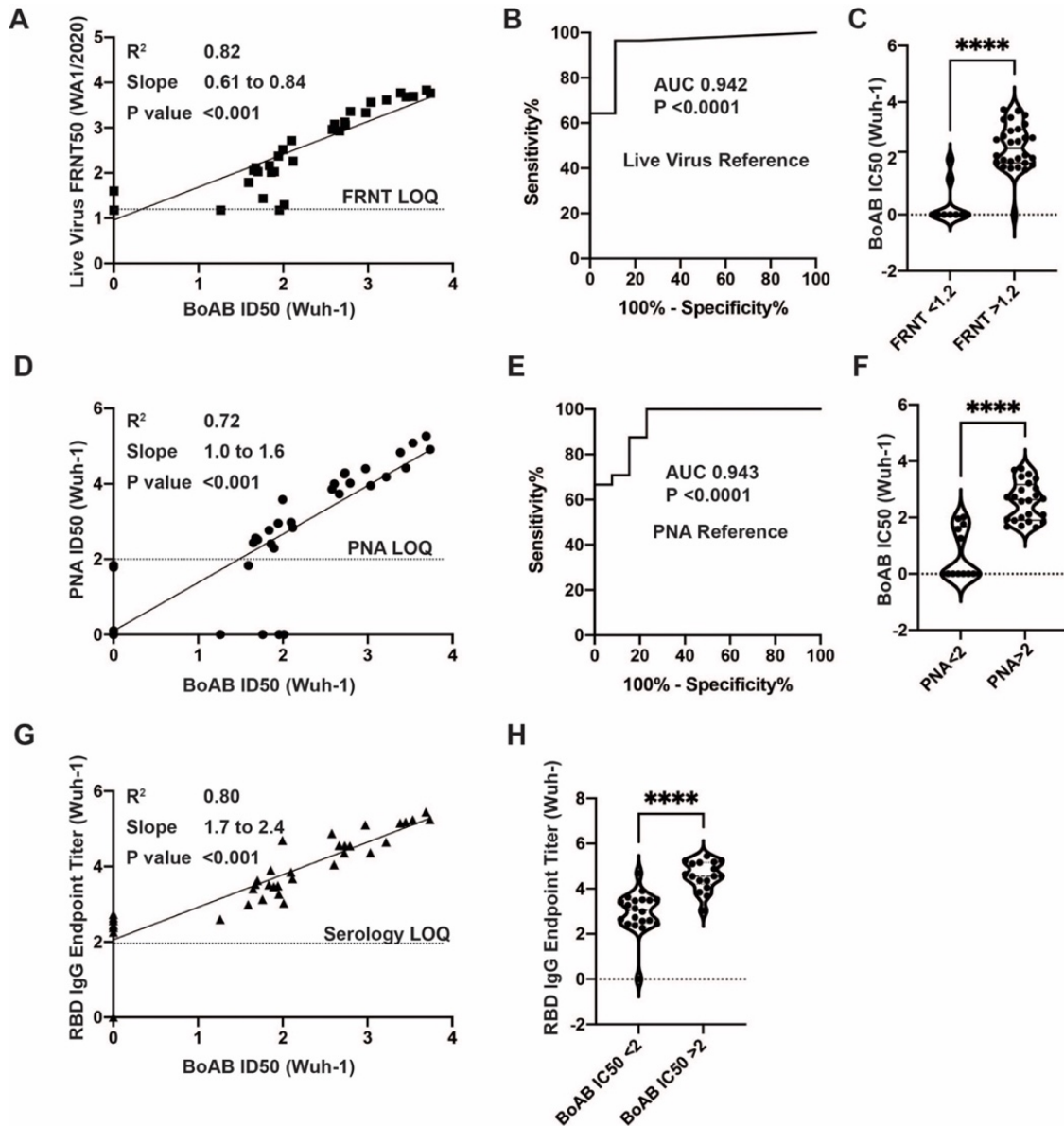


Figure 5.3. Correlation of vaccine strain BoAB IC50s with pseudovirus neutralization and live virus neutralization assays (LVN and PNA).

(A) Linear regression analysis of vaccine lineage (Wuh-1 & WA1/2020) live virus 50% focus reduction neutralization activity (FRNT50) against ID50s in the vaccine strain BoAB. The absolute value of the log dilution factor at which a sigmoidal curve (fit to duplicate eight-point dilution series for each sample) crossed 50% is plotted for the BoAb assay. (B,C) Receiver operator characteristic (ROC) curve and categorical comparison of the vaccine strain BoAB using a live virus FRNT cutoff of 1.17 (representing a linear dilution of 1 in 15) as the reference standard for neutralizing activity. (D) Linear regression analysis of vaccine strain (Wuh-1 & WA1/2020) pseudovirus 50% inhibitory dilution (ID50) against ID50s in the vaccine strain BoAB. (B,C) Receiver operator characteristic (ROC) curve and categorical comparison of the vaccine strain BoAB using a pseudovirus neutralization ID50 of 2 (representing a linear dilution of 1 in 100) as the reference standard for neutralizing activity. (G) Linear regression analysis of vaccine strain (Wuh-1 & WA1/2020) receptor binding domain (RBD) specific IgG titers against IC50s in the vaccine strain BoAB. Values are plotted as in (A) using an optical density cutoff of 0.2 to quantify levels of binding antibodies. (H) Comparison of RBD IgG endpoint titers in samples with vaccine strain BoAB activity less than or greater than a log IC50 of 2. Statistical significance was evaluated by unpaired non-parametric t tests ns=not significant,*P<0.05, **P<0.01, ***P<0.001,****P<0.0001.

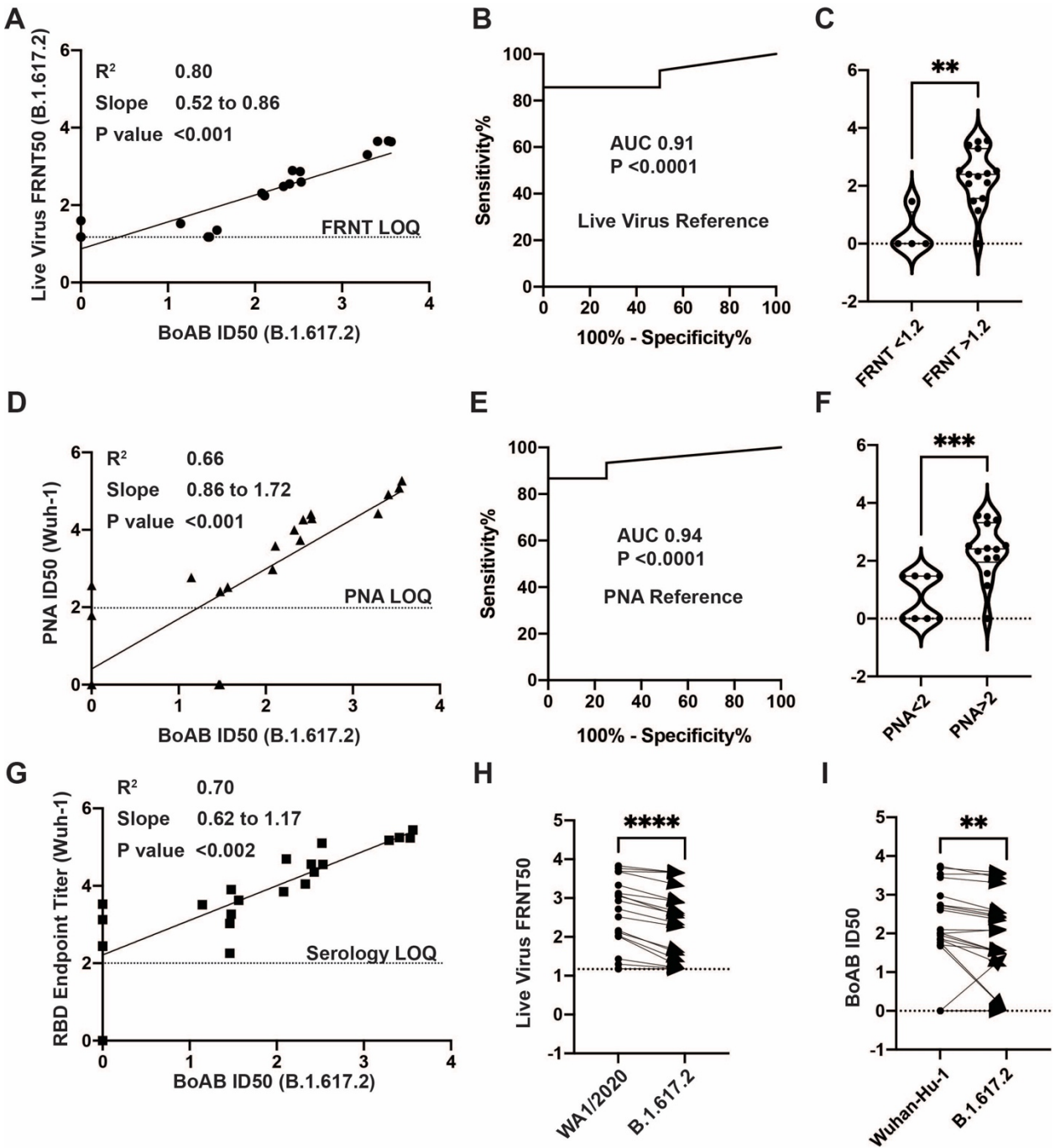


Figure 5.4. Correlation of delta variant BoAB ID50s with pseudovirus neutralization and live virus neutralization assays (PNA and LVN).

(A) Linear regression analysis of delta variant (B.1.617.2) live-virus FRNT 50% inhibitory concentration (ID50) against ID50s in the delta variant BoAB. Values are plotted as in (A). (B,C) Receiver operator characteristic (ROC) curve and categorical comparison of the delta variant BoAB using a live virus FRNT cutoff of 1.17 (representing a linear dilution of 1 in 15) as the reference standard for neutralizing activity. (D) Linear regression analysis of vaccine strain (Wuh-1 & WA1/2020) pseudovirus 50% inhibitory concentration (ID50) against ID50s in delta variant (B.1.617.2) BoAB. (E,F) Receiver operator characteristic (ROC) curve and categorical comparison of the delta variant BoAB using a pseudovirus neutralization ID50 of 2 (representing a linear dilution of 1 in 100) as the reference standard for neutralizing activity. (G) Linear regression analysis of vaccine strain (Wuh-1) receptor binding domain (RBD) specific IgG titers

against ID50 values in the delta variant BoAB. Values are plotted as in (A). (H,I) Paired comparison of live virus FRNT50 and BoAB ID50 values between vaccine strain lineage (Wuhan-Hu-1 or WA1/2020) and delta variant assays. Statistical significance was evaluated by paired non-parametric t tests ns=not significant, *P<0.05, **P<0.01, ***P<0.001,****P<0.0001.

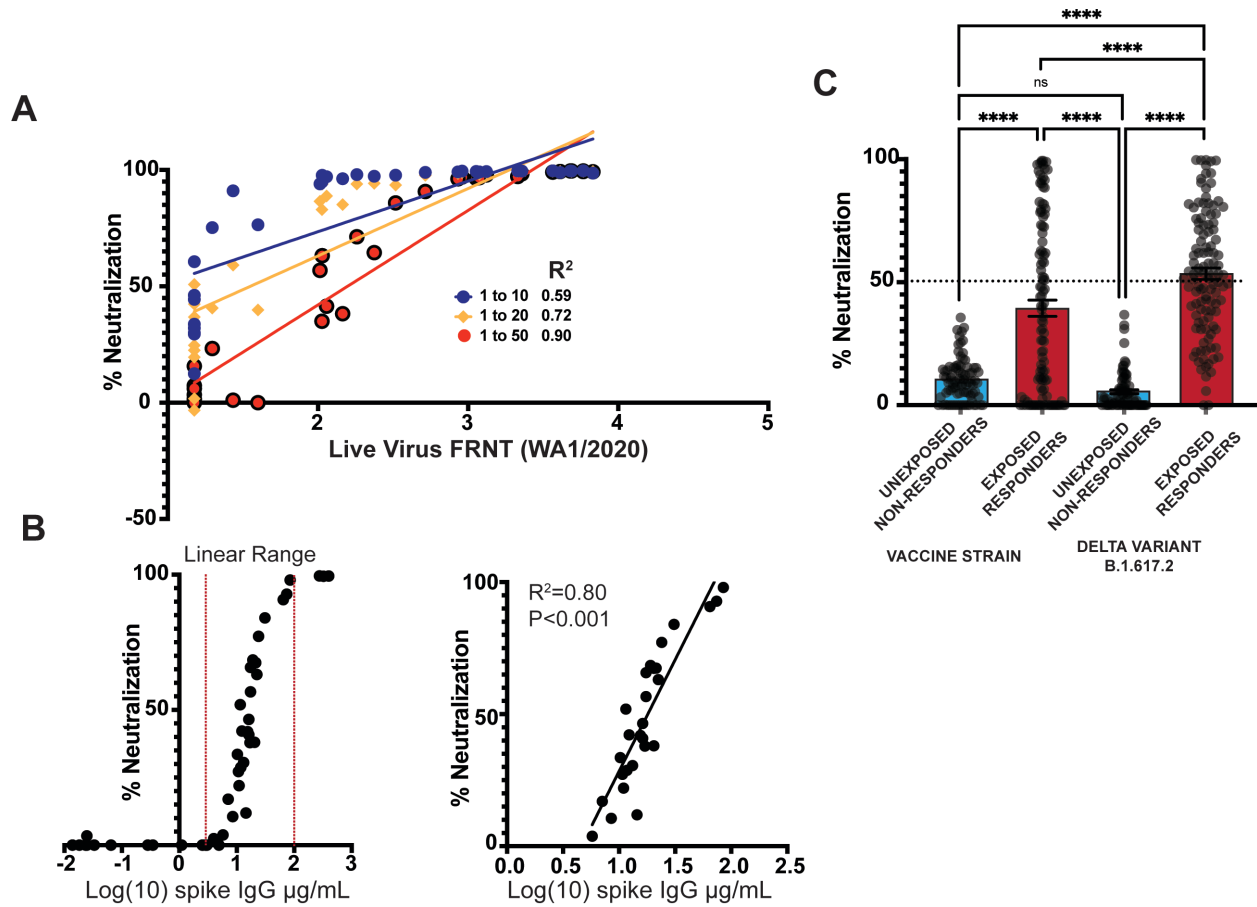


Figure 5.5. Detection of neutralizing antibodies by single dilution BoAB among SARS-CoV-2 exposed patients

(A) Screening by linear regression analysis of various single plasma dilution activities (1 to 10, 1 to 20, and 1 to 50) for correlation with WA1/2020 live virus FRNT ID50. R squared values are shown for each regression. (B) Correlation of quantitative anti-spike IgG levels in vaccinated individuals with 1:50 single dilution BoAb. Overall correlation is plotted with a separate linear regression censored to samples with inhibition in the linear range (C) Comparison of single dilution delta and vaccine strain neutralizing antibody activity in patients with or without evidence of SARS-CoV-2 exposure and seroconversion from a serosurvey conducted in the spring of 2021 at Emory University Hospital Midtown. Statistical significance was evaluated by unpaired non-parametric t tests ns=not significant, * $P<0.05$, ** $P<0.01$, *** $P<0.001$, **** $P<0.0001$.

Chapter 6 Conclusions and Outlook

SARS-CoV-2 Serological Tests: Then and Now

The role of serological testing in COVID-19 has shifted from possible diagnostic utility to primarily use as a correlate of protection after vaccination or natural infection. Our work in the early stages of the pandemic response contributed to the development of serological tests which were used by the Emory healthcare system early on as a confirmatory diagnostic or to evaluate evidence of exposure. We then leveraged these tests to evaluate the antibody components of convalescent plasma, finding significant heterogeneity in antibody class among units that were only screened for IgG content(14, 244). These studies added to the growing body of evidence that characterized convalescent plasma was needed in order to truly understand the efficacy of this therapy. This has been made evident in more clinical studies, which have shown that the early administration of CP with high neutralizing titer is necessary to see clinical benefit(245). This work has important implications for future pandemics, in which characterized CP with boosted efficacy may be the first line of defense against severe illness, prior to the development of transfusion products like virus-specific immune globulin or therapeutic monoclonal antibodies(246). In future work, more detailed considerations of IgA subclasses and configurations, including levels of IgA₁ and IgA₂ in addition to the relative concentration of dimeric versus monomeric IgA present in CP units and hospitalized patients may also be important when considering key characteristics of this therapy. The heterogeneity in IgA SARS-CoV-2 antibodies in both CP donors and patients, in addition to the more rapid decline of IgA than IgG SARS-CoV-2 antibodies following subsequent donations, suggest that unique features of humoral immunity may need to be considered when exploring ways to fully optimize or even determine whether CP is actually effective in treating this disease. Exploring these variables in larger studies may also be especially important when seeking to fully define the risk benefit ratio of this therapy. While early

studies suggest that CP therapy may be safe⁹, the long-term complications that may arise from this therapy, including thromboembolic events that commonly complicate COVID-19^{19,20}, have been more difficult to ascertain. Like delayed type hemolytic transfusion reactions²¹⁻²³, these complications may not be apparent during or even shortly following transfusion and therefore may be more easily missed given the propensity of hospitalized patients with COVID-19 to experience underlying thromboembolic complications^{19,20}. Thus, while intriguing, these observations are correlative in nature and therefore establishing the role of IgA in CP treatment efficacy is not possible with this study. However, our results suggest that IgA antibody levels may be an important consideration when seeking to characterize CP units and patients who may benefit from this approach.

Virus neutralizing activity is the functional capacity of serum antibodies to prevent cell entry by the virus. This activity appears rapidly after SARS-CoV-2 infection and vaccination and has been shown to persist for several months. As an extension of our serological test development activities, we developed a high-throughput blockade of binding assay which can be rapidly modified in response to emergent variants of concern. In addition to further validation and comparison with gold standard methods of detection, we have also begun to develop a multiplexed version of the test which will include omicron, delta and vaccine strain variants. These platforms, which are both adaptable and conform to the limitations and needs of clinical laboratory testing are needed for larger scale characterization of herd immunity and can be used to rapidly assess the consequences of new or putative mutations in the spike protein. This system fulfills one of our goals, which we set forth at the beginning of the pandemic, to establish a pipeline for rapid development and deployment of novel serological tests and other diagnostic platforms at Emory.

Viral antigenemia: Implications for diagnosis

COVID-19 manifests on a broad spectrum of clinical severity from asymptomatic or paucisymptomatic (~50%) to more severe disease requiring hospital care. Prior to the emergence of less pathological variants like omicron and widespread vaccination approximately 3-10% of patients required hospitalization(249, 250). Among those requiring hospitalization, approximately 20% progressed to life-threatening severity, which manifests as respiratory failure and ARDS as well as pulmonary and systemic microvascular complications leading to multi-system organ failure(118). Much of the early pathology associated with SARS-CoV-2 infection is directly driven by viral damage to infected lung tissue. Virus-mediated damage as well as pattern recognition pathways lead to cytokine production and recruitment of innate immune cell populations, which can further damage alveoli while clearing virally infected cells(251). Indeed, compared to other coronaviruses, SARS-CoV-2 has been shown to elicit more systemic cytokine production, particularly of IL1 and IL6(252). Together, these viral and immune factors lead to leak of viral nucleic acid and viral proteins, including nucleocapsid, into circulation.

In our studies describing this phenomenon, we first validated the use of nucleocapsid detection in blood samples as a high performing diagnostic tool particularly for acute SARS-CoV-2 infection(253). While the data from this study is highly suggestive of a link between the dynamics of nucleocapsid antigenemia and the kinetics of active viral replication (AVR), without paired respiratory sampling, we were unable to definitively describe viral antigenemia as a surrogate for AVR. To address this, we are following up the diagnostic component of this work by conducting a prospective study in which paired blood and respiratory samples will be collected for simultaneous evaluation of antigenemia and replication competent virus. These studies, motivated by the work we describe here, will-establish the relationship between nucleocapsid antigenemia and AVR more definitively. Importantly, or studies in rhesus macaques suggest that levels of

antigenemia may most closely be associated with levels of virus in the lung rather than the upper respiratory tract. Nevertheless, as a public health measure, routine screening of blood samples collected in the hospital or by blood banks for evidence of SARS-CoV-2 infection may offer a convenient alternative to continuous respiratory sampling. In addition, the capacity we describe of SARS-CoV-2 nucleocapsid to directly stimulate endothelial cells raises concerns over the safety of infusing blood products collected from those acutely infected with SARS-CoV-2.

Viral Antigenemia: implications for COVID-19 pathology

An important feature of severe COVID-19 is endothelial dysfunction(251), which results from both direct over activation of endothelial cells (endotheliitis) and from virus and immune mediated damage in the lung or other infected tissue. Direct and specific markers of endothelial damage are elevated in patients with severe disease—including glycocalyx constituents, circulating endothelial cells, and soluble VCAM1 (sVCAM1)(254). While endothelial dysfunction is surely driven in part by high levels of circulating cytokines and other inflammatory phenomena, our *in vitro* studies of nucleocapsid antigen and human endothelial cells suggest the possibility that high early levels of antigenemia may have the capacity to directly stimulate endotheliitis, which could contribute to local and systemic microthrombosis and predispose patients to more severe disease. A recent study by Qian et al., confirms that nucleocapsid can stimulate human endothelial cells derived from multiple compartments. They demonstrated that this stimulation could proceed through engagement of TLR2 in reporter cells and was inhibitable by statin treatment(196). However, while compelling, these studies employed nucleocapsid that was produced in mammalian cells and consequently glycosylated. While other studies have shown that nucleocapsid can be glycosylated when artificially targeted through the secretory pathway, impact of glycosylation on the native structure of the protein is unknown(255, 256).

In our work, we purified full-length and CTD nucleocapsid from non-pyrogenic *E. coli*. In addition, our work implicates the full-length protein and the RNA binding domain in particular in nucleocapsid-mediated endothelial activation. Interestingly, we also find that monoclonal antibodies mapped to two different epitopes in the N terminal RNA binding domain can modulate the activity of full-length N protein in an opposing fashion. M08 was shown to block this activity while R04 enhanced it. In preliminary data not included in this dissertation, we recently found that, in addition to enhancing VCAM1 expression, R04 was able to increase secretion of IL6. M08 moderately inhibited secretion in the same context. Additional studies will define the dose dependence of this interaction. In future and ongoing studies, we will also investigate the structural changes that occur with binding of each of these antibodies. In particular, we hypothesize that M08 may stabilize or prevent entry of nucleocapsid protein while the interaction with R04 may increase nucleocapsid processing in the endosomal compartment or destabilize interactions with associated nucleic acids, the release of which could activate pattern recognition pathways. Future studies will also expand upon our findings in endothelialized microfluidics models to better understand the functional consequences of nucleocapsid interactions with endothelial cells in the presence and absence of antibodies and potentially with concomitant inflammatory stimuli such as cytokine stimulation. Overall, the implications of our studies on nucleocapsid antigenemia range from describing its utility as a diagnostic and prognostic biomarker in human populations to a possible mechanism by which it drives systemic pathology in COVID-19.

Appendix 1 Supplementary materials to Chapter 2

Supplementary Tables

<i>Supplementary Table 1. Clinical details of patients with same-day positive SARS-CoV-2 nasopharyngeal NAAT and no antigenemia more than 14 days after diagnosis.</i>	<i>153</i>
<i>Supplementary Table 2. Clinical details for samples in convalescent group with detectable antigenemia.</i>	<i>154</i>
<i>Supplementary Table 3. Same-day negative patients with antigenemia.</i>	<i>157</i>
<i>Supplementary Table 4. Patients with antigenemia and positive SARS-CoV-2 respiratory testing between 14 days prior to and 3 days after sample collection but with more than 14 days of symptoms at the time of samples collection.</i>	<i>158</i>
<i>Supplementary Table 5. Samples categorized in the acute COVID group without antigenemia.</i>	<i>161</i>
<i>*if known.....</i>	<i>161</i>
<i>Supplementary Table 6. Summary of current literature</i>	<i>2</i>
<i>Supplementary Table 7. Outline of blood sample classification scheme and discussion of proposed reasons for variation from the antigenemia as a unique and universal marker of acute infection.</i>	<i>2</i>

Supplementary Figures

<i>Supplementary Figure 1. ROC curves for nucleocapsid antigenemia within subgroups defined by serostatus.</i>	<i>152</i>
<i>Supplementary Figure 2. Timeline of SARS-CoV-2 respiratory testing corresponding to samples with antigenemia in the convalescent group.....</i>	<i>155</i>
<i>Supplementary Figure 3. Comparison of prevalence of comorbidities based on ICD10 codes for samples without and with antigenemia in the convalescent group.....</i>	<i>156</i>
<i>Supplementary Figure 4. Timeline of SARS-CoV-2 respiratory testing corresponding to samples with antigenemia in the late-presenting group</i>	<i>159</i>
<i>Supplementary Figure 5. Timeline of SARS-CoV-2 respiratory testing corresponding to samples without antigenemia in the late-presenting group</i>	<i>160</i>
<i>Supplementary Figure 6. Timeline of SARS-CoV-2 respiratory testing corresponding to samples without antigenemia in the acute COVID group</i>	<i>162</i>

Supplementary Figure 7. Antigenemia levels in late-presenting group stratified by antibody serology..... 163

Supplementary Figure 8. Antigenemia levels in late COVID samples stratified by severity... 164

Supplementary Experimental Methods

Nucleocapsid antibody ELISA

For nucleocapsid antibody testing, 6x-histidine tagged recombinant nucleocapsid protein was produced in *E. coli* and purified by Ni-NTA chromatography before coating on high-binding ELISA plates at 1 µg/mL and 4°C overnight. ELISA plates were then blocked in PBS containing 1% bovine serum albumin (BSA) and 0.2% tween 20, before addition of patient samples pre-diluted at 1:500. After washing, anti-nucleocapsid IgG was detected using horseradish peroxidase (HRP)-conjugated anti-human IgG (Jackson Laboratory). Conjugate and sample dilutions were selected to optimize sensitivity and minimize background in control samples collected prior to the pandemic. ELISA optical density (OD) cutoffs for seroconversion were chosen by receiver operating characteristic (ROC) analysis with area under the curve for all assays greater than 0.95 in samples collected >14 days post symptom onset in PCR confirmed SARS-CoV-2 cases

Assignment of COVID-19 status to blood samples

Samples were categorized and labeled as follows. First, if the patient had *never tested positive* for SARS-CoV-2, a blood sample was labeled *negative* only if negative respiratory SARS-CoV-2 testing was recorded on the same day as the blood sample (**Figure 2.1A**). Blood samples with no record of positive SARS-CoV-2 testing and without same-day SARS-CoV-2 testing were excluded from analysis due to uncertainty of COVID-19 status at the time of blood sample collection.

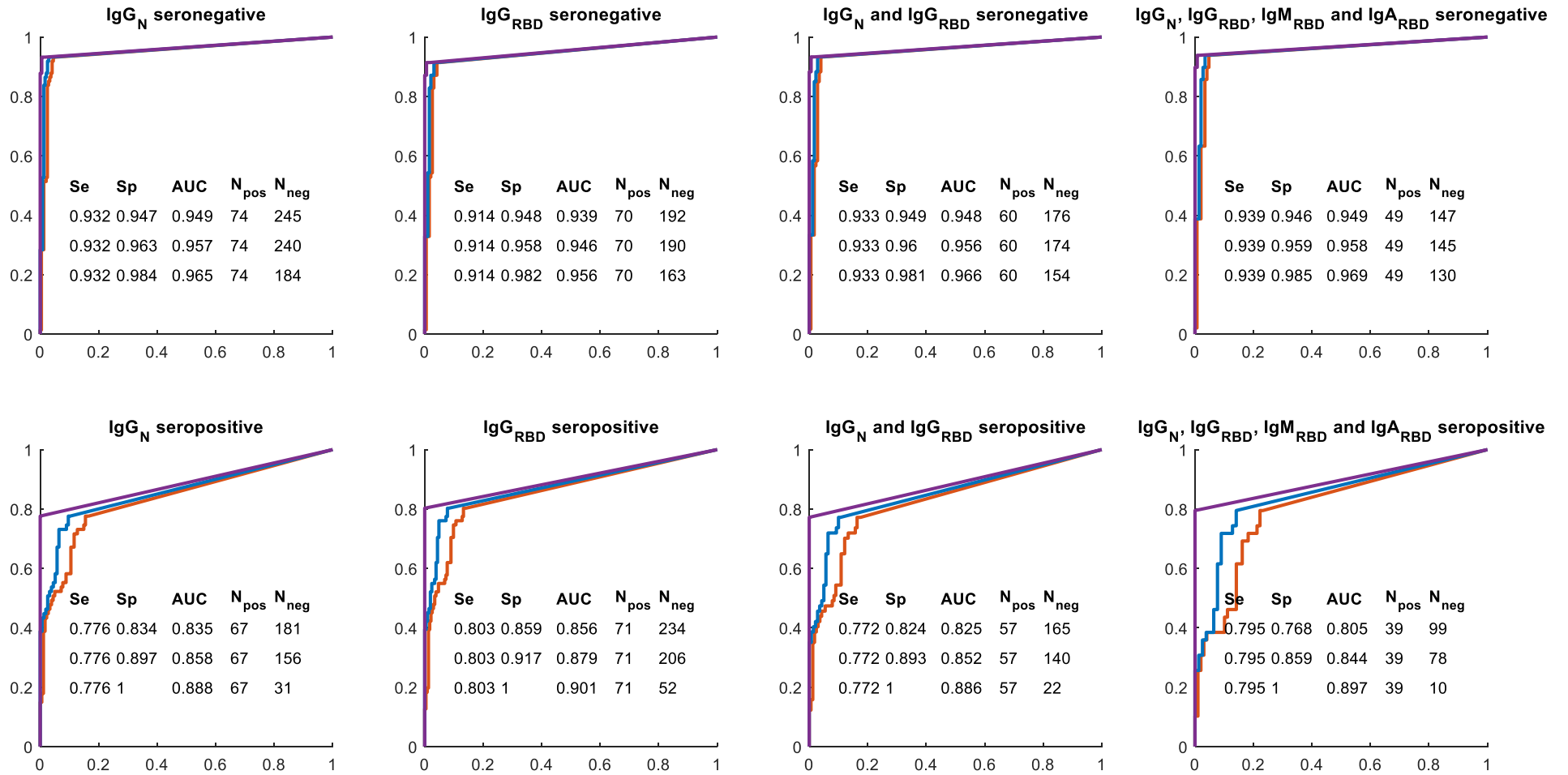
Next, any patient who had *ever tested positive* for SARS-CoV-2 was categorized based on date of the earliest positive test (**Figure 2.2A**). While CDC guidelines for the public recommend isolation for ten days following diagnosis with resolution of symptoms [3], local healthcare guidelines recommend discontinuation of isolation after fourteen days in most cases which has also been supported in the literature [19]. Meanwhile, a three-day period has been proposed as the typical time between infection and symptom onset [19]. Based on this timeframe, a blood sample was categorized as *convalescent* and labeled *negative* if the patient had positive respiratory testing more than fourteen days prior to sample collection as the sample would have been collected in the period following cessation of AVR in most hosts. Otherwise, the sample was categorized as *in-window positive* if the earliest positive respiratory test was within the -14-to-+3 day window or *post-window positive* if the earliest positive respiratory test was more than three days after the blood sample was collected.

Post-window positive samples were then further adjudicated based on whether interim testing was available between the date of the blood sample and the date of the positive respiratory test. If an interim negative SARS-CoV-2 respiratory test was available, the sample was labeled *negative*. If no interim testing was available, then the status was considered *unknown* and the sample was excluded from analysis.

Finally, *in-window positive* samples were further adjudicated based on symptom onset (**Figure 2.3A**). The same -14-to-+3 day window was considered. A patient with symptom onset more than 14 days prior to the blood sample was further categorized as *late COVID* and labeled *negative* because even though earliest positive respiratory testing was in the window, time since symptom onset would place the blood sample in the period after which AVR is expected to have ceased. Meanwhile, if symptom onset was in the window, then the patient is expected to have AVR and was categorized as *acute COVID* and labeled *positive*. Finally, a patient testing positive in the window but with symptom onset more than 3 days after the positive test was excluded due to the uncertainty of this testing-symptom onset sequence.

RT-PCR threshold cycle

All threshold cycle (Ct) values were obtained directly from reports produced by the manufacturer's software. Assays included the cobas® SARS-CoV-2 Test on the cobas® 6800 platform (Roche Diagnostics), the CDC 2019-Novel Coronavirus (2019-nCoV) Real-Time RT-PCR Diagnostic Panel or the TaqCheck™ SARS-CoV-2 Fast PCR Assay (Thermo Fisher) on the Applied Biosystems™ 7500 Real-Time PCR System (Thermo Fisher), and the Xpert® Xpress CoV-2/Flu/RSV on the GeneXpert platform (Cepheid).



Supplementary Figure 2.1. ROC curves for nucleocapsid antigenemia within subgroups defined by serostatus.

Curves correspond to the same reference standards as Figure 2B in main manuscript (Red: acute vs all non-acute, Blue: acute vs convalescent/negative, Purple: acute vs negative only).

Supplementary Figures and Tables

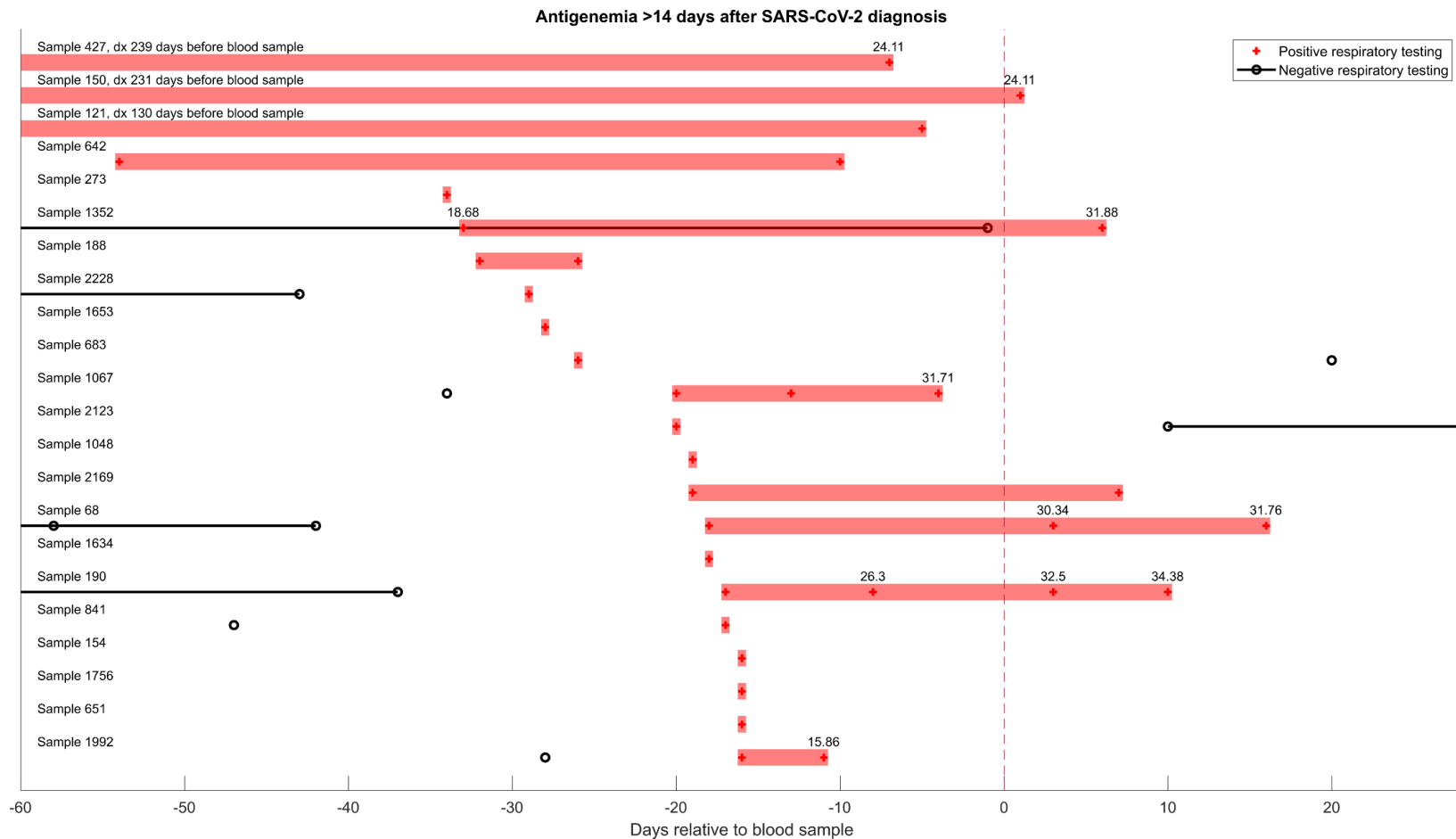
	Age range	Days Since COVID Diagnosis	IgG N	IgG RBD	Mech vent	Death	Ct values	Clinical summary
Sample 1050	71-80	39	Yes	Yes	No	Yes	Roche 31.21 (ORF) 34.56 (E)	Presented 39 days after earliest positive test with non-respiratory illness
Sample 2047	61-70	29	Yes	Yes	No	No	Roche 34.7 (ORF) E not detected	Pulmonary embolism > 1 week after resolution of primary COVID symptoms
Sample 255	71-80	21	Yes	Yes	No	No	GeneXpert 35.2	Presented with volume overload in the setting of missed dialysis
Sample 755	81-90	21	No	Yes	No	No	Roche 32.47 (ORF) 33.84 (E)	Presented with abdominal pain, nausea and vomiting
Sample 2056	71-80	21	Yes	Yes	No	No	CDC 34.69 (N1) 34.04 (N2)	Presented with hypoxic respiratory failure
Sample 141	41-50	16	Yes	Yes	No	No	GeneXpert 30.9	Presented with non-specific abdominal pain. No respiratory symptoms
Sample 995	61-70	15	Yes	Yes	No	No	Roche 32.09 (ORF) 34.54 (E)	Presented with syncope

Supplementary Table 2.1. Clinical details of patients with same-day positive SARS-CoV-2 nasopharyngeal NAAT and no antigenemia more than 14 days after diagnosis.

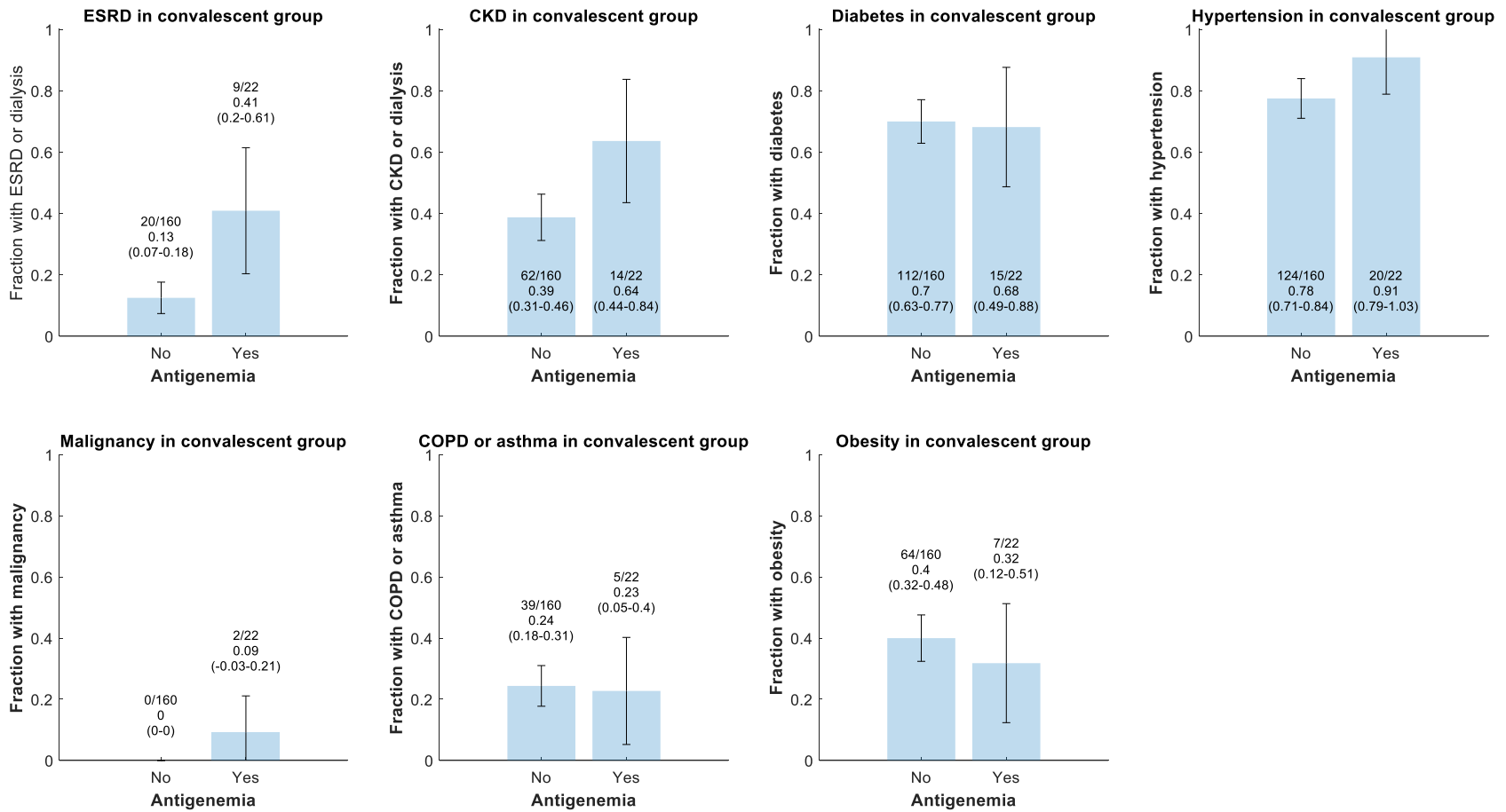
	Days since first dx	Age range	Nucleocapsid (pg/mL)	Log ₁₀ Nucleocapsid (pg/mL)	IgG N	IgG RBD	Intubated	Death	Comment	Likely category
Samples 427* and 150*	239	71-80	49.2	1.7	Yes	Yes	No	No	Negative SARS-CoV-2 NP RT-PCR 12 days before, evidence of seroconversion in samples gathered 8 days apart. High risk for exposure to active cases.	Re-infection
Sample 121	130	41-50	1.9	0.3	No	Yes	No	No	Recent high risk social gathering.	Re-infection
Sample 642	54	81-90	26	1.4	No	No	No	No	Immunocompromised with COVID-like symptoms	Persistent infection in immunocompromised host
Sample 273	34	71-80	1.2	0.1	Yes	Yes	Yes	Yes	Treated for hyper viscosity syndrome; same day blood transfusion	Severe COVID-19
Sample 1352	33	71-80	19.7	1.3	No	Yes	No	No	ESRD and recent chemotherapy; same day blood transfusion	Persistent infection in immunocompromised host
Sample 188	32	71-80	1	0	Yes	Yes	No	No	Required high-flow oxygen after diagnosis.	Severe COVID-19
Sample 2228	29	31-40	17.7	1.2	Yes	Yes	Yes	No	ESRD; blood transfusion 4 days prior	Severe COVID-19
Sample 1653	28	61-70	9.2	1	Yes	Yes	Yes	Yes	Immunocompromised; same-day and prior day blood transfusion	Severe COVID-19
Sample 683	26	61-70	0.9	0	Yes	Yes	Yes	Yes	Immunocompromised	Severe COVID-19
Sample 1067	20	41-50	2580.2	3.4	No	No	No	No	ESRD, asymptomatic infection but admitted for diarrhea	Uncertain
Sample 2123	20	51-60	1.2	0.1	Yes	Yes	Yes	No		Severe COVID-19
Sample 1048	19	41-50	76.4	1.9	Yes	Yes	Yes	No	Blood transfusion 3 days prior	Severe COVID-19
Sample 2169	19	71-80	14.4	1.2	Yes	No	No	Yes	Active malignancy; prior day blood transfusion	Uncertain
Sample 68	18	61-70	1.4	0.2	Yes	Yes	No	No	Blood transfusion 4 days prior	Uncertain
Sample 1634	18	71-80	24.6	1.4	Yes	Yes	No	No	Required high-flow oxygen	Uncertain
Sample 190	17	71-80	61.9	1.8	Yes	Yes	No	Yes	ESRD; blood transfusion 3 days prior	Uncertain
Sample 841	17	71-80	652.7	2.8	No	No	Yes	Yes	Blood transfusion 7 days prior	Severe COVID-19
Sample 154	16	51-60	116.4	2.1	Yes	Yes	Yes	No		Severe COVID-19
Sample 1756	16	71-80	18.3	1.3	Yes	Yes	Yes	Yes		Severe COVID-19
Sample 651	16	71-80	0.4	-0.4	Yes	Yes	Yes	Yes		Severe COVID-19
Sample 1992	16	71-80	5	0.7	Yes	Yes	No	No	Diarrhea, not hypoxia	Uncertain

Supplementary Table 2.2. Clinical details for samples in convalescent group with detectable antigenemia.

*Samples from the same patient. All other samples represent unique patients.



Supplementary Figure 2.2. Timeline of SARS-CoV-2 respiratory testing corresponding to samples with antigenemia in the convalescent group. Samples 427 and 150 are from the same individual. All other samples represent unique individuals. When available, Ct values are displayed above the markers for positive respiratory RT-PCR.



Supplementary Figure 2.3. Comparison of prevalence of comorbidities based on ICD10 codes for samples without and with antigenemia in the convalescent group. 95% confidence intervals are based on the standard error of the point estimate, i.e.

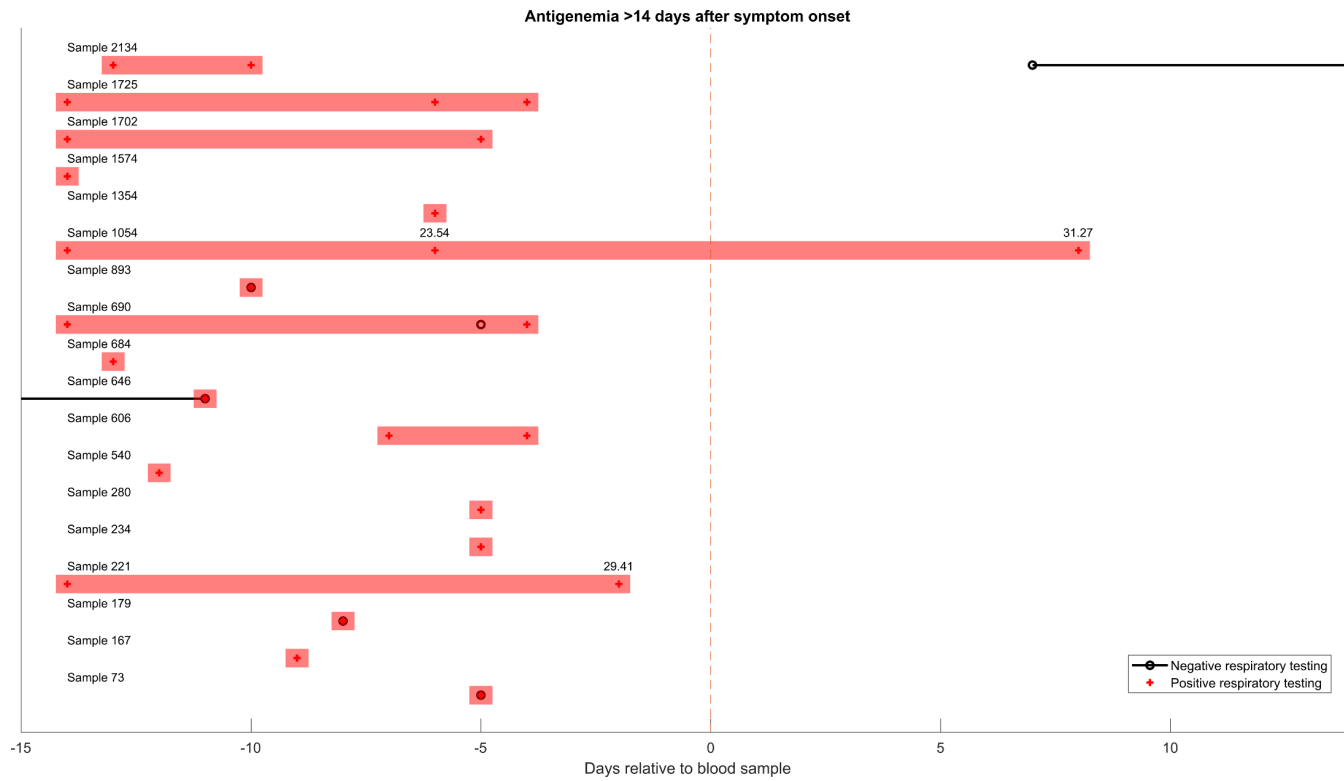
$$p \pm z \sqrt{p(1-p)/n} \text{ where } z = 1.96 \text{ and } n = \text{sample size.}$$

	Age	N	Log10	IgG	IgG	Comments
		protein	N protein	N	RBD	
Sample 158	61-70	0.6	-0.2	No	No	Acute back pain. No record of COVID-like symptoms.
Sample 1537	31-40	14.3	1.2	No	No	Outpatient pre-op testing ahead of surgery. No record of COVID-like symptoms.
Sample 1692	21-30	0.1	-0.9	No	No	Toxicology emergency. No record of COVID-like symptoms.

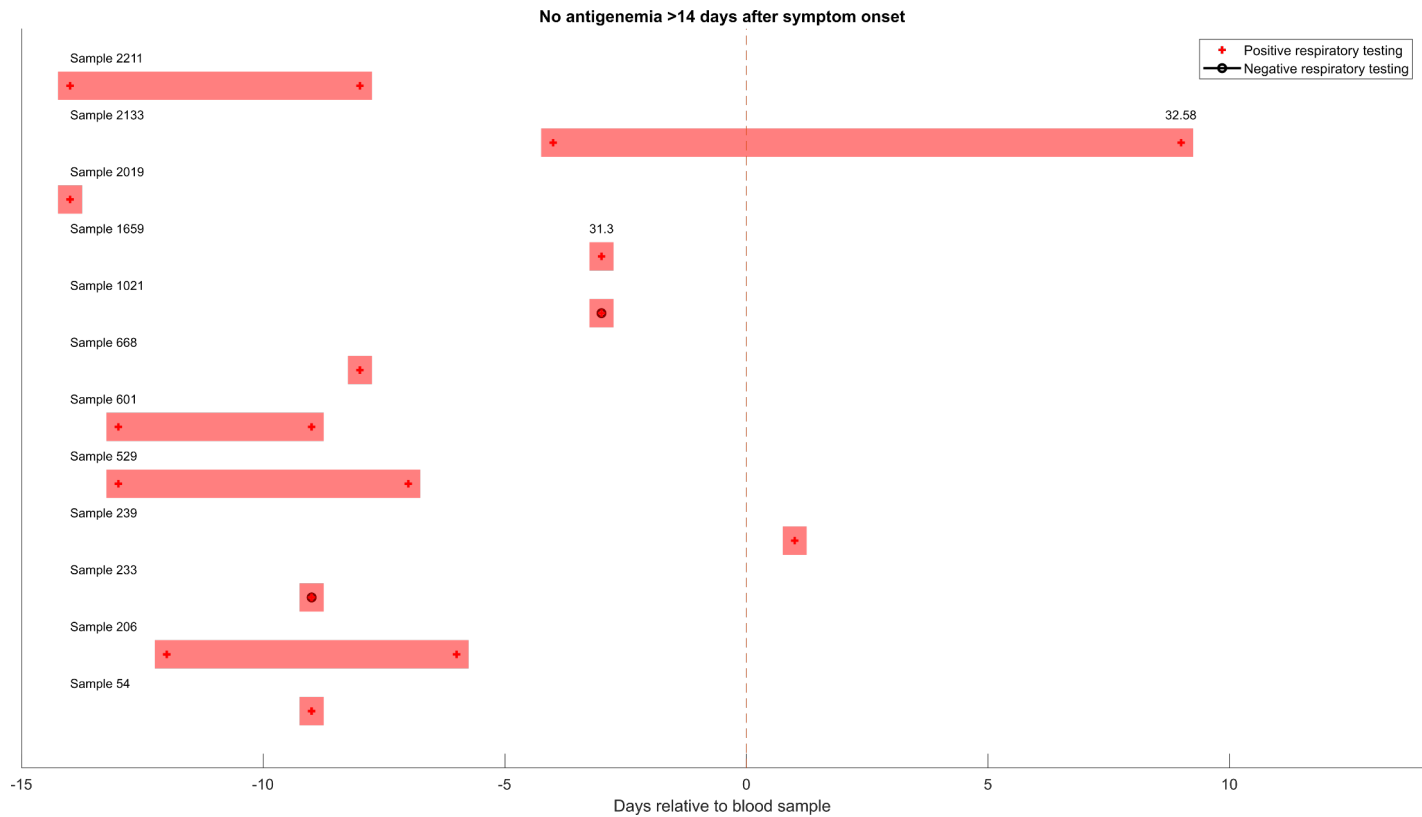
Supplementary Table 2.3. Same-day negative patients with ant

	Age	Days since positive respiratory testing	Days since symptom onset	N protein (pg/mL)	Log10 N protein	IgG N	IgG RBD	Mechanical ventilation	Death	Quality of symptom documentation
Sample 2134	71-80	13	24	5.9	0.8	Yes	Yes	Yes	No	Imprecise
Sample 540	81-90	12	19	27	1.4	Yes	Yes	No	No	Imprecise
Sample 1354	61-70	6	19	19.1	1.3	Yes	Yes	No	No	Imprecise
Sample 893	71-80	10	18	89332.6	5	No	No	Yes	Yes	Imprecise
Sample 606	51-60	7	18	0.1	-1	Yes	Yes	No	No	Precise
Sample 280	61-70	5	18	3.9	0.6	Yes	Yes	No	No	Imprecise
Sample 1702	21-30	14	17	11.9	1.1	Yes	Yes	No	No	Precise
Sample 1574	81-90	14	17	1451.1	3.2	Yes	Yes	No	Yes	Precise
Sample 1054	31-40	14	17	20.7	1.3	Yes	Yes	Yes	No	Precise
Sample 221	71-80	14	16	21	1.3	No	Yes	Yes	No	Imprecise
Sample 684	51-60	13	16	12.5	1.1	Yes	Yes	Yes	Yes	Precise
Sample 167	71-80	9	16	45.4	1.7	Yes	Yes	Yes	Yes	Imprecise
Sample 73	71-80	5	16	20.5	1.3	Yes	Yes	No	No	Precise
Sample 690	21-30	14	15	3.9	0.6	Yes	Yes	No	No	Precise
Sample 1725	71-80	14	15	773.6	2.9	No	Yes	No	No	Precise
Sample 646	71-80	11	15	716.9	2.9	No	No	Yes	Yes	Precise
Sample 179	71-80	8	15	942	3	Yes	Yes	Yes	Yes	Imprecise
Sample 234	61-70	5	15	17	1.2	Yes	Yes	No	No	Precise

Supplementary Table 2.4. Patients with antigenemia and positive SARS-CoV-2 respiratory testing between 14 days prior to and 3 days after sample collection but with more than 14 days of symptoms at the time of sample collection. Quality of symptom documentation is categorized. Calendar dates (e.g. “anosmia started on Jan 1”) or integer-quantified history (e.g. “anosmia started 5 days ago”) are considered precise whereas other descriptions are considered imprecise (e.g. “anosmia a few days ago”).



Supplementary Figure 2.4. Timeline of SARS-CoV-2 respiratory testing corresponding to samples with antigenemia in the late-presenting group (positive respiratory testing with 14 days prior to 3 days after the blood sample but with > 14 days of symptoms). When available, Ct value is indicated above positive tests.

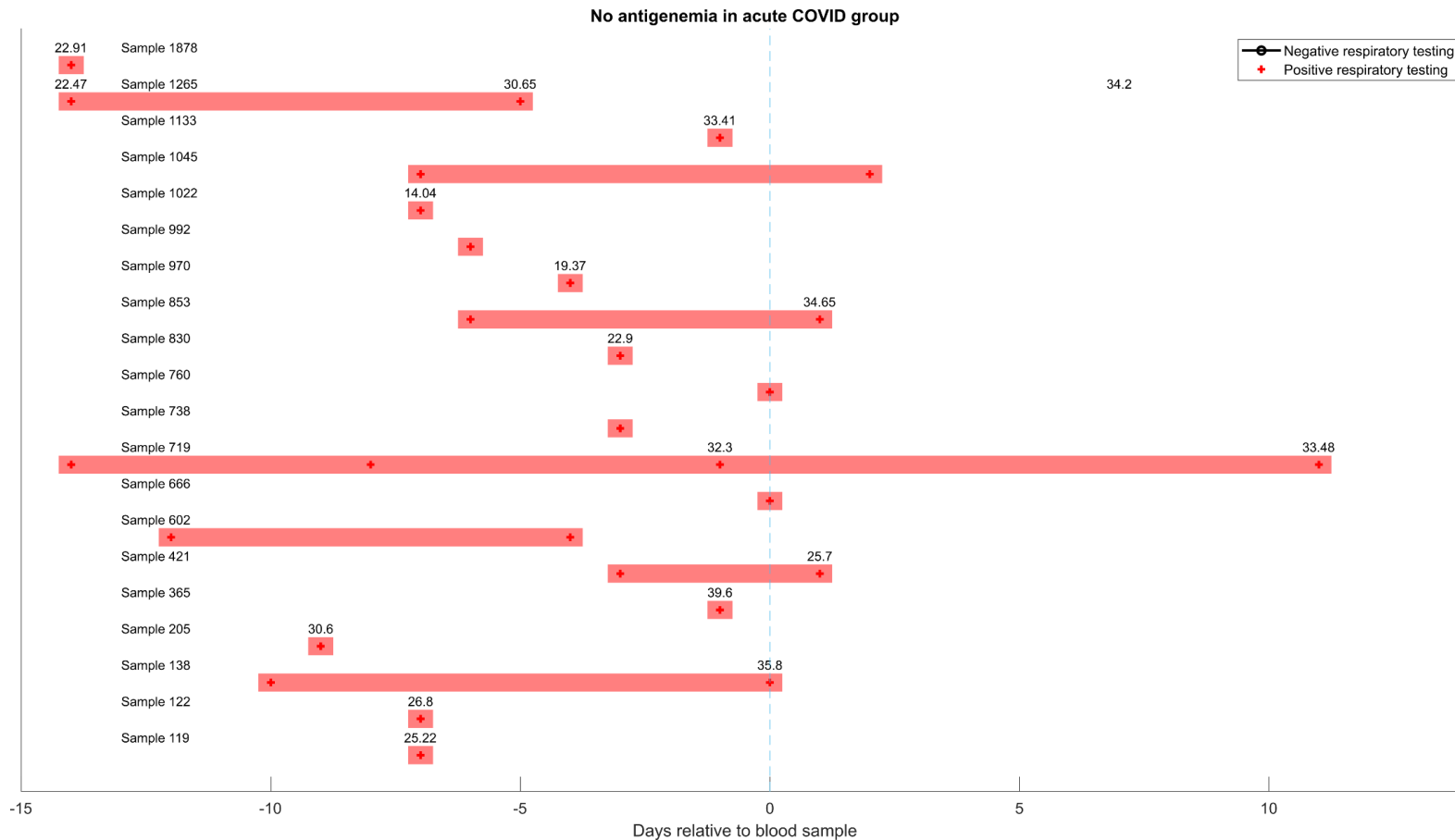


Supplementary Figure 2.5. Timeline of SARS-CoV-2 respiratory testing corresponding to samples without antigenemia in the late-presenting group (positive respiratory testing with 14 days prior to 3 days after the blood sample but with > 14 days of symptoms). When available, Ct value is indicated above positive test.

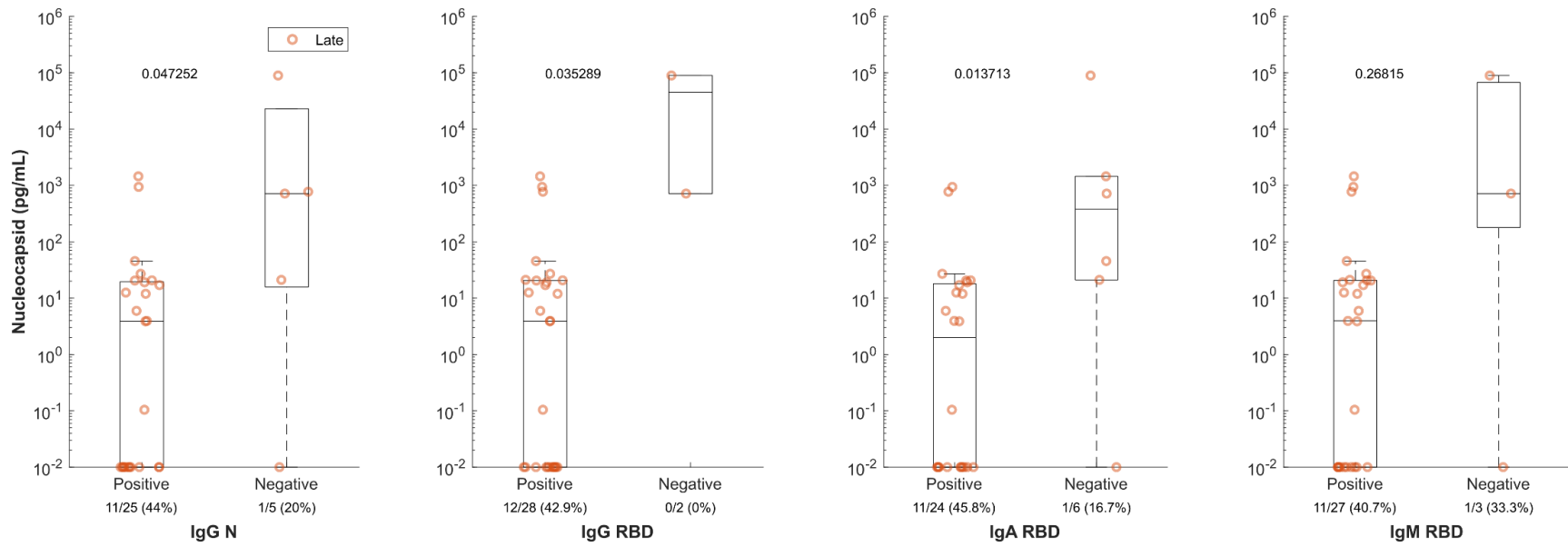
Sample	Age	Days since		Ct value*	IgG N	IgG RBD	Mechanical		Death	Quality of		Comments
		resp. test	symptom onset				ventilation			symptom	documentation	
Sample 719	81-90	14	14		Yes	Yes	No	Yes	Precise			
Sample 1265	51-60	14	14		No	Yes	No	No	Precise	Presented with fevers and chills.		
Sample 1045	51-60	7	7		Yes	Yes	No	No		Reported to have had prior COVID diagnosis.		
Sample 1878	61-70	14	14		Yes	No	No	No	Precise	Reported prior positive testing with date not documented. Likely more than 14 days since first positive test.		
Sample 119	31-40	7	14		Yes	Yes	No	No	Imprecise			
Sample 853	51-60	6	14		Yes	Yes	No	No	Precise			
Sample 122	71-80	7	13		Yes	Yes	No	No	Imprecise			
Sample 992	21-30	6	12		Yes	Yes	No	No	Imprecise	No in-house testing available.		
Sample 205	71-80	9	11		Yes	Yes	No	No	Precise			
Sample 602	41-50	12	10		Yes	Yes	No	No	Imprecise			
Sample 138	41-50	10	10	35.8	Yes	Yes	No	No	Imprecise	Symptoms improving at time of blood sample.		
Sample 1022	81-90	7	9		No	No	No	Yes	Precise			
Sample 421	71-80	3	8		Yes	No	No	No	Precise			
Sample 666	71-80	0	6		Yes	Yes	No	No	Imprecise			
Sample 970	71-80	4	5		No	No	No	Yes	Imprecise	History provided by family member		
Sample 738	21-30	3	5		No	No	No	No	Precise			
Sample 830	61-70	3	5		No	No	No	No	Precise			
Sample 1133	41-50	1	5		Yes	Yes	No	No	Imprecise			
Sample 365	51-60	1	1		Yes	Yes	No	No	Imprecise	History provided by family member		
Sample 760	71-80	0	0		Yes	Yes	Yes	No	Imprecise	Presented with new cough.		

Supplementary Table 2.5. Samples categorized in the acute COVID group without antigenemia.

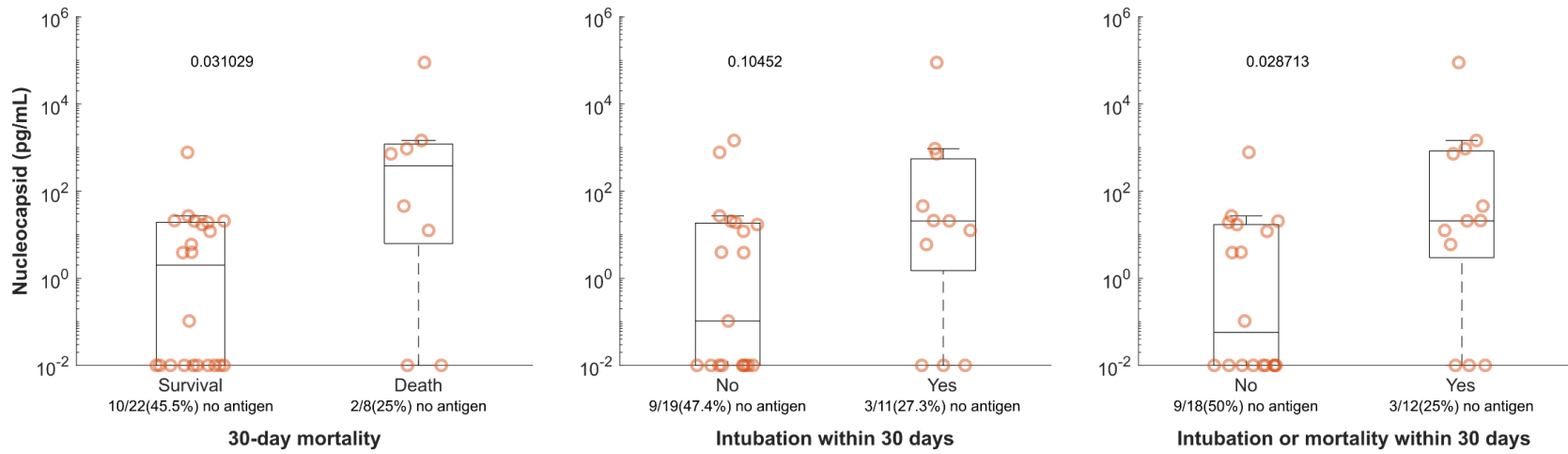
*if known



Supplementary Figure 2.6. Timeline of SARS-CoV-2 respiratory testing corresponding to samples without antigenemia in the acute COVID group (positive respiratory testing with 14 days prior to 3 days after the blood sample and < 14 days of symptoms). When available, Ct value is indicated above positive tests. Note that the patient corresponding to Sample 1265 had RT-PCR testing 7 days after blood sampling that was reported indeterminate (neither as positive nor negative) as only one of two targets amplified. Ct value for the target that did amplify appears here.



Supplementary Figure 2.7. Antigenemia levels in late-presenting group stratified by antibody serology.



Supplementary Figure 2.8. Antigenemia levels in late COVID samples stratified by severity.

	Pub date	Assay	Design	Definition of COVID positive	Definition of COVID negative	Sens	Spec	Other data
Li			40 COVID-19 patients from the First Affiliated Hospital of Anhui Medical University				633/633	
Front Cell Infect Microbiol [11]	9/4/20	ELISA	and	Included patients had positive RT-PCR and pathological changes on chest CT, but test performance only reported in those who also did not have N-protein antibodies.	633 with negative pharyngeal swab or sputum SARS-CoV-2 nucleic acid result and negative N protein antibody (369 of these from patients with other respiratory infections)	38/50 (76%)	-100%	Assay within-day & day-to-day precision
			30 COVID-19 patients from the Anhui Provincial Center for Disease Prevention and Control					
Lebedin [12]*	Pre-print posted 9/25/2020	ELISA (homebrew)	Patients with clinical signs of COVID-19 admitted to an redesigned facility	Unclear	Unclear		Unclear	..
Su	11/26/20	Simoa (Quanterix)	"89 plasma samples were obtained from 35 COVID-19 patients at different time points."	Time from earliest positive RT-PCR positivity or symptom onset is not described. Supplemental information states: "Among 89 plasma samples, 39 were collected when qPCR assay of SARS-CoV-2 in pharyngeal swabs were positive."	"healthy control"	29/39	34/50	..
Sci China Life Sci [13]						-74.40%	-68.00%	
Ogata		Simoa (Quanterix)	Adult patients presenting to Brigham and Women's Hospital or Massachusetts General Hospital	10-days from initial NP RT-PCR test (does not account for symptom onset)	17 RT-PCR negative	41/64		Clearance of plasma antigen
Clin Chem [14]	11/30/20				20 pre-pandemic healthy		NR	N positivity vs severity in Suppl. data
					14 pre-pandemic sick			Multiple biomarkers (emphasis on S1 not N)
Hingrat [15]	12/8/20	ELISA (COVID-Quantigene)	Study participants included in the French COVID and CoV-CONTACT cohorts	Serum samples after SARS-CoV-2 diagnosis within 14 days of symptom onset.	Pre-pandemic samples and 13 pandemic samples with other viral infection	132/142	62/63	N vs RNAemia N vs NP RT-PCR Ct
Ahava [16]*	Pre-print posted 1/13/2021	ELISA (Salofa)	Analysis of clinical samples sent to Helsinki University Hospital Laboratory	Positive upper respiratory testing; blood sample within 14 days from symptom onset.	Samples from 2019 and 2020	47/50	145/148	N vs Ct
Shan		Simoa (Quanterix)	SARS-CoV-2 RT-PCR+ samples from a commercial source (N = 20)	RT-PCR+; test characteristics are calculated from "first draw" sample data presented in supplement and based on cut-off of 1.25 pg/mL. Sample N according to days from positive PCR as follows:		39/40	100/100	Dried blood spots
Nat comm [17]	3/26/21		and	1-7 days: N = 27 8-14 days: N = 12 > 14 days: N = 1	Specificity is based on measurements of pre-pandemic samples.	-97.50%	-100%	Report antigenemia > 14 days in longitudinal cohort (53 samples) but all from six of ten total patients
Zhang [18]	8/6/21	ELISA (Biohit Healthcare)	Remnant serum from 208 randomly selected COVID cases at Zuckerberg San Francisco General Hospital.	RT-PCR positive within 24 hours, within 1 week of symptom onset.	RT-PCR negative	130/143	59/60	Absence of cross-reactivity for 5 individuals with other coronavirus infections
Thudium [21]	9/20/21	ELISA (Solsten Diagnostics)	Inpatients and outpatients	Confirmatory PCR-positive test within 13 days	Simultaneous upper respiratory RT-PCR negative	282/324	1/462	
Wang [19]	10/4/21	S-PLEX Direct Detection Assay (Meso Scale)	Remnant venipunctures from patients receiving blood draws between March to November 2020 at Stanford Healthcare.	Blood samples +/- 1 day from first positive NAAT, sensitivity summarized here are for those tested within 2 weeks of symptom onset.	SARS-CoV-2 NAAT negative	64/70	49/52	Comparison to Ct values
						-91.40%	-94.20%	Severity analysis
Favresse [20]*	Pre-print posted 11/21/2021	Simoa (Quanterix)	All patients with molecular diagnosis of SARS-CoV-2 infection between April 2020 and July 2021.	Within 10 days of symptom onset.	71 pre-pandemic serum samples collected before February 2020.	93/96	70/71	Severity analysis
						-96.90%	-98.60%	Also presents iFlash assay data

Supplementary Table 2.6. Summary of current literature

*preprint; NR = not reported.

	Convalescent	Late COVID	Acute COVID	Pre-COVID	Same-day negative
COVID status label	Negative	Negative	Positive	Negative	Negative
Earliest positive SARS-CoV-2 respiratory testing	> 14 days before blood sample	14 days before to 3 days after blood sample	14 days before to 3 days after blood sample	> 3 days after blood sample	Never
Negative SARS-CoV-2 respiratory testing	N/A	N/A	N/A	After blood sample and before earliest positive test	Same day as blood sample
Symptom onset	N/A	> 14 days before blood sample	14 days before to 3 days after blood sample	N/A	N/A
Proposed reasons for unexpected presence of antigenemia	Re-infection Critical illness (prolonged infection) Immune compromise (chronic infection)	Critical illness (prolonged infection) Immune compromise (chronic infection) Decreased antigen clearance (ESRD, CKD or AKI)	N/A	Undiagnosed COVID at time of blood sample with late respiratory testing	False-negative SARS-CoV-2 respiratory testing

Supplementary Table 2.7. Outline of blood sample classification scheme and discussion of proposed reasons for variation from the antigenemia as a unique and universal marker of acute infection

**Appendix 2 Galectins, An Ancient Family of Carbohydrate Binding
Proteins with Modern Functions**

Abstract

Galectins are a large family of carbohydrate binding proteins with members in nearly every lineage of multicellular life. Through tandem and en-mass genome duplications, over 15 known vertebrate galectins likely evolved from a single common ancestor extant in pre-chordate lineages. While galectins have divergently evolved numerous functions, some of which do not involve carbohydrate recognition, the vast majority of the galectins have retained the conserved ability to bind variably modified poly lactosamine (polyLacNAc) residues on glycans that modify proteins and lipids on the surface of host cells and pathogens. In addition to their direct role in microbial killing, many proposed galectin functions in the immune system and cancer involve crosslinking glycosylated receptors and modifying signaling pathways or sensitivity to antigen from the outside in. However, a large body of work has uncovered intracellular galectin functions mediated by carbohydrate- and non-carbohydrate-dependent interactions. In the cytoplasm, galectins can tune intracellular kinase and G-protein-coupled signaling cascades important for nutrient sensing, cell cycle progression, and transformation. Particularly, but interconnected pathways, cytoplasmic galectins serve the innate immune system as sensors of endolysosomal damage, recruiting and assembling the components of autophagosomes during intracellular infection through carbohydrate-dependent and -independent activities. In the nucleus, galectins participate in pre-mRNA splicing perhaps through interactions with non-coding RNAs required for assembly of spliceosomes. Together, studies of galectin function paint a picture of a functionally dynamic protein family recruited during eons of evolution to regulate numerous essential cellular processes in the context of multicellular life.

Introduction

Galectins are an ancient family of soluble β -galactoside carbohydrate binding proteins (CBPs) encoded by the *LGALS* gene family in humans. Members of the galectin family have evolved numerous intra- and extracellular functions in development and regeneration, innate immunity and pattern recognition, adaptive immune regulation(257–259), and pathogenesis of autoimmune diseases and cancer(260). Despite a large body of work investigating the biochemistry and effects of recombinant and endogenous galectins *in vitro*, detailed mechanistic studies have been limited for many proposed galectin functions *in vivo*. Such studies have proven challenging for several reasons including the number of galectins, their broad and varied tissue expression patterns, localization to multiple intracellular and extracellular compartments and the yet unproven, but likely confounding potential for galectins to complement one another by engaging similar or identical ligands. However, many consistent and compelling themes of galectin function have emerged since the discovery of the historically classified sulfhydryl- or S-type lectin, galectin-1 in 1975 among asialofetuin binding fractions from the electric organs of an electric eel(261).

Fundamentally, mammalian galectins mediate their pleiotropic functions through binding to both carbohydrate and non-carbohydrate ligands. They serve as adaptors within the cell to recruit enzymes, regulating pre-mRNA splicing in the nucleus as well as mRNA stability, autophagy, and apoptosis in the cytoplasm. Stimulated to non-classical secretion or released from damaged cells, they can engage or crosslink glycoprotein receptors on immune and neoplastic cells to modulate signaling pathways and dictate cell

fates; and free from their ECM they serve the innate immune system as direct anti-microbial effectors against pathogens employing molecular mimicry(262).

Perhaps the most important challenge in our mechanistic understanding of galectin functions is the complexity and ubiquity of their ligands: oligosaccharide modifications of proteins and lipids, known collectively as the glycome. The glycome is a complex network of linear and branched carbohydrate moieties, regulated at multiple levels by the flux of metabolites through major catabolic pathways, in turn dictating substrate availability in the tightly controlled anabolic pathways of glycan synthesis and addition, which occur in the endoplasmic reticulum (ER) and Golgi apparatus (GA) of eukaryotic cells. Terminal and internal glycan and non-glycan modifications including sulfates, phosphates, sialic acid, fucose, mannose, and xylose further enrich the glycan code: A complex and multifunctional set of interactions and responses mediated by glycans and glycan binding proteins. The functional significance of the glycan code has been particularly well studied in the mammalian immune system, where many innate and adaptive immune pathways have converged to utilize lectin recognition of specific glycan signatures in order to regulate cellular trafficking, pattern and damage recognition, signaling pathways, and differentiation(263). It is therefore essential to carefully consider the role of known and putative glycan ligands as well as the cell types and conditions which produce them in any rigorous study of physiologic galectin function.

Following the discovery of galectin-1 (Gal-1), more than 15 putative members of the galectin family (thus categorized in 1994(264)) have been identified in various mammalian species, including humans, wherein 12 functional galectin-encoding genes

have been found (LGALS 1, 2, 3, 4, 7, 8, 9, 10, 12, 13, 14, and 16). Galectins 5 and 6 emerged in contemporary rodent lineages while galectins 11, and 15 have thus far only been found in sheep and goats. In addition, galectin orthologues with yet unknown function have been identified in many lineages of vertebrate and invertebrate multicellular organisms (metazoans) including representative and model organisms from diverse evolutionary lineages: *Mus musculus*, *Ciona intestinalis* (sea squirt), *Drosophila melanogaster*, *Caenorhabditis elegans*, and even fungi and basal members of the metazoan lineage of Poriferan sponges. The ubiquity of galectin family members within nearly every branch of the multicellular tree of life and the highly conserved nature of the carbohydrate recognition domain (CRD), which defines them, supports the broad utility of galectin activity in multiple cellular processes and offers some explanation for experimental observations of their divergent and pleiotropic functions(265). In this introductory chapter to section 1, we aim to highlight important observations of galectin function, focusing on aspects of eukaryotic cell biology and vertebrate immunology set within the broader context of galectin evolution and biochemistry. In so doing, we hope to provide a conceptual framework for the evolving biology of this complex family of GBPs.

The Evolution of Carbohydrate Recognition

Glycans are perhaps the most enigmatic of the four major classes of macromolecules common to all organisms. The absence of a consistent genetic template and the complexity of their non-linear chemistry are just two intrinsic factors that have historically confounded the characterization of oligosaccharide modifications. By contrast, studies of biological function that traverse the familiar ladder from DNA (gene) to RNA

(transcript) to protein (enzyme) benefit from an enormous armamentarium of tools under development since Gregor Mendel elaborated his theory of inheritance in the mid 19th century(266). The relatively modern field of epigenetics has built on these fundamental tools in an effort to explain the influences of environment and development on the heredity of gene expression patterns, a study involving the extensive decoding of post and co replicative, transcriptional, and translational modification. Epigenetics has broadened the focus of life science from what is encoded to when and why it is expressed.

Carbohydrate adducts on proteins likely evolved in the earliest forms of life to stabilize and regulate the folding of an increasingly large and biochemically complex repertoire of enzymes and structural proteins. As the degree and complexity of these polar modifications expanded to obscure the surfaces of their protein substrates, carbohydrate recognition by catalytic enzymes and regulatory proteins within the evolving secretory and protein trafficking networks must have become imperative(267). According to this theory, many of the extracellular functions for protein glycosylation and the enzymatic pathways in the secretory system which produce them would have evolved and diverged later. Consistent with this “inside-out” model of glycan-GBP evolution, the major intracellular glycosyltransferases, glycosidases, and lectin chaperons within the ER (e.g. calnexin and calreticulin) are highly conserved both functionally and genetically in eukaryotic cells from plants, yeast, and mammals; while enzymes that prune, extend, and terminally modify these core structures within the Golgi apparatus are isolated and divergent within specific metazoan lineages. In addition, there is little evidence for ancient orthologues among GBPs with highly specialized extracellular functions within the

mammalian immune system such as the innate and B-cell regulating sialic acid-binding immunoglobulin-type lectins (Siglecs), which recognize specific terminal sialic acid moieties to modulate primary signaling pathways, or members of the C-type lectin (CLEC) family of selectins, which regulate leukocyte trafficking among other functions. These specialized GBPs, now critical components of the mammalian immune system, likely evolved to exploit and elaborate upon the more conserved functions like protein stabilization and trafficking common to all organisms. Importantly, all genomes including those from unicellular protists and bacterial lineages encode proteins, which have evolved convergently the ability to read or exploit aspects of their own glycan code or that of other species. What is known of the evolutionary history of galectins shares features of both the ancient and modern groups of lectins.

Galectin Evolution and Biochemistry

Members of the galectin family with conserved gene and protein structure have been found in nearly every lineage of multicellular life, suggesting the existence of a single common ancestor. However, through multiple tandem and en mass gene and genome duplications followed by structural and functional divergence, galectins have evolved specialized and accessory functions within specific lineages. While some poorly characterized galectin-like genes (e.g. GRIFIN) appear to have lost the residues necessary for carbohydrate recognition, all formally classified galectins have retained this functional domain. This conservation of structure and function highlights the importance of evaluating the evolutionary history of galectin carbohydrate recognition to appropriately contextualize functional observations in humans and model organisms.

Galectin Evolution

Historically, vertebrate galectins have been categorized by the number and linkage of their carbohydrate recognition domains (CRDs) into mono-CRD prototypical (Gal-1,2,5,7,10,11,14,15) and chimeric (Gal-3) galectins and bi-CRD tandem repeat (Gal-4,6,8,9,12) galectins(264). Much can be gleaned about these ubiquitous proteins from their gene structure, chromosomal location and sequence. All carbohydrate binding proteins classified as galectins share at least one ~135 amino acid β -sandwich carbohydrate recognition domain (CRD), composed of six (S1-S6) and five stranded (F1-F5) anti-parallel β -sheets. Strands S4-S6 contain the conserved amino acids which mediate carbohydrate recognition and are all encoded by the second of three consecutive exons in the CRD-encoding region(s) of *LGALS* loci (**Figure 1B**). The first exon consistently encodes F1 and S2 strands; while the second (middle), CRD-defining exon encodes strands S4, S5, and S6 but can either terminate at specific positions within the region encoding strands F3 or F4(268) (**Figure 1C**). These conserved exon structural and genomic features are found among all known chordate galectin genes, supporting a model in which a single mono-CRD common ancestor to chordate galectins arose and subsequently evolved through tandem duplication to produce the common ancestor of vertebrate bi-CRD galectins. Because the likelihood of a precise F3/F4 terminating gene structure arising independently for modern galectins is vanishingly small, this particular feature is useful in tracing relationships among different mono- and bi CRD galectins (i.e F3 or F4 terminating galectins likely arose from ancestral genes sharing the same exon structure)(268).

The specific nature of the first galectins is unknown, but the existence of mono-CRD galectins with the F4 terminating exon structure in both protostome and deuterostome (pre-chordate) lineages (and lack of the F3 exon structure in protostome galectins) implies that the original mono-CRD galectin may have also been F4-terminating. A subsequent tandem duplication of this ancestral galectin gene could then have given rise to the exon organization found in all chordate bi-CRD galectins (F4-linker-F3). The F3 terminating ancestors of galectins 1, 2, and 3 would then have arisen from further duplication of the C terminal F3 CRD of this bi-CRD galectin, found in the common ancestor of all vertebrates. Supporting the latter timeline is the unique sequence and dimeric interface in vertebrate orthologues of Gal-1 and Gal-2. Within this framework, all vertebrate galectins were derived from either an ancestral F4-linker-F3 bi CRD galectin or an F3 mono CRD galectin. The bi-CRD human galectins 4, 8, 9, and 12 are encoded by *LGALS* genes in highly paralogous regions of chromosomes 1, 11, 17, and 19. And the degree of synteny (similar flanking regions) among these members of the *LGALS* family, in addition to the existence of bi-CRD orthologues in similarly flanked regions of other vertebrate genomes, strongly supports chromosomal duplication of a single ancestral chordate bi-CRD galectin as the likely mechanism by which they arose—perhaps in the two putative mass genome duplications described in vertebrate evolution. More recently evolved mono-CRD mammalian galectins (5,6,7,10,13,14,15) most likely arose within more specific lineages from duplication of single domains of these original bi-CRD galectins. In this model, all extant prototypical galectins have emerged through partial duplications of either the F3 or F4 CRD of these core ancestral bi-CRD galectins while

mono-CRD orthologues of galectins 1, 2, and 3 evolved independently from a common F3 terminating ancestor. These relationships are important to consider when drawing inferences about galectin function in humans from studies of galectins in model organisms such as those which may have evolved independently for hundreds of millions of years. In **Figure 2** we outline the putative evolution of galectin gene structure.

The Galectin CRD

X-ray crystallographic studies of multiple galectin family members have revealed structural determinants of galectin activity. Despite considerable heterogeneity in their valency and quaternary structures, all galectins possess one or more structurally conserved CRDs with some degree of binding activity toward repeating units of N-acetyl lactosamine (polyLacNAc). Structurally, the galectin CRD forms a compact 11 stranded β -sandwich or jelly roll tertiary structure and confers specificity for the 4 and 6 hydroxyl functional groups of galactose and the 3 hydroxyl functionality of *N*-acetylglucosamine (GlcNAc) through amino acid side-chain hydrogen bonding and electrostatic interactions. Ring stacking by a highly conserved tryptophan (W) in the galectin CRD favors the stereochemistry of galactose over mannose; while additional interactions of backbone amines and side chains extend beyond the CRD to mediate differences in specificity and affinity for length and glycan modifications among galectin family members. In **Figure 1B** we detail structural features of the galectin CRD.

Despite overlapping specificity for LacNAc containing glycans, studies using increasingly comprehensive glycan microarrays in addition to more traditional

biochemical approaches suggest that each galectin exhibits unique ligand preferences(269–274). While glycans are the best characterized galectin ligands, it is important to also highlight the non-carbohydrate interactions which mediate galectin function, particularly in the intracellular compartment.

Galectin Quaternary Structure & Function

Prototypical galectins (e.g. Gal-1,2,7,10) have evolved to form homodimers with outward facing CRD domains, an orientation which facilitates ligand-crosslinking under certain conditions. These oligomers exist with their monomeric counterparts in dynamic equilibrium. The relationship between oligomeric structure and biological function has been a particular focus in biochemical characterizations of Gal-1. Gal-1 dimerization promotes ligand binding(275, 276), which in turn reduces the sensitivity of galectin-1 to oxidative inactivation(277). Oxidation of galectin-1 leads to stepwise formation of disulfide bonds among exposed thiols in six conserved cysteine residues Cys 2,16,42,60,88,130), four of which are solvent accessible in the predicted monomeric structure (Cys 2,16,88,130). Spectral studies have revealed that structural changes upon oxidation of galectin-1 are reversible, suggesting the ability of this protein to dynamically switch between a structure that favors dimerization and ligand binding and one that does not. The functional significance of this phenomenon has not been determined *in vivo*. However, the ability of galectin-1 to induces reversible phosphatidyl serine exposure on and phagocytosis of cultured neoplastic leukocytes and activated neutrophils is dependent on dimerization and ligand binding in the reduced conformation(278), an *in vitro* finding recapitulated for the C-terminus of Gal-8(279). These observations,

combined with the finding that *Lgals1* null mice exhibit increased susceptibility to tissue destruction in the context of autoimmunity, suggest a possible mechanism by which reduced Gal -1 is released from damaged tissue to limit leukocyte infiltration. The temporal and spatial regulation of this process could proceed automatically through reversible oxidative inactivation of secreted or released Gal-1. We summarize the redox properties of Gal-1 in **Figure 3**. Additional studies of inflammatory processes in galectin knockout models are needed to determine when Gal-1 is released *in vivo* and whether its activity is involved in limiting immune-mediated tissue damage.

Unique among vertebrate galectins, Galectin-3 has a modular N-terminal domain composed of a 21 amino acid long stretch, bearing two sites for serine phosphorylation, and a cleavable, nine triple-helix Proline/Glycine rich repeat domain similar in structure to collagen domains(280). Galectin-3 is monomeric in solution, but can form higher order structures at high concentration or in the presence of ligands, which can seed aggregation of multimeric complexes(281). The CRD of Galectin-3 also bares sites for tyrosine phosphorylation, which modulate carbohydrate recognition and secretion(282–284).

Synthesis of Galectin Carbohydrate Ligands

Analogous to promoters, transcription factor binding sites, or conserved nucleic acid structures in genetics and epigenetics, the study of protein glycosylation (and epiproteomics in general) has been guided by the presence of specific N and O-linked glycosylation motifs or sequons within the amino acid sequence of secreted proteins. For protein N glycosylation (PNG), glycans are built from covalent linkages to Asn-X-

Ser/Thr/Cys (N-X-S/T/C) amino acid sequences. The occupancy and complexity of glycan modifications at PNG sequons is both encoded and conditional—dependent on numerous genetic, structural, and environmental factors (**Figure 4**). In eukaryotes, PNG synthesis is initiated on the cytosolic face of the endoplasmic reticulum (ER) when a precursor glycan ($\text{Man}_5\text{GlcNAc}_2$) is transferred by dolichol lipid transporters. Subsequently, stepwise enzymatic reactions and chaperone binding within the ER lumen assemble, trim and stabilize a common PNG backbone ($\text{Glc}_3\text{Man}_9\text{GlcNAc}_2$), the recognition of which serves as a checkpoint for progression into the Golgi apparatus. Base structures for common galectin PNG ligands are formed in the medial golgi, first by sequential branching via N-acetylglucosaminyltransferase (MGAT1,2,3,4a/b, and MGAT5)-catalyzed β -1,4 addition of galactose, followed by extension of branches in the distal golgi by variable addition of N-acetyllactosamine (LacNAc) units. Gal-3, Gal-8, and Gal-9 have graded affinity for polyLacNAc ligands, increasing with degree and length of branching; while Gal-1 exhibits less of this effect. Furthermore, Gal-1 targets the terminal region of LacNAc structures while Gal-3 like the plant lectin PHA-L is able to bind to internal LacNAc residues(285). Thus, substrate availability and enzymatic activity of MGAT proteins regulate extracellular galectin activity toward PNG modified receptors.

Proteoglycan ligands for galectin binding are also formed through O-glycan synthesis. O-linked glycosylation (O-glycosylation) begins with the addition by GalNAc transferases (GALNTs) of N-acetylgalactosamine (GalNAc) to the side-chain oxygen atoms of hydroxyl containing amino acids, most commonly serine or threonine. Under normal conditions, T-synthase catalyzes addition of galactose to the $\text{GalNAc}\alpha$ 1-O-

Ser/Thr precursor, producing the O-glycan core-1 structure (T antigen). Branching of the Core-1 structure by addition of GlcNAc in $\beta 6$ or $\beta 3$ linkages form the O-glycan Core-2 and Core-3 structures respectively. Further modification of extended core structures by specific glycosyl-, sialyl, and fucosyl transferases in the golgi extends and modifies core-O-linked structures, resulting in functionally significant glycan structures including blood group antigens, Lewis and Sialyl Lewis epitopes for selectins and other immune lectins (Le^x & sLe^x), as well as the best characterized ligand for galectins: polyLacNAc. Failure of the cell to produce these structures is a hallmark of cancer, autoimmunity, and inconsistent with life in mouse models of embryonic development. The importance of normal O-glycan synthesis and extension is exemplified by the role of the human tumor-associated Thomsen-Friedreich (Tn) neoantigen (unmodified GalNAc $\alpha 1$ -O-Ser/Thr) and Sialyl Tn, which results from loss or mutation of the ER-localized chaperone *Cosmc* or its target T-synthase in malignancies(286). Expression and secretion of proteins bearing the Tn antigen is an important biomarker of certain cancers, particularly carcinomas(286, 287).

For both PNG and O-glycan synthesis, terminal and internal modification by transferases in the medial and trans golgi further control the binding behaviors of lectins, including galectins, upon secretion or surface exposure of the fully formed glycoprotein. Exemplifying this phenomenon is Gal-8, which contains two CRDs with different recognition of β -galactoside terminal modifications, with the N terminal CRD strongly preferring ligands containing terminal $\alpha 2$ -3-sialic acid containing β -galactosides. Like the N-terminal CRD of Gal-8, galectin-1 is also able to bind $\alpha 2$ -3-sialyl β -galactosides, but its

binding is strongly inhibited by the same modification in an α 2-6 linkage; while Gal-2 binding is inhibited by terminal sialic acid regardless of linkage. These important biochemical observations regarding galectin CRD specificity highlight an essential theme in galectin biology—the ability of specific cells, tissue types and neoplasms to control the extracellular effect of different extracellular galectins by branching and modification of N and O-linked glycan structures(288).

Mammalian Galectin Expression and Localization

Gal-1, Gal-3, and Gal-9 are first produced during mammalian embryogenesis and the patterns of their expression have been tracked using *in situ* hybridization and immunohistochemistry. Gal-1 and 3 are first expressed on the periphery of the developing blastocyst in cells of the trophectoderm. This observation led to the prediction that these two galectins might be necessary for the process and patterning of embryonic implantation. However, subsequent work found that global deletion of either or both galectins did not prevent implantation from occurring(289), suggesting accessory roles in this process. Following implantation, Gal-1 expression marks early muscle cell precursors localized to the myotomic pole of developing somites, a pattern which precedes and mirrors expression in skeletal and cardiac muscle of the adult animal. During the same embryonic timeframe Gal-3 is expressed primarily in cells of the notochord, or primordial nervous system(290–292). Gal-9 has also been identified in the developing mouse embryo, localized to the embryonic liver and thymus, where it may play a role regulating interactions between embryonic thymocytes and thymic epithelial cells(293). Patterning of galectin expression during embryogenesis is in part mediated by methylation of a small

region that encompasses Lgals transcriptional start sites(294); while upregulation of these genes requires demethylation and activation by certain transcription factors such as NF- κ B(295). Some galectin expression can also be hormonally regulated during placental development(296). Notably, three galectin genes with conserved function in placental development (LGALS13,14,15) cluster to human Chr19 and appear to have emerged during the evolution of semi-allogeneic fetal development in primates. Dysregulated expression patterns of these placental galectins is associated with pre-term preeclampsia in humans(297, 298) and they may also have roles in directly regulating immune tolerance of the fetus(299, 300), a function proposed for Gal-1 as well. In primate embryonic development, Gal-1 can be hormonally regulated and is expressed most prominently in maternal decidual stromal cells and uterine natural killer cells, possibly playing important role in regulating maternal-fetal tolerance(296, 301, 302). A comprehensive and inclusive survey of the galectinome during mammalian embryonic development would provide further insight into the evolutionary and developmental origins of the broad galectin expression patterns observed in adult mammals.

In adult mammals, Gal-1 is widely expressed at homeostatis in muscle (skeletal and smooth), skin, lung, lymphoid tissue (thymocytes, thymic epithelial cells, lymph nodes, and spleen), prostate, placenta, testes, and cells of the nervous system. In non-cancer tissues, Gal-3 expression has been documented in epithelial cells of different origins, dendritic cells, macrophages and virus infected T cells(303, 304). Gal-9 is also expressed in many cells of lymphoid origin but also cells of the lung and myocardium. Gal-10 appears to be solely expressed by immune cells including granulocytic neutrophils

and eosinophils (wherein it can comprise the principal component of Charcot-Leyden crystals) as well as regulatory T cells(305–307). Gal-7 expression is localized mostly to stratified squamous epithelial cells of the skin, while Gal-4 and Gal-6 are mostly found in the epithelium of the gastrointestinal tract. Rodent-specific Gal-5 is expressed in the erythroid lineage, but its specific function in the blood compartment of rodents has not been established. Gal-12 is highly expressed in adipocytes and may regulate their homeostasis, illustrated by the finding that Gal-12 null mice exhibit decreased adiposity(308). Further studies are needed to delineate patterns of basal and induced galectin expression as well as the regulation of galectin intracellular localization and secretion.

Many studies of galectin function *in vitro* have used cancer cells and exogenous addition of recombinant galectins. These studies have been critical in uncovering the scope of what galectins *can* do, but may also be misleading when delineating biological function *in vivo*. This challenge is confounded by overlapping and unique tissue expression patterns. Furthermore, galectin expression and secretion can be variably induced in stages of development, states of inflammation, or dysregulated during oncogenesis. It is therefore critical to determine which galectins are present in any experimental system and in which compartments they are localized when evaluating putative functions *in vivo*.

Nuclear and Cytoplasmic Galectins

While post-translational glycan modifications are predominantly found in secretory compartments and the extracellular space, nucleocytoplasmic proteins can also be modified by carbohydrate moieties (e.g. O-GlcNAc). However, these modifications are poor substrates for galectin binding as they have not been found to contain LacNAc. Despite the absence of canonical galectin ligands in the nucleocytoplasmic space, galectins have evolved intracellular functions through non-carbohydrate interactions. These interactions have been shown to mediate roles in pre-mRNA splicing and mRNA stabilization and the modification of intracellular signaling pathways. Cytoplasmic galectins have also been shown to regulate several important signaling pathways including apoptosis.

Galectin Secretion

Genes encoding conventional secretory proteins bare a leader or signal sequence which targets translating ribosomes to the endoplasmic reticulum, where the protein is co-translationally translocated to the ER lumen and trafficked to the golgi apparatus before secretion from the cell. However, many important secreted proteins, including galectins, lack a signal sequence, instead reaching the extracellular space by alternative mechanisms. The absence of a galectin signal sequence initially cast doubt on whether galectins were secreted, but metabolic labeling(309), immunohistochemical analysis(309), and detailed mechanistic studies have confirmed the phenomenon for several family members. Release of cytoplasmic galectin upon cellular damage is an additional potential mechanism by which galectins can reach the extracellular space.

Supporting the latter mechanism are studies of muscle degeneration and injury in which tissue damage is associated with increased extracellular localization of galectin-1 which may promote myogenesis(310, 311). Intriguingly, the regulated forms of galectin secretion appear to occur through diverse mechanisms. *In vitro*, export of active, surface bound Gal-1 appears to require the engagement of cell surface β -galactoside-modified counter receptors. Cells lacking these modifications are deficient for functional Gal-1 secretion and their presence is sufficient to drive secretion of Gal-1 orthologues(312). Using metabolic labeling, Cho et al. have further demonstrated that Lec8 CHO cell mutants (incapable of producing galactosylated glycoproteins) are indeed able to secrete Gal-1 into the extracellular space, but it is not retained on the surface and becomes inactivated in the absence of ligand and the reducing conditions of the cytoplasm⁵⁷. By contrast Gal-3 export occurs via exosome release and requires an N-terminal tetrapeptide P(S/T)AP motif for interaction with Tsg101 in the endosomal sorting complex required for transport (ESCRT)(313) pathway. Gal-8 secretion may in part be mediated by its association with damaged and recycling endosomes(314).

Modern Galectin Functions

Regulation of Pre-mRNA Splicing and mRNA Stability

In multiple studies, Gal-1 and Gal-3 have been associated with pre-mRNA splicing within the nucleus. Early experiments using cell-free-splicing assays in HeLa cell nuclear extracts found that addition of competitive galectin inhibitors—lactose or thiodigalactoside (TDG)—but not galactose alone or cellobiose potently inhibited formation of splicing

products from pre-mRNA substrates. Furthermore, after removal of nuclear lactose-binding proteins from these extracts using lactose affinity chromatography, addition of recombinant Gal-3 was sufficient to restore splicing activity *in vitro*(315). Further investigation revealed that both intracellular Gal-1 and Gal-3 microscopically localize within both the nucleus and cytoplasm of HeLa cells(316), directly interact with splicing complexes, and co-immunoprecipitated with pre-mRNA(317). For galectin-3, nuclear transport is, at least in part, dependent on interaction between a C-terminal poly-basic NLS sequence (HRVKKL), which mediates interaction with translocating nuclear importins(318). Return of Gal-3 to the cytosol and an enhancement of carbohydrate binding activity accompanies casein kinase 1 (CK1)(319) serine phosphorylation in the nucleus. These findings strongly support a model in which some galectin family members can function as nucleocytoplasmic proteins in addition to their extracellular roles(320). Additional mechanistic studies showed that Gal-3 specifically associates in the nucleus with U1 snRNP, an essential initiator of spliceosome assembly, to mediate its observed pro-splicing activity(321) through both the Gal-3 CRD and YPG-rich repeats in its N-terminus(322). Additional galectin-spliceosome interactions have also been uncovered using yeast two-hybrid screening, which identified survival of motor neuron (SMN) complexes containing Gem associated protein 4 (Gemin4) and additional snRNP components as Gal-1 and Gal-3 binding partners(323). Together, these findings strongly implicate Gal-1 and Gal-3 involvement in the process of pre-mRNA splicing through both protein-protein and protein-nucleic acid interactions.

Regulation of RNA by galectins has been recently confirmed in a study that demonstrated a role for Gal-3 in stabilizing transcripts of membrane-associated epithelial mucin, MUC4, in cancer cells. Mucins are important mediators of barrier function and homeostasis in healthy epithelial tissue, but their over-production promotes proliferation and motility in cancers, including pancreatic and bile-duct carcinomas, where their expression is strongly correlated with that of *LGALS3* mRNA levels. Because Gal-3 is also upregulated in these cancers and was previously shown to regulate RNA through direct and indirect mechanisms, the authors hypothesized that Gal-3 might alter *MUC* transcript stability. They found that cytoplasmic Gal-3 interacts with hnRNP-L in perinuclear granules to increase hnRNP-L association with a CA repeat element in the 3'UTR of *MUC4* mRNA, thus doubling the half-life of the *MUC4* transcript(324). Supporting this finding *in vivo*, they found that *LGALS3*^{-/-} mice had significantly lower levels of epithelial *MUC4* mRNA and hnRNP-L protein in the jejunum(325).

While together these findings clearly demonstrate that galectins can be involved in pre-mRNA and mRNA processing under certain conditions, it is important to recall that both *LGALS1* and *LGALS3* ^{-/-} mice are viable and exhibit grossly normal development and life-span. The latter observation is key to contextualizing the RNA-regulatory functions put forward for Gal-1 and Gal-3 because null mutations in the basal components of the spliceosome are almost universally lethal at the cellular level in both unicellular and multicellular eukaryotes(326). The only known human genetic diseases resulting from mutations in essential mRNA splicing components are sporadic autosomal dominant retinitis pigmentosa (RP) and spinal muscular atrophy (SMA), both of which result from

only partial loss of function mutations in essential spliceosome components. It is therefore most likely that the observed roles of Gal-1 and Gal-3 in this process are accessory, specific to certain transcripts, or induced in neoplasm or inflammation.

Intracellular Signaling: Proliferation and Apoptosis

Early studies of Gal-3 revealed that it was upregulated in human T-cell leukemia virus (HTLV) infected T cells and that its overexpression was sufficient to promote proliferation and confer resistance to apoptosis(304). These findings led to further investigation and the discovery of a functional BH1 (NWGR) domain, common to proto-oncogenes of the Bcl-2 family, in the C-terminus of Gal-3(327, 328). Consistent with a role in oncogenesis, Gal-3 has since emerged as a biomarker of numerous cancer types, in some cases correlating with disease progression and resistance to therapy (329–332). Interestingly, some have found opposing roles for cytoplasmic and nuclear Gal-3, with the latter localization promoting apoptosis(333). Additional work has demonstrated that this pro/anti-apoptotic switch is induced by chemotherapeutic agents and mediated by nuclear export upon Ser6 phosphorylation of Gal-3(334). The role of endogenous Gal-3 in homeostatic and developmental apoptosis remains to be thoroughly elucidated. Several studies have also investigated the observations that Gal-7 is downregulated in squamous cell carcinoma (SCC) and its overexpression in colon cancer cells can induce apoptosis(335).

The Galectin Lattice

The extracellular matrix is rich with variably modified beta-galactoside ligands, which can be crosslinked by specific galectins at the cell surface to form a functional lattice. *In vitro* binding studies using CHO cell glycosylation mutants have shown that the primary ligands for galectin-1, 3, 8, and 9 in particular are complex type N-glycans(336). N-glycan branching and extension is catalyzed in the medial golgi apparatus by a family of N-acetylglucosaminyltransferases encoded by MGAT1-5. The activity of these enzymes is regulated by flux through the hexosamine pathway, a primary metabolic route for synthesis of glycan building blocks, dependent on glycolysis. In addition to metabolic flux, the number of potential N-glycan sites on transmembrane receptors structurally encodes the graded affinity of a glycoprotein receptor for components of the galectin lattice. Interactions of these glycans and glycans produced by other anabolic pathways with various galectins and other carbohydrate binding proteins can regulate compartmentalization of the plasma membrane and control receptor exposure by modulating sensitivity to endocytosis(337). In general, growth/activation promoting receptors on cells encode a higher number of N-glycan sequons per extracellular amino acid (~70% occupied in the mammalian glycoproteome(338)); whereas arrest and differentiation promoting receptors encode fewer such sequons(338). Lau et al. used computational modeling and *in vitro* studies to show evidence that the number of N-glycan motifs coevolved with metabolic glycan branching enzymes to regulate the retention of specific receptors in the galectin lattice and control the transition between growth and arrest/differentiation in mammalian cells(339).

Determining the role of galectin lattices *in vivo* has been more challenging. One study by Smith et al., described a mechanism, which required galectin-3 mediated lattice formation on CD8+ T cells, by which the regulatory cytokine Interleukin-10 drives establishment of chronic viral infection. They demonstrated that IL-10 potently induces Mgat5 expression in antigen specific CD8+ T cells, which in turn enhances N-glycan branching and galectin-3 lattice formation. This lattice formation reduced antigen sensitivity of the affected cells and inhibited the ability of these antiviral effectors to clear chronic infection in mice(340). The latter finding suggests a fundamental role for galectin-lattice formation in tuning the sensitivity of the immune system, likely preventing unchecked activation and tissue damage at high levels of antigen exposure. In support of the theory that metabolic flux and environment influence N-glycan branching and galectin lattice formation *in vivo*, Demetriou et al have found that T cell receptor (TCR) clustering cross-linked by galectin-3 binding (and potentially other galectins) was deficient in T cells from Mgat5 null mice(341). Following up on these studies, the Demetriou group showed that genetic variants in Mgat enzymes altered surface retention of immune cell receptors in multiple human autoimmune diseases including multiple sclerosis and type 1 diabetes(342–344). A similar lattice-mediated stabilization may also be at play on the surface of B cells during antigen encounter. Obino et al. recently found that Gal-8 interacts with the B cell receptor(345).

Early studies of Gal-1 indicated its potential role in regulating immune cell functions. Exogenous administration of Gal-1 in a rabbit model of the autoimmune disease myasthenia gravis dampened immune cell-mediated damage(346). While the

latter finding demonstrated therapeutic potential of galectins, the role(s) of Gal-1 *in vivo* has remained more elusive. However, endogenous Gal-1 expression has been shown in lymphoid organs and implicated in the development and function of mature lymphocytes. Thymocyte-epithelial cells and thymocytes of the thymic cortex, but not medulla show surface expression of human galectin-1 *in vivo*. The association of Gal-1 with cortical epithelial cells is dependent on core 2 O glycans on T cell associated receptor CD43 and CD45, spatially and developmentally regulated during thymocyte development(347). Gal-3, Gal-8, and Gal-9 are also notable for being broadly expressed in immune cells and lymphoid organs and many intra and extracellular functions for them have been proposed in the mammalian immune system.

Homeostasis

Because many studies of cytoplasmic galectins in intracellular signaling rely on tumor cell models, the proposed functions and interactions resulting from them are often most relevant to the dysregulated signaling environment that drives cancer. However, galectins also appear to function in the maintenance and re-establishment of homeostasis under normal conditions in several tissue types including the vascular endothelium, blood, muscle, and epithelial barriers(348).

Epithelial Barrier

The process of re-epithelialization is a critical step in wound-healing. Several studies support a role for galectins in the re-establishment of epithelial homeostasis in various tissues. Galectin-7, which is primarily expressed by stratified epithelial cells in

skin, and galectin-3 are both important factors *in vitro* in models of skin and corneal wound-healing. Supporting these roles, both *LGALS3* and *LGALS7* null mice exhibit defects in corneal and keratinocyte wound healing(349, 350). A recent study by Robinson et al. found that galectin-9 null mice are more susceptible to intestinal epithelial damage. They further showed that galectin-9 deficient organoids developed abnormally and showed defects in signaling pathways associated with growth and regeneration. These observation indicate a homeostatic role for galectin-9 in maintaining and repairing healthy intestinal epithelial barriers(351). Together these findings implicate multiple galectins in the maintenance and repair of epithelial barriers.

Vascular Endothelium

The genesis and branching of new blood vessels involve activation and chemoregulation of endothelial cells to form the inner lining of a new vessel. Galectins 1, 3, and 9 are expressed by activated and resting endothelial cells and extracellular addition of these galectins regulate endothelial migration *in vitro*(352–354). Supporting a role in placental angiogenesis, Gal-1 null mice have vascular defects in formation of the placental decidua and tumor associated Gal-1 has been shown to be important for tumor vascularization(355). These findings suggest a basal role for galectins in the development of vascular networks through angiogenesis in normal and neoplastic tissue.

Hemostasis

Several studies have implicated gal-1 and gal-8 in primary hemostasis, mediated by the activation and aggregation of platelets in the clotting cascade. Specifically,

platelets were found to contain high levels of gal-8, which became exposed during activation by thrombin. This surface exposed gal-8 amplified platelet activation by promoting fibrinogen binding, mobilizing calcium and membrane spreading mechanisms, and enhancing thromboxane and P-selectin expression(356). Gal-1 can also activate similar pathways in platelets and its expression contributes to ADP-induced aggregation suggesting a potential role in clotting(357). The latter finding is supported by the observation of normal platelet number but dysfunctional primary hemostasis in *LGALS1*^{-/-} mice(358). In **Figure 5** we summarize the functional roles of several galectins in maintenance and homeostasis of different tissues.

Cancer

Transformation

Ras genes encode a family of small GTPases, which act as binary molecular switches to transduce intracellular signals and promote growth, proliferation, and differentiation at the cellular level(359). Constitutive activation of *Ras* mutants results in uncontrolled cellular proliferation and is a molecular hallmark of many human cancers. Gal-1 and Gal-3 have both been shown by colocalization, co-immunoprecipitation, and knockdown experiments to interact with transforming mutants of *Ras* proteins in cancer cells, specifically H-*Ras* and K-*Ras*(360, 361). Additional work in breast carcinoma cells has demonstrated that Gal-3 is in part responsible for the isoform switch and resulting constitutive activation of N-*Ras* to K-*Ras*(362). Consistent with this finding and also with a role of extracellular Gal-3 in the tumor microenvironment, Gal-3 null mice do not support xenograft lung tumor growth(363). In addition, Gal-1 association enhances H-*Ras*

localization to the inner leaflet of the plasma membrane, which is an important step in constitutive activation(360). The latter finding is intriguing given the non-conventional pathway involving membrane associated counter-receptors by which Gal-1 is secreted under homeostatic conditions⁹². Adding clinical relevance to these findings, Chung et al. found that tumor progression is strongly associated with Gal-1 expression in clinical isolates of lung adenocarcinoma. Using lung cancer cell lines they went on to confirm that effects of Gal-1 on the cellular level were attributable to an interaction with Ras, driving COX expression and cellular proliferation. Knockdown of Gal-1 was sufficient to inhibit proliferative and increase sensitivity to chemotherapeutic agents(364). The role of extracellular Gal-1 as a negative regulator of tumor infiltrating lymphocytes and angiogenesis(352, 365, 366) has also been well characterized, so studies of galectin deficiency in mouse tumor models must be carefully designed to isolate intracellular and extracellular functions.

Tumor Microenvironment

Tumor infiltration by lymphocytes has been linked to a survival benefit in multiple cancers and predicts responsiveness to immunotherapy(367–370). Intriguingly, multiple galectins including Gal-1 and Gal-3 are often over-expressed in the tumor microenvironment(371). While many of these studies are correlative, recent work has begun to dissect specific mechanisms by which these galectins may modulate the tumor microenvironment to promote cancer cell survival and progression of disease. Tumor secreted Gal-3 binds to glycosylated IFN- γ , inhibiting its diffusion through the tumor stroma, which is an important chemokine gradient for tumor infiltrating lymphocytes(372).

Furthermore, levels of Gal-1 in head and neck tumors are inversely correlated with therapeutic efficacy of immune checkpoint inhibitors (ICIs). Kong et al., used mouse models of head and neck cancer to investigate this correlation, finding that galectin-1 acted on endothelial cells in the tumor microenvironment to upregulate programmed death ligand 1 (PD-L1), which induces senescence in activated tumor infiltrating lymphocytes bearing PD1. Blocking galectin-1 in these models rendered the tumor microenvironment permissive to T cell infiltration and more responsive to anti-PD1 therapy. Together these findings suggest that tumors can use immune galectins to regulate the microenvironment and suppress the host immune response to cancer(366).

Roles in the Mammalian Immune System

A large body of work on galectin functions has focused on roles within the mammalian immune system. And while many of these studies have compellingly implicated galectins in immune processes involving specific cell types—from developmental programming to activation, effector function and resolution of inflammation—global deletion of individual or multiple galectins in mice does not cause gross immunodeficiency. Instead of fundamentally disrupting the immune system, the absence of galectins results in a host of subtle but important alterations in susceptibility to certain autoimmune conditions and pathogens, signaling pathways, antigen sensitivity, immune cell localization and interaction. Together these changes suggest that ancestral galectins may have evolved to more generally mediate multicellular cooperative interactions in early metazoan lineages. Further supporting this framework for galectin evolution, expression of galectins is broad and varied beyond cells of the immune

system—suggesting conserved functions in tissue organization and homeostasis more generally. In this model, the evolving vertebrate and mammalian immune systems would have adopted the primordial galectins—as they have other carbohydrate binding proteins to facilitate the myriad dynamic responses necessary for the emergent complexity of our innate and adaptive immune systems. Consistent with this model, it has become clear that immune and non-immune cells regulate galectin expression for numerous functions. Rather than exhaustively detail observations of galectin function in specific immune cell populations, we seek here to highlight themes of galectin function within the mammalian immune system which occur in multiple cell types. In **Figure 6** we summarize major roles for galectins in the regulation and function of the immune system.

Engagement and Crosslinking of Surface Receptors

Early efforts to determine the activity of electrolectin (EL or Gal-1) led investigators to administer the recombinant protein as a therapeutic for autoimmune myasthenia gravis in rabbits. Surprisingly, administration of Gal-1 in this context, prevented myasthenic symptom onset and resolved the autoimmune disease completely. The researchers further noted that the therapeutic lectin had no direct effect on the magnitude of the humoral antibody response induced in the model or on the diseased muscular junction itself. Rather, the galectin was seen to bind and act upon lymphocytes(346). These initial observations led to a host of studies investigating the therapeutic effect of Gal-1 in animal models of autoimmune disease, many of which found that administration of Gal-1 consistently reduced the pathogenesis of T-cell mediated autoimmunity(373–376). Building on these observations, Perillo et al. experimentally tested the hypothesis that

Gal-1 directly killed T cells, finding that both recombinant Gal-1 and Gal-1 expressed on the cell surface of cultured endothelial cells was capable of inducing apoptotic cell death in activated, but not resting human T cells. Using antibody inhibition assays and swainsonine treatment, they further demonstrated that this effect was dependent on an interaction between Gal-1 and glycans decorating specific surface receptors including the common activated leukocyte antigen CD45RO and CD43. Antibodies against other prominent T cell receptors CD5, CD11a, CD28 and CD44 failed to inhibit Gal-1 induced apoptosis(377). While future studies by Stowell et al. demonstrated that aspects of these *in vitro* observations were mediated in part by the effect of certain reducing agents on the T cells themselves(278, 279), the ability of extracellular Gal-1 to alter immune cell fate and function by engaging specific glycoprotein receptors was established as a key mechanistic theme of galectin biology. Supporting these findings *in vivo*, endogenous Gal-1 expression has been shown in lymphoid organs and implicated in the development and function of mature T lymphocytes. Thymocyte-epithelial cells and thymocytes of the thymic cortex, but not medulla show surface expression of human galectin-1 *in vivo*. And the association of Gal-1 with cortical epithelial cells is dependent on core 2 O glycans on T cell associated receptor CD43 and CD45, spatially and developmentally regulated during thymocyte development(347). Gal-1 has also more recently been identified as a component of CD8+ T cell cytotoxic granules and may regulate FAS/FasL dependent death of target cells by altering cell death receptor endocytosis(378). Later studies of galectin-receptor interactions showed that Gal-3 could also induce cell death in T cells and bound to a host of cell surface receptors not all bound by Gal-1 including CD29,

CD98, CD71, CD43, and CD45(379). Gal-3 can also bind directly to the T cell receptor (TCR) to decrease antigen sensitivity under conditions of chronic infection in a manner dependent on metabolic flux, IL-10 mediated upregulation of MGAT branching enzymes, and nano-scale membrane compartmentalization of CD8 and TCR(340).

A similar cell surface receptor engagement mechanism has been proposed for the regulation by Gal-1 of dendritic cell trafficking. Dendritic cells bridge innate and adaptive immunity through their numerous roles in pattern recognition, cytokine production, and potent antigen presentation. DCs develop from circulating monocytes which differentiate into mature subsets in specific tissues. In response to inflammation and pathogen recognition, activated DCs traverse the extracellular matrix and endothelial cell layers to reach lymphatic channels in draining lymph nodes. Several studies have demonstrated a role for endothelial Gal-1 in regulating this process. Gal-1 is highly expressed in lymphatic endothelial cells and vascular endothelium of inflamed tissues as well as the inflamed tissue itself. Thiemann et al., demonstrated that Gal-1 in this context may inhibit egress of immunogenic dendritic cells bearing different core 2 O-glycans on CD43, while permitting the extravasation of tolerogenic DCs(380). In addition to controlling entry of inflammatory DCs to lymphoid compartments, Gal-1 exposure itself may reprogram DCs to a more tolerogenic phenotype. Ilarregue et al., found that Gal-1 primes mature DCs to enhance IL-10 production of CD4+ T cells in co-culture. While the latter experiments relied on exogenous treatment with Gal-1, they suggest the capacity of Gal-1 to modulate a multicellular circuit in the immune system in a specific and reproducible manner(381).

Gal-9 may also act by a similar mechanism on CD4+ T helper type 1 (Th1) cells through a direct interaction with glycans on T cell immunoglobulin and mucin protein 3 (TIM-3). Zhu et al., found that Gal-9 can bind to TIM-3 *in vitro* in a carbohydrate dependent manner and induce calcium dependent cell death of ex vivo Th1 but not Th2 cells. In the same study, injection of Gal-9 also resulted in a reduction in Th1 mediated pathology in a mouse model of multiple sclerosis. These findings are particularly interesting in the context of resolution of antiviral and antitumoral CD8+ T cell mediated immunity and the establishment of stable T cell memory as recent studies have defined a long-lived pool of CXCR5+, TIM3- CD8+ T cells, presumably refractory to the effects of Gal-9, that remain after chronic infection and mediate the proliferative burst after PD-1 blockade during chronic infection(382).

Regulation of Immune Cell Turnover

Neutrophils and neutrophil-like phagocytic immune cells execute some of the most primordial functions of multicellular immune systems. Neutrophils develop in the bone marrow (accounting for up to 60% of hematopoietic derived cells at homeostasis) and travel to sites of inflammation through blood vessels. Egress of neutrophils from the vasculature proceeds in a well-characterized cascade of selectin and integrin-mediated interactions with activated endothelial cells, which precede para or transcellular migration into infected and inflamed tissues. Recruited to these sites of inflammation, neutrophils execute effector functions to eliminate microbes and infected cells. The latter functions include phagocytosis of opsonized cells, production of reactive oxygen species and neutrophil extracellular traps, cytotoxic and microbicidal degranulation. In the mammalian

immune system, neutrophils can also bridge innate and adaptive immune responses by acting as antigen presenting cells and modulating inflammation through direct interactions with antigen specific T and B cells.

Galectins can regulate neutrophils through several well-defined pathways. Galectin-3 was originally discovered as a high affinity binding partner for IgE in rat basophilic leukemia cells(383). The over production of immunoglobulin E (IgE) with reactivity toward common environmental allergens and self-antigen drives type I hypersensitivity reactions associated with asthma and atopic dermatitis. During the late stages of asthmatic reactions, neutrophils accumulate at sites of inflammation in a manner requiring binding to IgE. However, neutrophils do not express either of two canonical IgE (Fc ϵ) receptor. Instead, this interaction has been shown to be mediated via galectin-3 IgE binding activity. Neutrophil associated galectin-3 binds IgE and activates the respiratory burst needed for ROS effector functions(384). Galectins may also serve as tissue factors that regulate neutrophil turnover, a key process in the resolution of inflammation. Early studies demonstrated that Gal-1, Gal-2, Gal-3, Gal-4 and Gal-8 are able to induce non-apoptotic phosphatidyl serine exposure in promyelocytic HL-60 cells as well as neutrophils(385, 386). These observations combined with data from galectin null animals, which can exhibit defects in neutrophil turnover in tissues are consistent with a model in which galectins can induce PS exposure on immune cells to mark them for a non-inflammatory turnover through phagocytosis. The reversible oxidative inactivation of galectin-1 may also serve to limit the activity of this galectin to sites of tissue damage, thereby preventing further localized damage while allowing the immune response to

proceed systemically(387). In **Figure 4** we illustrate the redox modulation of Gal-1 activity. While *in vivo* studies have provided some evidence consistent with this mechanism, studies using conditional and tissue specific knockout animals as well as immune cell transfers are needed to parse the contributions of immune cell intrinsic and tissue derived galectins in the resolution of inflammation following infection.

Modulation of Inflammatory Intracellular Signaling Pathways

As in cancer signaling networks, inflammatory signaling pathways have evolved to adopt intracellular galectins as accessory proteins and adaptors in the assembly of their most essential components. While galectins do not typically take center stage in these pathways, they have clearly evolved important modulatory roles in the amplitude and outcome of their activation. Intracellular Gal-3 in macrophages has been shown to mediate Nod-like receptor family, pyrin domain containing 3 (NLRP3) inflammasome activation during cholestatic liver injury(388). This observation was recapitulated in studies demonstrating that Gal-3 may act to indirectly regulate viral pathogenesis by modulating inflammasome activity during H5N1 infection, enhancing IL1b production and promoting inflammatory lung pathology(389).

Mature DCs extensively remodel membranous structures to maximize surface exposure to the environment and to mediate phagocytosis and other uptake mechanisms. Intracellular Gal-9 has been shown to regulate these membrane dynamics by modulating Rac1 dependent actin-cytoskeleton organization. Gal-9 is consequently essential for

maintaining the membrane integrity of dendritic cells *in vitro*(390). Consistent with this finding, Gal-9 null dendritic cells exhibit impaired phagocytic capacity.

Galectin-3 is highly expressed by macrophages and has been shown to antagonize pro-inflammatory polarization, favoring a fibrotic phenotype in several model systems(391) including mouse models of atherosclerosis(392). Galectin-3 promotes these fibrotic phenotypes, which can be either pathological or adaptive depending on the disease state, by driving alternative over classical activation of recruited macrophages in a positive feedback loop involving extracellular crosslinking of CD98 and PI3K signaling. The absence or inhibition of Gal-3 is sufficient to skew macrophages away from the alternative pathway toward classical activation(393).

Intracellular Pattern Recognition and Damage Sensing

In addition to interacting with signaling complexes, cytoplasmic galectins can restrict the invasion of intracellular pathogens through recognition of host and pathogen glycans exposed during endolysosomal damage. Recognition of pathogen and danger associated molecular patterns (PAMPs & DAMPs) by pattern recognition receptors (PRRs) is a hallmark of the innate immune system. In addition to cytoplasmic and endolysosomal membrane-associated sensors of viral RNA and DNA (RIG-I/MDA5, TLR3/7/8/9, and STING) immune lectins, which can recognize pathogen specific glycan signatures, have also been well characterized as innate immune effectors. However, the best studied examples of glycan sensing by host receptors occur in the extracellular space. Examples include mannose binding lectin (MBL), a C-type lectin, which binds

specifically to mannosylated glycans produced in abundance by certain pathogenic bacteria and parasites, initiating formation of bactericidal MBL attack complexes or recruitment of phagocytes within the lectin arm of the complement cascade(394, 395). In addition, Dectin-1 on macrophages and dendritic cells directly recognizes β -glucans on fungal pathogens, resulting in downstream Syk activation of an NF κ B mediated inflammatory program, which in turn stimulates metabolic reprogramming, phagocytosis and production of inflammatory cytokines: IL-6, IL-2, IL-23 and TNF(396).

While the cytosolic localization of galectins has long made them prime candidate sensors of intracellular pathogen glycan signatures, few studies have rigorously demonstrated this phenomenon experimentally. However, Thurston et al., have elegantly shown that intracellular galectin-8 can initiate anti-bacterial autophagy during invasion of the cell by *Salmonella Typhimurium*(314). Mechanistically, cytoplasmic galectin-8 is recruited to *S. Typhimurium* containing vesicles (SCVs) as they rupture, exposing host and bacterial glycans to the cytosol. The 2,3 sialyl-binding N-terminus of galectin 8 is required for recruitment to these damaged vesicles. Host and bacterial glycan-bound galectin-8 then serves as an adaptor for the autophagy initiating NDP52, the recruitment of which is necessary for galectin-8-mediated restriction of *S. Typhimurium* invasion and replication. Consistent with its role as a damage sensor during *S. Typhimurium* infection, galectin-8 also localizes to lysosomes damaged by the vacuolating cytotoxin A (Vac-A) produced by *H. pylori* where it also induces autophagy. Mechanistically this process was found to be dependent on toxin production by the bacteria and host O-glycan synthesis(397). Intriguingly, intracellular galectin-3 and galectin-9 (but not Gal-

1,2,4,7,10,12,13,14, or HSPC159) were also recruited to damaged vesicles in these studies. While they were not required to induce autophagy or restrict infection by the specific bacterial isolates tested, the ability of galectin-3 and galectin-9 to recognize endolysosomal damage are likely to have alternative immune or homeostatic functions. Indeed, galectin-3 has been shown to interact with the E3 ubiquitin ligase TRIM16 to mediate selective autophagy during *Mycobacterium tuberculosis* infection(398). In addition, earlier studies using immuno-electron microscopy observed accumulation of galectin-3 in and around *Shigella flexnari* containing vesicles in a glycan-binding dependent manner(399). Together these findings implicate specific cytosolic galectins as damage associated molecular pattern sensors for the endolysosomal system, a common site of invasion for intracellular pathogens.

Galectin-Pathogen Interactions

A major strategy used to probe the endogenous roles of galectins in the immune system has been to infect galectin-null systems (mice or cells) with various types and subtypes of bacterial, viral, fungal, or parasitic pathogens and monitor alterations in pathogenesis and immune response attributable to the missing galectin(400). In some cases, there is evidence that galectins can directly engage glycan ligands on the pathogen causing death, blocking infection or altering some aspect of its life cycle. This function is exemplified by work showing that bacterially expressed blood group antigen mimetics are targets for bactericidal activity of Gal-4 and Gal-8(401). In other studies, intracellular and extracellular galectin functions within or on responding immune cells or affected tissues are at cause. In the following section we highlight studies which suggest

that a direct interaction may occur between galectins and invading or commensal microorganisms. In **Figure 7** we detail significant galectin-pathogen interactions.

Bacteria

The role of galectins in direct immunity against microorganisms was first suggested by studies of galectin binding to glycan structures on lipopolysaccharide (LPS) from important human bacterial pathogens including *Neisseria meningitidis*, *Escherichia coli*, *Klebsiella pneumoniae*, and *Pseudomonas aeruginosa*. These studies largely focused on galectin-3 and demonstrated binding to isolated structures on LPS. Use of glycan microarrays and genetic variants of live bacteria demonstrated that among the innate immune lectins, galectin-3, 4 and 8 had remarkable specificity for bacterial molecular mimics of human ABO(H) blood group antigens(401). The possible evolutionary reason for these observations involving the host response to molecular mimicry was demonstrated by several recent studies. Pathogens have evolved glycosylation enzymes that produce terminal glycans structurally similar or identical to human ABO(H) blood group antigens(402). These modifications are thought to subvert the mammalian adaptive immune system, which has evolved a system of negative selection that deletes effector immune cells carrying receptors with autoreactive specificity(403, 404). As a result, individuals of each blood group are unable to produce antibodies with binding specificity to self-blood group antigens which may decorate an invading pathogen. Stowell et al. demonstrated a mechanism by which galectins (in particular galectins 4 and 8) may fill this gap in adaptive immunity by directly killing microbes bearing ABO(H) glycan structures(400). The many proposed and elucidated functions of specific galectins within

immune cells poses a major challenge to demonstrating galectin functions as direct anti-microbial effectors. Additional studies using global and conditional knockout models are needed to dissect the role of this activity *in vivo*. Despite the ability of galectin-3 to bind both bacterial pathogens *in vitro*, studies demonstrating increased susceptibility of galectin-3 null mice to *Helicobacter pylori* and *Neisseria meningitidis* could equally be due to deficits in immune cell function(405, 406).

Viruses

Galectins can act in the innate antiviral immune response on multiple levels—either directly interacting with viral glycoproteins or components of viral assembly factories or by modifying innate immune signaling pathways such as the inflammasome. Some studies have shown that galectin-1 can be upregulated in the lung during influenza A virus infection and may directly interact with the virus(407). Supporting a potential role for galectin-1 in influenza virus infection, a genome wide association study found that certain variants of human *LGALS1* were associated with significant reduction in mortality during poultry farm derived influenza A (H7N9) infection(408). It remains unknown, however what role(s) endogenous galectin-1 might play in IAV infection. *In vitro* studies have also shown that galectin-1 can bind to Nipah virus F glycoprotein to inhibit infection-induced syncytia formation in multiple cell types(409, 410). On the other hand, extracellular galectin-1 may also serve to mediate HIV infection or reservoir establishment as it enhances infection *in vitro* and exhibits broad and stable expression in lymphoid tissues(411). HIV has been shown to exploit intracellular galectin-3 activity in the ESCRT pathway to stabilize assembly and budding of new virions(412). While the aforementioned

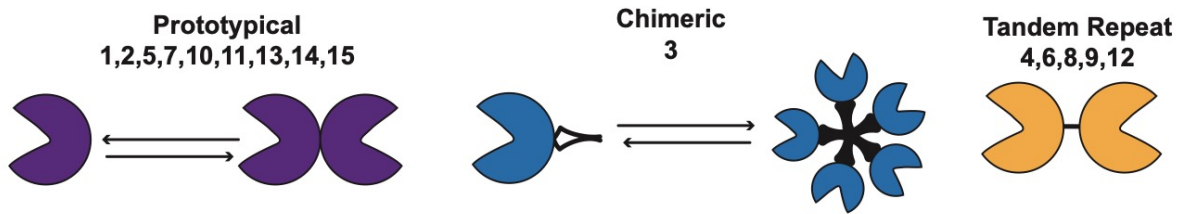
role of Gal-8 in intracellular endolysosomal damage sensing has mostly been studied in the context of intracellular bacteria, this function may also be at play during adenovirus infection, where gal-8 can recognize a PPxY motif in the viral capsid protein to initiate autophagy(413).

Summary and Conclusions

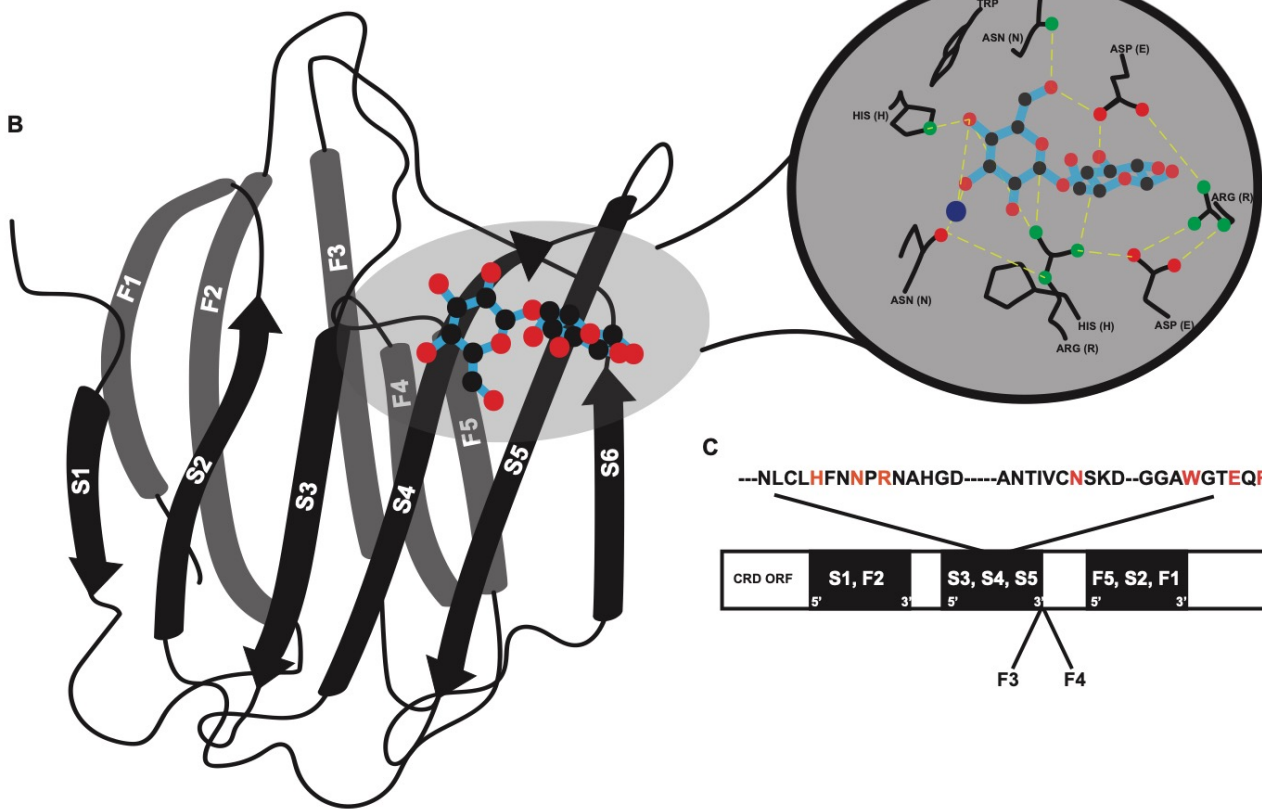
Many of the evolving mechanisms of galectin function point to a common theme in the evolution of ancient protein families: the layering and elaboration of multiple functions on proteins with single core functions. In the case of galectins, the conservation of carbohydrate recognition and its role in stabilizing and regulating the components of the ECM may well have been essential for the evolution of multicellular life. The primordial extracellular role may well have evolved within the mammalian immune system to encompass a host of specific galectin-receptor interactions important for development, activation, differentiation, and interaction of multiple immune cell populations. However, just as components of the cytoskeleton play numerous roles not just in reinforcing the cell structurally but also in signaling, metabolite sensing, cell division, and oncogenesis, galectin functions have diverged to include intracellular danger and pattern recognition, direct microbial killing, and even stabilization of pre-mRNA splicing components. The ubiquity and multi-compartmentalization of these galectin localization and functions and the potential for galectins to complement one another likely explain their roles in oncogenic transformation and progression of disease.

Figures Appendix 2

A



B



C

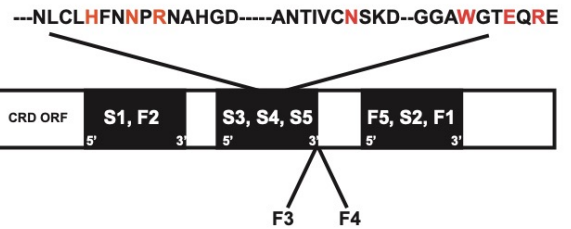


Figure 1. The galectin family of β -galactoside binding proteins.

A. Galectins are classified into three distinct groups based on their quaternary structure: prototypical, chimeric and tandem repeat. Prototypical: Gal-1, Gal-2, Gal-7, Gal-10, Gal-13 and Gal-14. Chimeric: Gal-3. Tandem repeat: Gal-4, Gal-8, Gal-9 and Gal-12. **B.** The galectin CRD is composed of six (S1-S6) and five stranded (F1-F5) anti parallel β -sheets oriented in a “jelly-roll” fold. **C.** Strands and amino acids required for ligand-binding (red) are encoded by LGALS loci with conserved exon structure and orientation.

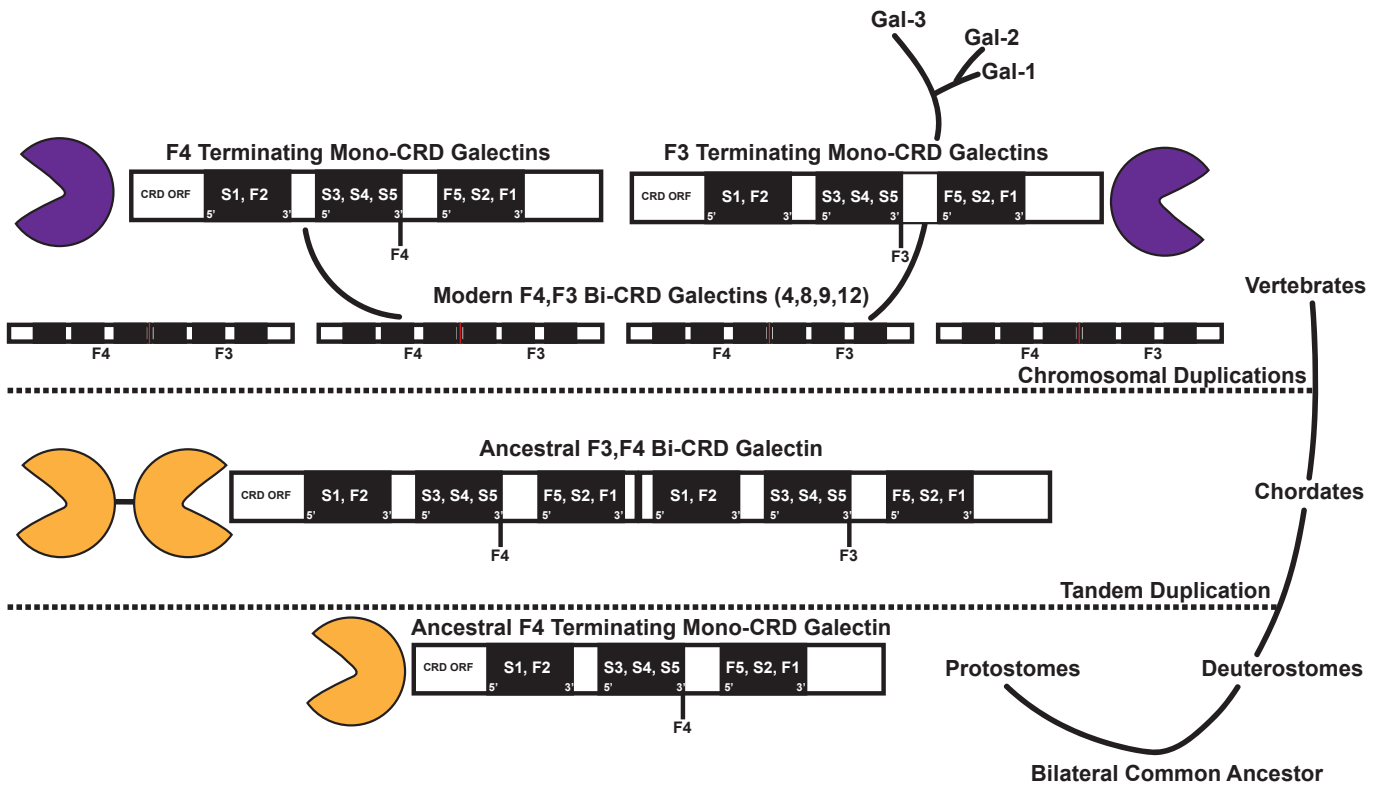


Figure 2. Evolution of galectins.

Analysis of gene structure and organization in extant lineages of multicellular life support the existence of a single ancestral mono-CRD galectin in the bilateral common ancestor of protostomes and deuterostomes with a middle exon terminating in a gene region encoding an F4 beta strand. The structural and functional diversity of vertebrate galectins seen today is likely to have subsequently arisen through first tandem, then en-masse gene duplication followed by additional duplications and divergent adaptations

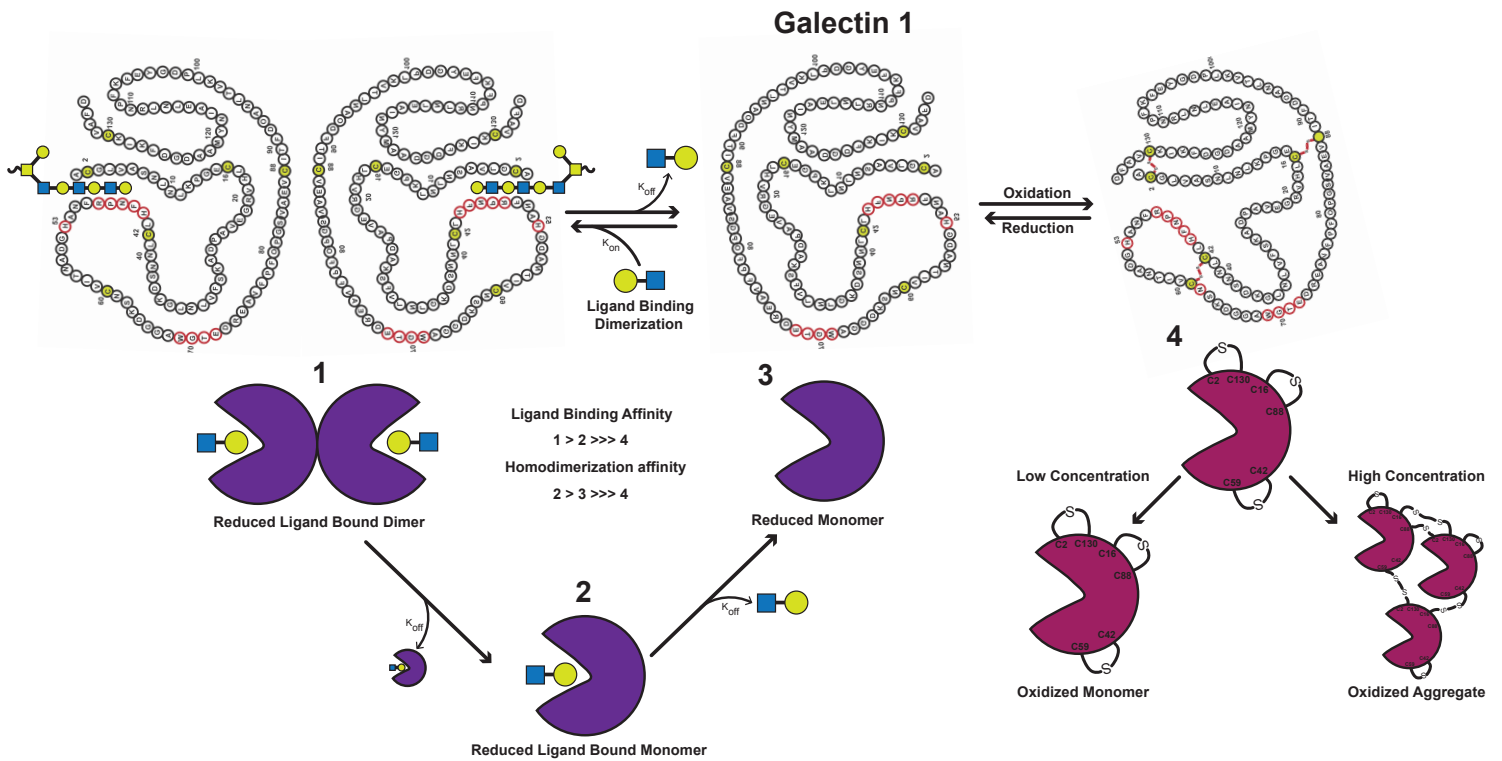


Figure 3. Galectin-1 is regulated by redox environment.

Galectins, first called S-type lectins due to the requirement of several galectins maintaining reduced thiols to enhance carbohydrate recognition activity, can form intra- and inter-molecular disulfide bridges that often result in significant conformational changes that preclude carbohydrate recognition. Upon oxidation Gal-1 can form three disulfide bonds resulting in an inactivating conformational change that dramatically inhibits ligand binding and oligomerization. At high concentration, bridges can form between Gal-1 monomers, resulting in aggregation and the potential for irreversible inactivation. By contrast, reducing environments activate Gal-1, promoting carbohydrate binding and dimerization. Dimerization also enhances ligand binding affinity of Gal-1.

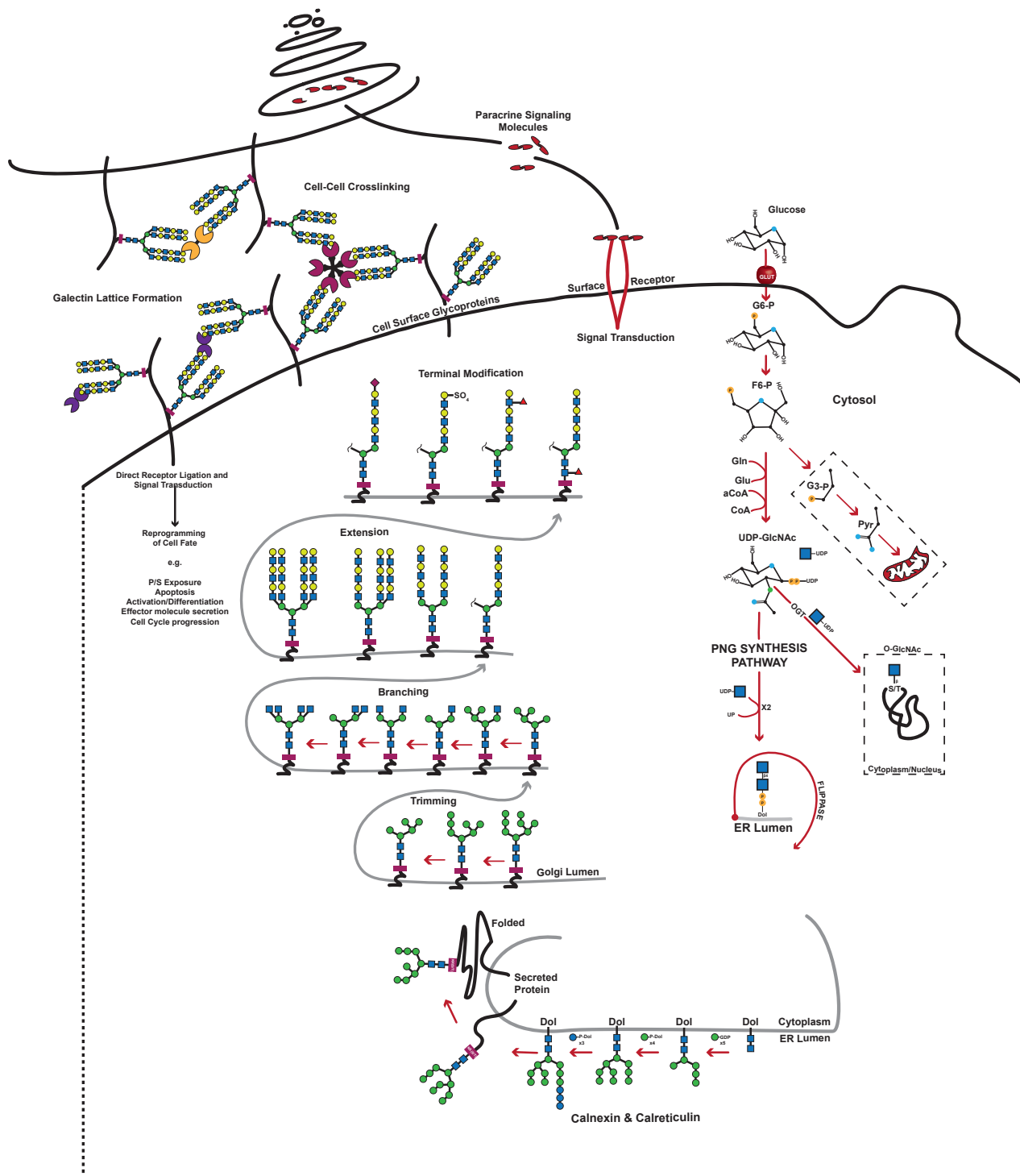


Figure 4. Glycan synthesis and lattice formation.

Metabolic flux through the glycolytic pathway forms substrates for protein N glycan synthesis (PNG), including UDP-GlcNAc, which is transferred onto dolichol phosphate on the cytosolic face of the ER. Following co-translational transfer of this PNG stem structure onto a newly synthesized glycoprotein, stepwise synthesis in the ER lumen builds a precursor glycan, $\text{Man}_5\text{GlcNAc}_2$, which is then trimmed and further modified to form the common PNG backbone $\text{Glc}_3\text{Man}_9\text{GlcNAc}_2$. Recognition of this precursor in the ER licenses glycoprotein transport to the cisternae of the golgi apparatus, where trimming, branching, extension and terminal modifications exponentially increase the repertoire of possible glycan adducts on secreted and membrane associated glycoproteins. In the extracellular space, these modifications can be recognized by non-classically secreted galectins whose multivalency can form lattice like structures, mediating cell-cell adhesion and nano-scale localization of membrane proteins. Galectins can also directly bind receptors bearing specific glycans resulting in signal transduction and cell reprogramming. Galectin-mediated cell-cell adhesion can also mediate paracrine signaling.

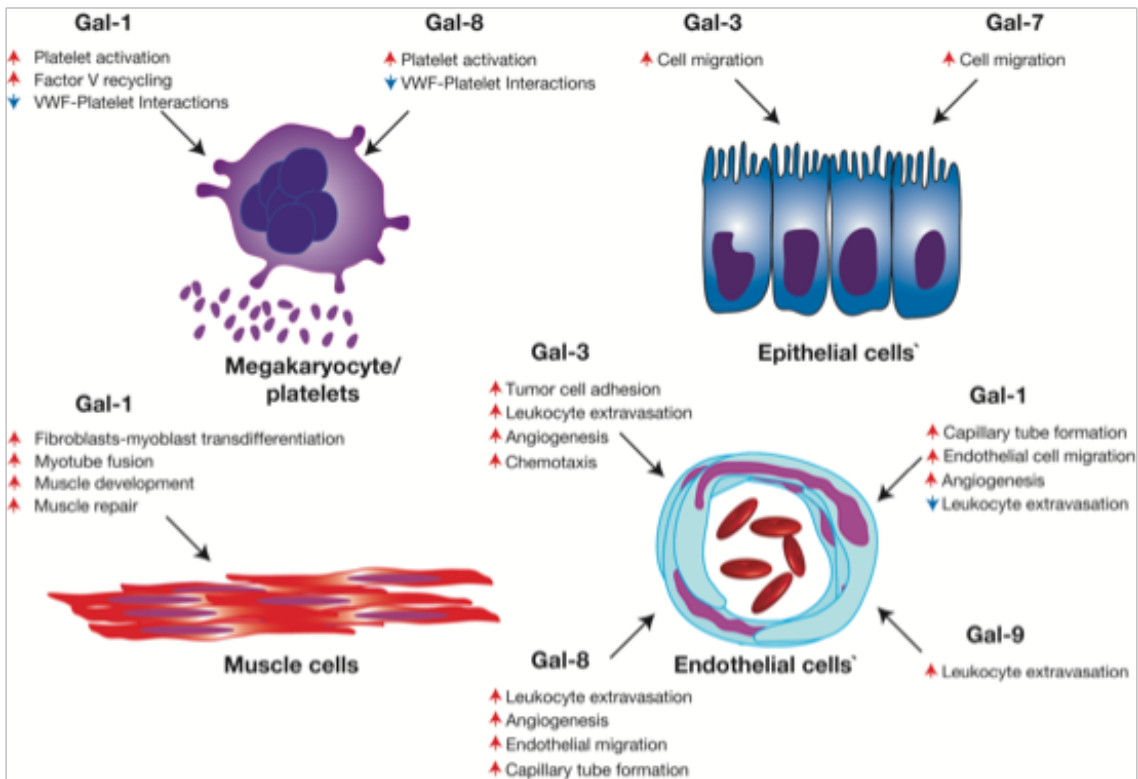


Figure 5. Galectins regulate hemostasis, angiogenesis and tissue repair.

Various members of the galectin family regulate megakaryocyte activity, hemostasis, angiogenesis, epithelial migration and general tissue repair following injury. Representative galectin-regulated activities are shown. Red arrows indicate an activity that the respective galectin increases, while blue arrows signify galectin-induced decreases in the accompanying activity. Plt = platelet.

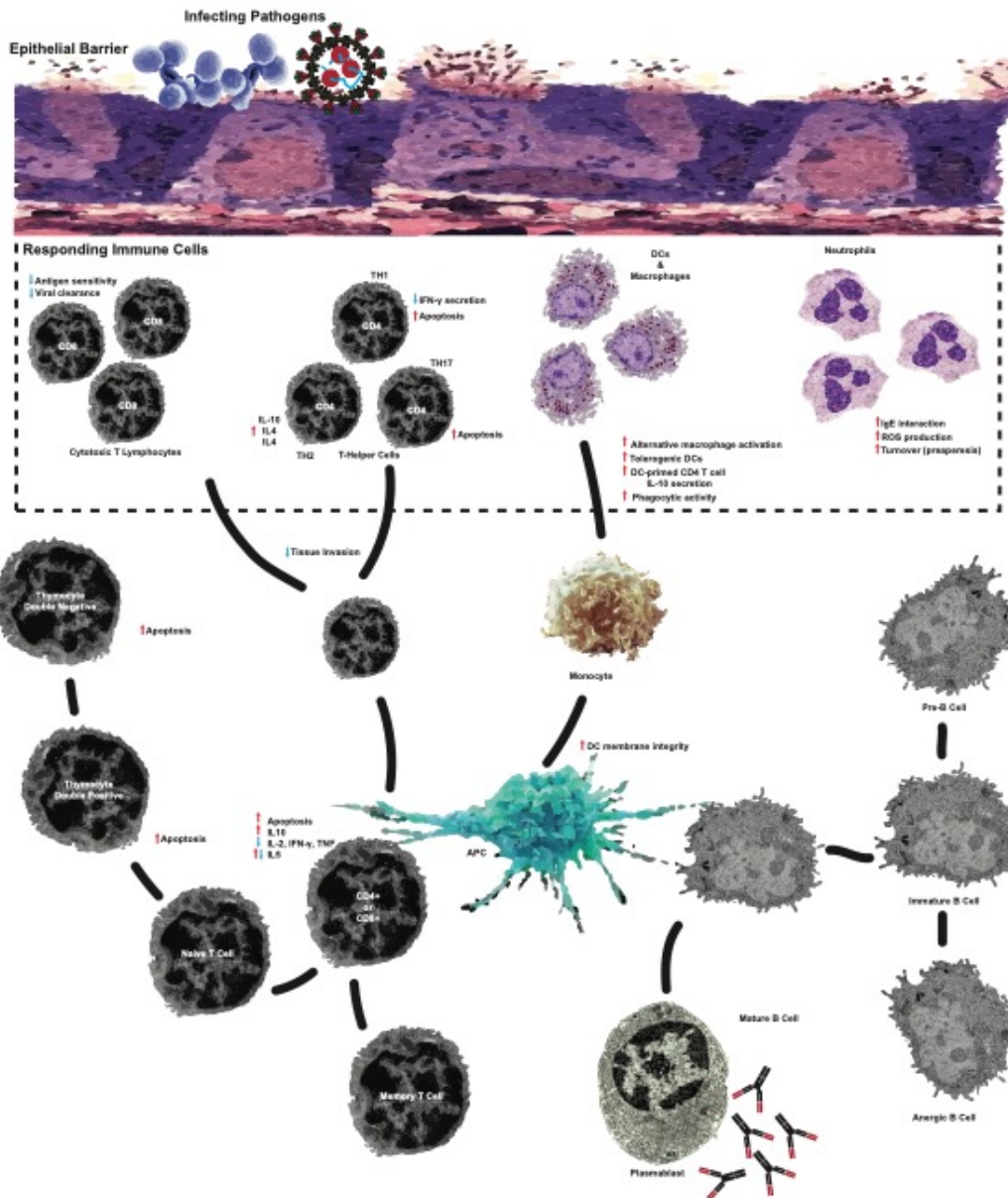


Figure 6. Galectin regulation of immune cell function.

Galectins have many putative functions in development and functioning of the mammalian immune system. Early studies suggested that galectins could influence T cell viability and cytokine secretion through their direct interactions with surface receptors. In parallel, researchers uncovered the ability of galectins to regulate granulocyte activation and turnover through a non-apoptotic mechanism termed preapoptosis. Later studies utilizing galectin null animal models revealed significant roles for galectins in the development of immature B and T lymphocytes and their polarization toward different inflammatory states.

As intracellular functions for galectins were uncovered, their relevance to innate and adaptive immune cell differentiation has been studied—revealing roles in modulation of intracellular signaling pathway, membrane integrity and remodeling, as well as cell cycle progression and differentiation.

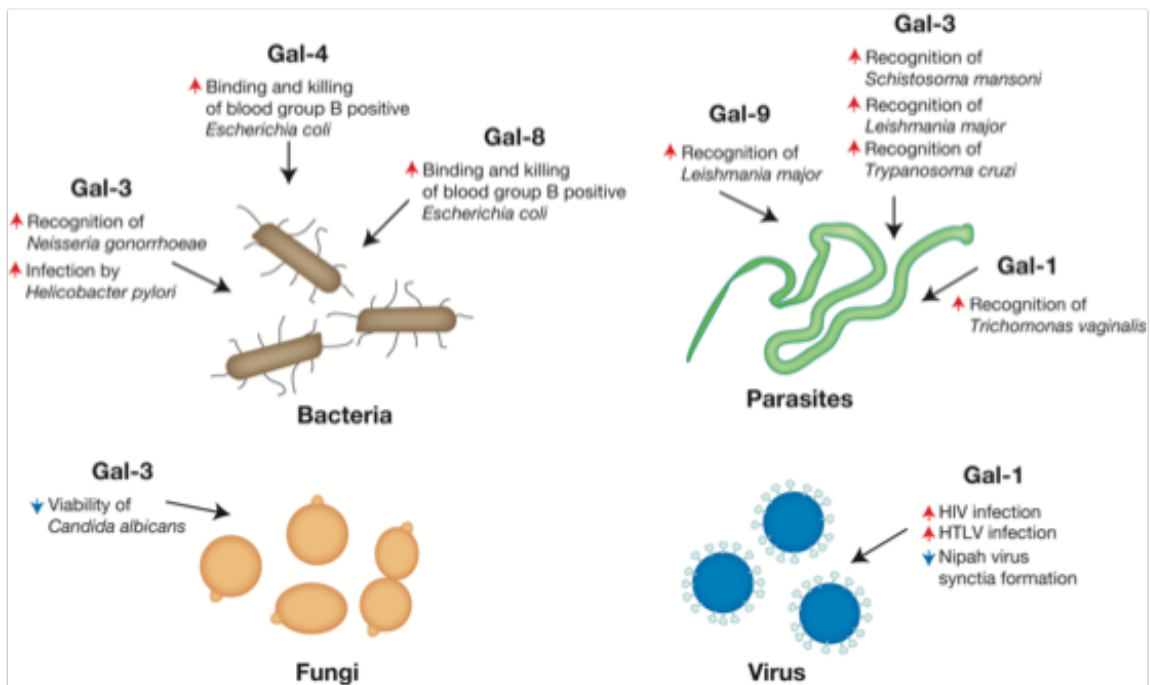


Figure 7. Galectins recognize a diverse range of pathogens.

While the immunoregulatory roles of galectins likely represent some of their most well-known functions, the ability of galectins to recognize a diverse range of pathogens may reflect some of their earliest evolutionary activities. Galectins recognition of pathogens can result in opsonization or direct microbial killing. In contrast, pathogens may utilize galectins to facilitate attachment and invasion. Representative galectin-regulated activities are shown. Red arrows indicate an activity that the respective galectin increases, while blue arrows signify galectin-induced decreases in the accompanying activity.

**Appendix 3
Infection**

Evaluating the Role of Galectin-1 during Influenza A Virus

Abstract

Galectins are a large ancient family of carbohydrate binding proteins with numerous intra- and extracellular functions in innate and adaptive immunity. Dissecting specific mechanisms of galectin function in these complex systems has been challenging due to the size of the family and overlapping, broad glycan specificity. Gal-1, the first identified member of this family, has putative functions in regulating autoimmunity, leukocyte turnover, and viral infection based largely on effects of its therapeutic administration in animal models and *ex vivo* activity in isolated immune cells. However, endogenous function(s) of Gal-1 in the mammalian immune system remain poorly defined. To explore possible endogenous Gal-1 immune functions, we employed a well-characterized model of influenza A virus infection in Gal-1 deficient mice finding that global Gal-1 knockout paradoxically results in attenuated weight loss and increased early lung viral load relative to wildtype animals. Levels of antiviral cytokines including type I interferons were also elevated early in the lung of IAV infected *Lgals*^{-/-} mice. To dissect the immune compartment contributing to this phenotype, we performed bulk RNA sequencing separately on lung resident lymphocytes and pulmonary epithelial cells finding that the heightened interferon signature in Gal-1 knockout animals is reflected in the differentially expressed genes of the lymphocyte, but not the epithelial compartment early on. These findings were bolstered by results from bone marrow chimera experiments, which showed that transfer of Gal-1 deficient hematopoietic cells into wildtype animals was sufficient to confer an increase in lung viral load and cytokine response. While these studies are ongoing, we have identified the tissue resident lymphocyte compartment as the most likely source of altered immune function in the

absence of Gal-1. Future and ongoing studies will seek to identify specific cell types within this compartment where Gal-1 plays a role in antiviral immunity.

Introduction

Galectins are an evolutionarily ancient family of proteins that recognize the diverse, modifiable carbohydrate glycoconjugates that decorate host and pathogen surface receptors, lipid conjugates, and secreted proteins. While many studies of galectins in the mammalian immune system have revealed functions in the adaptive immunity, growing evidence suggests that galectins also serve as innate immune lectins with antimicrobial activity against select bacteria(401). However, the role of specific galectins during viral infection has not been defined.

Galectin-1 (Gal-1) forms a homodimer with specificity for terminal Gal β 1-4GlcNAc. Gal-1 is variably secreted by a non-canonical golgi-independent mechanism or retained within the cytoplasm of numerous cell types, including lymphocytes(414, 415). The earliest studies of Gal-1 function revealed its ability to suppress immune function in an autoimmune model of myasthenia gravis. Follow-up to this work suggested that Gal-1 might inhibit autoimmunity by enhancing T cell regulatory function and altering the interactions between developing T and thymic epithelial cells(416). Supporting these findings are the more recent observations that Gal-1 treatment enhances IL-10 secretion and inhibits IFN- γ secretion by both CD4+ and CD8+ T-cells. Gal-1 may also directly alter T cell activation and induce apoptosis, though the studies supporting these conclusions used Gal-1 preparations containing the reducing agent DTT, later shown to be essential for induction of apoptosis in this context(417, 418).

The activity of exogenous Gal-1 has varying consequences in viral infection. Exogenous addition of Gal-1 can inhibit Nipa virus mediated syncytia formation through interactions with the viral F glycoprotein(409, 410). In addition, Yang et al, showed that intranasal Gal-1 therapy could

reduce influenza A/WSN/33 virus replication *in vitro* and that Gal-1 can bind to IAV hemagglutinin. However, they did not directly test the ability of exogenous Gal-1 to block viral entry and replication as their model relied on transfection rather than treatment. By contrast, exogenous Gal-1 has been shown to enhance infection by certain viruses such as HIV-1 by stabilizing host-virus interactions(411, 419).

Studies of galectin function in the many cell types and compartments of the immune system are complicated by the varying localization and tissue distribution of galectins, including Gal-1 which can be nuclear, cytoplasmic, and extracellular. Even in the extracellular space, galectins can have autocrine or paracrine effects depending on their ability to transit the glycocalyxes of cells from which they are secreted. To address this, we sought to systematically study the Gal-1 deficient immune response to a well characterized viral infection *in vivo*. To this end, we challenged *Lgals*^{-/-} mice with Influenza A virus (Hong Kong/X31) and unexpectedly found that Gal-1 deficiency attenuated weight loss compared to *Wt* mice starting early during infection. Paradoxically, *Lgals*^{-/-} mice also exhibited increases in viral load during the early phase of infection and we observed a corresponding increase in antiviral cytokine responses in the lung. Because Gal-1 is ubiquitously expressed in both immune and non-immune compartments, we performed bulk RNA sequencing on sorted, lung resident lymphocytes and pulmonary epithelial cells early during infection to develop hypotheses about the level at which Gal-1 might be acting in response to IAV infection. Our analysis suggested that the increased cytokine and interferon signature was largely lymphocyte derived as top differentially regulated genes included type I interferons and ISGs. These findings were supported in a bone marrow chimera model where transfer of Gal-1 deficient hematopoietic cells was sufficient to increase viral load and cytokine responses in

irradiated wildtype recipients. Together, our ongoing investigation into the function of Gal-1 in the immune response to IAV infection have revealed that Gal-1 may restrict viral replication through actions in the early cellular innate immune response. The intriguing finding that Gal-1 deficiency increases viral load while attenuating weight loss also represents an opportunity to better understand the interaction between viral load dynamics and respiratory viral pathology. Ongoing and future studies will seek to identify specific immune cells involved in these phenotypes and dissect the specific role of Gal-1 in their biology.

Results

Galectin-1 deficient mice exhibit attenuated weight loss, increased viral load, and enhance cytokine responses during IAV infection.

To evaluate the role of Galectin-1 in the antiviral immune response, we intranasally challenged *Lgals1* ^{-/-} mice with Influenza A virus (Hong Kong/X31) and tracked weight loss, lung viral loads, and early cytokine responses. Gal-1 deficiency resulted in attenuation of weight loss compared to equivalently challenged Wt animals (**Figure 1A**). Paradoxically, we observed an increase in viral load associated with Gal-1 deficiency (**Figure 1B**), which was also associated with a higher early antiviral cytokine response at day 2 post infection (**Figure 1C**). These phenotypes led us to further explore the potential role of Gal-1 in the innate response to IAV infection.

Bulk RNA sequencing of Gal-1 deficient lymphocytes and epithelial cells during IAV infection

To identify the compartment (immune cells or epithelial barrier) involved in the phenotypes described above, we conducted bulk RNA sequencing in sorted lung resident lymphocytes and epithelial cells from naïve and day 2 infected *Lgals*^{-/-} and Wt mice (Experimental design and gating shown in **Figure 3A**). Gal-1 protein and transcript are both abundant in lung tissue (**Figure 2A and 2B**), however, at the transcript level *Lgals1* is more highly expressed in the lymphocyte compartment than the epithelial compartment. Furthermore, while Gal-1 does not appear to be induced by IAV infection in this model, expression of several other galectins were, including *Lgals3*, *Lgals3bp*, and *Lgals9*. Intriguingly, the expression of *Lgals3* is significantly elevated in the epithelial and lymphoid compartments during the response to IAV infection in Gal-1 knockout mice compared to Wt. This suggests a potential compensatory role for Gal-3 in the Gal-1 deficient immune system or may simply be a byproduct of differences we observed in the level of inflammation and dynamics of viral replication.

RNA sequencing analysis of Gal-1 deficiency in the epithelial and lymphocyte compartments during acute IAV infection

Bulk RNA sequencing of the lymphocyte compartment at day 2 post infection revealed gene signatures that are highly consistent with our observed phenotype of increased cytokine responses in the lung of Gal-1 deficient animals. Top upregulated genes included multiple type I interferons, cytokines, and chemokines as well as genes involved in T and NK cell function (**Figure 3C**). Interestingly, Gal-1 deficient mice had significantly higher levels of *IL1B* and *IL1R2*, suggesting possible baseline differences in sensitivity to immune stimuli (**Figure 3B**). The same differential gene expression patterns

were not observed in isolated epithelial cells, where the primary pathways enriched at day 2 post infection were related to kinase and metabolic pathways as well as carbohydrate recognition. These findings suggest that the increase in cytokine production observed in Gal-1 deficient mice is likely attributable to Gal-1 deficient lymphocytes.

Gal-1 in the lymphocyte compartment is sufficient to reduce viral load and cytokine response

In order to confirm that the Gal-1 deficient lymphocyte compartment was sufficient to confer the immune and virologic phenotypes we observed, we conducted a bone marrow chimera experiment in which Gal-1 deficient hematopoietic cells were transferred into irradiated *Wt* mice (experimental outline in **Figure 5A**). After transfer and recovery, we infected groups of mice who received *Lgals* *-/-* or *Wt* bone marrow with IAV X31 and monitored viral load as well as type I interferon responses in the lung. Consistent with our RNA sequencing results, we observed elevated viral load and cytokine responses in the mice that received Gal-1 deficient bone marrow (**Figure 5B and 5C**). Together these findings suggest that Gal-1 plays a role in the magnitude and function of the early cellular immune response to IAV infection. Future and ongoing work will seek to identify specific cells in which Gal-1 acts to exert its antiviral function.

Conclusion

In summary, we have shown that Gal-1 deficiency alters the immune response to IAV infection, increasing viral load in the lung and cytokine responses while paradoxically

attenuating the severity of disease, as assessed by weight loss. We followed up these studies using bulk RNA sequencing to further evaluate the source of these differences, isolating tissue resident lymphocytes and epithelial cells early during IAV infection. This analysis showed baseline differences in IL1 and IL1B expression and numerous interferon and interferon related genes differentially expressed in the Gal-1 deficient lymphocyte compartment after day 2 of infection. The epithelial compartment did not share these differential gene signatures. In addition, we find that transfer of Gal-1 deficient hematopoietic cells into *wt* animals recapitulated the viral load and cytokine response phenotypes seen in intact animals. These findings point to a lymphocyte source for these phenotypes and have prompted us to pursue further studies into the specific immune cell types involved and the mechanistic role that Gal-1 may play in their function. While previous studies have demonstrated the immunomodulatory and potential direct interactions of Gal-1(387, 407), none have systematically evaluated the role of endogenous Gal-1 in during IAV infection.

Experimental Procedures

Experimental models

8-10 weeks old C57BL/6 mice from Jackson Laboratory were used in this study as wildtype controls. PepBoy/J and Galectin-1^{-/-} mice were originally obtained from Jackson Laboratory and subsequently bred and maintained in our AAALAC accredited facility. All procedures were approved in observance of national guidelines by the Emory University IACUC.

Bone Marrow Chimeras

To generate bone marrow chimeras, Gal-1 knockout and *Wt* mice were euthanized and their femurs were harvested before processing to isolate bone marrow. Recipients were irradiated using X-rays twice with 6h between doses. 15E6 donor cells were transferred to each recipient mouse. Chimeras were then maintained on a solid food diet supplemented with 1.2% sulfamethoxazole and 0.2% trimethoprim for 4 weeks. Diets were supplemented every other day with wet food for the first 2 weeks following transfer. An additional 2 weeks were allowed for immune reconstitution and chimerism was assessed prior to infection using congenic markers CD45.2 and CD45.1

Viral infection

Mice receiving an intranasal (i.n.) challenge with influenza A/Hong Kong/X31(X31) were first anaesthetized in an isoflurane chamber before inoculation with 90,000 EID₅₀ of the virus in 30ul HBSS. Mice were weighed daily to generate weight curves and sacrificed by exsanguination after i.p. injection with avertin. For analysis of tissue resident lymphocytes, mice were intravenously injected with 1.5ug anti-CD45.2 or anti-CD3 [145-2C11] fluorophore conjugated antibody in 200ul PBS by the tail vein route 5 minutes prior to sacrifice.

Tissue preparation

BAL and other tissues were harvested after sacrifice(420). Briefly, to isolate single cell suspensions from lungs for flow cytometry, lungs were dissected and digested in 5g/L Collagenase D (Roche) and 2E6 units/L DNase (Sigma) for 30 minutes at 37C. 40%/80% Percoll gradients were used to enrich for lymphocytes. Spleens and mesenteric lymph

nodes were also mechanically dissociated and filtered through a 70 μ m filter before pelleting and staining for flow cytometry.

Flow Cytometry

Pelleted lymphocytes were Fc blocked with α CD16/32 before surface staining with various fluorescently conjugated antibodies along with influenza NP and PA specific class 1 restricted tetramers. Cell suspensions were also stained with live/dead stain Zombie NIR. Tetramers were provided by the NIH tetramer core facility.

Cell Sorting and Bulk RNA sequencing

Lung homogenates from naïve and Day 2 IAV X31 infected Wt and *Lgals*^{-/-} mice were prepared as described above without percoll gradient enrichment. Circulating cells were marked by i.v. labeling as described with anti-CD45.2 in PE. Cells were then surface stained with anti-CD45.2 in BV650 and anti-EPCAM-1 in BV421. 200,000 tissue resident lymphocytes or epithelial cells were sorted directly into RLT buffer on a BD FACS Aria with the help of the Emory Pediatrics Flow Cytometry core. Library preparation and bulk RNA sequencing were performed by the Emory Integrated Genomics Core.

Data analysis

RNA sequencing data were analyzed using ROSALIND®, which employs a HyperScale architecture developed by ROSALIND, Inc.. Read trimming was accomplished using cutadapt and quality scores were assessed using FASTQC. Read alignment to the *Mus musculus* genome build mm10 was done using STAR. Sample reads were quantified by HTseq and normalized via RLE using DESeq1 R library. Read

distribution percentages, violin plots, identity heatmaps, and sample MDS plots were generated as QC using RSeQC. P values were generated by DEseq2 with covariate correction. Gene lists were fed into DAVID for gene ontology and KEGG pathway analysis to determine fold enrichment scores. Other statistical analyses conducted in this appendix were accomplished using GraphPad Prism and the appropriate non-parametric Wilcoxon rank-sum for comparison of means. Statistical significance thresholds were set at $p=0.05$.

MDCK Plaque Assays

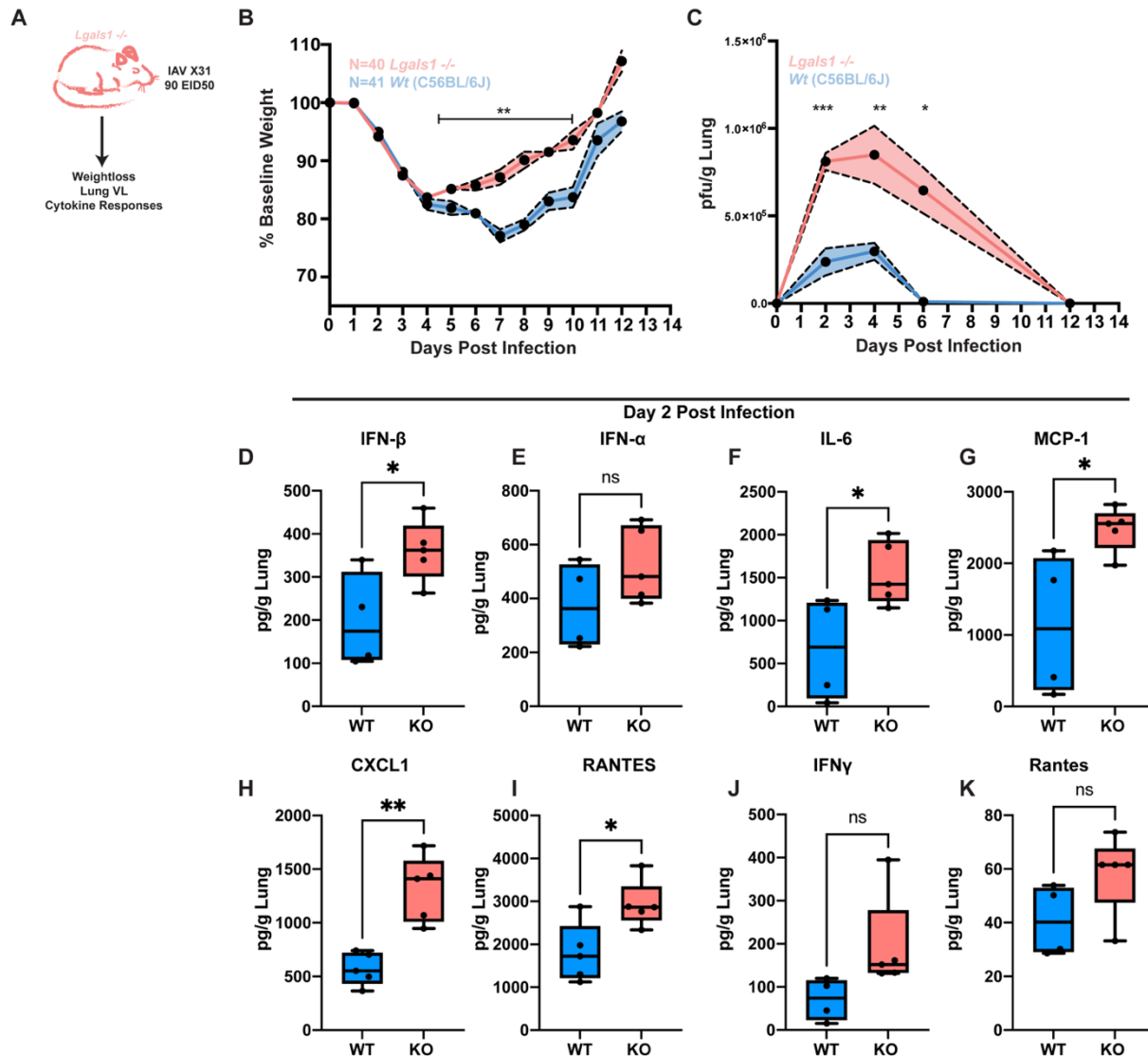
Lungs were weighed prior to sterile Dounce homogenization in RPMI supplemented with 1% BSA. Homogenates were then centrifuged at 600g for 10 minutes at 4C and supernatants were aliquoted and frozen. 0.8×10^6 MDCK cells per well were seeded in 6 well plates the night prior to performing plaque assays. After thawing on ice, supernatants were 10-fold serially diluted in PBS and inoculates were added in 200ul to MDCK monolayers. Infection was allowed to proceed for 1hr at 37C with rocking every 15 minutes to prevent drying of the monolayers. Monolayers were washed with PBS before being overlaid with 2mL of oxid agar (0.6%) in MEM supplemented with DEAE dextran and TPCK trypsin. Plaque assays were then incubated for 48hrs before fixing in 4% formaldehyde in PBS and staining with 0.08% crystal violet. Plaques were counted in multiple wells for each sample and the concentration of plaque forming units was determined using the following formula:

$$(\text{Average \# plaques/well} \times \text{Dilution factor} \times 5) = \text{PFU/mL}$$

Cytokine analysis

Lungs were Dounce homogenized for cytokine analysis as described above. Homogenates were diluted 1:2 prior to analysis using either bead-based legendplex mouse inflammation or antiviral cytokine assays (Biolegend). Duplicate standard curves were included in each assay run for quantification using the LegendPlex software. Cytokine concentrations were then used to determine a pg/g lung tissue for each animal.

Figures for Appendix 3



Galectin-1 deficiency alters weight loss, kinetics of viral replication and early cytokine responses during IAV infection. (A) Experimental challenge of *Lgals1*^{-/-} mice with 90 plaque forming units of influenza A virus X31 (IAV X31) (B) Daily weight loss curves expressed as a percentage weight loss from baseline. (C) Kinetics for IAV viral load as assessed by plaque assay in the lungs of *LGALS1*^{-/-} and C57/B6 WT mice expressed as pfu/gram of lung tissue. (D) Early antiviral cytokine levels in lung homogenates at day 2 post infection.

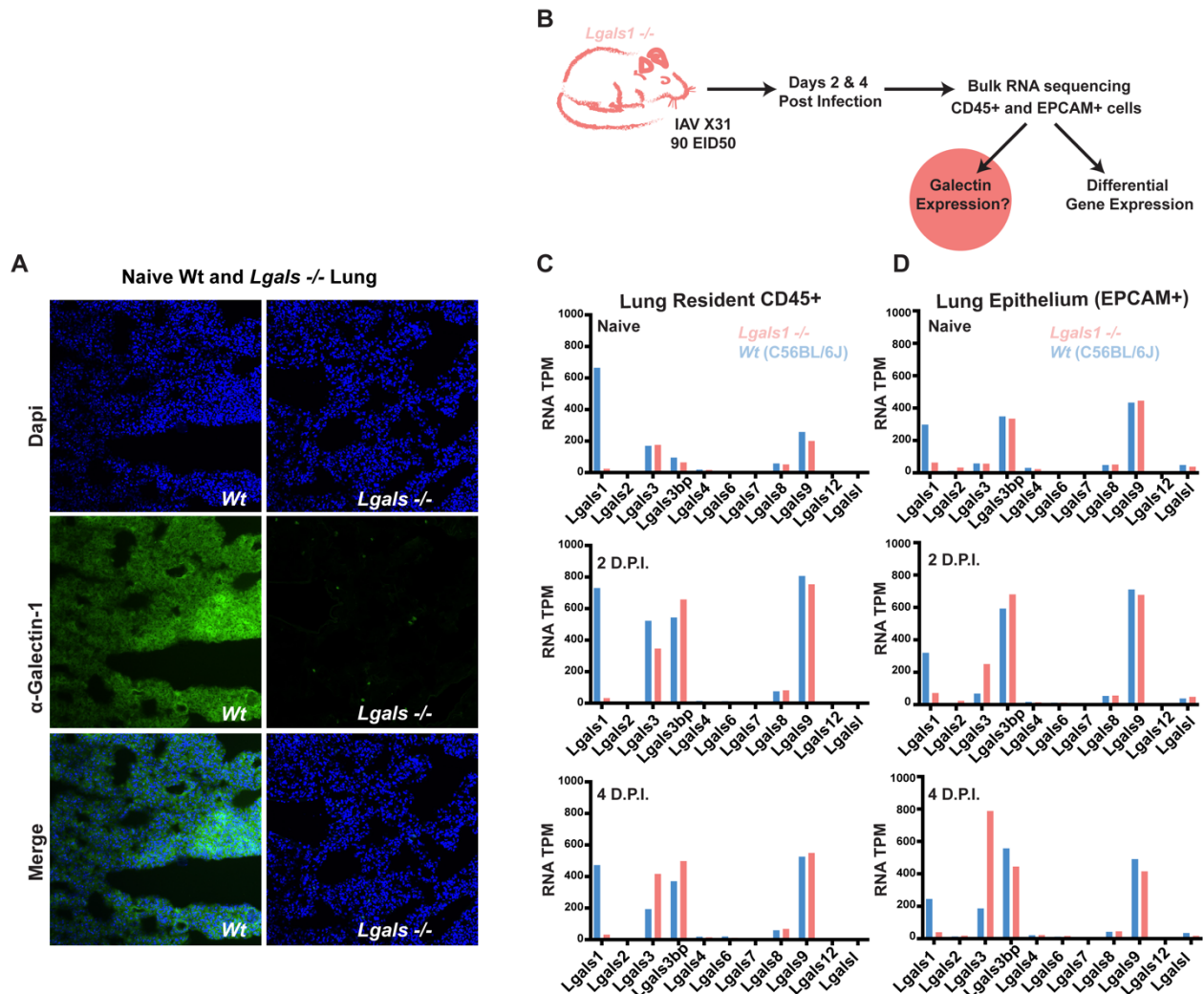


Figure 7.2 Expression of galectin-1 and other galectins in the lung. (A) Immunofluorescence microscopy of lung sections from Wt and *Lgals*^{-/-} mice at 20x magnification. (B) Experimental outline of bulk RNA sequencing approach to evaluate galectin and differential gene expression in immune and epithelial cells of the lung during IAV infection. (C) *Lgals* gene expression in lung resident CD45+ lymphocytes sorted from naïve and IAV infected *Lgals*^{-/-} and Wt mice at days 2 and 4 post infection expressed as transcripts per kilobase million (TPM). (D) *Lgals* gene expression in sorted lung EPCAM+ epithelial cells from the same experimental groups described in (C).

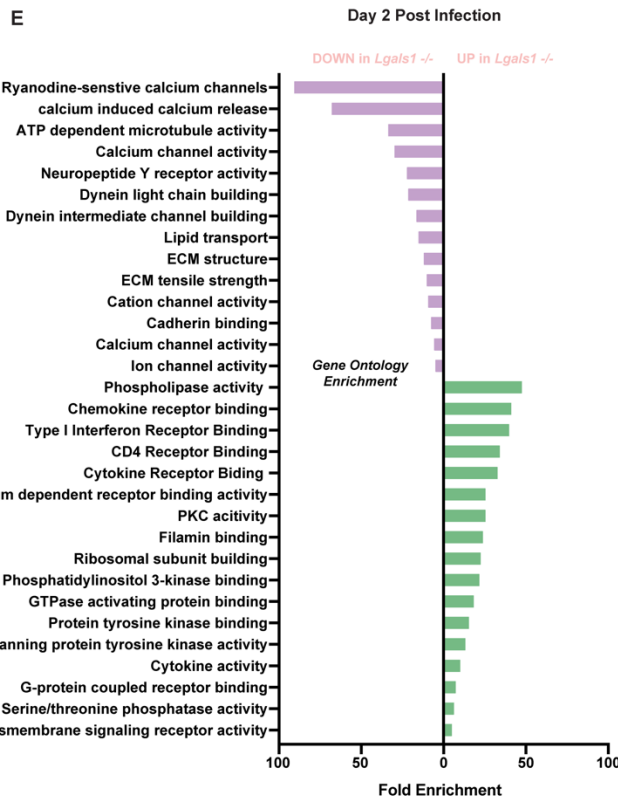
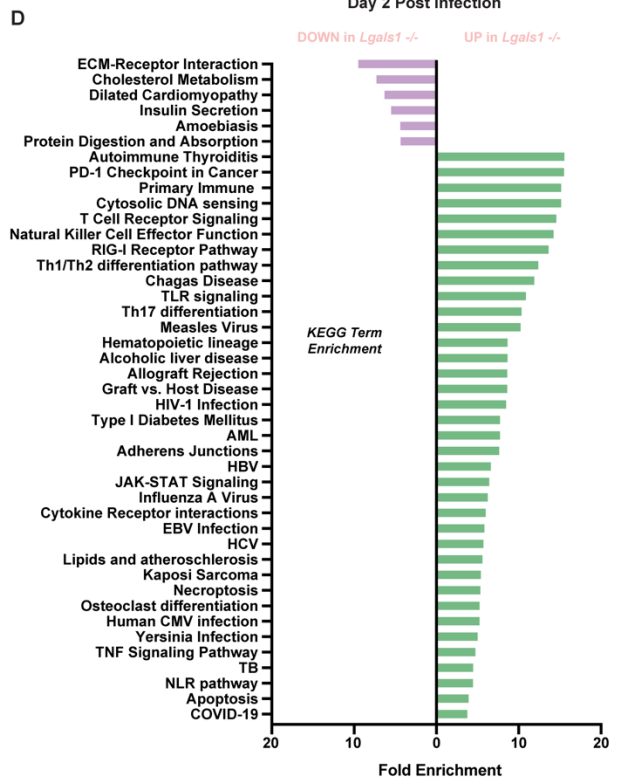
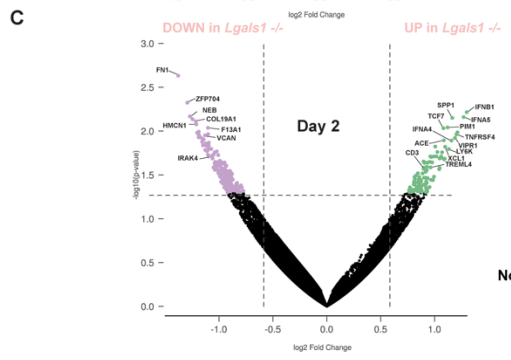
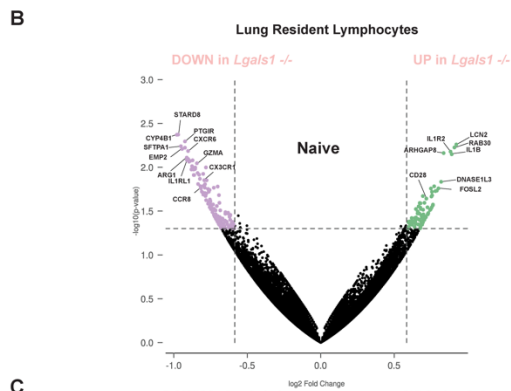
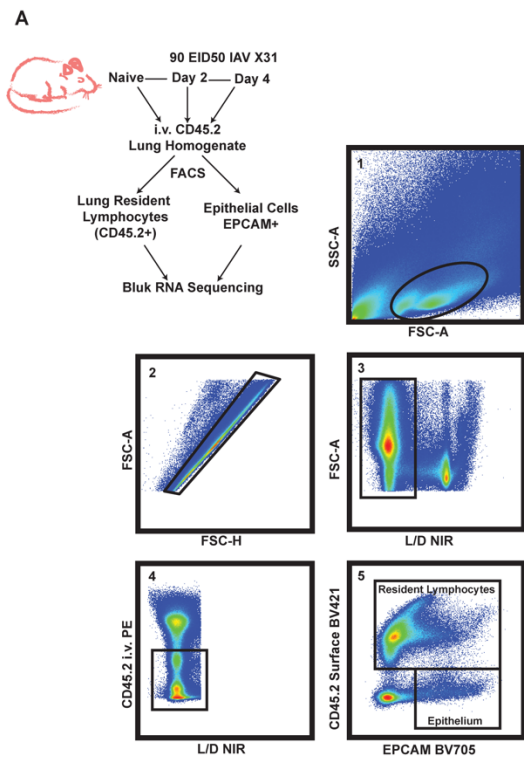


Figure 7.3 Early differentially regulated gene signatures in IAV infected *Lgals1*^{-/-} mice. (A) Experimental workflow for bulk RNA sequencing experiment and gating strategy for sorting of

CD45+ lung resident lymphocytes and EPCAM+ epithelial cells. (B) Volcano plot of differentially regulated genes in naïve *Wt* and *Lgals1* *-/-* mice. (C) Volcano plot showing DEGs at day 2 post infection. (D) KEGG pathway enrichment analysis of gene sets differentially regulated relative to *Wt* at day 2 post infection in the *Lgals1* *-/-* mouse. Pathways enriched for the gene set that was upregulated in the knockout relative to *Wt* are shown with green bars, while downregulated pathways in the knockout are shown with purple bars. (E) The same enrichment analysis is shown with gene ontology.

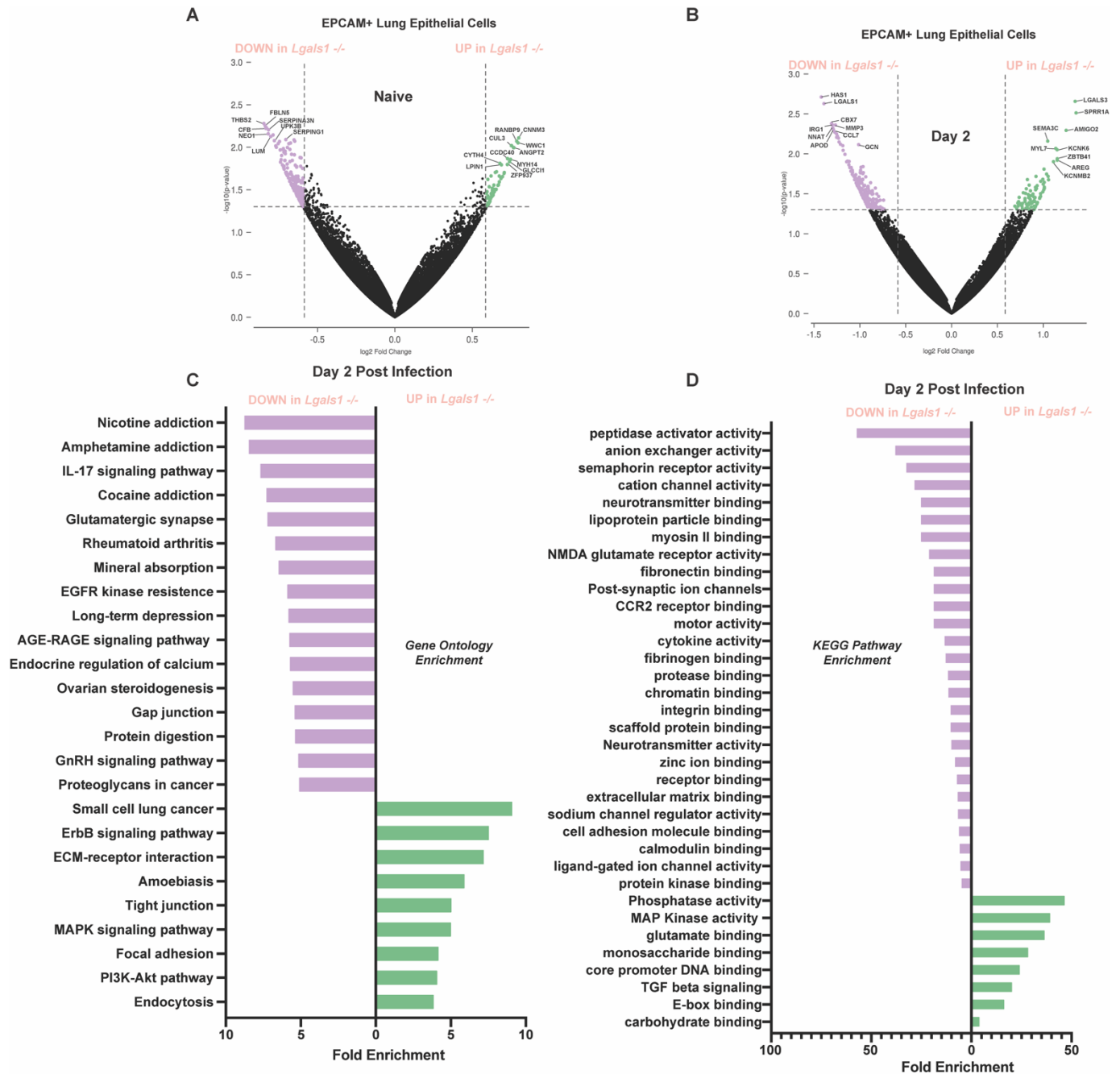


Figure 7.4 Differentially regulated genes in the galectin-1 deficient epithelial compartment during IAV infection. (A) Volcano plot showing differences in genes expressed in naïve *Lgals1*^{-/-} mice compared to *Wt* animals. (B) Volcano plot showing differences in genes upregulated during IAV infection at day 2 post infection in *Lgals1*^{-/-} mice relative to *Wt*. (C) Gene ontology enrichment analysis of ontologies overrepresented in gene sets that were up (green bars) or down (purple bars) regulated in the knockout relative to *Wt* at day 2 post IAV X31 infection. (D) KEGG pathways enriched in gene sets up (green bars) or down (purple bars) regulated in the galectin-1 knockout relative to *Wt* at day 2 post IAV X31 infection.

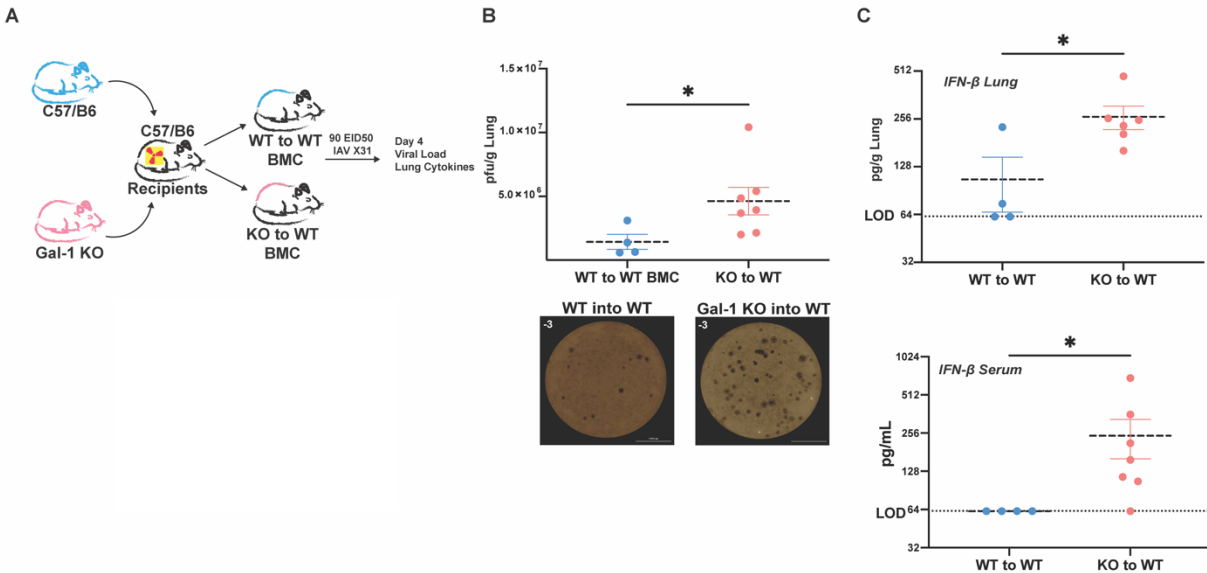


Figure 7.5 Gal-1 mediated restriction of viral load and enhancement of type I interferon is mediated by Gal-1 deficiency in the hematopoietic compartment. (A) Experimental design for bone marrow transfer. Groups of CD45.1 pepboy recipients were irradiated before receiving equivalent bone marrow from either Gal-1 KO or C57/B6 donors. (B) IAV X31 viral loads by plaque assay. (C) Levels of type I Interferon in the lung and serum of each recipient group.

References

1. WHO Coronavirus (COVID-19) Dashboard. <https://covid19.who.int>. Retrieved 30 March 2022.
2. Berlin DA, Gulick RM, Martinez FJ. 2020. Severe Covid-19. *N Engl J Med* 0:null.
3. Dupont A, Rauch A, Staessens S, Moussa M, Rosa M, Corseaux D, Jeanpierre E, Goutay J, Caplan M, Varlet P, Lefevre G, Lassalle F, Bauters A, Faure K, Lambert M, Duhamel A, Labreuche J, Garrigue D, De Meyer SF, Staels B, Vincent F, Rousse N, Kipnis E, Lenting P, Poissy J, Susen S, null null. 2021. Vascular Endothelial Damage in the Pathogenesis of Organ Injury in Severe COVID-19. *Arterioscler Thromb Vasc Biol* 41:1760–1773.
4. Chu DKW, Pan Y, Cheng SMS, Hui KPY, Krishnan P, Liu Y, Ng DYM, Wan CKC, Yang P, Wang Q, Peiris M, Poon LLM. 2020. Molecular Diagnosis of a Novel Coronavirus (2019-nCoV) Causing an Outbreak of Pneumonia. *Clin Chem* 66:549–555.
5. Kevadiya BD, Machhi J, Herskovitz J, Oleynikov MD, Blomberg WR, Bajwa N, Soni D, Das S, Hasan M, Patel M, Senan AM, Gorantla S, McMillan J, Edagwa B, Eisenberg R, Gurumurthy CB, Reid SPM, Punyadeera C, Chang L, Gendelman HE. 2021. Diagnostics for SARS-CoV-2 infections. 5. *Nat Mater* 20:593–605.
6. Rapid isolation and profiling of a diverse panel of human monoclonal antibodies targeting the SARS-CoV-2 spike protein | *Nature Medicine*. <https://www.nature.com/articles/s41591-020-0998-x>. Retrieved 12 April 2022.
7. Preanalytical issues affecting the diagnosis of COVID-19 | *Journal of Clinical Pathology*. <https://jcp.bmj.com/content/74/4/207>. Retrieved 31 March 2022.
8. Choi B, Choudhary MC, Regan J, Sparks JA, Padera RF, Qiu X, Solomon IH, Kuo H-H, Boucau J, Bowman K, Adhikari UD, Winkler ML, Mueller AA, Hsu TY-T, Desjardins M, Baden LR, Chan BT, Walker BD, Lichterfeld M, Brigl M, Kwon DS, Kanjilal S, Richardson ET, Jonsson AH, Alter G, Barczak AK, Hanage WP, Yu XG, Gaiha GD, Seaman MS, Cernadas M, Li JZ. 2020. Persistence and Evolution of SARS-CoV-2 in an Immunocompromised Host. *N Engl J Med* 383:2291–2293.
9. Wang J, Hang X, Wei B, Li D, Chen F, Liu W, Yang C, Miao X, Han L. 2020. Persistent SARS-COV-2 RNA positivity in a patient for 92 days after disease onset. *Medicine (Baltimore)* 99:e21865.
10. Owusu D, Pomeroy MA, Lewis NM, Wadhwa A, Yousaf AR, Whitaker B, Dietrich E, Hall AJ, Chu V, Thornburg N, Christensen K, Kiphibane T, Willardson S, Westergaard R, Dasu T, Pray IW, Bhattacharyya S, Dunn A, Tate JE, Kirking HL, Matanock A, Household Transmission Study Team. 2021. Persistent SARS-CoV-2 RNA Shedding Without Evidence of Infectiousness: A Cohort Study of Individuals With COVID-19. *J Infect Dis* 224:1362–1371.
11. Mina MJ, Parker R, Larremore DB. 2020. Rethinking Covid-19 Test Sensitivity — A Strategy for Containment. *N Engl J Med* 383:e120.
12. Connor BA, Rogova M, Garcia J, Patel D, Couto-Rodriguez M, Nagy-Szkal D, Rendel M. 2022. Comparative Effectiveness of Single vs Repeated Rapid SARS-CoV-2 Antigen Testing Among Asymptomatic Individuals in a Workplace Setting. *JAMA Netw Open* 5:e223073.

13. Lee CC, Segaloff HE, Cole D, Rosenblum HG, Morgan CN, Somers T, Desamunthorpe R, Foster MA, Currie D, Ruff J, Payne D, Whyte TJ, Abedi GR, Bigouette JP, Kahrs J, Langolf K, Remington P, Sterkel A, Kelly P, Westergaard RP, Bateman AC, Hsu CH, Tate JE, Kirking HL. 2022. A cohort study measuring SARS-CoV-2 seroconversion and serial viral testing in university students. *BMC Infect Dis* 22:314.
14. Verkerke H, Horwath M, Saeedi B, Boyer D, Allen JW, Owens J, Arthur CM, Nakahara H, Rha J, Patel K, Wu S-C, Paul A, Yasin N, Wang J, Shin S, Brown D, Normile K, Cole L, Meyers M, Lin H, Woods E, Isaac J, Broder K, Wade J, Kauffman RC, Patel R, Josephson CD, Reynolds S, Sherman M, Wrammert J, Alter D, Guarner J, Roback JD, Neish A, Stowell SR. 2021. Comparison of Antibody Class-Specific SARS-CoV-2 Serologies for the Diagnosis of Acute COVID-19. *J Clin Microbiol* 59:e02026-20.
15. Yong G, Yi Y, Tuantuan L, Xiaowu W, Xiuyong L, Ang L, Mingfeng H. 2020. Evaluation of the auxiliary diagnostic value of antibody assays for the detection of novel coronavirus (SARS-CoV-2). *J Med Virol* 92:1975–1979.
16. Yan Y, Chang L, Wang L. 2020. Laboratory testing of SARS-CoV, MERS-CoV, and SARS-CoV-2 (2019-nCoV): Current status, challenges, and countermeasures. *Rev Med Virol* 30:e2106.
17. Jin Y, Wang M, Zuo Z, Fan C, Ye F, Cai Z, Wang Y, Cui H, Pan K, Xu A. 2020. Diagnostic value and dynamic variance of serum antibody in coronavirus disease 2019. *Int J Infect Dis IJID Off Publ Int Soc Infect Dis* 94:49–52.
18. Loeffelholz MJ, Tang Y-W. 2020. Laboratory diagnosis of emerging human coronavirus infections - the state of the art. *Emerg Microbes Infect* 9:747–756.
19. Charlton CL, Kanji JN, Johal K, Bailey A, Plitt SS, MacDonald C, Kunst A, Buss E, Burnes LE, Fonseca K, Berenger BM, Schnabl K, Hu J, Stokes W, Zelyas N, Tipples G. 2020. Evaluation of Six Commercial Mid- to High-Volume Antibody and Six Point-of-Care Lateral Flow Assays for Detection of SARS-CoV-2 Antibodies. *J Clin Microbiol* 58:e01361-20.
20. Han X, Wang Y, Li S, Hu C, Li T, Gu C, Wang K, Shen M, Wang J, Hu J, Wu R, Mu S, Gong F, Chen Q, Gao F, Huang J, Long Y, Luo F, Song S, Long S, Hao Y, Li L, Wu Y, Xu W, Cai X, Gao Q, Zhang G, He C, Deng K, Du L, Nai Y, Wang W, Xie Y, Qu D, Huang A, Tang N, Jin A. 2021. A Rapid and Efficient Screening System for Neutralizing Antibodies and Its Application for SARS-CoV-2. *Front Immunol* 12.
21. Kongsuphol P, Jia H, Cheng HL, Gu Y, Shunmuganathan BD, Chen MW, Lim SM, Ng SY, Tambyah PA, Nasir H, Gao X, Tay D, Kim S, Gupta R, Qian X, Kozma MM, Purushotorman K, McBee ME, MacAry PA, Sikes HD, Preiser PR. 2021. A rapid simple point-of-care assay for the detection of SARS-CoV-2 neutralizing antibodies. 1. *Commun Med* 1:1–12.
22. Walls AC, Park Y-J, Tortorici MA, Wall A, McGuire AT, Veesler D. 2020. Structure, Function, and Antigenicity of the SARS-CoV-2 Spike Glycoprotein. *Cell* 181:281-292.e6.
23. Yan R, Zhang Y, Li Y, Xia L, Guo Y, Zhou Q. 2020. Structural basis for the recognition of SARS-CoV-2 by full-length human ACE2. *Science* 367:1444–1448.

24. Wang Q, Zhang Y, Wu L, Niu S, Song C, Zhang Z, Lu G, Qiao C, Hu Y, Yuen K-Y, Wang Q, Zhou H, Yan J, Qi J. 2020. Structural and Functional Basis of SARS-CoV-2 Entry by Using Human ACE2. *Cell* 181:894-904.e9.
25. Matsuyama S, Nagata N, Shirato K, Kawase M, Takeda M, Taguchi F. 2010. Efficient activation of the severe acute respiratory syndrome coronavirus spike protein by the transmembrane protease TMPRSS2. *J Virol* 84:12658–12664.
26. Petersen E, Koopmans M, Go U, Hamer DH, Petrosillo N, Castelli F, Storgaard M, Al Khalili S, Simonsen L. 2020. Comparing SARS-CoV-2 with SARS-CoV and influenza pandemics. *Lancet Infect Dis* 20:e238–e244.
27. Delgado JM, Duro N, Rogers DM, Tkatchenko A, Pandit SA, Varma S. 2021. Molecular basis for higher affinity of SARS-CoV-2 spike RBD for human ACE2 receptor. *Proteins* 89:1134–1144.
28. Cheng H-Y, Jian S-W, Liu D-P, Ng T-C, Huang W-T, Lin H-H, Taiwan COVID-19 Outbreak Investigation Team. 2020. Contact Tracing Assessment of COVID-19 Transmission Dynamics in Taiwan and Risk at Different Exposure Periods Before and After Symptom Onset. *JAMA Intern Med* 180:1156–1163.
29. Cevik M, Tate M, Lloyd O, Maraolo AE, Schafers J, Ho A. 2021. SARS-CoV-2, SARS-CoV, and MERS-CoV viral load dynamics, duration of viral shedding, and infectiousness: a systematic review and meta-analysis. *Lancet Microbe* 2:e13–e22.
30. Wölfel R, Corman VM, Guggemos W, Seilmaier M, Zange S, Müller MA, Niemeyer D, Jones TC, Vollmar P, Rothe C, Hoelscher M, Bleicker T, Brünink S, Schneider J, Ehmann R, Zwirgmaier K, Drosten C, Wendtner C. 2020. Virological assessment of hospitalized patients with COVID-2019. 7809. *Nature* 581:465–469.
31. Hui KPY, Cheung M-C, Perera RAPM, Ng K-C, Bui CHT, Ho JCW, Ng MMT, Kuok DIT, Shih KC, Tsao S-W, Poon LLM, Peiris M, Nicholls JM, Chan MCW. 2020. Tropism, replication competence, and innate immune responses of the coronavirus SARS-CoV-2 in human respiratory tract and conjunctiva: an analysis in ex-vivo and in-vitro cultures. *Lancet Respir Med* 8:687–695.
32. Li M-Y, Li L, Zhang Y, Wang X-S. 2020. Expression of the SARS-CoV-2 cell receptor gene ACE2 in a wide variety of human tissues. *Infect Dis Poverty* 9:45.
33. Cheung KS, Hung IFN, Chan PPY, Lung KC, Tso E, Liu R, Ng YY, Chu MY, Chung TWH, Tam AR, Yip CCY, Leung K-H, Fung AY-F, Zhang RR, Lin Y, Cheng HM, Zhang AJX, To KKW, Chan K-H, Yuen K-Y, Leung WK. 2020. Gastrointestinal Manifestations of SARS-CoV-2 Infection and Virus Load in Fecal Samples From a Hong Kong Cohort: Systematic Review and Meta-analysis. *Gastroenterology* 159:81–95.
34. SARS-CoV-2 productively infects human gut enterocytes. <https://www.science.org/doi/10.1126/science.abc1669>. Retrieved 30 March 2022.
35. Metz-Zumaran C, Kee C, Doldan P, Guo C, Stanifer ML, Boulant S. Increased Sensitivity of SARS-CoV-2 to Type III Interferon in Human Intestinal Epithelial Cells. *J Virol* 0:e01705-21.
36. Lehmann M, Allers K, Heldt C, Meinhardt J, Schmidt F, Rodriguez-Sillke Y, Kunkel D, Schumann M, Böttcher C, Stahl-Hennig C, Elezkurtaj S, Bojarski C, Radbruch

- H, Corman VM, Schneider T, Loddenkemper C, Moos V, Weidinger C, Kühl AA, Siegmund B. 2021. Human small intestinal infection by SARS-CoV-2 is characterized by a mucosal infiltration with activated CD8+ T cells. *Mucosal Immunol* 14:1381–1392.
37. Zhou J, Li C, Liu X, Chiu MC, Zhao X, Wang D, Wei Y, Lee A, Zhang AJ, Chu H, Cai J-P, Yip CC-Y, Chan IH-Y, Wong KK-Y, Tsang OT-Y, Chan K-H, Chan JF-W, To KK-W, Chen H, Yuen KY. 2020. Infection of bat and human intestinal organoids by SARS-CoV-2. *Nat Med* 26:1077–1083.
 38. Mao R, Qiu Y, He J-S, Tan J-Y, Li X-H, Liang J, Shen J, Zhu L-R, Chen Y, Iacucci M, Ng SC, Ghosh S, Chen M-H. 2020. Manifestations and prognosis of gastrointestinal and liver involvement in patients with COVID-19: a systematic review and meta-analysis. *Lancet Gastroenterol Hepatol* 5:667–678.
 39. Yeoh YK, Zuo T, Lui GC-Y, Zhang F, Liu Q, Li AY, Chung AC, Cheung CP, Tso EY, Fung KS, Chan V, Ling L, Joynt G, Hui DS-C, Chow KM, Ng SSS, Li TC-M, Ng RW, Yip TC, Wong GL-H, Chan FK, Wong CK, Chan PK, Ng SC. 2021. Gut microbiota composition reflects disease severity and dysfunctional immune responses in patients with COVID-19. *Gut* 70:698–706.
 40. Cevik M, Tate M, Lloyd O, Maraolo AE, Schafers J, Ho A. 2021. SARS-CoV-2, SARS-CoV, and MERS-CoV viral load dynamics, duration of viral shedding, and infectiousness: a systematic review and meta-analysis. *Lancet Microbe* 2:e13–e22.
 41. Guo M, Tao W, Flavell RA, Zhu S. 2021. Potential intestinal infection and faecal–oral transmission of SARS-CoV-2. *Nat Rev Gastroenterol Hepatol* 18:269–283.
 42. Cavanagh D. 2005. Coronaviruses in poultry and other birds. *Avian Pathol J WVPA* 34:439–448.
 43. Masters PS. 2006. The molecular biology of coronaviruses. *Adv Virus Res* 66:193–292.
 44. Weiss SR, Navas-Martin S. 2005. Coronavirus pathogenesis and the emerging pathogen severe acute respiratory syndrome coronavirus. *Microbiol Mol Biol Rev* 69:635–664.
 45. Origin and evolution of pathogenic coronaviruses | *Nature Reviews Microbiology*. <https://www.nature.com/articles/s41579-018-0118-9>. Retrieved 30 March 2022.
 46. Paules CI, Marston HD, Fauci AS. 2020. Coronavirus Infections—More Than Just the Common Cold. *JAMA* 323:707–708.
 47. Fung TS, Liu DX. 2019. Human Coronavirus: Host-Pathogen Interaction. *Annu Rev Microbiol* 73:529–557.
 48. Jackson CB, Farzan M, Chen B, Choe H. 2022. Mechanisms of SARS-CoV-2 entry into cells. *Nat Rev Mol Cell Biol* 23:3–20.
 49. Shang J, Wan Y, Luo C, Ye G, Geng Q, Auerbach A, Li F. 2020. Cell entry mechanisms of SARS-CoV-2. *Proc Natl Acad Sci* 117:11727–11734.
 50. Bayati A, Kumar R, Francis V, McPherson PS. 2021. SARS-CoV-2 infects cells after viral entry via clathrin-mediated endocytosis. *J Biol Chem* 296.
 51. Inhibitors of cathepsin L prevent severe acute respiratory syndrome coronavirus entry | *PNAS*. <https://www.pnas.org/doi/10.1073/pnas.0505577102>. Retrieved 30 March 2022.

52. Belouzard S, Chu VC, Whittaker GR. 2009. Activation of the SARS coronavirus spike protein via sequential proteolytic cleavage at two distinct sites. *Proc Natl Acad Sci U S A* 106:5871–5876.
53. Irigoyen N, Firth AE, Jones JD, Chung BY-W, Siddell SG, Brierley I. 2016. High-Resolution Analysis of Coronavirus Gene Expression by RNA Sequencing and Ribosome Profiling. *PLoS Pathog* 12:e1005473.
54. Schubert K, Karousis ED, Jomaa A, Scaiola A, Echeverria B, Gurzeler L-A, Leibundgut M, Thiel V, Mühlemann O, Ban N. 2020. SARS-CoV-2 Nsp1 binds the ribosomal mRNA channel to inhibit translation. *Nat Struct Mol Biol* 27:959–966.
55. Shuvalov A, Shuvalova E, Biziaev N, Sokolova E, Evmenov K, Pustogarov N, Arnautova A, Matrosova V, Egorova T, Alkalaeva E. 2021. Nsp1 of SARS-CoV-2 stimulates host translation termination. *RNA Biol* 18:804–817.
56. Mendez AS, Ly M, González-Sánchez AM, Hartenian E, Ingolia NT, Cate JH, Glaunsinger BA. 2021. The N-terminal domain of SARS-CoV-2 nsp1 plays key roles in suppression of cellular gene expression and preservation of viral gene expression. *Cell Rep* 37:109841.
57. Finkel Y, Mizrahi O, Nachshon A, Weingarten-Gabbay S, Morgenstern D, Yahalom-Ronen Y, Tamir H, Achdout H, Stein D, Israeli O, Beth-Din A, Melamed S, Weiss S, Israely T, Paran N, Schwartz M, Stern-Ginossar N. 2021. The coding capacity of SARS-CoV-2. *Nature* 589:125–130.
58. Knoops K, Kikkert M, Worm SHE van den, Zevenhoven-Dobbe JC, van der Meer Y, Koster AJ, Mommaas AM, Snijder EJ. 2008. SARS-coronavirus replication is supported by a reticulovesicular network of modified endoplasmic reticulum. *PLoS Biol* 6:e226.
59. Snijder EJ, Limpens RWAL, de Wilde AH, de Jong AWM, Zevenhoven-Dobbe JC, Maier HJ, Faas FFGA, Koster AJ, Bárcena M. 2020. A unifying structural and functional model of the coronavirus replication organelle: Tracking down RNA synthesis. *PLoS Biol* 18:e3000715.
60. Snijder EJ, Decroly E, Ziebuhr J. 2016. The Nonstructural Proteins Directing Coronavirus RNA Synthesis and Processing. *Adv Virus Res* 96:59–126.
61. Sawicki SG, Sawicki DL. 1995. Coronaviruses use discontinuous extension for synthesis of subgenome-length negative strands. *Adv Exp Med Biol* 380:499–506.
62. Sawicki SG, Sawicki DL. 1998. A new model for coronavirus transcription. *Adv Exp Med Biol* 440:215–219.
63. Scherer KM, Mascheroni L, Carnell GW, Wunderlich LCS, Makarchuk S, Brockhoff M, Mela I, Fernandez-Villegas A, Barysevich M, Stewart H, Suau Sans M, George CL, Lamb JR, Kaminski-Schierle GS, Heeney JL, Kaminski CF. 2022. SARS-CoV-2 nucleocapsid protein adheres to replication organelles before viral assembly at the Golgi/ERGIC and lysosome-mediated egress. *Sci Adv* 8:eabl4895.
64. Saraste J, Prydz K. 2021. Assembly and Cellular Exit of Coronaviruses: Hijacking an Unconventional Secretory Pathway from the Pre-Golgi Intermediate Compartment via the Golgi Ribbon to the Extracellular Space. *Cells* 10:503.
65. Ghosh S, Dellibovi-Ragheb TA, Kerviel A, Pak E, Qiu Q, Fisher M, Takvorian PM, Bleck C, Hsu VW, Fehr AR, Perlman S, Achar SR, Straus MR, Whittaker GR, de

- Haan CAM, Kehrl J, Altan-Bonnet G, Altan-Bonnet N. 2020. β -Coronaviruses Use Lysosomes for Egress Instead of the Biosynthetic Secretory Pathway. *Cell* 183:1520-1535.e14.
66. Xiong X, Qu K, Ciazynska KA, Hosmillo M, Carter AP, Ebrahimi S, Ke Z, Scheres SHW, Bergamaschi L, Grice GL, Zhang Y, Nathan JA, Baker S, James LC, Baxendale HE, Goodfellow I, Doffinger R, Briggs JAG. 2020. A thermostable, closed SARS-CoV-2 spike protein trimer. *Nat Struct Mol Biol* 1–8.
 67. Huang H-C, Lai Y-J, Liao C-C, Yang W-F, Huang K-B, Lee I-J, Chou W-C, Wang S-H, Wang L-H, Hsu J-M, Sun C-P, Kuo C-T, Wang J, Hsiao T-C, Yang P-J, Lee T-A, Huang W, Li F-A, Shen C-Y, Lin Y-L, Tao M-H, Li C-W. 2021. Targeting conserved N-glycosylation blocks SARS-CoV-2 variant infection in vitro. *EBioMedicine* 74:103712.
 68. Zhang S, Go EP, Ding H, Anang S, Kappes JC, Desaire H, Sodroski JG. 2022. Analysis of Glycosylation and Disulfide Bonding of Wild-Type SARS-CoV-2 Spike Glycoprotein. *J Virol* 96:e0162621.
 69. Yao H, Song Y, Chen Y, Wu N, Xu J, Sun C, Zhang J, Weng T, Zhang Z, Wu Z, Cheng L, Shi D, Lu X, Lei J, Crispin M, Shi Y, Li L, Li S. 2020. Molecular Architecture of the SARS-CoV-2 Virus. *Cell* 183:730-738.e13.
 70. Pirone L, Del Gatto A, Di Gaetano S, Saviano M, Capasso D, Zaccaro L, Pedone E. 2020. A Multi-Targeting Approach to Fight SARS-CoV-2 Attachment. *Front Mol Biosci* 7.
 71. The SARS-CoV-2 receptor-binding domain preferentially recognizes blood group A | Blood Advances | American Society of Hematology. <https://ashpublications.org/bloodadvances/article/5/5/1305/475250/The-SARS-CoV-2-receptor-binding-domain>. Retrieved 30 March 2022.
 72. Liu J, Lu F, Chen Y, Plow E, Qin J. 2022. Integrin mediates cell entry of the SARS-CoV-2 virus independent of cellular receptor ACE2. *J Biol Chem* 298.
 73. Yan R, Zhang Y, Li Y, Ye F, Guo Y, Xia L, Zhong X, Chi X, Zhou Q. 2021. Structural basis for the different states of the spike protein of SARS-CoV-2 in complex with ACE2. *Cell Res* 31:717–719.
 74. Benton DJ, Wrobel AG, Xu P, Roustan C, Martin SR, Rosenthal PB, Skehel JJ, Gamblin SJ. 2020. Receptor binding and priming of the spike protein of SARS-CoV-2 for membrane fusion. *Nature* 588:327–330.
 75. A noncompeting pair of human neutralizing antibodies block COVID-19 virus binding to its receptor ACE2. <https://www.science.org/doi/full/10.1126/science.abc2241>. Retrieved 11 April 2022.
 76. Garrett ME, Galloway JG, Wolf C, Logue JK, Franko N, Chu HY, Matsen FA IV, Overbaugh JM. 2022. Comprehensive characterization of the antibody responses to SARS-CoV-2 Spike protein finds additional vaccine-induced epitopes beyond those for mild infection. *eLife* 11:e73490.
 77. Yang H, Rao Z. 2021. Structural biology of SARS-CoV-2 and implications for therapeutic development. *Nat Rev Microbiol* 19:685–700.

78. Lu X, Pan J, Tao J, Guo D. 2011. SARS-CoV nucleocapsid protein antagonizes IFN- β response by targeting initial step of IFN- β induction pathway, and its C-terminal region is critical for the antagonism. *Virus Genes* 42:37–45.
79. Mu J, Xu J, Zhang L, Shu T, Wu D, Huang M, Ren Y, Li X, Geng Q, Xu Y, Qiu Y, Zhou X. 2020. SARS-CoV-2-encoded nucleocapsid protein acts as a viral suppressor of RNA interference in cells. *Sci China Life Sci* 63:1413–1416.
80. Chang C, Hou M-H, Chang C-F, Hsiao C-D, Huang T. 2014. The SARS coronavirus nucleocapsid protein--forms and functions. *Antiviral Res* 103:39–50.
81. Hsieh Y-C, Li H-C, Chen S-C, Lo S-Y. 2008. Interactions between M protein and other structural proteins of severe, acute respiratory syndrome-associated coronavirus. *J Biomed Sci* 15:707–717.
82. Sui L, Zhao Y, Wang W, Wu P, Wang Z, Yu Y, Hou Z, Tan G, Liu Q. 2021. SARS-CoV-2 Membrane Protein Inhibits Type I Interferon Production Through Ubiquitin-Mediated Degradation of TBK1. *Front Immunol* 12.
83. Wang Y, Liu L. The Membrane Protein of Severe Acute Respiratory Syndrome Coronavirus Functions as a Novel Cytosolic Pathogen-Associated Molecular Pattern To Promote Beta Interferon Induction via a Toll-Like-Receptor-Related TRAF3-Independent Mechanism. *mBio* 7:e01872-15.
84. Yang Y, Wu Y, Meng X, Wang Z, Younis M, Liu Y, Wang P, Huang X. 2022. SARS-CoV-2 membrane protein causes the mitochondrial apoptosis and pulmonary edema via targeting BOK. *Cell Death Differ* 1–14.
85. Mandala VS, McKay MJ, Shcherbakov AA, Dregni AJ, Kolocouris A, Hong M. 2020. Structure and drug binding of the SARS-CoV-2 envelope protein transmembrane domain in lipid bilayers. *Nat Struct Mol Biol* 27:1202–1208.
86. Schnell JR, Chou JJ. 2008. Structure and mechanism of the M2 proton channel of influenza A virus. 7178. *Nature* 451:591–595.
87. Nieto-Torres JL, Verdiá-Báguena C, Jimenez-Guardeño JM, Regla-Nava JA, Castaño-Rodríguez C, Fernandez-Delgado R, Torres J, Aguilera VM, Enjuanes L. 2015. Severe acute respiratory syndrome coronavirus E protein transports calcium ions and activates the NLRP3 inflammasome. *Virology* 485:330–339.
88. Siu K-L, Yuen K-S, Castaño-Rodríguez C, Ye Z-W, Yeung M-L, Fung S-Y, Yuan S, Chan C-P, Yuen K-Y, Enjuanes L, Jin D-Y. 2019. Severe acute respiratory syndrome coronavirus ORF3a protein activates the NLRP3 inflammasome by promoting TRAF3-dependent ubiquitination of ASC. *FASEB J* 33:8865–8877.
89. Ren Y, Shu T, Wu D, Mu J, Wang C, Huang M, Han Y, Zhang X-Y, Zhou W, Qiu Y, Zhou X. 2020. The ORF3a protein of SARS-CoV-2 induces apoptosis in cells. 8. *Cell Mol Immunol* 17:881–883.
90. Thorne LG, Bouhaddou M, Reuschl A-K, Zuliani-Alvarez L, Polacco B, Pelin A, Batra J, Whelan MVX, Hosmillo M, Fossati A, Ragazzini R, Jungreis I, Ummadi M, Rojc A, Turner J, Bischof ML, Obernier K, Braberg H, Soucheray M, Richards A, Chen K-H, Harjai B, Memon D, Hiatt J, Rosales R, McGovern BL, Jahun A, Fabius JM, White K, Goodfellow IG, Takeuchi Y, Bonfanti P, Shokat K, Jura N, Verba K, Noursadeghi M, Beltrao P, Kellis M, Swaney DL, García-Sastre A, Jolly C, Towers GJ, Krogan NJ. 2022. Evolution of enhanced innate immune evasion by SARS-CoV-2. 7897. *Nature* 602:487–495.

91. Zhang J, Cruz-cosme R, Zhuang M-W, Liu D, Liu Y, Teng S, Wang P-H, Tang Q. 2020. A systemic and molecular study of subcellular localization of SARS-CoV-2 proteins. *Signal Transduct Target Ther* 5:269.
92. Michel CJ, Mayer C, Poch O, Thompson JD. 2020. Characterization of accessory genes in coronavirus genomes. *Virology* 17:131.
93. Interferon-Stimulated Genes: A Complex Web of Host Defenses | Annual Review of Immunology. <https://www.annualreviews.org/doi/10.1146/annurev-immunol-032713-120231>. Retrieved 11 April 2022.
94. Xia H, Cao Z, Xie X, Zhang X, Chen JY-C, Wang H, Menachery VD, Rajsbaum R, Shi P-Y. 2020. Evasion of Type I Interferon by SARS-CoV-2. *Cell Rep* 33:108234.
95. Diamond MS, Kanneganti T-D. 2022. Innate immunity: the first line of defense against SARS-CoV-2. 2. *Nat Immunol* 23:165–176.
96. Ye Q, Zhou J, He Q, Li R-T, Yang G, Zhang Y, Wu S-J, Chen Q, Shi J-H, Zhang R-R, Zhu H-M, Qiu H-Y, Zhang T, Deng Y-Q, Li X-F, Liu J-F, Xu P, Yang X, Qin C-F. 2021. SARS-CoV-2 infection in the mouse olfactory system. 1. *Cell Discov* 7:1–13.
97. Tang AT, Buchholz DW, Szigety KM, Imbhiaka B, Gao S, Frankfurter M, Wang M, Yang J, Hewins P, Mericko-Ishizuka P, Adrian Leu N, Sterling S, Monreal IA, Sahler J, August A, Zhu X, Jurado KA, Xu M, Morrissey EE, Millar SE, Aguilar HC, Kahn ML. 2021. SARS-CoV-2 infection of olfactory epithelial cells and neurons drives acute lung injury and lethal COVID-19 in mice. *BioRxiv Prepr Serv Biol* 2021.12.04.471245.
98. Salman AA, Waheed MH, Ali-Abdulsahib AA, Atwan ZW. 2021. Low type I interferon response in COVID-19 patients: Interferon response may be a potential treatment for COVID-19. *Biomed Rep* 14:43.
99. Hadjadj J, Yatim N, Barnabei L, Corneau A, Boussier J, Pere H, Charbit B, Bondet V, Chenevier-Gobeaux C, Breillat P, Carlier N, Gauzit R, Morbieu C, Pene F, Marin N, Roche N, Szwebel T-A, Smith N, Merckling S, Treluyer J-M, Veyer D, Mouthon L, Blanc C, Tharaux P-L, Rozenberg F, Fischer A, Duffy D, Rieux-Laucat F, Kerneis S, Terrier B. 2020. Impaired type I interferon activity and exacerbated inflammatory responses in severe Covid-19 patients. preprint. *Infectious Diseases (except HIV/AIDS)*.
100. Channappanavar R, Fehr AR, Vijay R, Mack M, Zhao J, Meyerholz DK, Perlman S. 2016. Dysregulated Type I Interferon and Inflammatory Monocyte-Macrophage Responses Cause Lethal Pneumonia in SARS-CoV-Infected Mice. *Cell Host Microbe* 19:181–193.
101. Wang N, Zhan Y, Zhu L, Hou Z, Liu F, Song P, Qiu F, Wang X, Zou X, Wan D, Qian X, Wang S, Guo Y, Yu H, Cui M, Tong G, Xu Y, Zheng Z, Lu Y, Hong P. 2020. Retrospective Multicenter Cohort Study Shows Early Interferon Therapy Is Associated with Favorable Clinical Responses in COVID-19 Patients. *Cell Host Microbe* 28:455-464.e2.
102. Zhou R, To KK-W, Wong Y-C, Liu L, Zhou B, Li X, Huang H, Mo Y, Luk T-Y, Lau TT-K, Yeung P, Chan W-M, Wu AK-L, Lung K-C, Tsang OT-Y, Leung W-S, Hung IF-N, Yuen K-Y, Chen Z. 2020. Acute SARS-CoV-2 Infection Impairs Dendritic Cell and T Cell Responses. *Immunity* 53:864-877.e5.

103. Pérez-Gómez A, Vitallé J, Gasca-Capote C, Gutierrez-Valencia A, Trujillo-Rodriguez M, Serna-Gallego A, Muñoz-Muela E, Jiménez-Leon M de los R, Rafii-El-Idrissi Benhnia M, Rivas-Jeremias I, Sotomayor C, Roca-Oporto C, Espinosa N, Infante-Domínguez C, Crespo-Rivas JC, Fernández-Villar A, Pérez-González A, López-Cortés LF, Poveda E, Ruiz-Mateos E. 2021. Dendritic cell deficiencies persist seven months after SARS-CoV-2 infection. 9. *Cell Mol Immunol* 18:2128–2139.
104. Reizis B. 2019. Plasmacytoid Dendritic Cells: Development, Regulation, and Function. *Immunity* 50:37–50.
105. Sposito B, Broggi A, Pandolfi L, Crotta S, Clementi N, Ferrarese R, Sisti S, Criscuolo E, Spreafico R, Long JM, Ambrosi A, Liu E, Frangipane V, Saracino L, Bozzini S, Marongiu L, Facchini FA, Bottazzi A, Fossali T, Colombo R, Clementi M, Tagliabue E, Chou J, Pontiroli AE, Meloni F, Wack A, Mancini N, Zanoni I. 2021. The interferon landscape along the respiratory tract impacts the severity of COVID-19. *Cell* 184:4953-4968.e16.
106. Moss P. 2022. The T cell immune response against SARS-CoV-2. 2. *Nat Immunol* 23:186–193.
107. Mateus J, Grifoni A, Tarke A, Sidney J, Ramirez SI, Dan JM, Burger ZC, Rawlings SA, Smith DM, Phillips E, Mallal S, Lammers M, Rubiro P, Quiambao L, Sutherland A, Yu ED, da Silva Antunes R, Greenbaum J, Frazier A, Markmann AJ, Premkumar L, de Silva A, Peters B, Crotty S, Sette A, Weiskopf D. 2020. Selective and cross-reactive SARS-CoV-2 T cell epitopes in unexposed humans. *Science* 370:89–94.
108. Kundu R, Narean JS, Wang L, Fenn J, Pillay T, Fernandez ND, Conibear E, Koycheva A, Davies M, Tolosa-Wright M, Hakki S, Varro R, McDermott E, Hammett S, Cutajar J, Thwaites RS, Parker E, Rosadas C, McClure M, Tedder R, Taylor GP, Dunning J, Lalvani A. 2022. Cross-reactive memory T cells associate with protection against SARS-CoV-2 infection in COVID-19 contacts. 1. *Nat Commun* 13:80.
109. Cross-reactive CD4+ T cells enhance SARS-CoV-2 immune responses upon infection and vaccination. <https://www.science.org/doi/10.1126/science.abh1823>. Retrieved 31 March 2022.
110. Cross-reactive memory T cells and herd immunity to SARS-CoV-2 - PubMed. <https://pubmed.ncbi.nlm.nih.gov/33024281/>. Retrieved 11 April 2022.
111. Lung epithelial and endothelial damage, loss of tissue repair, inhibition of fibrinolysis, and cellular senescence in fatal COVID-19. <https://www.science.org/doi/10.1126/scitranslmed.abj7790>. Retrieved 11 April 2022.
112. Gupta A, Madhavan MV, Sehgal K, Nair N, Mahajan S, Sehrawat TS, Bikdeli B, Ahluwalia N, Ausiello JC, Wan EY, Freedberg DE, Kirtane AJ, Parikh SA, Maurer MS, Nordvig AS, Accili D, Bathon JM, Mohan S, Bauer KA, Leon MB, Krumholz HM, Uriel N, Mehra MR, Elkind MSV, Stone GW, Schwartz A, Ho DD, Bilezikian JP, Landry DW. 2020. Extrapulmonary manifestations of COVID-19. 7. *Nat Med* 26:1017–1032.

113. Prozan L, Shusterman E, Ablin J, Mitelpunkt A, Weiss-Meilik A, Adler A, Choshen G, Kehat O. 2021. Prognostic value of neutrophil-to-lymphocyte ratio in COVID-19 compared with Influenza and respiratory syncytial virus infection. 1. *Sci Rep* 11:21519.
114. Zeng Z-Y, Feng S-D, Chen G-P, Wu J-N. 2021. Predictive value of the neutrophil to lymphocyte ratio for disease deterioration and serious adverse outcomes in patients with COVID-19: a prospective cohort study. *BMC Infect Dis* 21:80.
115. Diao B, Wang C, Tan Y, Chen X, Liu Y, Ning L, Chen L, Li M, Liu Y, Wang G, Yuan Z, Feng Z, Zhang Y, Wu Y, Chen Y. 2020. Reduction and Functional Exhaustion of T Cells in Patients With Coronavirus Disease 2019 (COVID-19). *Front Immunol* 11:827.
116. Rha M-S, Shin E-C. 2021. Activation or exhaustion of CD8+ T cells in patients with COVID-19. 10. *Cell Mol Immunol* 18:2325–2333.
117. Xiang Q, Feng Z, Diao B, Tu C, Qiao Q, Yang H, Zhang Y, Wang G, Wang H, Wang C, Liu L, Wang C, Liu L, Chen R, Wu Y, Chen Y. 2021. SARS-CoV-2 Induces Lymphocytopenia by Promoting Inflammation and Decimates Secondary Lymphoid Organs. *Front Immunol* 12.
118. Multiple organ infection and the pathogenesis of SARS | *Journal of Experimental Medicine* | Rockefeller University Press.
<https://rupress.org/jem/article/202/3/415/52686/Multiple-organ-infection-and-the-pathogenesis-of>. Retrieved 11 April 2022.
119. Veras FP, Pontelli MC, Silva CM, Toller-Kawahisa JE, de Lima M, Nascimento DC, Schneider AH, Caetité D, Tavares LA, Paiva IM, Rosales R, Colón D, Martins R, Castro IA, Almeida GM, Lopes MIF, Benatti MN, Bonjorno LP, Giannini MC, Luppino-Assad R, Almeida SL, Vilar F, Santana R, Bollela VR, Auxiliadora-Martins M, Borges M, Miranda CH, Pazin-Filho A, da Silva LLP, Cunha LD, Zamboni DS, Dal-Pizzol F, Leiria LO, Siyuan L, Batah S, Fabro A, Mauad T, Dolhnikoff M, Duarte-Neto A, Saldiva P, Cunha TM, Alves-Filho JC, Arruda E, Louzada-Junior P, Oliveira RD, Cunha FQ. 2020. SARS-CoV-2–triggered neutrophil extracellular traps mediate COVID-19 pathology SARS-CoV-2 directly triggers ACE-dependent NETs. *J Exp Med* 217:e20201129.
120. Zheng J, Deng Y, Zhao Z, Mao B, Lu M, Lin Y, Huang A. 2022. Characterization of SARS-CoV-2-specific humoral immunity and its potential applications and therapeutic prospects. 2. *Cell Mol Immunol* 19:150–157.
121. Natarajan H, Crowley AR, Butler SE, Xu S, Weiner JA, Bloch EM, Littlefield K, Wieland-Alter W, Connor RI, Wright PF, Benner SE, Bonny TS, Laeyendecker O, Sullivan D, Shoham S, Quinn TC, Larman HB, Casadevall A, Pekosz A, Redd AD, Tobian AAR, Ackerman ME. 2020. SARS-CoV-2 antibody signatures robustly predict diverse antiviral functions relevant for convalescent plasma therapy. *medRxiv* 2020.09.16.20196154.
122. Jarlhelt I, Nielsen SK, Jahn CXH, Hansen CB, Pérez-Alós L, Rosbjerg A, Bayarri-Olmos R, Skjoedt M-O, Garred P. 2021. SARS-CoV-2 Antibodies Mediate Complement and Cellular Driven Inflammation. *Front Immunol* 12.

123. Eguia RT, Crawford KHD, Stevens-Ayers T, Kelnhofer-Millevolte L, Greninger AL, Englund JA, Boeckh MJ, Bloom JD. 2021. A human coronavirus evolves antigenically to escape antibody immunity. *PLOS Pathog* 17:e1009453.
124. Cervia C, Nilsson J, Zurbuchen Y, Valaperti A, Schreiner J, Wolfensberger A, Raeber ME, Adamo S, Weigang S, Emmenegger M, Hasler S, Bosshard PP, De Cecco E, Bächli E, Rudiger A, Stüssi-Helbling M, Huber LC, Zinkernagel AS, Schaer DJ, Aguzzi A, Kochs G, Held U, Probst-Müller E, Rampini SK, Boyman O. 2021. Systemic and mucosal antibody responses specific to SARS-CoV-2 during mild versus severe COVID-19. *J Allergy Clin Immunol* 147:545-557.e9.
125. Pérez-Alós L, Armenteros JJA, Madsen JR, Hansen CB, Jarlhelt I, Hamm SR, Heftdal LD, Pries-Heje MM, Møller DL, Fogh K, Hasselbalch RB, Rosbjerg A, Brunak S, Sørensen E, Larsen MAH, Ostrowski SR, Frikke-Schmidt R, Bayarri-Olmos R, Hilsted LM, Iversen KK, Bundgaard H, Nielsen SD, Garred P. 2022. Modeling of waning immunity after SARS-CoV-2 vaccination and influencing factors. 1. *Nat Commun* 13:1614.
126. Frøberg J, Gillard J, Philipsen R, Lanke K, Rust J, van Tuijl D, Teelen K, Bousema T, Simonetti E, van der Gaast-de Jongh CE, Bos M, van Kuppeveld FJ, Bosch B-J, Nabuurs-Franssen M, van der Geest-Blankert N, van Daal C, Huynen MA, de Jonge MI, Diavatopoulos DA. 2021. SARS-CoV-2 mucosal antibody development and persistence and their relation to viral load and COVID-19 symptoms. 1. *Nat Commun* 12:5621.
127. Echeverría G, Guevara Á, Coloma J, Ruiz AM, Vasquez MM, Tejera E, de Waard JH. 2021. Pre-existing T-cell immunity to SARS-CoV-2 in unexposed healthy controls in Ecuador, as detected with a COVID-19 Interferon-Gamma Release Assay. *Int J Infect Dis* 105:21–25.
128. Wang EY, Mao T, Klein J, Dai Y, Huck JD, Jaycox JR, Liu F, Zhou T, Israelow B, Wong P, Coppi A, Lucas C, Silva J, Oh JE, Song E, Perotti ES, Zheng NS, Fischer S, Campbell M, Fournier JB, Wyllie AL, Vogels CBF, Ott IM, Kalinich CC, Petrone ME, Watkins AE, Dela Cruz C, Farhadian SF, Schulz WL, Ma S, Grubaugh ND, Ko AI, Iwasaki A, Ring AM. 2021. Diverse functional autoantibodies in patients with COVID-19. 7866. *Nature* 595:283–288.
129. Autoantibodies against type I IFNs in patients with life-threatening COVID-19. <https://www.science.org/doi/full/10.1126/science.abd4585>. Retrieved 31 March 2022.
130. Prothrombotic autoantibodies in serum from patients hospitalized with COVID-19. <https://www.science.org/doi/full/10.1126/scitranslmed.abd3876>. Retrieved 31 March 2022.
131. Ferrara JL, Deeg HJ. 1991. Graft-versus-host disease. *N Engl J Med* 324:667–674.
132. Henden AS, Hill GR. 2015. Cytokines in Graft-versus-Host Disease. *J Immunol* 194:4604–4612.
133. Schnaubelt S, Tihanyi D, Strassl R, Schmidt R, Anders S, Laggner AN, Agis H, Domanovits H. 2021. Hemophagocytic lymphohistiocytosis in COVID-19: Case reports of a stepwise approach. *Medicine (Baltimore)* 100:e25170.

134. Engelmann B, Massberg S. 2013. Thrombosis as an intravascular effector of innate immunity. 1. *Nat Rev Immunol* 13:34–45.
135. Carter SJ, Tattersall RS, Ramanan AV. 2019. Macrophage activation syndrome in adults: recent advances in pathophysiology, diagnosis and treatment. *Rheumatol Oxf Engl* 58:5–17.
136. Nile SH, Nile A, Qiu J, Li L, Jia X, Kai G. 2020. COVID-19: Pathogenesis, cytokine storm and therapeutic potential of interferons. *Cytokine Growth Factor Rev* 53:66–70.
137. Ronit A, Berg RMG, Bay JT, Haugaard AK, Ahlström MG, Burgdorf KS, Ullum H, Rørvig SB, Tjelle K, Foss NB, Benfield T, Marquart HV, Plovsing RR. 2021. Compartmental immunophenotyping in COVID-19 ARDS: A case series. *J Allergy Clin Immunol* 147:81–91.
138. McElvaney OJ, McEvoy NL, McElvaney OF, Carroll TP, Murphy MP, Dunlea DM, Ní Choileáin O, Clarke J, O'Connor E, Hogan G, Ryan D, Sulaiman I, Gunaratnam C, Branagan P, O'Brien ME, Morgan RK, Costello RW, Hurley K, Walsh S, de Barra E, McNally C, McConkey S, Boland F, Galvin S, Kiernan F, O'Rourke J, Dwyer R, Power M, Geoghegan P, Larkin C, O'Leary RA, Freeman J, Gaffney A, Marsh B, Curley GF, McElvaney NG. 2020. Characterization of the Inflammatory Response to Severe COVID-19 Illness. *Am J Respir Crit Care Med* 202:812–821.
139. Lucas C, Wong P, Klein J, Castro TBR, Silva J, Sundaram M, Ellingson MK, Mao T, Oh JE, Israelow B, Takahashi T, Tokuyama M, Lu P, Venkataraman A, Park A, Mohanty S, Wang H, Wyllie AL, Vogels CBF, Earnest R, Lapidus S, Ott IM, Moore AJ, Muenker MC, Fournier JB, Campbell M, Odio CD, Casanovas-Massana A, Yale IMPACT Team, Herbst R, Shaw AC, Medzhitov R, Schulz WL, Grubaugh ND, Dela Cruz C, Farhadian S, Ko AI, Omer SB, Iwasaki A. 2020. Longitudinal analyses reveal immunological misfiring in severe COVID-19. *Nature* 584:463–469.
140. Azkur AK, Akdis M, Azkur D, Sokolowska M, van de Veen W, Brügger M-C, O'Mahony L, Gao Y, Nadeau K, Akdis CA. 2020. Immune response to SARS-CoV-2 and mechanisms of immunopathological changes in COVID-19. *Allergy* 75:1564–1581.
141. Ruan Q, Yang K, Wang W, Jiang L, Song J. 2020. Clinical predictors of mortality due to COVID-19 based on an analysis of data of 150 patients from Wuhan, China. *Intensive Care Med* 46:846–848.
142. Caricchio R, Gallucci M, Dass C, Zhang X, Gallucci S, Fleece D, Bromberg M, Criner GJ, Temple University COVID-19 Research Group. 2021. Preliminary predictive criteria for COVID-19 cytokine storm. *Ann Rheum Dis* 80:88–95.
143. Rosas IO, Bräu N, Waters M, Go RC, Hunter BD, Bhagani S, Skiest D, Aziz MS, Cooper N, Douglas IS, Savic S, Youngstein T, Del Sorbo L, Cubillo Gracian A, De La Zerda DJ, Ustianowski A, Bao M, Dimonaco S, Graham E, Matharu B, Spotswood H, Tsai L, Malhotra A. 2021. Tocilizumab in Hospitalized Patients with Severe Covid-19 Pneumonia. *N Engl J Med* 384:1503–1516.
144. 2021. Interleukin-6 Receptor Antagonists in Critically Ill Patients with Covid-19. *N Engl J Med* 384:1491–1502.

145. Lowenstein CJ, Solomon SD. 2020. Severe COVID-19 Is a Microvascular Disease. *Circulation* 142:1609–1611.
146. Klok FA, Kruip MJHA, van der Meer NJM, Arbous MS, Gommers D, Kant KM, Kaptein FHJ, van Paassen J, Stals MAM, Huisman MV, Endeman H. 2020. Confirmation of the high cumulative incidence of thrombotic complications in critically ill ICU patients with COVID-19: An updated analysis. *Thromb Res* 191:148–150.
147. 2021. An organoid-derived bronchioalveolar model for SARS-CoV-2 infection of human alveolar type II-like cells. *EMBO J* 40:e105912.
148. Hamming I, Timens W, Bulthuis M, Lely A, Navis G, van Goor H. 2004. Tissue distribution of ACE2 protein, the functional receptor for SARS coronavirus. A first step in understanding SARS pathogenesis. *J Pathol* 203:631–637.
149. Legrand M, Bell S, Forni L, Joannidis M, Koyner JL, Liu K, Cantaluppi V. 2021. Pathophysiology of COVID-19-associated acute kidney injury. 11. *Nat Rev Nephrol* 17:751–764.
150. Levi M, Iba T. 2021. COVID-19 coagulopathy: is it disseminated intravascular coagulation? *Intern Emerg Med* 16:309–312.
151. McFadyen JD, Stevens H, Peter K. 2020. The Emerging Threat of (Micro)Thrombosis in COVID-19 and Its Therapeutic Implications. *Circ Res* 127:571–587.
152. Cugno M, Meroni PL, Gualtierotti R, Griffini S, Grovetti E, Torri A, Lonati P, Grossi C, Borghi MO, Novembrino C, Boscolo M, Uceda Renteria SC, Valenti L, Lamorte G, Manunta M, Prati D, Pesenti A, Blasi F, Costantino G, Gori A, Bandera A, Tedesco F, Peyvandi F. 2021. Complement activation and endothelial perturbation parallel COVID-19 severity and activity. *J Autoimmun* 116:102560.
153. Cugno M, Meroni PL, Gualtierotti R, Griffini S, Grovetti E, Torri A, Panigada M, Aliberti S, Blasi F, Tedesco F, Peyvandi F. 2020. Complement activation in patients with COVID-19: A novel therapeutic target. *J Allergy Clin Immunol* 146:215–217.
154. Ma L, Sahu SK, Cano M, Kuppuswamy V, Bajwa J, McPhatter J, Pine A, Meizlish M, Goshua G, Chang C-H, Zhang H, Price C, Bahel P, Rinder H, Lei T, Day A, Reynolds D, Wu X, Schriefer R, Rauseo AM, Goss CW, O'Halloran JA, Presti RM, Kim AH, Gelman AE, Cruz CD, Lee AI, Mudd P, Chun HJ, Atkinson JP, Kulkarni HS. 2021. Increased complement activation is a distinctive feature of severe SARS-CoV-2 infection. *BioRxiv Prepr Serv Biol* 2021.02.22.432177.
155. Minet C, Potton L, Bonadona A, Hamidfar-Roy R, Somohano CA, Lugosi M, Cartier J-C, Ferretti G, Schwebel C, Timsit J-F. 2015. Venous thromboembolism in the ICU: main characteristics, diagnosis and thromboprophylaxis. *Crit Care* 19:287.
156. Ahmed S, Zimba O, Gasparyan AY. 2020. Thrombosis in Coronavirus disease 2019 (COVID-19) through the prism of Virchow's triad. *Clin Rheumatol* 39:2529–2543.
157. Yan D, Zhang X, Chen C, Jiang D, Liu X, Zhou Y, Huang C, Zhou Y, Guan Z, Ding C, Chen L, Lan L, Fu X, Wu J, Li L, Yang S. 2021. Characteristics of Viral

- Shedding Time in SARS-CoV-2 Infections: A Systematic Review and Meta-Analysis. *Front Public Health* 9.
158. Rapid Diagnostic Testing for SARS-CoV-2 | NEJM. <https://www.nejm.org/doi/full/10.1056/NEJMcp2117115>. Retrieved 21 February 2022.
 159. CDC, CDC. 2022. Quarantine & Isolation. *Cent Dis Control Prev*. <https://www.cdc.gov/coronavirus/2019-ncov/your-health/quarantine-isolation.html>. Retrieved 21 February 2022.
 160. CDC updates and shortens recommended isolation and quarantine period for general population : media statement for immediate release : Monday, December 27, 2021. <https://stacks.cdc.gov/view/cdc/112951>. Retrieved 21 February 2022.
 161. Binnicker MJ. Can Testing Predict SARS-CoV-2 Infectivity? The Potential for Certain Methods To Be Surrogates for Replication-Competent Virus. *J Clin Microbiol* 59:e00469-21.
 162. Chin ET, Huynh BQ, Chapman LAC, Murrill M, Basu S, Lo NC. 2020. Frequency of routine testing for COVID-19 in high-risk healthcare environments to reduce outbreaks. *medRxiv* 2020.04.30.20087015.
 163. Che X-Y, Hao W, Wang Y, Di B, Yin K, Xu Y-C, Feng C-S, Wan Z-Y, Cheng VCC, Yuen K-Y. 2004. Nucleocapsid Protein as Early Diagnostic Marker for SARS. *Emerg Infect Dis* 10:1947–1949.
 164. Li Y-H, Li J, Liu X-E, Wang L, Li T, Zhou Y-H, Zhuang H. 2005. Detection of the nucleocapsid protein of severe acute respiratory syndrome coronavirus in serum: comparison with results of other viral markers. *J Virol Methods* 130:45–50.
 165. Li T, Wang L, Wang H, Li X, Zhang S, Xu Y, Wei W. 2020. Serum SARS-COV-2 Nucleocapsid Protein: A Sensitivity and Specificity Early Diagnostic Marker for SARS-COV-2 Infection. *Front Cell Infect Microbiol* 10:470.
 166. Su B, Yin J, Lin X, Zhang T, Yao X, Xu Y, Lu Y, Wang W, Liu K, Zhang J, Xie L, Jin R, Feng Y. 2021. Quantification of SARS-CoV-2 antigen levels in the blood of patients with COVID-19. *Sci China Life Sci* 64:1193–1196.
 167. Hingrat QL 2021. Detection of SARS-CoV-2 N-antigen in blood during acute COVID-19 provides a sensitive new marker and new testing alternatives. *Clin Microbiol Infect* 27:789.e1-789.e5.
 168. Ahava MJ, Kurkela S, Kuivanen S, Lappalainen M, Jarva H, Jääskeläinen AJ. 2022. Detection of SARS-CoV-2 nucleocapsid antigen from serum can aid in timing of COVID-19 infection. *J Virol Methods* 302:114469.
 169. Shan D, Johnson JM, Fernandes SC, Suib H, Hwang S, Wuelfing D, Mendes M, Holdridge M, Burke EM, Beauregard K, Zhang Y, Cleary M, Xu S, Yao X, Patel PP, Plavina T, Wilson DH, Chang L, Kaiser KM, Nattermann J, Schmidt SV, Latz E, Hrusovsky K, Mattoon D, Ball AJ. 2021. N-protein presents early in blood, dried blood and saliva during asymptomatic and symptomatic SARS-CoV-2 infection. 1. *Nat Commun* 12:1931.
 170. Zhang Y, Ong CM, Yun C, Mo W, Whitman JD, Lynch KL, Wu AHB. 2021. Diagnostic Value of Nucleocapsid Protein in Blood for SARS-CoV-2 Infection. *Clin Chem* 68:240–248.

171. Wang H, Hogan CA, Verghese M, Solis D, Sibai M, Huang C, Röltgen K, Stevens BA, Yamamoto F, Sahoo MK, Zehnder J, Boyd SD, Pinsky BA. 2022. SARS-CoV-2 Nucleocapsid Plasma Antigen for Diagnosis and Monitoring of COVID-19. *Clin Chem* 68:204–213.
172. Favresse J, Bayart J-L, David C, Gillot C, Wieërs G, Roussel G, Sondag G, Elsen M, Eucher C, Dogné J-M, Douxfils J. 2021. Serum SARS-CoV-2 Antigens for the Determination of COVID-19 Severity. *medRxiv* <https://doi.org/10.1101/2021.11.18.21266478>.
173. Thudium RF, Stoico MP, Høgdall E, Høgh J, Krarup HB, Larsen MAH, Madsen PH, Nielsen SD, Ostrowski SR, Palombini A, Rasmussen DB, Foged NT. Early laboratory diagnosis of covid-19 by antigen detection in blood samples of the sars-cov-2 nucleocapsid protein. *J Clin Microbiol* 0:JCM.01001-21.
174. Lebedin YS, Lyang OV, Galstyan AG, Panteleeva AV, Belousov VV, Rebrikov DV. 2020. Serum SARS-CoV-2 nucleocapsid antigen detection is essential for primary diagnostics of SARS-CoV-2-associated pneumonia. *medRxiv* <https://doi.org/10.1101/2020.09.24.20200303>.
175. Ogata AF, Maley AM, Wu C, Gilboa T, Norman M, Lazarovits R, Mao C-P, Newton G, Chang M, Nguyen K, Kamkaew M, Zhu Q, Gibson TE, Ryan ET, Charles RC, Marasco WA, Walt DR. 2020. Ultra-Sensitive Serial Profiling of SARS-CoV-2 Antigens and Antibodies in Plasma to Understand Disease Progression in COVID-19 Patients with Severe Disease. *Clin Chem* 66:1562–1572.
176. Avanzato VA, Matson MJ, Seifert SN, Pryce R, Williamson BN, Anzick SL, Barbian K, Judson SD, Fischer ER, Martens C, Bowden TA, de Wit E, Riedo FX, Munster VJ. 2020. Case Study: Prolonged Infectious SARS-CoV-2 Shedding from an Asymptomatic Immunocompromised Individual with Cancer. *Cell* 183:1901-1912.e9.
177. Aydililo T, Gonzalez-Reiche AS, Aslam S, van de Guchte A, Khan Z, Obla A, Dutta J, van Bakel H, Aberg J, Garcia-Sastre A, Shah G, Hohl T, Papanicolaou G, Perales M-A, Sepkowitz K, Babady NE, Kamboj M. 2020. Shedding of Viable SARS-CoV-2 after Immunosuppressive Therapy for Cancer. *N Engl J Med* 383:2586–2588.
178. McCarthy KR, Rennick LJ, Nambulli S, Robinson-McCarthy LR, Bain WG, Haidar G, Duprex WP. 2021. Recurrent deletions in the SARS-CoV-2 spike glycoprotein drive antibody escape. *Science* 371:1139–1142.
179. Gottlieb RL, Vaca CE, Paredes R, Mera J, Webb BJ, Perez G, Oguchi G, Ryan P, Nielsen BU, Brown M, Hidalgo A, Sachdeva Y, Mittal S, Osiyemi O, Skarbinski J, Juneja K, Hyland RH, Osinusi A, Chen S, Camus G, Abdelghany M, Davies S, Behenna-Renton N, Duff F, Marty FM, Katz MJ, Ginde AA, Brown SM, Schiffer JT, Hill JA, GS-US-540-9012 (PINETREE) Investigators. 2022. Early Remdesivir to Prevent Progression to Severe Covid-19 in Outpatients. *N Engl J Med* 386:305–315.
180. Ortega-Paz L, Capodanno D, Montalescot G, Angiolillo DJ. 2021. Coronavirus Disease 2019–Associated Thrombosis and Coagulopathy: Review of the

- Pathophysiological Characteristics and Implications for Antithrombotic Management. *J Am Heart Assoc* 10:e019650.
181. Giannis D, Ziogas IA, Gianni P. 2020. Coagulation disorders in coronavirus infected patients: COVID-19, SARS-CoV-1, MERS-CoV and lessons from the past. *J Clin Virol Off Publ Pan Am Soc Clin Virol* 127:104362.
 182. Guan W, Ni Z, Hu Y, Liang W, Ou C, He J, Liu L, Shan H, Lei C, Hui DSC, Du B, Li L, Zeng G, Yuen K-Y, Chen R, Tang C, Wang T, Chen P, Xiang J, Li S, Wang J, Liang Z, Peng Y, Wei L, Liu Y, Hu Y, Peng P, Wang J, Liu J, Chen Z, Li G, Zheng Z, Qiu S, Luo J, Ye C, Zhu S, Zhong N. 2020. Clinical Characteristics of Coronavirus Disease 2019 in China. *N Engl J Med* 382:1708–1720.
 183. Han H, Yang L, Liu R, Liu F, Wu K, Li J, Liu X, Zhu C. 2020. Prominent changes in blood coagulation of patients with SARS-CoV-2 infection. *Clin Chem Lab Med CCLM* 58:1116–1120.
 184. Autopsy Findings and Venous Thromboembolism in Patients With COVID-19: A Prospective Cohort Study: *Annals of Internal Medicine*: Vol 173, No 4. <https://www.acpjournals.org/doi/10.7326/M20-2003>. Retrieved 5 April 2022.
 185. Calvet J, Berenguer-Llargo A, M, Costa E, Clotet B, Vilaseca M, Blanco J, Gratacós J. 2022. Biomarker candidates for progression and clinical management of COVID-19 associated pneumonia at time of admission. 1. *Sci Rep* 12:640.
 186. Malik P, Patel U, Mehta D, Patel N, Kelkar R, Akrmah M, Gabrilove JL, Sacks H. 2021. Biomarkers and outcomes of COVID-19 hospitalisations: systematic review and meta-analysis. *BMJ Evid-Based Med* 26:107–108.
 187. Lasso G, Khan S, Allen SA, Mariano M, Florez C, Orner EP, Quiroz JA, Quevedo G, Massimi A, Hegde A, Wirchnianski AS, Iii RHB, Malonis RJ, Georgiev GI, Tong K, Herrera NG, Morano NC, Garforth SJ, Malaviya A, Khokhar A, Laudermilch E, Dieterle ME, Fels JM, Haslwanter D, Jangra RK, Barnhill J, Almo SC, Chandran K, Lai JR, Kelly L, Daily JP, Vergnolle O. 2022. Longitudinally monitored immune biomarkers predict the timing of COVID-19 outcomes. *PLOS Comput Biol* 18:e1009778.
 188. The TH, van der Bij W, van den Berg AP, van der Giessen M, Weits J, Sprenger HG, van Son WJ. 1990. Cytomegalovirus antigenemia. *Rev Infect Dis* 12 Suppl 7:S734-744.
 189. Lanini S, Portella G, Vairo F, Kobinger GP, Pesenti A, Langer M, Kabia S, Brogiato G, Amone J, Castilletti C, Miccio R, Capobianchi MR, Strada G, Zumla A, Di Caro A, Ippolito G, INMI-EMERGENCY EBOV Sierra Leone Study Group. 2018. Relationship Between Viremia and Specific Organ Damage in Ebola Patients: A Cohort Study. *Clin Infect Dis* 66:36–44.
 190. Hingrat QL, Visseaux B, Laouenan C, Tubiana S, Bouadma L, Yazdanpanah Y, Duval X, Ichou H, Damond F, Bertine M, Benmalek N, Committee FC cohort management, Group C-C study, Choquet C, Timsit J-F, Ghosn J, Charpentier C, Descamps D, Houhou-Fidouh N. 2020. SARS-CoV-2 N-antigenemia: A new alternative to nucleic acid amplification techniques. *medRxiv* 2020.09.14.20191759.

191. Ahava MJ, Kurkela S, Kuivanen S, Lappalainen M, Jarva H, Jääskeläinen AJ. 2021. Detection of SARS-CoV-2 nucleocapsid antigen from serum can aid in timing of COVID-19 infection. medRxiv 2021.01.08.20248771.
192. Lu S, Ye Q, Singh D, Cao Y, Diedrich JK, Yates JR, Villa E, Cleveland DW, Corbett KD. 2021. The SARS-CoV-2 nucleocapsid phosphoprotein forms mutually exclusive condensates with RNA and the membrane-associated M protein. 1. Nat Commun 12:502.
193. The SARS-CoV-2 nucleocapsid protein is dynamic, disordered, and phase separates with RNA | Nature Communications. <https://www.nature.com/articles/s41467-021-21953-3>. Retrieved 5 April 2022.
194. Major J, Crotta S, Llorian M, McCabe TM, Gad HH, Priestnall SL, Hartmann R, Wack A. 2020. Type I and III interferons disrupt lung epithelial repair during recovery from viral infection. Science <https://doi.org/10.1126/science.abc2061>.
195. Kim Y-M, Shin E-C. 2021. Type I and III interferon responses in SARS-CoV-2 infection. 5. Exp Mol Med 53:750–760.
196. Qian Y, Lei T, Patel PS, Lee CH, Monaghan-Nichols P, Xin H-B, Qiu J, Fu M. 2021. Direct activation of endothelial cells by SARS-CoV-2 nucleocapsid protein is blocked by Simvastatin. bioRxiv 2021.02.14.431174.
197. Mannino RG, Qiu Y, Lam WA. 2018. Endothelial cell culture in microfluidic devices for investigating microvascular processes. Biomicrofluidics 12:042203.
198. Pino M, Abid T, Pereira Ribeiro S, Edara VV, Floyd K, Smith JC, Latif MB, Pacheco-Sanchez G, Dutta D, Wang S, Gumber S, Kirejczyk S, Cohen J, Stammen RL, Jean SM, Wood JS, Connor-Stroud F, Pollet J, Chen W-H, Wei J, Zhan B, Lee J, Liu Z, Strych U, Shenvi N, Easley K, Weiskopf D, Sette A, Pollara J, Mielke D, Gao H, Eisel N, LeBranche CC, Shen X, Ferrari G, Tomaras GD, Montefiori DC, Sekaly RP, Vanderford TH, Tomai MA, Fox CB, Suthar MS, Kozlowski PA, Hotez PJ, Paiardini M, Bottazzi ME, Kasturi SP. 2021. A yeast-expressed RBD-based SARS-CoV-2 vaccine formulated with 3M-052-alum adjuvant promotes protective efficacy in non-human primates. Sci Immunol 6:eabh3634.
199. Hoang TN, Pino M, Boddapati AK, Viox EG, Starke CE, Upadhyay AA, Gumber S, Nekorchuk M, Busman-Sahay K, Strongin Z, Harper JL, Tharp GK, Pellegrini KL, Kirejczyk S, Zandi K, Tao S, Horton TR, Beagle EN, Mahar EA, Lee MYH, Cohen J, Jean SM, Wood JS, Connor-Stroud F, Stammen RL, Delmas OM, Wang S, Cooney KA, Sayegh MN, Wang L, Filev PD, Weiskopf D, Silvestri G, Waggoner J, Piantadosi A, Kasturi SP, Al-Shakhshir H, Ribeiro SP, Sekaly RP, Levit RD, Estes JD, Vanderford TH, Schinazi RF, Bosinger SE, Paiardini M. 2021. Baricitinib treatment resolves lower-airway macrophage inflammation and neutrophil recruitment in SARS-CoV-2-infected rhesus macaques. Cell 184:460-475.e21.
200. Zhou P, Yang X-L, Wang X-G, Hu B, Zhang L, Zhang W, Si H-R, Zhu Y, Li B, Huang C-L, Chen H-D, Chen J, Luo Y, Guo H, Jiang R-D, Liu M-Q, Chen Y, Shen X-R, Wang X, Zheng X-S, Zhao K, Chen Q-J, Deng F, Liu L-L, Yan B, Zhan F-X, Wang Y-Y, Xiao G-F, Shi Z-L. 2020. A pneumonia outbreak associated with a new coronavirus of probable bat origin. 7798. Nature 579:270–273.

201. Huang C, Wang Y, Li X, Ren L, Zhao J, Hu Y, Zhang L, Fan G, Xu J, Gu X, Cheng Z, Yu T, Xia J, Wei Y, Wu W, Xie X, Yin W, Li H, Liu M, Xiao Y, Gao H, Guo L, Xie J, Wang G, Jiang R, Gao Z, Jin Q, Wang J, Cao B. 2020. Clinical features of patients infected with 2019 novel coronavirus in Wuhan, China. *Lancet Lond Engl* 395:497–506.
202. Zhou P, Yang X-L, Wang X-G, Hu B, Zhang L, Zhang W, Si H-R, Zhu Y, Li B, Huang C-L, Chen H-D, Chen J, Luo Y, Guo H, Jiang R-D, Liu M-Q, Chen Y, Shen X-R, Wang X, Zheng X-S, Zhao K, Chen Q-J, Deng F, Liu L-L, Yan B, Zhan F-X, Wang Y-Y, Xiao G-F, Shi Z-L. 2020. Discovery of a novel coronavirus associated with the recent pneumonia outbreak in humans and its potential bat origin. *bioRxiv* 2020.01.22.914952.
203. Winichakoon P, Chaiwarith R, Liwsrisakun C, Salee P, Goonna A, Limsukon A, Kaewpoowat Q. 2020. Negative Nasopharyngeal and Oropharyngeal Swabs Do Not Rule Out COVID-19. *J Clin Microbiol* 58.
204. Patel R, Babady E, Theel ES, Storch GA, Pinsky BA, George KS, Smith TC, Bertuzzi S. 2020. Report from the American Society for Microbiology COVID-19 International Summit, 23 March 2020: Value of Diagnostic Testing for SARS–CoV-2/COVID-19. *mBio* 11.
205. Zou L, Ruan F, Huang M, Liang L, Huang H, Hong Z, Yu J, Kang M, Song Y, Xia J, Guo Q, Song T, He J, Yen H-L, Peiris M, Wu J. 2020. SARS-CoV-2 Viral Load in Upper Respiratory Specimens of Infected Patients. *N Engl J Med* 382:1177–1179.
206. Suthar MS, Zimmerman MG, Kauffman RC, Mantus G, Linderman SL, Hudson WH, Vanderheiden A, Nyhoff L, Davis CW, Adekunle O, Affer M, Sherman M, Reynolds S, Verkerke HP, Alter DN, Guarner J, Bryksin J, Horwath MC, Arthur CM, Saakadze N, Smith GH, Edupuganti S, Scherer EM, Hellmeister K, Cheng A, Morales JA, Neish AS, Stowell SR, Frank F, Ortlund E, Anderson EJ, Menachery VD, Roupheal N, Mehta AK, Stephens DS, Ahmed R, Roback JD, Wrammert J. 2020. Rapid Generation of Neutralizing Antibody Responses in COVID-19 Patients. *Cell Rep Med* 1:100040.
207. Rogers TF, Zhao F, Huang D, Beutler N, Burns A, He W, Limbo O, Smith C, Song G, Woehl J, Yang L, Abbott RK, Callaghan S, Garcia E, Hurtado J, Parren M, Peng L, Ramirez S, Ricketts J, Ricciardi MJ, Rawlings SA, Wu NC, Yuan M, Smith DM, Nemazee D, Teijaro JR, Voss JE, Wilson IA, Andrabi R, Briney B, Landais E, Sok D, Jardine JG, Burton DR. 2020. Isolation of potent SARS-CoV-2 neutralizing antibodies and protection from disease in a small animal model. *Science* <https://doi.org/10.1126/science.abc7520>.
208. Long Q-X, Liu B-Z, Deng H-J, Wu G-C, Deng K, Chen Y-K, Liao P, Qiu J-F, Lin Y, Cai X-F, Wang D-Q, Hu Y, Ren J-H, Tang N, Xu Y-Y, Yu L-H, Mo Z, Gong F, Zhang X-L, Tian W-G, Hu L, Zhang X-X, Xiang J-L, Du H-X, Liu H-W, Lang C-H, Luo X-H, Wu S-B, Cui X-P, Zhou Z, Zhu M-M, Wang J, Xue C-J, Li X-F, Wang L, Li Z-J, Wang K, Niu C-C, Yang Q-J, Tang X-J, Zhang Y, Liu X-M, Li J-J, Zhang D-C, Zhang F, Liu P, Yuan J, Li Q, Hu J-L, Chen J, Huang A-L. 2020. Antibody responses to SARS-CoV-2 in patients with COVID-19. *Nat Med* 1–4.

209. Ma H, Zeng W, He H, Zhao D, Jiang D, Zhou P, Cheng L, Li Y, Ma X, Jin T. 2020. Serum IgA, IgM, and IgG responses in COVID-19. *Cell Mol Immunol* 1–3.
210. Dahlke C, Heidepriem J, Kobbe R, Santer R, Koch T, Fathi A, Ly ML, Schmiedel S, Seeberger PH, Group I-UC-19 study, Addo MM, Loeffler FF. 2020. Distinct early IgA profile may determine severity of COVID-19 symptoms: an immunological case series. *medRxiv* 2020.04.14.20059733.
211. Wang Z, Lorenzi JCC, Muecksch F, Finkin S, Viant C, Gaebler C, Cipolla M, Hoffmann H-H, Oliveira TY, Oren DA, Ramos V, Nogueira L, Michailidis E, Robbiani DF, Gazumyan A, Rice CM, Hatzioannou T, Bieniasz PD, Caskey M, Nussenzweig MC. 2020. Enhanced SARS-CoV-2 neutralization by dimeric IgA. *Sci Transl Med* <https://doi.org/10.1126/scitranslmed.abf1555>.
212. Sterlin D, Mathian A, Miyara M, Mohr A, Anna F, Claër L, Quentric P, Fadlallah J, Devilliers H, Ghillani P, Gunn C, Hockett R, Mudumba S, Guihot A, Luyt C-E, Mayaux J, Beurton A, Fourati S, Bruel T, Schwartz O, Lacorte J-M, Yssel H, Parizot C, Dorgham K, Charneau P, Amoura Z, Gorochov G. 2020. IgA dominates the early neutralizing antibody response to SARS-CoV-2. *Sci Transl Med* <https://doi.org/10.1126/scitranslmed.abd2223>.
213. Early High-Titer Plasma Therapy to Prevent Severe Covid-19 in Older Adults | NEJM. <https://www.nejm.org/doi/full/10.1056/NEJMoa2033700>. Retrieved 22 March 2022.
214. Hansen IS, Baeten DLP, den Dunnen J. 2019. The inflammatory function of human IgA. *Cell Mol Life Sci CMLS* 76:1041–1055.
215. Rossato E, Ben Mkaddem S, Kanamaru Y, Hurtado-Nedelec M, Hayem G, Descatoire V, Vonarburg C, Miescher S, Zuercher AW, Monteiro RC. 2015. Reversal of Arthritis by Human Monomeric IgA Through the Receptor-Mediated SH2 Domain-Containing Phosphatase 1 Inhibitory Pathway. *Arthritis Rheumatol Hoboken NJ* 67:1766–1777.
216. Bradfute SB, Hurwitz I, Yingling AV, Ye C, Cheng Q, Noonan TP, Raval JS, Sosa NR, Mertz GJ, Perkins DJ, Harkins MS. 2020. SARS-CoV-2 Neutralizing Antibody Titers in Convalescent Plasma and Recipients in New Mexico: An Open Treatment Study in COVID-19 Patients. *J Infect Dis* <https://doi.org/10.1093/infdis/jiaa505>.
217. Hou H, Wang T, Zhang B, Luo Y, Mao L, Wang F, Wu S, Sun Z. 2020. Detection of IgM and IgG antibodies in patients with coronavirus disease 2019. *Clin Transl Immunol* 9.
218. Tré-Hardy M, Blairon L, Wilmet A, Beukinga I, Malonne H, Dogné J-M, Douxfils J. 2020. The role of serology for COVID-19 control: Population, kinetics and test performance do matter. *J Infect* <https://doi.org/10.1016/j.jinf.2020.05.019>.
219. Health C for D and R. 2020. In Vitro Diagnostics EUAs. FDA.
220. Corthésy B. 2013. Multi-faceted functions of secretory IgA at mucosal surfaces. *Front Immunol* 4:185.
221. Brochot E, Demey B, Handala L, François C, Duverlie G, Castelain S. 2020. Comparison of different serological assays for SARS-CoV-2 in real life. *J Clin Virol Off Publ Pan Am Soc Clin Virol* 130:104569.

222. Deeks JJ, Dinnes J, Takwoingi Y, Davenport C, Spijker R, Taylor-Phillips S, Adriano A, Beese S, Dretzke J, Ferrante di Ruffano L, Harris IM, Price MJ, Dittrich S, Emperador D, Hooft L, Leeflang MM, Van den Bruel A, Cochrane COVID-19 Diagnostic Test Accuracy Group. 2020. Antibody tests for identification of current and past infection with SARS-CoV-2. *Cochrane Database Syst Rev* 6:CD013652.
223. Lisboa Bastos M, Tavaziva G, Abidi SK, Campbell JR, Haraoui L-P, Johnston JC, Lan Z, Law S, MacLean E, Trajman A, Menzies D, Benedetti A, Ahmad Khan F. 2020. Diagnostic accuracy of serological tests for covid-19: systematic review and meta-analysis. *BMJ* 370:m2516.
224. Rongqing Z, Li M, Song H, Chen J, Ren W, Feng Y, Gao GF, Song J, Peng Y, Su B, Guo X, Wang Y, Chen J, Li J, Sun H, Bai Z, Cao W, Zhu J, Zhang Q, Sun Y, Sun S, Mao X, Su J, Chen X, He A, Gao W, Jin R, Jiang Y, Sun L. 2020. Early Detection of Severe Acute Respiratory Syndrome Coronavirus 2 Antibodies as a Serologic Marker of Infection in Patients With Coronavirus Disease 2019. *Clin Infect Dis Off Publ Infect Dis Soc Am* 71:2066–2072.
225. Tea F, Stella AO, Aggarwal A, Darley DR, Pilli D, Vitale D, Merheb V, Lee FXZ, Cunningham P, Walker GJ, Fichter C, Brown DA, Rawlinson WD, Isaacs SR, Mathivanan V, Hoffmann M, Pöhlman S, Mazigi O, Christ D, Dwyer DE, Rockett RJ, Sintchenko V, Hoad VC, Irving DO, Dore GJ, Gosbell IB, Kelleher AD, Matthews GV, Brilot F, Turville SG. 2021. SARS-CoV-2 neutralizing antibodies: Longevity, breadth, and evasion by emerging viral variants. *PLOS Med* 18:e1003656.
226. Khoury DS, Cromer D, Reynaldi A, Schlub TE, Wheatley AK, Juno JA, Subbarao K, Kent SJ, Triccas JA, Davenport MP. 2021. Neutralizing antibody levels are highly predictive of immune protection from symptomatic SARS-CoV-2 infection. *Nat Med* 27:1205–1211.
227. Overbaugh J, Morris L. 2012. The Antibody Response against HIV-1. *Cold Spring Harb Perspect Med* 2:a007039.
228. Pan-Sarbecovirus Neutralizing Antibodies in BNT162b2-Immunized SARS-CoV-1 Survivors | *NEJM*. <https://www.nejm.org/doi/full/10.1056/NEJMoa2108453>. Retrieved 12 April 2022.
229. Wang Z, Muecksch F, Schaefer-Babajew D, Finkin S, Viant C, Gaebler C, Hoffmann H-H, Barnes CO, Cipolla M, Ramos V, Oliveira TY, Cho A, Schmidt F, Da Silva J, Bednarski E, Aguado L, Yee J, Daga M, Turroja M, Millard KG, Jankovic M, Gazumyan A, Zhao Z, Rice CM, Bieniasz PD, Caskey M, Hatziioannou T, Nussenzweig MC. 2021. Naturally enhanced neutralizing breadth against SARS-CoV-2 one year after infection. *Nature* 595:426–431.
230. Does infection with or vaccination against SARS-CoV-2 lead to lasting immunity? - *The Lancet Respiratory Medicine*. [https://www.thelancet.com/journals/lanres/article/PIIS2213-2600\(21\)00407-0/fulltext](https://www.thelancet.com/journals/lanres/article/PIIS2213-2600(21)00407-0/fulltext). Retrieved 12 April 2022.
231. Levine-Tiefenbrun M, Yelin I, Alapi H, Katz R, Herzel E, Kuint J, Chodick G, Gazit S, Patalon T, Kishony R. 2021. Viral loads of Delta-variant SARS-CoV-2 breakthrough infections after vaccination and booster with BNT162b2. *Nat Med* 27:2108–2110.

232. Wang M-Y, Zhao R, Gao L-J, Gao X-F, Wang D-P, Cao J-M. 2020. SARS-CoV-2: Structure, Biology, and Structure-Based Therapeutics Development. *Front Cell Infect Microbiol* 10:587269.
233. Ke Z, Oton J, Qu K, Cortese M, Zila V, McKeane L, Nakane T, Zivanov J, Neufeldt CJ, Cerikan B, Lu JM, Peukes J, Xiong X, Kräusslich H-G, Scheres SHW, Bartenschlager R, Briggs JAG. 2020. Structures and distributions of SARS-CoV-2 spike proteins on intact virions. *Nature* 588:498–502.
234. Yao H, Song Y, Chen Y, Wu N, Xu J, Sun C, Zhang J, Weng T, Zhang Z, Wu Z, Cheng L, Shi D, Lu X, Lei J, Crispin M, Shi Y, Li L, Li S. 2020. Molecular Architecture of the SARS-CoV-2 Virus. *Cell* 183:730-738.e13.
235. Seyran M, Takayama K, Uversky VN, Lundstrom K, Palù G, Sherchan SP, Attrish D, Rezaei N, Aljabali AAA, Ghosh S, Pizzol D, Chauhan G, Adadi P, Mohamed Abd El-Aziz T, Soares AG, Kandimalla R, Tambuwala M, Hassan SkS, Azad GK, Pal Choudhury P, Baetas-da-Cruz W, Serrano-Aroca Á, Brufsky AM, Uhal BD. 2021. The structural basis of accelerated host cell entry by SARS-CoV-2†. *FEBS J* 288:5010–5020.
236. Tomassetti F, Nuccetelli M, Sarubbi S, Gisone F, Ciotti M, Spinazzola F, Ricotta C, Cagnoli M, Borgatti M, Iannetta M, Andreoni M, Calugi G, Pieri M, Bernardini S. 2021. Evaluation of S-RBD and high specificity ACE-2-binding antibodies on SARS-CoV-2 patients after six months from infection. *Int Immunopharmacol* 99:108013.
237. Lan J, Ge J, Yu J, Shan S, Zhou H, Fan S, Zhang Q, Shi X, Wang Q, Zhang L, Wang X. 2020. Structure of the SARS-CoV-2 spike receptor-binding domain bound to the ACE2 receptor. 7807. *Nature* 581:215–220.
238. Xia X. 2021. Domains and Functions of Spike Protein in Sars-Cov-2 in the Context of Vaccine Design. *Viruses* 13:109.
239. Piccoli L, Park Y-J, Tortorici MA, Czudnochowski N, Walls AC, Beltramello M, Silacci-Fregni C, Pinto D, Rosen LE, Bowen JE, Acton OJ, Jaconi S, Guarino B, Minola A, Zatta F, Sprugasci N, Bassi J, Peter A, De Marco A, Nix JC, Mele F, Jovic S, Rodriguez BF, Gupta SV, Jin F, Piumatti G, Lo Presti G, Pellanda AF, Biggiogero M, Tarkowski M, Pizzuto MS, Cameroni E, Havenar-Daughton C, Smithey M, Hong D, Lepori V, Albanese E, Ceschi A, Bernasconi E, Elzi L, Ferrari P, Garzoni C, Riva A, Snell G, Sallusto F, Fink K, Virgin HW, Lanzavecchia A, Corti D, Veesler D. 2020. Mapping Neutralizing and Immunodominant Sites on the SARS-CoV-2 Spike Receptor-Binding Domain by Structure-Guided High-Resolution Serology. *Cell* 183:1024-1042.e21.
240. Bewley KR, Coombes NS, Gagnon L, McInroy L, Baker N, Shaik I, St-Jean JR, St-Amant N, Buttigieg KR, Humphries HE, Godwin KJ, Brunt E, Allen L, Leung S, Brown PJ, Penn EJ, Thomas K, Kulnis G, Hallis B, Carroll M, Funnell S, Charlton S. 2021. Quantification of SARS-CoV-2 neutralizing antibody by wild-type plaque reduction neutralization, microneutralization and pseudotyped virus neutralization assays. 6. *Nat Protoc* 16:3114–3140.
241. Xiong H-L, Wu Y-T, Cao J-L, Yang R, Liu Y-X, Ma J, Qiao X-Y, Yao X-Y, Zhang B-H, Zhang Y-L, Hou W-H, Shi Y, Xu J-J, Zhang L, Wang S-J, Fu B-R, Yang T, Ge S-X, Zhang J, Yuan Q, Huang B-Y, Li Z-Y, Zhang T-Y, Xia N-S. 2020. Robust

- neutralization assay based on SARS-CoV-2 S-protein-bearing vesicular stomatitis virus (VSV) pseudovirus and ACE2-overexpressing BHK21 cells. *Emerg Microbes Infect* 9:2105–2113.
242. Nie J, Li Q, Wu J, Zhao C, Hao H, Liu H, Zhang L, Nie L, Qin H, Wang M, Lu Q, Li X, Sun Q, Liu J, Fan C, Huang W, Xu M, Wang Y. 2020. Establishment and validation of a pseudovirus neutralization assay for SARS-CoV-2. *Emerg Microbes Infect* 9:680–686.
 243. Hu J, Gao Q, He C, Huang A, Tang N, Wang K. 2020. Development of cell-based pseudovirus entry assay to identify potential viral entry inhibitors and neutralizing antibodies against SARS-CoV-2. *Genes Dis* 7:551–557.
 244. Verkerke H, Saeedi BJ, Boyer D, Allen JW, Owens J, Shin S, Horwath M, Patel K, Paul A, Wu S-C, Wang J, Ho A, Maier CL, Zerra PE, Chonat S, Arthur CM, Roback JD, Neish AS, Lough C, Josephson CD, Stowell SR. 2021. Are We Forgetting About IgA? A Re-examination of Coronavirus Disease 2019 Convalescent Plasma. *Transfusion (Paris)* 61:1740–1748.
 245. Sullivan DJ, Gebo KA, Shoham S, Bloch EM, Lau B, Shenoy AG, Mosnaim GS, Gniadek TJ, Fukuta Y, Patel B, Heath SL, Levine AC, Meisenberg BR, Spivak ES, Anjan S, Huaman MA, Blair JE, Currier JS, Paxton JH, Gerber JM, Petrini JR, Broderick PB, Rausch W, Cordisco M-E, Hammel J, Greenblatt B, Cluzet VC, Cruser D, Oei K, Abinante M, Hammitt LL, Sutcliffe CG, Forthal DN, Zand MS, Cachay ER, Raval JS, Kassaye SG, Foster EC, Roth M, Marshall CE, Yarava A, Lane K, McBee NA, Gawad AL, Karlen N, Singh A, Ford DE, Jabs DA, Appel LJ, Shade DM, Ehrhardt S, Baksh SN, Laeyendecker O, Pekosz A, Klein SL, Casadevall A, Tobian AAR, Hanley DF. 2022. Early Outpatient Treatment for Covid-19 with Convalescent Plasma. *N Engl J Med* 0:null.
 246. Verkerke HP, Maier CL. 2020. Towards characterized convalescent plasma for COVID-19: The dose matters. *eClinicalMedicine* 26.
 247. Immunological memory to SARS-CoV-2 assessed for up to 8 months after infection. <https://www.science.org/doi/10.1126/science.abf4063>. Retrieved 12 April 2022.
 248. Durability of Responses after SARS-CoV-2 mRNA-1273 Vaccination | *NEJM*. <https://www.nejm.org/doi/full/10.1056/NEJMc2032195>. Retrieved 12 April 2022.
 249. Pathophysiology, Transmission, Diagnosis, and Treatment of Coronavirus Disease 2019 (COVID-19): A Review | *Critical Care Medicine* | *JAMA* | *JAMA Network*. <https://jamanetwork.com/journals/jama/fullarticle/2768391>. Retrieved 12 April 2022.
 250. Berlin DA, Gulick RM, Martinez FJ. 2020. Severe Covid-19. *N Engl J Med* 383:2451–2460.
 251. Endothelial dysfunction and immunothrombosis as key pathogenic mechanisms in COVID-19 | *Nature Reviews Immunology*. <https://www.nature.com/articles/s41577-021-00536-9>. Retrieved 12 April 2022.
 252. Blanco-Melo D, Nilsson-Payant BE, Liu W-C, Uhl S, Hoagland D, Møller R, Jordan TX, Oishi K, Panis M, Sachs D, Wang TT, Schwartz RE, Lim JK, Albrecht RA, tenOever BR. 2020. Imbalanced Host Response to SARS-CoV-2 Drives Development of COVID-19. *Cell* 181:1036-1045.e9.

253. Verkerke HP, Damhorst GL, Graciaa DS, McLendon K, O'Sick W, Robichaux C, Cheedarla N, Potlapalli S, Wu S-C, Harrington KRV, Webster A, Kraft C, Rostad CA, Waggoner JJ, Gandhi NR, Guarner J, Auld SC, Neish A, Roback JD, Lam WA, Shah NS, Stowell SR. 2022. Nucleocapsid antigenemia is a marker of acute SARS-CoV-2 infection. medRxiv <https://doi.org/10.1101/2022.01.23.22269354>.
254. Guervilly C, Burtey S, Sabatier F, Cauchois R, Lano G, Abdili E, Daviet F, Arnaud L, Brunet P, Hraiech S, Jourde-Chiche N, Koubi M, Lacroix R, Pietri L, Berda Y, Robert T, Degioanni C, Velier M, Papazian L, Kaplanski G, Dignat-George F. 2020. Circulating Endothelial Cells as a Marker of Endothelial Injury in Severe COVID -19. *J Infect Dis* 222:1789–1793.
255. Sun Z, Zheng X, Ji F, Zhou M, Su X, Ren K, Li L. 2021. Mass Spectrometry Analysis of SARS-CoV-2 Nucleocapsid Protein Reveals Camouflaging Glycans and Unique Post-Translational Modifications. *Infect Microbes Dis* 3:149–157.
256. Supekar NT, Shajahan A, Gleinich AS, Rouhani D, Heiss C, Azadi P. 2020. SARS-CoV-2 Nucleocapsid protein is decorated with multiple N- and O-glycans. bioRxiv <https://doi.org/10.1101/2020.08.26.269043>.
257. Thiemann S, Baum LG. 2016. Galectins and Immune Responses—Just How Do They Do Those Things They Do? *Annu Rev Immunol* 34:243–264.
258. Robinson BS, Arthur CM, Evavold B, Roback E, Kamili NA, Stowell CS, Vallecillo-Zúniga ML, Van Ry PM, Dias-Baruffi M, Cummings RD, Stowell SR. 2019. The Sweet-Side of Leukocytes: Galectins as Master Regulators of Neutrophil Function. *Front Immunol* 10.
259. Johannes L, Jacob R, Leffler H. 2018. Galectins at a glance. *J Cell Sci* 131:jcs208884.
260. Girotti MR, Salatino M, Dalotto-Moreno T, Rabinovich GA. 2020. Sweetening the hallmarks of cancer: Galectins as multifunctional mediators of tumor progression. *J Exp Med* 217.
261. Teichberg VI, Silman I, Beitsch DD, Resheff G. 1975. A beta-D-galactoside binding protein from electric organ tissue of *Electrophorus electricus*. *Proc Natl Acad Sci U S A* 72:1383–1387.
262. Arthur CM, Kamili NA, Patel SR, Mener A, Fasano RM, Meyer E, Winkler AM, Sola-Visner M, Josephson CD, Stowell SR. 2015. Innate Immunity Against Molecular Mimicry: Examining Galectin-Mediated Antimicrobial Activity. *BioEssays News Rev Mol Cell Dev Biol* 37:1327–1337.
263. Lowe JB. 2001. Glycosylation, Immunity, and Autoimmunity. *Cell* 104:809–812.
264. Barondes SH, Castronovo V, Cooper DN, Cummings RD, Drickamer K, Feizi T, Gitt MA, Hirabayashi J, Hughes C, Kasai K. 1994. Galectins: a family of animal beta-galactoside-binding lectins. *Cell* 76:597–598.
265. Arthur CM, Baruffi MD, Cummings RD, Stowell SR. 2015. Evolving mechanistic insights into galectin functions. *Methods Mol Biol Clifton NJ* 1207:1–35.
266. Mendel G. EXPERIMENTS IN PLANT HYBRIDIZATION (1865) 41.
267. Lauc G, Krištić J, Zoldoš V. 2014. Glycans – the third revolution in evolution. *Front Genet* 5.

268. D H, Ir G, Aj F, Ss S, Dn C, K D, H L, F P. 2004. Phylogenetic analysis of the vertebrate galectin family. *Mol Biol Evol.* <https://pubmed.ncbi.nlm.nih.gov/14963092/>. Retrieved 14 October 2020.
269. Brewer CF. 2002. Thermodynamic binding studies of galectin-1, -3 and -7. *Glycoconj J* 19:459–465.
270. Stowell SR, Arthur CM, Mehta P, Slanina KA, Blixt O, Leffler H, Smith DF, Cummings RD. 2008. Galectin-1, -2, and -3 Exhibit Differential Recognition of Sialylated Glycans and Blood Group Antigens. *J Biol Chem* 283:10109–10123.
271. Arthur CM, Rodrigues LC, Baruffi MD, Sullivan HC, Heimbürg-Molinaro J, Smith DF, Cummings RD, Stowell SR. 2015. Examining galectin binding specificity using glycan microarrays. *Methods Mol Biol Clifton NJ* 1207:115–131.
272. Hirabayashi J, Hashidate T, Arata Y, Nishi N, Nakamura T, Hirashima M, Urashima T, Oka T, Futai M, Muller WEG, Yagi F, Kasai K. 2002. Oligosaccharide specificity of galectins: a search by frontal affinity chromatography. *Biochim Biophys Acta* 1572:232–254.
273. Sun Y, Cheng L, Gu Y, Xin A, Wu B, Zhou S, Guo S, Liu Y, Diao H, Shi H, Wang G, Tao S-C. 2016. A Human Lectin Microarray for Sperm Surface Glycosylation Analysis. *Mol Cell Proteomics MCP* 15:2839–2851.
274. Carlsson S, Oberg CT, Carlsson MC, Sundin A, Nilsson UJ, Smith D, Cummings RD, Almkvist J, Karlsson A, Leffler H. 2007. Affinity of galectin-8 and its carbohydrate recognition domains for ligands in solution and at the cell surface. *Glycobiology* 17:663–676.
275. Di Lella S, Martí MA, Croci DO, Guardia CMA, Díaz-Ricci JC, Rabinovich GA, Caramelo JJ, Estrin DA. 2010. Linking the structure and thermal stability of beta-galactoside-binding protein galectin-1 to ligand binding and dimerization equilibria. *Biochemistry* 49:7652–7658.
276. Di Lella S, Sundblad V, Cerliani JP, Guardia CM, Estrin DA, Vasta GR, Rabinovich GA. 2011. When Galectins Recognize Glycans: From Biochemistry to Physiology and Back Again. *Biochemistry* 50:7842–7857.
277. Stowell SR, Cho M, Feasley CL, Arthur CM, Song X, Colucci JK, Karmakar S, Mehta P, Dias-Baruffi M, McEver RP, Cummings RD. 2009. Ligand Reduces Galectin-1 Sensitivity to Oxidative Inactivation by Enhancing Dimer Formation. *J Biol Chem* 284:4989–4999.
278. Dias-Baruffi M, Zhu H, Cho M, Karmakar S, McEver RP, Cummings RD. 2003. Dimeric galectin-1 induces surface exposure of phosphatidylserine and phagocytic recognition of leukocytes without inducing apoptosis. *J Biol Chem* 278:41282–41293.
279. Stowell SR, Arthur CM, Slanina KA, Horton JR, Smith DF, Cummings RD. 2008. Dimeric Galectin-8 Induces Phosphatidylserine Exposure in Leukocytes through Polylactosamine Recognition by the C-terminal Domain. *J Biol Chem* 283:20547–20559.
280. Arthur CM, Rodrigues LC, Dias Baruffi M, Sullivan HC, Cummings RD, Stowell SR. 2015. Detection of Phosphatidylserine Exposure on Leukocytes Following Treatment with Human Galectins. *Methods Mol Biol Clifton NJ* 1207:185–200.

281. Flores-Ibarra A, Vértesy S, Medrano FJ, Gabius H-J, Romero A. 2018. Crystallization of a human galectin-3 variant with two ordered segments in the shortened N-terminal tail. 1. *Sci Rep* 8:9835.
282. Mazurek N, Conklin J, Byrd JC, Raz A, Bresalier RS. 2000. Phosphorylation of the beta-galactoside-binding protein galectin-3 modulates binding to its ligands. *J Biol Chem* 275:36311–36315.
283. Yoshii T, Fukumori T, Honjo Y, Inohara H, Kim H-RC, Raz A. 2002. Galectin-3 phosphorylation is required for its anti-apoptotic function and cell cycle arrest. *J Biol Chem* 277:6852–6857.
284. Menon S, Kang C-M, Beningo KA. 2011. Galectin-3 Secretion and Tyrosine Phosphorylation is Dependent on the Calpain Small Subunit, Calpain 4. *Biochem Biophys Res Commun* 410:91.
285. Kamili NA, Arthur CM, Gerner-Smidt C, Tafesse E, Blenda A, Dias-Baruffi M, Stowell SR. 2016. Key regulators of galectin-glycan interactions. *Proteomics* 16:3111–3125.
286. Ju T, Lanneau GS, Gautam T, Wang Y, Xia B, Stowell SR, Willard MT, Wang W, Xia JY, Zuna RE, Laszik Z, Benbrook DM, Hanigan MH, Cummings RD. 2008. Human tumor antigens Tn and sialyl Tn arise from mutations in Cosmc. *Cancer Res* 68:1636–1646.
287. Stowell SR, Ju T, Cummings RD. 2015. Protein glycosylation in cancer. *Annu Rev Pathol* 10:473–510.
288. Arthur CM, Cummings RD, Stowell SR. 2014. Using glycan microarrays to understand immunity. *Curr Opin Chem Biol* 18:55–61.
289. Colnot C, Fowlis D, Ripoche M-A, Bouchaert I, Poirier F. 1998. Embryonic implantation in galectin 1/galectin 3 double mutant mice. *Dev Dyn* 211:306–313.
290. Poirier F, Robertson EJ. 1993. Normal development of mice carrying a null mutation in the gene encoding the L14 S-type lectin. *Development* 119:1229–1236.
291. Poirier F, Timmons PM, Chan CT, Guénet JL, Rigby PW. 1992. Expression of the L14 lectin during mouse embryogenesis suggests multiple roles during pre- and post-implantation development. *Dev Camb Engl* 115:143–155.
292. Colnot C, Ripoche MA, Scaerou F, Fowlis D, Poirier F. 1996. Galectins in mouse embryogenesis. *Biochem Soc Trans* 24:141–146.
293. Wada J, Ota K, Kumar A, Wallner EI, Kanwar YS. 1997. Developmental regulation, expression, and apoptotic potential of galectin-9, a beta-galactoside binding lectin. *J Clin Invest* 99:2452–2461.
294. Benvenuto G, Carpentieri ML, Salvatore P, Cindolo L, Bruni CB, Chiariotti L. 1996. Cell-specific transcriptional regulation and reactivation of galectin-1 gene expression are controlled by DNA methylation of the promoter region. *Mol Cell Biol* 16:2736–2743.
295. Toscano MA, Campagna L, Molinero LL, Cerliani JP, Croci DO, Ilarregui JM, Fuertes MB, Nojek IM, Fededa JP, Zwirner NW, Costas MA, Rabinovich GA. 2011. Nuclear factor (NF)- κ B controls expression of the immunoregulatory glycan-binding protein galectin-1. *Mol Immunol* 48:1940–1949.

296. Than NG, Romero R, Erez O, Weckle A, Tarca AL, Hotra J, Abbas A, Han YM, Kim S-S, Kusanovic JP, Gotsch F, Hou Z, Santolaya-Forgas J, Benirschke K, Papp Z, Grossman LI, Goodman M, Wildman DE. 2008. Emergence of hormonal and redox regulation of galectin-1 in placental mammals: Implication in maternal–fetal immune tolerance. *Proc Natl Acad Sci* 105:15819–15824.
297. Than NG, Romero R, Xu Y, Erez O, Xu Z, Bhatti G, Leavitt R, Chung TH, El-Azzamy H, LaJeunesse C, Wang B, Balogh A, Szalai G, Land S, Dong Z, Hassan SS, Chaiworapongsa T, Krispin M, Kim CJ, Tarca AL, Papp Z, Bohn H. 2014. Evolutionary origins of the placental expression of Chromosome 19 cluster galectins and their complex dysregulation in preeclampsia. *Placenta* 35:855–865.
298. Za E, Jm M, Gr S, Ak S, Xx S, Al L, J M, Ja C, A R. 2019. The Impact of Natural Selection on the Evolution and Function of Placentally Expressed Galectins. *Genome Biol Evol.* *Genome Biol Evol.* <https://pubmed.ncbi.nlm.nih.gov/31504490/>. Retrieved 14 October 2020.
299. Than NG, Romero R, Goodman M, Weckle A, Xing J, Dong Z, Xu Y, Tarquini F, Szilagyi A, Gal P, Hou Z, Tarca AL, Kim CJ, Kim J-S, Haidarian S, Uddin M, Bohn H, Benirschke K, Santolaya-Forgas J, Grossman LI, Erez O, Hassan SS, Zavodszky P, Papp Z, Wildman DE. 2009. A primate subfamily of galectins expressed at the maternal–fetal interface that promote immune cell death. *Proc Natl Acad Sci* 106:9731–9736.
300. Than NG, Romero R, Kim CJ, McGowen MR, Papp Z, Wildman DE. 2012. Galectins: guardians of eutherian pregnancy at the maternal-fetal interface. *Trends Endocrinol Metab* 23:23–31.
301. Human Decidual Natural Killer Cells Are a Unique NK Cell Subset with Immunomodulatory Potential | *Journal of Experimental Medicine* | Rockefeller University Press. <https://rupress.org/jem/article/198/8/1201/39806/Human-Decidual-Natural-Killer-Cells-Are-a-Unique>. Retrieved 30 November 2020.
302. Garín MI, Chu C-C, Golshayan D, Cernuda-Morollón E, Wait R, Lechler RI. 2007. Galectin-1: a key effector of regulation mediated by CD4+CD25+ T cells. *Blood* 109:2058–2065.
303. Liu FT. 2000. Galectins: a new family of regulators of inflammation. *Clin Immunol Orlando Fla* 97:79–88.
304. Hsu DK, Hammes SR, Kuwabara I, Greene WC, Liu FT. 1996. Human T lymphotropic virus-I infection of human T lymphocytes induces expression of the beta-galactoside-binding lectin, galectin-3. *Am J Pathol* 148:1661–1670.
305. Ackerman SJ, Corrette SE, Rosenberg HF, Bennett JC, Mastrianni DM, Nicholson-Weller A, Weller PF, Chin DT, Tenen DG. 1993. Molecular cloning and characterization of human eosinophil Charcot-Leyden crystal protein (lysophospholipase). Similarities to IgE binding proteins and the S-type animal lectin superfamily. *J Immunol Baltim Md* 150:456–468.
306. Dor PJ, Ackerman SJ, Gleich GJ. 1984. Charcot-Leyden crystal protein and eosinophil granule major basic protein in sputum of patients with respiratory diseases. *Am Rev Respir Dis* 130:1072–1077.
307. Selective Recognition of Mannose by the Human Eosinophil Charcot-Leyden Crystal Protein (Galectin-10): A Crystallographic Study at 1.8 Å Resolution, |

- Biochemistry. <https://pubs.acs.org/doi/abs/10.1021/bi990756e>. Retrieved 1 December 2020.
308. Yang R-Y, Yu L, Graham JL, Hsu DK, Lloyd KCK, Havel PJ, Liu F-T. 2011. Ablation of a galectin preferentially expressed in adipocytes increases lipolysis, reduces adiposity, and improves insulin sensitivity in mice. *Proc Natl Acad Sci* 108:18696–18701.
 309. Cooper DN, Barondes SH. 1990. Evidence for export of a muscle lectin from cytosol to extracellular matrix and for a novel secretory mechanism. *J Cell Biol* 110:1681–1691.
 310. Cerri DG, Rodrigues LC, Stowell SR, Araujo DD, Coelho MC, Oliveira SR, Bizario JCS, Cummings RD, Dias-Baruffi M, Costa MCR. 2008. Degeneration of dystrophic or injured skeletal muscles induces high expression of Galectin-1. *Glycobiology* 18:842–850.
 311. Vallecillo-Zúniga ML, Rathgeber MF, Poulson PD, Hayes S, Luddington JS, Gill HN, Teynor M, Kartchner BC, Valdoz J, Stowell C, Markham AR, Arthur C, Stowell S, Ry PMV. 2020. Treatment with galectin-1 improves myogenic potential and membrane repair in dysferlin-deficient models. *PLOS ONE* 15:e0238441.
 312. Seelenmeyer C, Wegehingel S, Tews I, Künzler M, Aebi M, Nickel W. 2005. Cell surface counter receptors are essential components of the unconventional export machinery of galectin-1. *J Cell Biol* 171:373–381.
 313. Bänfer S, Schneider D, Dewes J, Strauss MT, Freibert S-A, Heimerl T, Maier UG, Elsässer H-P, Jungmann R, Jacob R. 2018. Molecular mechanism to recruit galectin-3 into multivesicular bodies for polarized exosomal secretion. *Proc Natl Acad Sci* 115:E4396–E4405.
 314. Thurston TLM, Wandel MP, von Muhlinen N, Foeglein A, Randow F. 2012. Galectin 8 targets damaged vesicles for autophagy to defend cells against bacterial invasion. *Nature* 482:414–418.
 315. Dagher SF, Wang JL, Patterson RJ. 1995. Identification of galectin-3 as a factor in pre-mRNA splicing. *Proc Natl Acad Sci* 92:1213–1217.
 316. Vyakarnam A, Lenneman AJ, Lakkides KM, Patterson RJ, Wang JL. 1998. A Comparative Nuclear Localization Study of Galectin-1 with Other Splicing Components. *Exp Cell Res* 242:419–428.
 317. Wang W, Park JW, Wang JL, Patterson RJ. 2006. Immunoprecipitation of spliceosomal RNAs by antisera to galectin-1 and galectin-3. *Nucleic Acids Res* 34:5166–5174.
 318. Nakahara S, Hogan V, Inohara H, Raz A. 2006. Importin-mediated Nuclear Translocation of Galectin-3. *J Biol Chem* 281:39649–39659.
 319. Huflejt ME, Turck CW, Lindstedt R, Barondes SH, Leffler H. 1993. L-29, a soluble lactose-binding lectin, is phosphorylated on serine 6 and serine 12 in vivo and by casein kinase I. *J Biol Chem* 268:26712–26718.
 320. Wang JL, Gray RM, Haudek KC, Patterson RJ. 2004. Nucleocytoplasmic lectins. *Biochim Biophys Acta* 1673:75–93.
 321. Haudek KC, Voss PG, Locascio LE, Wang JL, Patterson RJ. 2009. A mechanism for incorporation of galectin-3 into the spliceosome through its association with U1 snRNP. *Biochemistry* 48:7705–7712.

322. Gray RM, Davis MJ, Ruby KM, Voss PG, Patterson RJ, Wang JL. 2008. Distinct Effects on Splicing of Two Monoclonal Antibodies Directed against the Amino-terminal Domain of Galectin-3. *Arch Biochem Biophys* 475:100–108.
323. Park JW, Voss PG, Grabski S, Wang JL, Patterson RJ. 2001. Association of galectin-1 and galectin-3 with Gemin4 in complexes containing the SMN protein. *Nucleic Acids Res* 29:3595–3602.
324. Coppin L, Vincent A, Frénois F, Duchêne B, Lahdaoui F, Stechly L, Renaud F, Villenet C, Van Seuninghen I, Leteurtre E, Dion J, Grandjean C, Poirier F, Figeac M, Delacour D, Porchet N, Pigny P. 2017. Galectin-3 is a non-classic RNA binding protein that stabilizes the mucin MUC4 mRNA in the cytoplasm of cancer cells. 1. *Sci Rep* 7:43927.
325. Bafna S, Kaur S, Batra S. 2010. Membrane-bound mucins: the mechanistic basis for alterations in the growth and survival of cancer cells. *Oncogene* 29:2893–2904.
326. Golling G, Amsterdam A, Sun Z, Antonelli M, Maldonado E, Chen W, Burgess S, Haldi M, Artzt K, Farrington S, Lin S-Y, Nissen RM, Hopkins N. 2002. Insertional mutagenesis in zebrafish rapidly identifies genes essential for early vertebrate development. 2. *Nat Genet* 31:135–140.
327. Yang RY, Hsu DK, Liu FT. 1996. Expression of galectin-3 modulates T-cell growth and apoptosis. *Proc Natl Acad Sci* 93:6737–6742.
328. Akahani S, Kim C. Galectin-3: A Novel Antiapoptotic Molecule with A Functional BH1 (NWGR) Domain of Bcl-2 Family' 6.
329. Wang Y, Balan V, Gao X, Reddy PG, Kho D, Tait L, Raz A. 2013. The significance of galectin-3 as a new basal cell marker in prostate cancer. 8. *Cell Death Dis* 4:e753–e753.
330. Cheng D, Liang B, Li Y. 2015. Serum Galectin-3 as a Potential Marker for Gastric Cancer. *Med Sci Monit Int Med J Exp Clin Res* 21:755–760.
331. Mazurek N, Byrd JC, Sun Y, Hafley M, Ramirez K, Burks J, Bresalier RS. 2012. Cell-surface galectin-3 confers resistance to TRAIL by impeding trafficking of death receptors in metastatic colon adenocarcinoma cells. 3. *Cell Death Differ* 19:523–533.
332. Transient silencing of galectin-3 expression promotes both in vitro and in vivo drug-induced apoptosis of human pancreatic carcinoma cells. <https://www.infona.pl/resource/bwmeta1.element.springer-75fbf91d-6b9f-34d7-b85a-e359a257fea3>. Retrieved 30 November 2020.
333. Califice S, Castronovo V, Bracke M, van den Brûle F. 2004. Dual activities of galectin-3 in human prostate cancer: tumor suppression of nuclear galectin-3 vs tumor promotion of cytoplasmic galectin-3. 45. *Oncogene* 23:7527–7536.
334. Takenaka Y, Fukumori T, Yoshii T, Oka N, Inohara H, Kim H-RC, Bresalier RS, Raz A. 2004. Nuclear Export of Phosphorylated Galectin-3 Regulates Its Antiapoptotic Activity in Response to Chemotherapeutic Drugs. *Mol Cell Biol* 24:4395–4406.
335. Bernerd F, Sarasin A, Magnaldo T. 1999. Galectin-7 overexpression is associated with the apoptotic process in UVB-induced sunburn keratinocytes. *Proc Natl Acad Sci U S A* 96:11329–11334.

336. Patnaik SK, Potvin B, Carlsson S, Sturm D, Leffler H, Stanley P. 2006. Complex N-glycans are the major ligands for galectin-1, -3, and -8 on Chinese hamster ovary cells. *Glycobiology* 16:305–317.
337. Nabi IR, Shankar J, Dennis JW. 2015. The galectin lattice at a glance. *J Cell Sci* 128:2213–2219.
338. Apweiler R, Hermjakob H, Sharon N. 1999. On the frequency of protein glycosylation, as deduced from analysis of the SWISS-PROT database. *Biochim Biophys Acta* 1473:4–8.
339. Lau KS, Partridge EA, Grigorian A, Silvescu CI, Reinhold VN, Demetriou M, Dennis JW. 2007. Complex N-Glycan Number and Degree of Branching Cooperate to Regulate Cell Proliferation and Differentiation. *Cell* 129:123–134.
340. Smith LK, Boukhaled GM, Condotta SA, Mazouz S, Guthmiller JJ, Vijay R, Butler NS, Bruneau J, Shoukry NH, Krawczyk CM, Richer MJ. 2018. Interleukin-10 Directly Inhibits CD8+ T Cell Function by Enhancing N-Glycan Branching to Decrease Antigen Sensitivity. *Immunity* 48:299-312.e5.
341. Demetriou M, Granovsky M, Quaggin S, Dennis JW. 2001. Negative regulation of T-cell activation and autoimmunity by Mgat5 N-glycosylation. *Nature* 409:733–739.
342. Mkhikian H, Grigorian A, Li CF, Chen H-L, Newton B, Zhou RW, Beeton C, Torossian S, Tatariyan GG, Lee S-U, Lau K, Walker E, Siminovich KA, Chandy KG, Yu Z, Dennis JW, Demetriou M. 2011. Genetics and the environment converge to dysregulate N-glycosylation in multiple sclerosis. *Nat Commun* 2:334.
343. Li CF, Zhou RW, Mkhikian H, Newton BL, Yu Z, Demetriou M. 2013. Hypomorphic MGAT5 polymorphisms promote multiple sclerosis cooperatively with MGAT1 and interleukin-2 and 7 receptor variants. *J Neuroimmunol* 256:71–76.
344. Yu Z, Li CF, Mkhikian H, Zhou RW, Newton BL, Demetriou M. 2014. Family studies of type 1 diabetes reveal additive and epistatic effects between MGAT1 and three other polymorphisms. *Genes Immun* 15:218–223.
345. Obino D, Fetter L, Soza A, Malbec O, Saez JJ, Labarca M, Oyanadel C, Del Valle Batalla F, Goles N, Chikina A, Lankar D, Segovia-Miranda F, Garcia C, Léger T, Gonzalez A, Espéli M, Lennon-Duménil A-M, Yuseff M-I. 2018. Galectin-8 Favors the Presentation of Surface-Tethered Antigens by Stabilizing the B Cell Immune Synapse. *Cell Rep* 25:3110-3122.e6.
346. Levi G, Tarrab-Hazdai R, Teichberg VI. 1983. Prevention and therapy with electrolectin of experimental autoimmune myasthenia gravis in rabbits. *Eur J Immunol* 13:500–507.
347. 1995. Human thymic epithelial cells express an endogenous lectin, galectin-1, which binds to core 2 O-glycans on thymocytes and T lymphoblastoid cells. *J Exp Med* 181:877–887.
348. Lee-Sundlov MM, Stowell SR, Hoffmeister KM. 2020. Multifaceted role of glycosylation in transfusion medicine, platelets, and red blood cells. *J Thromb Haemost JTH* 18:1535–1547.
349. Gendronneau G, Sidhu SS, Delacour D, Dang T, Calonne C, Houzelstein D, Magnaldo T, Poirier F. 2008. Galectin-7 in the control of epidermal homeostasis after injury. *Mol Biol Cell* 19:5541–5549.

350. Panjwani N. 2014. Role of galectins in re-epithelialization of wounds. *Ann Transl Med* 2.
351. Robinson BS, Saeedi B, Naudin C, Arthur C, Darby T, Jones R, Stowell S, Neish A. 2018. Galectin-9 is a Novel Modulator of Epithelial Restitution. *FASEB J* 32:414.1-414.1.
352. Thijssen VLJL, Postel R, Brandwijk RJMGE, Dings RPM, Nesmelova I, Satijn S, Verhofstad N, Nakabeppu Y, Baum LG, Bakkers J, Mayo KH, Poirier F, Griffioen AW. 2006. Galectin-1 is essential in tumor angiogenesis and is a target for antiangiogenesis therapy. *Proc Natl Acad Sci* 103:15975–15980.
353. D’Haene N, Sauvage S, Maris C, Adanja I, Mercier ML, Decaestecker C, Baum L, Salmon I. 2013. VEGFR1 and VEGFR2 Involvement in Extracellular Galectin-1- and Galectin-3-Induced Angiogenesis. *PLOS ONE* 8:e67029.
354. Nangia-Makker P, Honjo Y, Sarvis R, Akahani S, Hogan V, Pienta KJ, Raz A. 2000. Galectin-3 Induces Endothelial Cell Morphogenesis and Angiogenesis. *Am J Pathol* 156:899–909.
355. Freitag N, Tirado-González I, Barrientos G, Herse F, Thijssen VLJL, Weedon-Fekjær SM, Schulz H, Wallukat G, Klapp BF, Nevers T, Sharma S, Staff AC, Dechend R, Blois SM. 2013. Interfering with Gal-1-mediated angiogenesis contributes to the pathogenesis of preeclampsia. *Proc Natl Acad Sci* 110:11451–11456.
356. Romaniuk MA, Tribulatti MV, Cattaneo V, Laponi MJ, Molinas FC, Campetella O, Schattner M. 2010. Human platelets express and are activated by galectin-8. *Biochem J* 432:535–547.
357. Pacienza N, Pozner RG, Bianco GA, D’Atri LP, Croci DO, Negrotto S, Malaver E, Gómez RM, Rabinovich GA, Schattner M. 2008. The immunoregulatory glycan-binding protein galectin-1 triggers human platelet activation. *FASEB J Off Publ Fed Am Soc Exp Biol* 22:1113–1123.
358. Romaniuk MA, Croci DO, Laponi MJ, Tribulatti MV, Negrotto S, Poirier F, Campetella O, Rabinovich GA, Schattner M. 2012. Binding of galectin-1 to $\alpha\text{IIb}\beta_3$ integrin triggers “outside-in” signals, stimulates platelet activation, and controls primary hemostasis. *FASEB J Off Publ Fed Am Soc Exp Biol* 26:2788–2798.
359. Pylayeva-Gupta Y, Grabocka E, Bar-Sagi D. 2011. RAS oncogenes: weaving a tumorigenic web. *Nat Rev Cancer* 11:761–774.
360. Paz A, Haklai R, Elad-Sfadia G, Ballan E, Kloog Y. 2001. Galectin-1 binds oncogenic H-Ras to mediate Ras membrane anchorage and cell transformation. *Oncogene* 20:7486–7493.
361. Elad-Sfadia G, Haklai R, Balan E, Kloog Y. 2004. Galectin-3 augments K-Ras activation and triggers a Ras signal that attenuates ERK but not phosphoinositide 3-kinase activity. *J Biol Chem* 279:34922–34930.
362. Shalom-Feuerstein R, Cooks T, Raz A, Kloog Y. 2005. Galectin-3 regulates a molecular switch from N-Ras to K-Ras usage in human breast carcinoma cells. *Cancer Res* 65:7292–7300.
363. Vuong L, Kouverianou E, Rooney CM, McHugh BJ, Howie SEM, Gregory CD, Forbes SJ, Henderson NC, Zetterberg FR, Nilsson UJ, Leffler H, Ford P, Pedersen A, Gravelle L, Tantawi S, Schambye H, Sethi T, MacKinnon AC. 2019.

- An Orally Active Galectin-3 Antagonist Inhibits Lung Adenocarcinoma Growth and Augments Response to PD-L1 Blockade. *Cancer Res* 79:1480–1492.
364. Chung L-Y, Tang S-J, Sun G-H, Chou T-Y, Yeh T-S, Yu S-L, Sun K-H. 2012. Galectin-1 promotes lung cancer progression and chemoresistance by upregulating p38 MAPK, ERK, and cyclooxygenase-2. *Clin Cancer Res Off J Am Assoc Cancer Res* 18:4037–4047.
 365. Banh A, Zhang J, Cao H, Bouley DM, Kwok S, Kong C, Giaccia AJ, Koong AC, Le Q-T. 2011. Tumor galectin-1 mediates tumor growth and metastasis through regulation of T-cell apoptosis. *Cancer Res* 71:4423–4431.
 366. Nambiar DK, Aguilera T, Cao H, Kwok S, Kong C, Bloomstein J, Wang Z, Rangan VS, Jiang D, Eyben R von, Liang R, Agarwal S, Colevas AD, Korman A, Allen CT, Uppaluri R, Koong AC, Giaccia A, Le QT. 2019. Galectin-1–driven T cell exclusion in the tumor endothelium promotes immunotherapy resistance. *J Clin Invest* 129:5553–5567.
 367. Galon J, Costes A, Sanchez-Cabo F, Kirilovsky A, Mlecnik B, Lagorce-Pagès C, Tosolini M, Camus M, Berger A, Wind P, Zinzindohoué F, Bruneval P, Cugnenc P-H, Trajanoski Z, Fridman W-H, Pagès F. 2006. Type, Density, and Location of Immune Cells Within Human Colorectal Tumors Predict Clinical Outcome. *Science* 313:1960–1964.
 368. Predictive correlates of response to the anti-PD-L1 antibody MPDL3280A in cancer patients | *Nature*. <https://www.nature.com/articles/nature14011?page=1>. Retrieved 12 November 2020.
 369. Peranzoni E, Lemoine J, Vimeux L, Feuillet V, Barrin S, Kantari-Mimoun C, Bercovici N, Guérin M, Biton J, Ouakrim H, Régnier F, Lupo A, Alifano M, Damotte D, Donnadieu E. 2018. Macrophages impede CD8 T cells from reaching tumor cells and limit the efficacy of anti-PD-1 treatment. *Proc Natl Acad Sci* 115:E4041–E4050.
 370. Savas P, Virassamy B, Ye C, Salim A, Mintoff CP, Caramia F, Salgado R, Byrne DJ, Teo ZL, Dushyanthen S, Byrne A, Wein L, Luen SJ, Poliness C, Nightingale SS, Skandarajah AS, Gyorki DE, Thornton CM, Beavis PA, Fox SB, Darcy PK, Speed TP, Mackay LK, Neeson PJ, Loi S. 2018. Single-cell profiling of breast cancer T cells reveals a tissue-resident memory subset associated with improved prognosis. *Nat Med* 24:986–993.
 371. Thijssen VL, Heusschen R, Caers J, Griffioen AW. 2015. Galectin expression in cancer diagnosis and prognosis: A systematic review. *Biochim Biophys Acta* 1855:235–247.
 372. Gordon-Alonso M, Hirsch T, Wildmann C, van der Bruggen P. 2017. Galectin-3 captures interferon-gamma in the tumor matrix reducing chemokine gradient production and T-cell tumor infiltration. *Nat Commun* 8:793.
 373. Santucci L, Fiorucci S, Cammilleri F, Servillo G, Federici B, Morelli A. 2000. Galectin-1 exerts immunomodulatory and protective effects on concanavalin a–induced hepatitis in mice. *Hepatology* 31:399–406.
 374. Santucci L, Fiorucci S, Rubinstein N, Mencarelli A, Palazzetti B, Federici B, Rabinovich GA, Morelli A. 2003. Galectin-1 suppresses experimental colitis in mice. *Gastroenterology* 124:1381–1394.

375. Toscano MA, Commodaro AG, Illarregui JM, Bianco GA, Liberman A, Serra HM, Hirabayashi J, Rizzo LV, Rabinovich GA. 2006. Galectin-1 suppresses autoimmune retinal disease by promoting concomitant Th2- and T regulatory-mediated anti-inflammatory responses. *J Immunol Baltim Md 1950* 176:6323–6332.
376. Baum LG, Blackall DP, Arias-Magallano S, Nanigian D, Uh SY, Browne JM, Hoffmann D, Emmanouilides CE, Territo MC, Baldwin GC. 2003. Amelioration of graft versus host disease by galectin-1. *Clin Immunol Orlando Fla* 109:295–307.
377. Perillo NL, Pace KE, Seilhamer JJ, Baum LG. 1995. Apoptosis of T cells mediated by galectin-1. 6558. *Nature* 378:736–739.
378. Proteomic and functional analysis identifies galectin-1 as a novel regulatory component of the cytotoxic granule machinery | *Cell Death & Disease*. <https://www.nature.com/articles/cddis2017506>. Retrieved 29 November 2020.
379. Stillman BN, Hsu DK, Pang M, Brewer CF, Johnson P, Liu F-T, Baum LG. 2006. Galectin-3 and Galectin-1 Bind Distinct Cell Surface Glycoprotein Receptors to Induce T Cell Death. *J Immunol* 176:778–789.
380. Thiemann S, Man JH, Chang MH, Lee B, Baum LG. 2015. Galectin-1 Regulates Tissue Exit of Specific Dendritic Cell Populations. *J Biol Chem* 290:22662–22677.
381. Illarregui JM, Croci DO, Bianco GA, Toscano MA, Salatino M, Vermeulen ME, Geffner JR, Rabinovich GA. 2009. Tolerogenic signals delivered by dendritic cells to T cells through a galectin-1-driven immunoregulatory circuit involving interleukin 27 and interleukin 10. *Nat Immunol* 10:981–991.
382. Im SJ, Hashimoto M, Gerner MY, Lee J, Kissick HT, Burger MC, Shan Q, Hale JS, Lee J, Nasti TH, Sharpe AH, Freeman GJ, Germain RN, Nakaya HI, Xue H-H, Ahmed R. 2016. Defining CD8+ T cells that provide the proliferative burst after PD-1 therapy. *Nature* 537:417–421.
383. Robertson MW, Albrandt K, Keller D, Liu FT. 1990. Human IgE-binding protein: a soluble lectin exhibiting a highly conserved interspecies sequence and differential recognition of IgE glycoforms. *Biochemistry* 29:8093–8100.
384. 1993. Human neutrophils express immunoglobulin E (IgE)-binding proteins (Mac-2/epsilon BP) of the S-type lectin family: role in IgE-dependent activation. *J Exp Med* 177:243–248.
385. Stowell SR, Karmakar S, Stowell CJ, Dias-Baruffi M, McEver RP, Cummings RD. 2007. Human galectin-1, -2, and -4 induce surface exposure of phosphatidylserine in activated human neutrophils but not in activated T cells. *Blood* 109:219–227.
386. Stowell SR, Qian Y, Karmakar S, Koyama NS, Dias-Baruffi M, Leffler H, McEver RP, Cummings RD. 2008. Differential Roles of Galectin-1 and Galectin-3 in Regulating Leukocyte Viability and Cytokine Secretion. *J Immunol* 180:3091–3102.
387. Stowell SR, Karmakar S, Arthur CM, Ju T, Rodrigues LC, Riul TB, Dias-Baruffi M, Miner J, McEver RP, Cummings RD. 2009. Galectin-1 induces reversible phosphatidylserine exposure at the plasma membrane. *Mol Biol Cell* 20:1408–1418.
388. Tian J, Yang G, Chen H-Y, Hsu DK, Tomilov A, Olson KA, Dehnad A, Fish SR, Cortopassi G, Zhao B, Liu F-T, Gershwin ME, Török NJ, Jiang JX. 2016. Galectin-

- 3 regulates inflammasome activation in cholestatic liver injury. *FASEB J Off Publ Fed Am Soc Exp Biol* 30:4202–4213.
389. Galectin-3 Enhances Avian H5N1 Influenza A Virus-Induced Pulmonary Inflammation by Promoting NLRP3 Inflammasome Activation | Elsevier Enhanced Reader.
<https://reader.elsevier.com/reader/sd/pii/S0002944017308660?token=226DDEC555EF9B2F96158481FEC6925164CAB88E83C42778F537B2A9FBFD4D1FB1CFE8E7488EB4CEA5ADB6405ABCBCB>. Retrieved 15 November 2020.
390. Querol Cano L, Tagit O, Dolen Y, van Duffelen A, Dieltjes S, Buschow SI, Niki T, Hirashima M, Joosten B, van den Dries K, Cambi A, Figdor CG, van Sriel AB. 2019. Intracellular Galectin-9 Controls Dendritic Cell Function by Maintaining Plasma Membrane Rigidity. *iScience* 22:240–255.
391. Henderson NC, Mackinnon AC, Farnworth SL, Kipari T, Haslett C, Iredale JP, Liu F-T, Hughes J, Sethi T. 2008. Galectin-3 Expression and Secretion Links Macrophages to the Promotion of Renal Fibrosis. *Am J Pathol* 172:288–298.
392. Di Gregoli Karina, Somerville Michelle, Bianco Rosaria, Thomas Anita C., Frankow Aleksandra, Newby Andrew C., George Sarah J., Jackson Christopher L., Johnson Jason L. 2020. Galectin-3 Identifies a Subset of Macrophages With a Potential Beneficial Role in Atherosclerosis. *Arterioscler Thromb Vasc Biol* 40:1491–1509.
393. MacKinnon AC, Farnworth SL, Hodgkinson PS, Henderson NC, Atkinson KM, Leffler H, Nilsson UJ, Haslett C, Forbes SJ, Sethi T. 2008. Regulation of Alternative Macrophage Activation by Galectin-3. *J Immunol* 180:2650–2658.
394. Takahashi K, Ezekowitz RAB. 2005. The Role of the Mannose-Binding Lectin in Innate Immunity. *Clin Infect Dis* 41:S440–S444.
395. Garred P, Larsen F, Seyfarth J, Fujita R, Madsen HO. 2006. Mannose-binding lectin and its genetic variants. 2. *Genes Immun* 7:85–94.
396. Brown GD. 2006. Dectin-1: a signalling non-TLR pattern-recognition receptor. 1. *Nat Rev Immunol* 6:33–43.
397. Li F-Y, Weng I-C, Lin C-H, Kao M-C, Wu M-S, Chen H-Y, Liu F-T. 2019. *Helicobacter pylori* induces intracellular galectin-8 aggregation around damaged lysosomes within gastric epithelial cells in a host O-glycan-dependent manner. *Glycobiology* 29:151–162.
398. Chauhan S, Kumar S, Jain A, Ponpuak M, Mudd MH, Kimura T, Choi SW, Peters R, Mandell M, Bruun J-A, Johansen T, Deretic V. 2016. TRIMs and Galectins Globally Cooperate and TRIM16 and Galectin-3 Co-direct Autophagy in Endomembrane Damage Homeostasis. *Dev Cell* 39:13–27.
399. I P, M S, N D, J M, C C, J E, H L, F P, Mc P, F L, P S. 2010. Galectin-3, a marker for vacuole lysis by invasive pathogens. *Cell Microbiol. Cell Microbiol.*
<https://pubmed.ncbi.nlm.nih.gov/19951367/>. Retrieved 14 October 2020.
400. Vasta GR. 2009. Roles of galectins in infection. 6. *Nat Rev Microbiol* 7:424–438.
401. Stowell SR, Arthur CM, Dias-Baruffi M, Rodrigues LC, Gourdine J-P, Heimburg-Molinaro J, Ju T, Molinaro RJ, Rivera-Marrero C, Xia B, Smith DF, Cummings RD. 2010. Innate immune lectins kill bacteria expressing blood group antigen. *Nat Med* 16:295–301.

402. Stowell SR, Arthur CM, McBride R, Berger O, Razi N, Heimbürg-Molinaro J, Rodrigues LC, Gourdine J-P, Noll AJ, von Gunten S, Smith DF, Knirel YA, Paulson JC, Cummings RD. 2014. Microbial glycan microarrays define key features of host-microbial interactions. *Nat Chem Biol* 10:470–476.
403. Springer GF, Williamson P, Brandes WC. 1961. BLOOD GROUP ACTIVITY OF GRAM-NEGATIVE BACTERIA. *J Exp Med* 113:1077–1093.
404. Stowell SR, Stowell CP. 2019. Biologic roles of the ABH and Lewis histo-blood group antigens part II: thrombosis, cardiovascular disease and metabolism. *Vox Sang* 114:535–552.
405. Quattroni P, Li Y, Lucchesi D, Lucas S, Hood DW, Herrmann M, Gabius H-J, Tang CM, Exley RM. 2012. Galectin-3 binds *Neisseria meningitidis* and increases interaction with phagocytic cells. *Cell Microbiol* 14:1657–1675.
406. Park A-M, Hagiwara S, Hsu DK, Liu F-T, Yoshie O. 2016. Galectin-3 Plays an Important Role in Innate Immunity to Gastric Infection by *Helicobacter pylori*. *Infect Immun* 84:1184–1193.
407. Yang M-L, Chen Y-H, Wang S-W, Huang Y-J, Leu C-H, Yeh N-C, Chu C-Y, Lin C-C, Shieh G-S, Chen Y-L, Wang J-R, Wang C-H, Wu C-L, Shiau A-L. 2011. Galectin-1 Binds to Influenza Virus and Ameliorates Influenza Virus Pathogenesis. *J Virol* 85:10010–10020.
408. Chen Y, Zhou J, Cheng Z, Yang S, Chu H, Fan Y, Li C, Wong BH-Y, Zheng S, Zhu Y, Yu F, Wang Y, Liu X, Gao H, Yu L, Tang L, Cui D, Hao K, Bossé Y, Obeidat M, Brandsma C-A, Song Y-Q, To KK-W, Sham PC, Yuen K-Y, Li L. 2015. Functional variants regulating LGALS1 (Galectin 1) expression affect human susceptibility to influenza A(H7N9). 1. *Sci Rep* 5:8517.
409. Levroney EL, Aguilar HC, Fulcher JA, Kohatsu L, Pace KE, Pang M, Gurney KB, Baum LG, Lee B. 2005. Novel Innate Immune Functions for Galectin-1: Galectin-1 Inhibits Cell Fusion by Nipah Virus Envelope Glycoproteins and Augments Dendritic Cell Secretion of Proinflammatory Cytokines. *J Immunol Baltim Md* 175:413–420.
410. Endothelial Galectin-1 Binds to Specific Glycans on Nipah Virus Fusion Protein and Inhibits Maturation, Mobility, and Function to Block Syncytia Formation. <https://journals.plos.org/plospathogens/article?id=10.1371/journal.ppat.1000993>. Retrieved 15 November 2020.
411. Ouellet M, Mercier S, Pelletier I, Bounou S, Roy J, Hirabayashi J, Sato S, Tremblay MJ. 2005. Galectin-1 Acts as a Soluble Host Factor That Promotes HIV-1 Infectivity through Stabilization of Virus Attachment to Host Cells. *J Immunol* 174:4120–4126.
412. Wang S-F, Tsao C-H, Lin Y-T, Hsu DK, Chiang M-L, Lo C-H, Chien F-C, Chen P, Arthur Chen Y-M, Chen H-Y, Liu F-T. 2014. Galectin-3 promotes HIV-1 budding via association with Alix and Gag p6. *Glycobiology* 24:1022–1035.
413. Montespan C, Marvin SA, Austin S, Burrage AM, Roger B, Rayne F, Faure M, Campell EM, Schneider C, Reimer R, Grünewald K, Wiethoff CM, Wodrich H. 2017. Multi-layered control of Galectin-8 mediated autophagy during adenovirus cell entry through a conserved PPxY motif in the viral capsid. *PLoS Pathog* 13:e1006217.

414. Arthur CM, Baruffi MD, Cummings RD, Stowell SR. 2015. Evolving Mechanistic Insights into Galectin Functions. *Methods Mol Biol Clifton NJ* 1207:1–35.
415. Kamili NA, Arthur CM, Gerner-Smidt C, Tafesse E, Blenda A, Dias-Baruffi M, Stowell SR. 2016. Key regulators of galectin–glycan interactions. *Proteomics* 16:3111–3125.
416. Hafer-Macko C, Pang M, Seilhamer JJ, Baum LG. 1996. Galectin-1 is expressed by thymic epithelial cells in myasthenia gravis. *Glycoconj J* 13:591–597.
417. Stowell SR, Qian Y, Karmakar S, Koyama NS, Dias-Baruffi M, Leffler H, McEver RP, Cummings RD. 2008. Differential roles of galectin-1 and galectin-3 in regulating leukocyte viability and cytokine secretion. *J Immunol Baltim Md 1950* 180:3091–3102.
418. Stowell SR, Karmakar S, Stowell CJ, Dias-Baruffi M, McEver RP, Cummings RD. 2007. Human galectin-1, -2, and -4 induce surface exposure of phosphatidylserine in activated human neutrophils but not in activated T cells. *Blood* 109:219–227.
419. Mercier S, St-Pierre C, Pelletier I, Ouellet M, Tremblay MJ, Sato S. 2008. Galectin-1 promotes HIV-1 infectivity in macrophages through stabilization of viral adsorption. *Virology* 371:121–129.
420. McMaster SR, Wilson JJ, Wang H, Kohlmeier JE. 2015. Airway-Resident Memory CD8 T Cells Provide Antigen-Specific Protection against Respiratory Virus Challenge through Rapid IFN- γ Production. *J Immunol Baltim Md 1950* 195:203–209.